End Group Functionalised Highly Branched Poly(*N*-isopropylacrylamides) in Biomaterials

Richard Plenderleith

A thesis submitted to the University of Sheffield in fulfilment of the requirements for the degree of Doctor of Philosophy

2015

Contents

Acknowledgements

I would like to thank the following people and groups for their input:

My supervisors; Stephen Rimmer and Frederik Claeyssens, who have provided a wealth of knowledge experience and in Fred's case, unwavering optimism and excitement. Both Fred and Steve have been invaluable in their support and innovation.

A special mention to Prof. John Haycock and Dr Chris Sammon who in spite of not being official supervisors, have gone beyond the call of duty in their assistance to me during the project.

My colleague and friend Christopher Pateman with whom I worked closely throughout the project.

Members of the Rimmer group and f-floor past, present and future: In particular Ryan Taylor, Andrew McKenzie, Thomas Swift, Laura Platt, Adam Ellis and Luke Cartwright.

Melanie Hannah for fixing all of the equipment all of the time, calming influence and unfortunate discontinuation of otherwise ongoing support due to geographic botheration.

The EPSRC and the University of Sheffield for providing 4 years of funding for my PhD.

My gym buddies aka 'northern swole': Dr John Ormond-Prout aka 'The Naked Swole Rat', Dr Mike 'fingers' Walker, Dr Lewis Williams aka 'Dr Worldwide', Dr Adam Ellis aka 'Elephant Baba.' For getting up at 6am every morning train before work.

Dr Ed Cochrane, who has been my longest standing housemate and has provided a wide array of scents, aromas and drawers full of mysterious liquids. Homelessness would no doubt have had a deleterious effect on my work, for this I must thank Ed.

My family; mother, father and brother (Pauline, Alistair and Calum respectively), for providing my genetic code (Calum not included), a non-traumatic upbringing, love and support (often financial).

List of Abbreviations

Abbreviation	Full Name
4-VBPCD	4-vinylbenzylpyrrolecarbodithioate
BS-IPN	Branched semi-interpenetrating polymer network
COOH	Carboxylic acid
DEGDA	Dithylene glycol diacrylate
ECM	Extracellular matrix
EGDA	Ethylene glycol diacrylate
ESI	Electrospray Ionisation
FDA	Food and Drug Administration
GPC	Gel Permeation Chromatography
HA	Hyaluronic acid
HB-PNIPAM	Highly branched poly(N-isopropyl acrylamide)
HB-PNIPAM-COOH	Acid ended highly branched poly(N-isopropyl acrylamide
HMPP	2-hydroxy-2-methyl-1-phenyl-1-propanone
HPLC	High pressure liquid chromatography
LCST	Lower critical solution temperature
MADIX	Macromolecular design via the interchange of xanthates
NB	Nile Blue
MTT assay	Assay for cell metabolic rate using 3-(4,5-dimethylthiazol-2-yl)-2,5-diphenyltetrazolium bromide
NMR	Nuclear Magnetic Resonance
NVP	N-vinyl pyrrolidone
PAA	Poly(acrylic acid)
PCL	Poly(caprolactone)
PEG	Poly(ethylene glycol)
PGA	Poly(glycolic acid)
PLA	Poly(lactic acid)
PLGA	Poly(lactic acid-co-glycolic acid)
PNIPAM	Poly(N-isopropyl acrylamide)
PTMC	Poly(trimethylene carbonate)
PVP	Poly(vinyl pyrrolidone
RAFT	reversible Addition Fragmentation Chain Transfer
SEC	Size Exclusion Chromatography
S-IPN	Semi-interpenetrating polymer network
TFA	Trifluoroacetic acid
TIPS	Triisopropylsilane
TMC	Trimethylene carbonate
Vanc	Vancomycin
X-PEG	Crosslinked poly(ethylene glycol)
X-PVP	Crosslinked poly(vinyl pyrrolidone)
X-TMC	Crosslinked poly(trimethylene carbonate)

Thesis Abstract

In these projects highly branched poly(*N*-isopropylacrylamide) (HB-PNIPAM) have been functionalised with peptides or bioactive molecules to control cell behaviour using polymers in solution and immobilised within crosslinked membranes.

A set of HB-PNIPAM polymers have been synthesised, with varying feed ratios of NIPAM to 4-vinylbenzyl pyrrolecarbodithioate (4-VBPCD). This had a significant effect on the degree of branching, and influenced properties of the polymers such as, the number of acid ends per unit mass, the number of pyrrole ends per unit mass, molecular weight distributions and the lower critical solution temperature (LCST). These properties were thoroughly investigated by nuclear magnetic resonance (NMR), solution cell differential scanning calorimetry (VP-DSC), gel permeation chromatography (GPC), ultra violet (UV) spectroscopy and fluorescence spectroscopy. The bimodal distributions of the molecular weights for these polymers were analysed using the traditional means but also by an alternative method, which should only be used for non-Gaussian distributions. This alternative method was based on the median and quartiles of the distribution and thus takes into account the whole distribution. Evidence for a core shell morphology of the polymer particles has been elucidated by using a fluorescent dye dissolved within the polymer core.

The highly branched polymers have been functionalised with cell adhesive peptide sequences and used to lift cells from tissue culture plastic before redepositing them into new cell culture wells. This is made possible by affecting the availability of the cell adhesive peptide for cell binding via the LCST of the polymer. These polymers were not as efficient as Trypsin when transferring cells. However, a non-enzymatic method for passaging cells may by favourable for sensitive cell types.

Branched semi-Interpenetrating polymer networks (BS-IPNs) have been synthesised from the peptide functional HB-PNIPAM polymers and polymer matrices based on PEG and PVP. Changing the concentration of the HB-PNIPAM-GRGDS has been shown to influence the adhesion and proliferation of cells in culture. It is suggested that the improvement in adhesion and proliferation of cultured cells on these materials could lead to the development of biomaterials with improved biological properties. The materials have been fabricated by microstereolithography to produce tube type structures. These could be used

in the area of peripheral nerve repair. However, these materials could be suitable for a range of other biomaterials.

A biodegradeable monomer system, based on PTMC, has been developed. Testing has shown the relationship between the molecular weight of the prepolymers used and the mechanical properties of the resulting crosslinked polymer. BS-IPNs were formed with the added HB-PNIPAM-GRGDS additive. This was shown to have a positive effect on the behaviour of cells cultured *in vitro.*

The HB-PNIPAM polymers have been end functionalised with the antibiotic vancomycin and the solvatochromic dye Nile Blue. This produced a molecule which could bind to bacteria. It was hoped that the binding of the bacteria would trigger the coil to globule transition which would give rise to a colour change from the Nile Blue. However, the position of the dye on the polymer chain end meant that this colour change was not observed as the environment of the dye does not change upon coil collapse.

1. Introduction

1.1 Tissue Engineering

Tissue engineering has been described by Langer and Vacanti as "An interdisciplinary field that applies the principles of engineering and life sciences toward the development of biological substitutes that restore, maintain, or improve tissue function or a whole organ."[1]

The potential impact of this could have great implications. Further research into engineered tissues could reduce the need for organ donors by repairing damaged tissues or organs or even replacing them with synthetic systems. Using tissue engineered models could greatly accelerate the testing of new drugs allowing better treatment of patients.[2]

In order to carry out tissue engineering and tissue regeneration structural support is often required in the damaged area. These materials are known as biomaterials. Their job is to provide support to an area and often to allow cell ingrowth eventually leading to normal or improved function of the affected area. Functional synthetic polymeric biomaterials will be the focus of this project, but other alternatives include processed natural polymers and decellularised matrices of human or animal tissue. Although these materials have been shown to be highly biocompatible, produce low inflammatory response and be resorbed by the body, there are serious concerns with batch-to-batch variability. For decellularised matrixes, there are ethical concerns and a limited supply of mammalian tissue from which matrixes can be obtained.

1.1.1 Biomaterials

Modern polymer chemistry can allow a virtually unlimited number of polymer systems to be synthesised from existing monomers and new monomers being synthesised all of the time. These polymer systems can be tailored to fit the properties required to replicate natural tissues to restore functionality. It is often the case that the biomaterial is not required permanently. In this case it is advantageous for the material to fulfil its duty and to degrade and be resorbed and excreted by the body.

There are two main groups of polymers used in biomaterials; these are naturally derived polymers and synthetic polymers. A great deal of research into natural polymers focuses on collagen. Collagen has a 'rope' type structure made from three peptide chains. There are many different types of collagen, and it is the most abundant material in mammalian tissues.[3] This important structural polymer is a common component of the extra cellular matrix where it provides support and structure for cells to grow.[4] The uses of collagen within the body include strengthening tendons, forming sheets that provide support to skin and organs and forming the main constituent of bone and teeth to which minerals such as hydroxyapatite are added.

Hyaluronic acid, Alginate and Chitosan are also very commonly used natural polymers and all three are based on linear polysaccharides. Hyaluronic acid is a glycosaminoglycan polymer, made from alternating units of D-glucuronic acid and N-acetyl-D-glucosamine,[5] alginate is a copolymer made from β-D-mannuronic acid and α-L-guluronic acid [6] and chitosan is made from N-acetyl-D-glucosamine and D-glucosamine.[7] These natural polymers have found many uses as biomaterials and have been used to form composite materials containing natural and synthetic polymers. The blending of natural and synthetic polymers can be used to give materials with good mechanical properties and biocompatibility compared to the isolated constituent parts.[8] These composite materials or polymer blends have been called biosynthetic or bioartificial materials.[8] The idea of blending polymeric materials to create a composite material with improved properties has become very important in this project. Branched semi-interpenetrating polymer networks (BS-IPNs) will be used as a platform to introduce functionalities to hydrogel systems.

Although natural polymers have advantages such as resorbability and often low immune response, they do have drawbacks. There are serious issues with the batch-to-batch reproducibility of natural polymers and thus problems with reproducibility of results with their use. Furthermore, there are ethics based problems with the use of polymers from human and animal tissues and a limited supply of raw material from which polymer can be extracted. In some cases there may also be a threat of transmission of disease from the donor to the patient. Synthetic polymers suffer from none of the above drawbacks and they will be the focus of this work.

There are examples of biomaterials which have been in used routinely for many years.[9] For tissue engineering of bone these include; poly(methyl methacrylate) which is used as bone cement[10] and poly(glycolic-co-lactic acid) which is used in plates and screws used in bone fixation.[11] Many polymer systems are used in the field of drug delivery. Many polymers such as poly(ethylene glycol), poly(N-*iso*propylacrylamide) and poly(acrylic acid) have been used to improve targeting of drugs by triggered release. [12-14] In ophthalmology poly(vinyl alcohol) and poly(hydroxyethyl methacrylate) have been used as soft contact lenses for many years.[15-17]

For the design of synthetic biomaterials one of the most important considerations is biocompatibility. If a biomaterial is attacked or encapsulated by the body it will cause severe problems and rejection. It is therefore important that a biomaterial does not cause a strong immune response. One such group of materials is hydrogels, which often have low inflammatory response and can be functionalised by several strategies to help support cellular adhesion and proliferation

1.1.2 Hydrogels

A hydrogel is a three dimensional network of polymer chains crosslinked to form an insoluble polymer matrix. Although insoluble the polymer can be swollen by water (or other solvents), and can often contain very high weight percentages of water. Hydrogels are usually soft and elastic materials but work with synthetic polymers has developed some much tougher variants.[18-19] Hydrogels often have good biocompatibility,[20] do not cause an inflammatory response[21] and have easily adjustable permeability to oxygen and nutrients.[22] These properties make hydrogels ideal candidates for tissue engineering of soft tissues.

For biomaterials three areas have been identified for hydrogel application:

1. Space filling agents.[23]
2. Bioactive molecule delivery.[23]
3. Cell and tissue delivery.[23]

The useful and easily tailored properties of hydrogels has resulted in their widespread use in many medical applications. They are often used in controlled release of drugs,[24] growth

factors,[25] or other bioactive factors such as proteins or DNA.[26-27] They can be fine-tuned to give a constant and continuous release of the agent over extended time periods. They are well suited to this role as the rate of release of the specific molecule can be controlled by tailoring properties such as swelling, crosslink density and rate of degradation. Correct application can allow bioactive molecules to be incorporated into the scaffold which can degrade over time slowly releasing a consistent concentration of drug or other bioactive molecule. [23, 28]

Hydrogels are also often used in filling applications, for cosmetic tissue augmentation.[29] They are selected for filler applications because of their low inflammatory response. Although, these polymers generally have a low inflammatory response introducing a non-degradable polymer system to the body indefinitely may eventually lead to complications.[30] Hydrogels may be seen as foreign bodies thus triggering an immune response, resulting in formation of inflammatory nodules at injection sites.[31]

Injectable hydrogels are used as a vehicle for cell delivery and have been used for delivery of many cell types for specific tissue engineering applications. These include (but are not limited to): delivery of chondrocytes for regeneration of cartridge,[32] delivery of stem cells for retinal regeneration[33] and complex composite polymer systems including cells and growth factors to promote differentiation and proliferation of specific cell types.[34] The properties of hydrogels can also be adjusted so that they mimic the environment of soft tissues. This has made them popular materials for regeneration of a multitude of soft tissues such as cartilage, bone, fat, liver, neurones and vascular structures.[28, 35]

There are a variety of synthetic and naturally derived materials which are commonly used in tissue engineering. Polymers derived from natural sources have been used as they have similar properties to polymers of the ECM. Whereas synthetic systems have the advantage that the chemistry is controlled and reproducible.[23]

The high hydrophillicity and water content of hydrogels renders them ’non-fouling’. Therefore extracellular matrix proteins which regulate cellular adhesion cannot bind to the hydrogel.[36] Thus, hydrogels are often non-cell-adhesive.[37] This can be an advantage in some applications where cell adhesion would be disastrous. For example, cellular adhesion on contact lenses or barriers to post-operative adhesion would cause major problems. In other applications where hydrogel systems need to support cell adhesion, proliferation and

migration, cell adhesive moieties must be included. Some strategies to improve cellular adhesion to non-cell-adhesive hydrogels include;[38] inclusion of hydrophobic moieties,[39] inclusion of acid or amine surface functionalities, [38, 40] surface modification with extra cellular matrix proteins such as fibronectin, vitronectin and laminin [41] or inclusion of cell adhesive peptides.[37, 42-44] The idea of introducing cell adhesive peptides into a hydrogel system will become increasingly important in the projects undertaken. There are many strategies for introducing cell adhesive peptides, and a new method of using a peptide functional highly branched polymer to create an interpenetrating polymer network will be used.

1.1.3 Cellular Adhesion

Cellular adhesion is mediated by extra cellular matrix proteins such as fibronectin and vitronectin and the corresponding cell surface receptors, known as integrins. The action of these integrins can be replicated by the use of much smaller peptide sequences which can be derived from the active site of a protein. For example the arginine-glycine-aspartic acid (RGD) sequence, which mimics the fibronectin extracellular matrix protein, can improve cellular adhesion when attached to a surface. This peptide sequence behaves similarly to fibronectin, allowing cell surface integrins to attach so cells can spread grow and migrate normally. As well as RGD containing peptides, there are many other non-RGD containing sequences that can be used to control cell adhesion. These include; LDV, REDV, YIGSR, PDSGR and VTXG.[45] These peptides can bind different extra cellular matrix proteins such as fibronectin, virtonectin, laminin A/B1/B2, collagen I and thrombospodin. However, in this project the focus will be on RGD sequences, which usually bind fibronectin or vitronectin receptors most strongly.

1.1.3.1 RGD Containing Sequences

The general structure of the RGD peptide sequence is shown in Figure 1.1. Flanking amino acid groups can be added to the minimum sequence (RGD) to improve binding affinity to specific receptors or selectivity to a specific cell surface integrin.

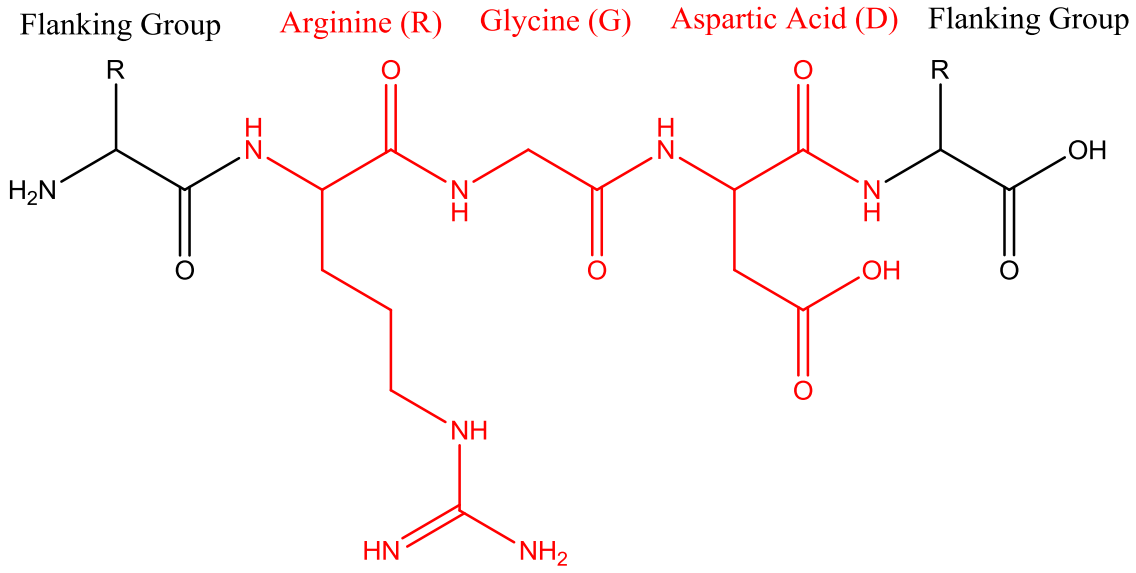

Figure 1.1 - General structure of RGD sequence with flanking amino acid groups. RGD shown in red with flanking residues shown in black.

Typically, the binding interaction of RGD containing sequences is assessed by lifting adherent cells from coatings of fibronectin and vitronectin using the free peptide in solution.[46-47] The peptide competes for these binding sites, causing the cells to detach from the substrate.

The strength of this interaction relies on two competing factors; the non-covalent interactions of the peptide chain with the receptor and the loss of entropy upon binding. This can be affected by altering the RGD flanking residues and thus the orientation of the peptide. Addition and alteration of flanking groups has been shown to have a positive effect on the binding affinity of peptides to fibronectin in the order GRGDSP>RGDS>RGD-NH2>RGD.[48-49] GRGDSP was the most effective of the peptide sequences studied whereas the minimum RGD sequence was shown to lift very few cells from a fibronectin coated surface. It was also shown that the selectivity of the binding can be altered by the flanking groups as GRGDSPC and GRGDNPC were shown to be active on coatings of vitronectin as well as the fibronectin.

The flanking groups can cause changes in the conformation of the peptide sequence.[50] These conformational changes present the peptide functionality in differing orientations, which can yield not only a higher binding affinity, but also highly specific binding interactions for various ECM proteins.

Conformational effects have been demonstrated particularly well for cyclic peptides, which have been shown to have improved binding affinity when compared to their linear analogues. This has been exhibited with peptide immobilised on a surface,[51-52] and in competitive binding to detach cells from a surface.[53] Work by Hiromichi *et al.* showed that cyclo(GRGDSP) > cyclo(GRGDS) > cyclo(RGDSP) and that cyclo(GRGDSP) was twenty times more effective than its linear analogue. Research has shown that electrostatic interactions and spatial arrangement play a large role in binding affinity.[54] Binding can also be highly specific for one protein over another, [55] Pierschabacher *et al.* synthesised a cyclic GRGDSP peptide which showed almost no interaction with fibronectin receptors but a strong binding affinity to the vitronectin receptor.

Simply adding a peptide to a system to improve cellular adhesion is often not enough. An accurate measurement of the surface concentration of peptide available for binding is needed to predict cellular behaviours. Much of the experimental work in peptide densities comes from studies by Hubbell. It was shown that a density of 0.1 fmol cm^{-1} (440 nm spacing) allowed adhesion of fibroblasts but not spreading, 1 fmol cm^{-1} produced higher spreading of fibroblasts and concentrations of 10 fmol cm^{-1} and above (140 nm spacing) caused focal contact and stress fiber formation yielding cells with a normal actin cytoskeleton.[56] These samples showed that the RGD sequence was enough to allow morphologically complete cell spreading. Additionally, concentrations of RGD which are too low have been shown to have little effect on adhesion.[57] Whereas high concentrations may reduce migration rates.[58]

It has been demonstrated that the density of the RGD sequence will directly affect the rate of migration of cells.[58] The rate of migration of cells has been shown practically and experimentally to affect the rate of proliferation.[59-60]These factors will become increasingly important in the design of biocompatible medical devices which support cell adhesion and promote ingrowth of cells.

1.1.4 Peptide Synthesis

There are two methods for peptide synthesis, the first is solution phase peptide synthesis where all of the reagents are in solution. This method can cause a number of problems with isolation and separation of products, which makes the synthesis of longer peptide chains

problematic. Peptide synthesis was revolutionised by R.B. Merrifield in 1963 when solid phase peptide synthesis was first reported.[61] The first amino acid in the chain is attached to an insoluble polymeric resin. The remaining amino acids are then deprotected and added sequentially to the growing peptide chain. Once formed the complete peptide sequences are removed from the resin by cleavage with a Tetrafluoroacetic acid (TFA) cleavage cocktail. This increases the speed of the synthesis by removing the need for difficult purification procedures. Excess reagents and byproducts can now be washed away leaving the peptide bound to the solid polymeric support.[61-62]

During peptide synthesis or modification of peptides, protection of the nucleophilic α-amino group is often required. Unwanted side reactions can be prevented by using large sterically bulky groups to screen the nucleophilicity of the amino group. There are several requirements for a protecting group. Firstly, protecting groups should not introduce any further complications to the reaction such as unwanted side reactions or interactions. They must also remain bound to the α-amino group for the duration of the reactions but should be removed with relative ease when necessary. Without the aid of the protecting groups these syntheses would be made impossible by many dominating side reactions. The final requirement is that the chirality of the α-carbon should not be affected by the presence of these groups.[62]

There are many protecting groups for the α-amino group which have been developed the most common of which are t-butoxycarbonyl (^{t}BOC) and 9-flourenylmethoxycarbonyl (Fmoc). The structures of these protectiong groups is shown in Figure 1.2.

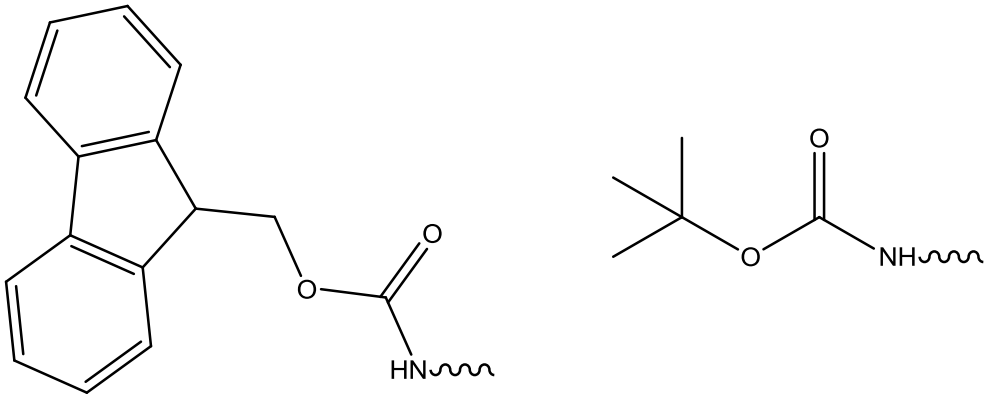

Fmoc ^{t}BOC

Figure 1.2 - Structures of Fmoc and tBOC protecting groups attached to N-terminus of amino acid/peptide

1.1.5 Peptide Modification Strategies

There are many examples in the literature of peptide sequences being physically bound (adsorbed) to the substrate rather than chemically bound by a covalent bond. These coating methods often use concentration dependent deposition of a peptide in solution.[63] There are obvious problems that can be caused by this passive method of peptide inclusion; firstly availability of the peptide sequence can be reduced as the electrostatic interactions used to bind to the sequences to the substrate can change the conformation and reduce binding affinity to the target.[64] The second problem is leaching of the sequence from the surface. There are no covalent bonds holding the peptide to the surface and this will lead to a time dependent loss of the adsorbed peptide functionality into the solution phase.[65] This will lead to a reduction in proliferation over time caused by the reduction in adsorbed binding sites. [66] Surface desorption will quickly reduce the benefit of using a peptide sequence in this way. The increased concentration of peptide in solution could be detrimental to cell adhesion due to competitive binding. These factors rule out this mode of binding for this project. For this application a chemical bond between the polymer and peptide sequence will be created. There are numerous methods used to create these bonds, the most commonly used are; coupling to carboxylic acids[44] and amide[67], using a coupling agent (such as EDC) with a protected peptide to avoid unwanted side reactions between peptides or the formation of an activated group to which the peptide is added. This technique is

usually favoured as it negates the formation of oligo peptides, which can be problematic in the 'one step' EDC reaction. Thus, N-hydroxysuccinimide (NHS) is used with (EDC) or (DCC) to produce a succinimide ester which can be stored and reacted with a peptide sequence in a second step at a later date.[68-69] This will be the most appropriate technique for coupling peptides to the highly branched polymers used in this project. The aim of this work is to optimise the peptide functionality so that the polymers could then be used to create interpenetrating polymer networks which add functionality to medical devices.

1.1.6 PNIPAM in Detachment of Cell Sheets

PNIPAM surfaces can be used to culture cells and then release them as an intact sheet using the thermal transition of the polymer.[70] Above the LCST, the cells can adhere to a 'hydrophobic' surface. When cooled there is a large change in the swelling of the substrate, which has a huge effect on the dimensions and water content. Most of the volume of the substrate is now water, so that there is minimal surface for the cell sheet to adhere to. Using this method, whole cell sheets with intact extra cellular matrix can be detached.

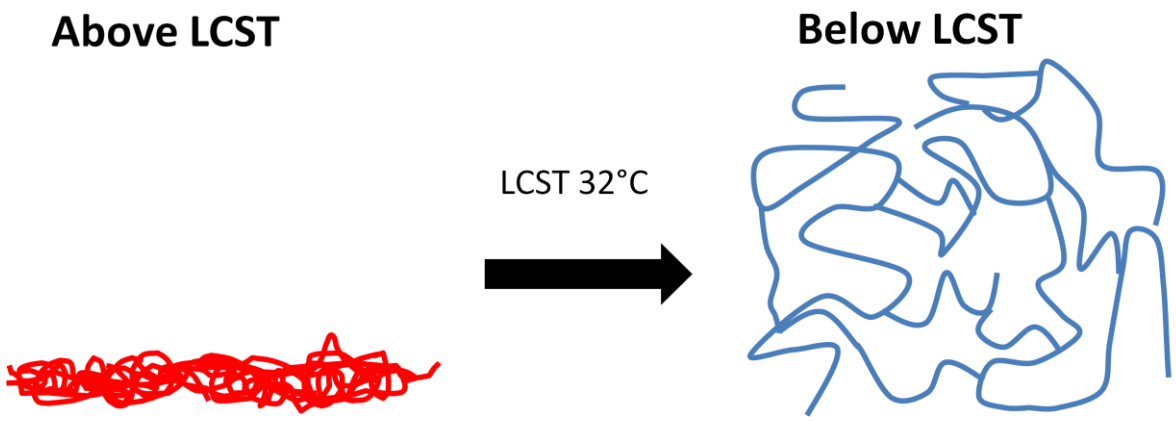

Figure 1.3 – A diagram showing the structure of PNIPAM hydrogel above and below LCST.

The advantages of using this low temperature detachment technique over mechanical scraping or enzymatic digestion, are that an intact cell sheet can be removed without damage to the ECM or cells.[71-72] Canavan *et al.* have shown by ToF-SIMS, that fibronectin and vitronectin are generally removed with the cell sheet, and that only trace quantities remain on the culture surface.[71-72] It has also been shown by XPS and ToF-

SIMS, that when cells are cultured on substrates coated with fibronectin and vitronectin these ECM proteins reside within the cell sheet.

Although fibronectin and vitronectin have been shown to detach with the cell sheet, it has also been shown by the Canavan *et al.* that the surfaces remaining after cell detachment are rich in glycine and proline.[73] It was concluded that the presence of collagen explained this.

Evidence for the mechanism of this cell sheet detachment has been provided by Okano *et al.* Cell sheets were detached from PNIPAM surfaces by lowering the temperature.[74] The rounded morphologies of cells observed after detachment prompted the suggestion of a two phase detachment process. The change in swelling PNIPAM starts the detachment, followed by a cellular metabolic process which allows full cell sheet detachment. This claim was substantiated by using a lower temperature or sodium azide, which reduce metabolic activity. This reduced the metabolic activity inhibited the detachment of the sheet. Counter claims have been made to this proposal,[75] that state that very low detachment temperatures (4°C) favour the fastest cell sheet detachment rates. However, differences in experimental design make it difficult to give a definitive answer as to what is the best approach.

Improvements to these systems have focussed on attachment and detachment of the cell sheets. Improvements in the rate of detachment have been made by copolymerising NIPAM with 2-carboxyisopropylacrylamide,[76] increasing the porosity of the membranes,[77] altering the density of polymer chains at the surface,[78] and altering the metabolic rate of cells by using low temperature and serum free media.[75] Improvements in the attachment of PNIPAM surfaces have often been observed when implemented RGD based peptide sequences were grafted to the polymer.[44, 79]

1.1.7 Cell Lifting Using Peptide Functional PNIPAM Particles

The current method for detaching cells in culture uses trypsin to digest the ECM, which can damage adhesion receptors. [80] PNIPAM hydrogels have been used to create temperature responsive sheets for cell growth which are cell adhesive above and non-cell adhesive below the LCST.[81] These can be used to culture then detach an intact cell sheet. PNIPAM hydrogels with cell adhesive properties due to the inclusion of a cell adhesive GRGDSP

peptide have been investigated.[82] It was found that cell migration rate was increased by inclusion of the peptide up to a concentration of 1.5 pmol cm^{-2} where it reached a plateau. Further increases in the surface concentration (up to 2 pmol cm^{-2}) of peptide caused a decrease in cell mobility. Thermally responsive sheets circumvent the use of trypsin and centrifuging of cells, which can have adverse effects on some cell types. Importantly, PNIPAM has been shown not to be cytotoxic; for example Cooperstein *et al.* rigorously tested the cytotoxicity of PNIPAM.[83-84] The results showed that PNIPAM was not cytotoxic to endothelial, epithelial, smooth muscle, and fibroblast cells cultured on PNIPAM coated surfaces or with PNIPAM in solution. Differences in the initial rate of proliferation (48 hours assay) of cells on PNIPAM coated surfaces were attributed to poorer cell adhesion to PNIPAM compared to controls.

This aspect of the work aims to build on previous work by Rimmer *et al*, which explored an alternative strategy for cell detachment.[80] Above the LCST, HB-PNIPAM-GRGDS collapsed to a globule and aggregated into sub-micron particles to which cells bond to in preference to TCP. [80, 85] When cooled, polymer particles passed through the LCST and the cells were released. In this extension of that work, the peptide functionality will be optimised.

Figure 1.4 shows the conformation of the polymer above and below its LCST. It has been observed that, above the LCST, these polymers form core shell particles with the hydrophilic peptides as the shell and the globular polymer in the core.[85]

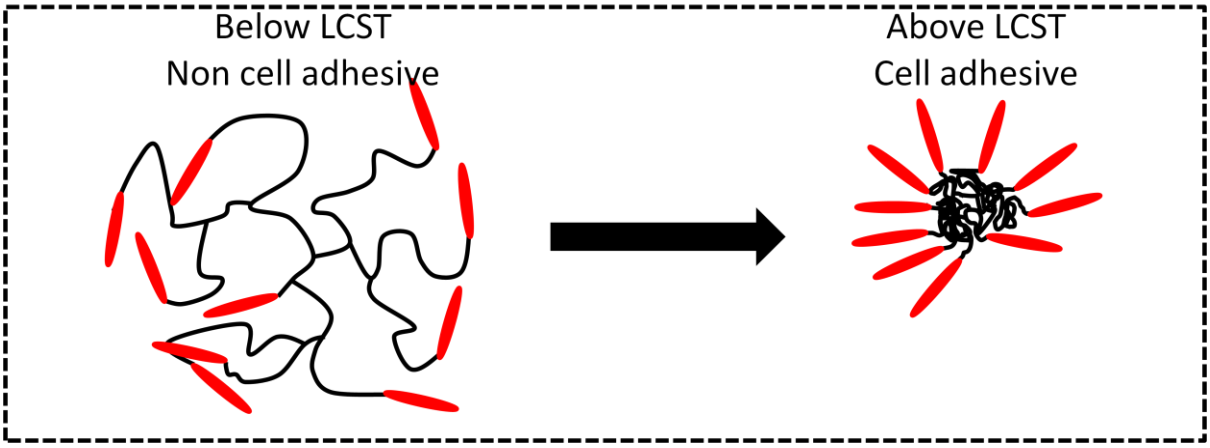

Figure 1.4 – A diagram showing the availability of peptide functionality above and below LCST of the polymer.

This gives a polymer with two distinct states:

1. Below the LCST; the polymer is in the hydrated coil conformation, polymer chains are tangled around the peptide. The peptides are poorly orientated for integrin binding, and the binding affinity of the functional polymer is low.
2. Above the LCST; the polymer is in the dehydrated globular conformation, forming a core with a peptide shell. The peptide is well orientated for integrin binding and the binding affinity of the functional polymer is high.

This change in binding affinity means these polymers can be used to reversibly bind to cells.

1.1.8 Poly(*N*-isopropylacrylamide) PNIPAM

PNIPAM is a temperature responsive polymer with a LCST of around 32°C. The PNIPAM undergoes a phase separation upon heating in aqueous solution. When cooled the dispersion clears to form a single homogeneous phase. It has been shown using acenapthalene labelled systems that a coil collapse mechanism is responsible for this behaviour. Time Resolved Anisotoropy Measurements (TRAMS) have shown a large decrease in segmental mobility at the LCST and a reduced availability of quencher to the label in the collapsed state. [86-87]

The temperature response of PNIPAM can be controlled by several means. Creating copolymers with hydrophilic or hydrophobic monomers will increase or decrease the LCST respectively. Alternatively, control of branching has been shown to have a substantial effect on the LCST. Increasing the degree of branching decreased the LCST but also increased branching produces increased concentrations of end groups. The nature of the end group can have a large effect on the LCST behaviour.[88] RAFT polymerisation can be used to create a pyrrole dithioester ended highly branched poly(N-isporopyl acrylamides). When compared to similar linear PNIPAM there is a reduction in the LCST.[88] It was suggested that this might be due to the aggregation of imidazole end groups because of the hydrophobic influence of the aryl branching point.[89] However, this is an evolving theory which has been revised several times and the aggregation of imidazole and groups in now considered to be incorrect. The current theory is that these polymers form biphasic core-

shell particles with a collapsed globular core and a hydrated open coil shell. The extent of these phases depends upon the degree of branching. [90]

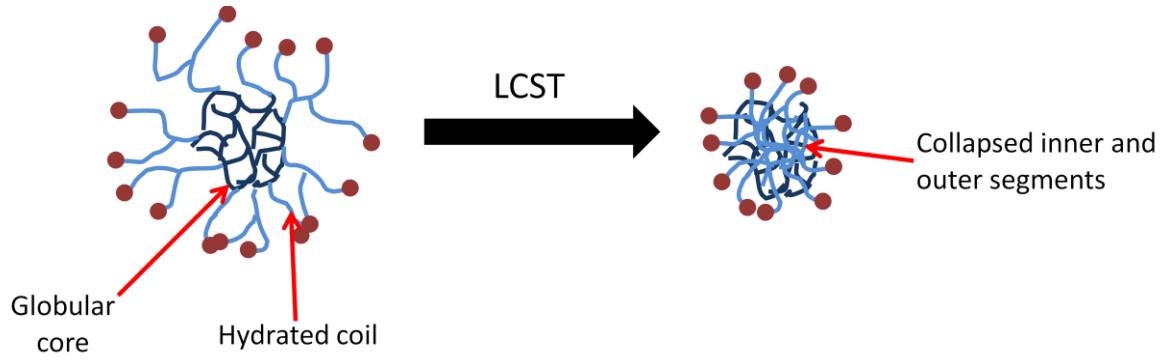

Figure 1.5 – A diagram showing the core shell nature of some HB-PNIPAM formulations.

The fact that PNIPAM shows this tuneable temperature response between the hydrated hydrophilic chain and the collapsed hydrophobic coil has made it attractive for tissue engineering.

Highly branched PNIPAM can also be functionalised with peptides This is a multi-step reaction where the pyrrole dithioate end groups of the Reversible Addition Fragmentation Chain Transfer (RAFT) polymer are replaced to give an acid end group using 4,4'-Azobis(4-cyanovaleric acid) (ACVA). This can then be converted to the succinimide ester which can be converted to a peptide.[80] These polymers go through the same reversible aggregation process as the unfunctionalised RAFT PNIPAM. Above the LCST it forms a stable colloid due to electrostatic repulsions from the polar COOH or peptide (RGD) end groups located at the particle surface. [16, 85]. These particles have been used in the detachment and deposition of cultured cells. Above the LCST the particles form globules with peptides on the outside.[85]

In this state the particles bind to the cell surface integrins of dermal fibroblasts and endothelial cells removing the cells from their substrate. When cooled to room temperature (below the LCST) the polymer releases the cells allowing them to bind to their new substrate. This avoids the need for trypsin and centrifugation during passaging of cells. [80]

Although PNIPAM is often described as existing in a hydrophobic and hydrophilic state it must be remembered that the hydrophobic state is only hydrophobic relative to its hydrophilic state. The water content of NIPAM in the collapsed state is often still very high

thus care should be taken when describing the states of PNIPAM. This is described in detail in the paper Poly(N-Isopropylacrylamide) (PNIPAM) is never hydrophobic by P. Robert.[91]

1.1.9 Free Radical Polymerisation

Free radical polymerisation is a type of chain polymerisation that typically uses unsaturated monomers such as acrylates, methacrylates and vinyl compounds. The polymerisation proceeds via a series of steps outlined in Figure 1.6. These steps will be discussed in further detail.

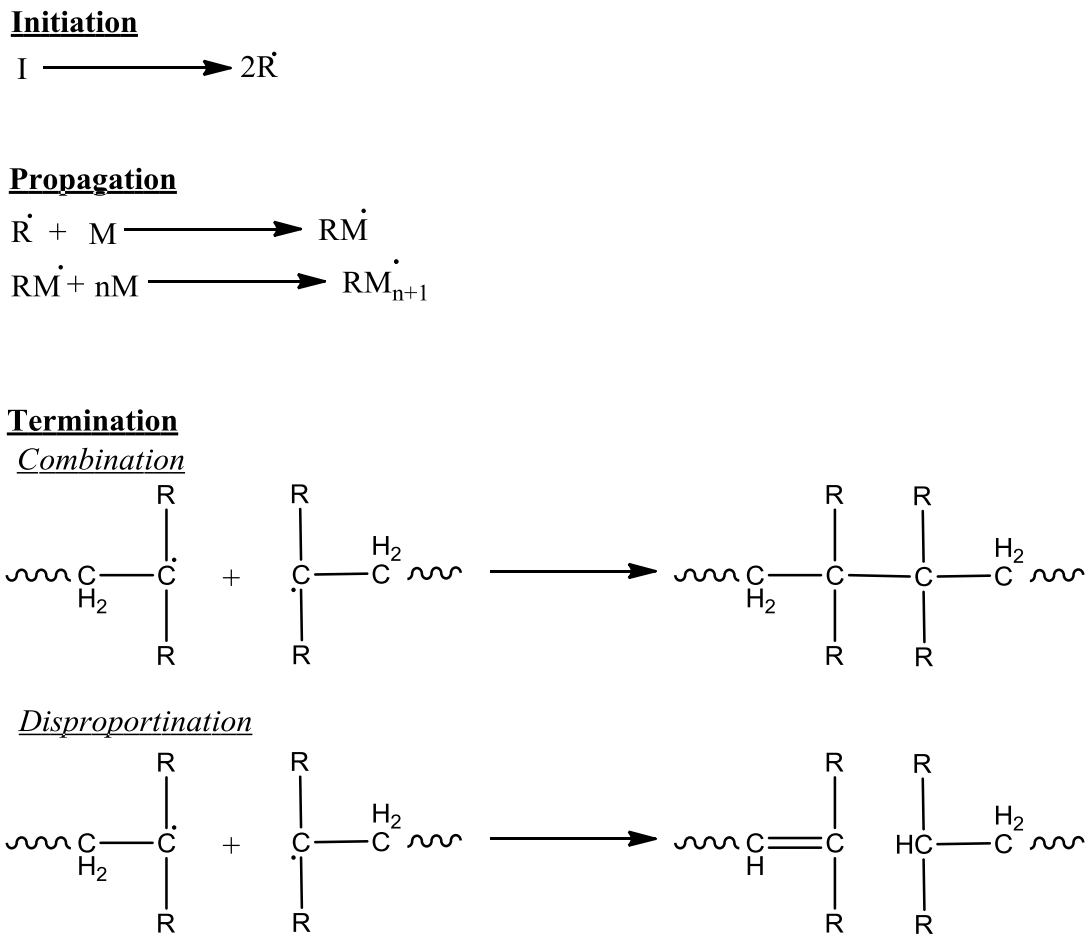

Figure 1.6 - The reactions involved in free radical polymerisation

Initiators for polymerisations are compounds which can undergo homolytic fission to form radicals. Typically this decomposition will occur as a result of thermal or UV irradiation. The example of the initiation reaction shown in Figure 1.6 shows an initiator fragmenting to give two radicals.[92] The homolysis of the initiator can be caused by different stimuli such as

thermolysis, photolysis, redox reactions or the use of ionising radiation. Initiators which decompose by homolysis are termed Norrish type I initiators.[93]

There is another type of initiator, Norrish type II initiators.[93] These work by abstraction of hydrogen from another molecule (a synergist), which is often an amine or a thio. This creates two radicals which can go on to cause polymerisations to occur.

When an initiator molecule decomposed to form the radicals there is an efficiency factor (f), which is a measure of the amount of initiator that goes on to form polymers.[92] This number is always less than 1 as initiator fragments can easily be consumed by unwanted side reactions.

In the propagation step the initiator radical reacts with a monomer unit. The chain then propagates rapidly to give a linear polymer. In radical polymerisation this step will occur very quickly. The rate of polymerisation is limited by the decomposition of the initiator not the addition of monomer to the active radical.

Termination can occur when two radicals come into contact and can proceed *via* two mechanisms, combination and disproportionation. As shown in Figure 1.6 the disproportionation reaction involves a bimolecular interaction between two radicals where one radical abstracts a hydrogen from the other.[92] This results in two terminated molecules one of which is saturated and the other is unsaturated. Hence, a high radical concentration will give to more radical-radical interactions, more termination reactions and a low molecular weight polymer.

Other reactions that can result in a termination are reaction of the propagation polymer chain with an initiator radical, transfer of the active centre (chain transfer) or reaction of the radical with molecular oxygen to give an unreactive peroxy radical.

1.1.9.1 Features of Free Radical Polymerisations

There are several features which are characteristic of free radical polymerisations. There are;

1. A high molar mass polymer is formed immediately. Over the course of the reaction the average polymer molecular weight does not very significantly. Hence, longer reaction times will not result in an increased molecular weight.

2. The concentration of monomer decreases steadily over the reaction time. Hence, longer reaction times result in higher conversion not higher molecular weights.
3. Only the active centre can react with monomer.
4. Increasing the temperature of the reaction will increase the rate of polymerisation but will also increase the rate of termination. This will result in a reduced molecular weight.

1.1.10 Living Polymerisation

A living polymerisation is defined by IUPAC as, "a chain polymerisation from which chain transfer and chain termination are absent."[94] It is generally claimed that this method of polymerisation will give narrow dispersities but can also be used to control the end group functionality of the polymer. Ionic polymerisation methods can be used to remove the termination because the propagating polymer chain is charged and as such will repel other similar chains. This effectively stops termination by combination and disproportionation.

Methods of living radical polymerisation include Atom Transfer Radical Polymerisation (ATRP), Nitroxide mediated living radical polymerisation and Reversible Addition Fragmentation Chain Transfer (RAFT) which will be discussed in detail. The common theme of these methods is that the propagating polymer chains maintain a dormant state most of the time. Thus, reducing the concentration of radical chain ends in solution and reducing the probability of two polymer chains meeting and terminating.

1.1.11 Reversible Addition Fragmentation Chain Transfer (RAFT) Polymerisation

The first reports of chain transfer agents came in the 1970s when they were used for irreversible reactions in organic synthesis.[95] These chain transfer agents were of little use to polymer chemistry at this stage. In the 1980s there were reports or 'potential' reversible transfer agents,[96] although, it wasn't until 1995-1998 when a reversible chain transfer step exhibiting some properties of a living polymerisation was reported by Rizzado at the Commonwealth Scientific and Industrial Research Organisation.[97-98] Researchers in France had developed another approach in parallel. This was called Macromolecular design

via the Interchange of Xanthates (MADIX), and proceeded *via* an almost identical mechanism to the proposed RAFT mechanism.[99] The work from both groups built upon previous work by Zard *et al*. [100]zard

RAFT polymerisation is a mode of polymerisation, which gives some of the characteristics of living polymerisation. This occurs by reducing the concentration of active radicals which lowers the rate of termination by radical radical interaction. This can allow precise control over the polymerisation process, while retaining the versatility of conventional radical polymerisation. RAFT polymerisation has made the synthesis of complex polymer architectures possible by radical polymerisation.[101] What differentiates RAFT polymerisation from other forms of living polymerisation is that it can be done with a wide range of monomers and reaction conditions in a way that will produce polymers of a controlled molecular weight and narrow dispersity.[97]

The generic structure of a RAFT agent used for these radical polymerisations is shown in Figure 1.8. There are many types of thiocarbonyl compounds now in use including thiocarbonates, xanthates and dithiocarbamates.

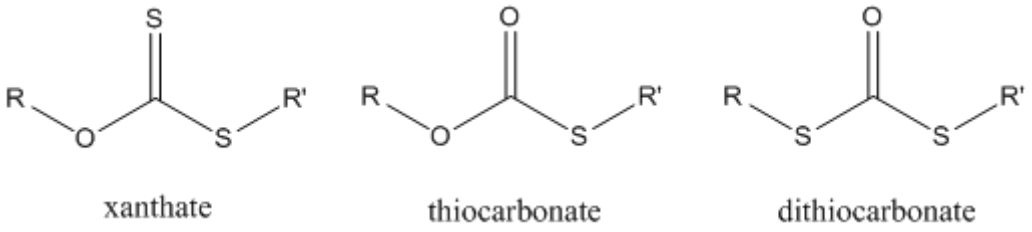

Figure 1.7 - Generic structures of xanthates, thiocarbonates and dithiocarbonates.

The effectiveness of the RAFT agent depends on the monomer being used. This is strongly affected by the radical leaving group R and by Z.[102-104] The generic structure of a RAFT agent is shown in Figure 1.8.

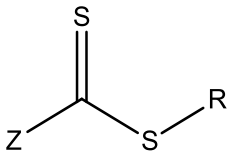

Figure 1.8 - Generic Structure of a RAFT agent

1.1.12 RAFT Mechanism

The fundamental feature of RAFT polymerisation is the addition fragmentation equilibria shown in Figure 1.9.

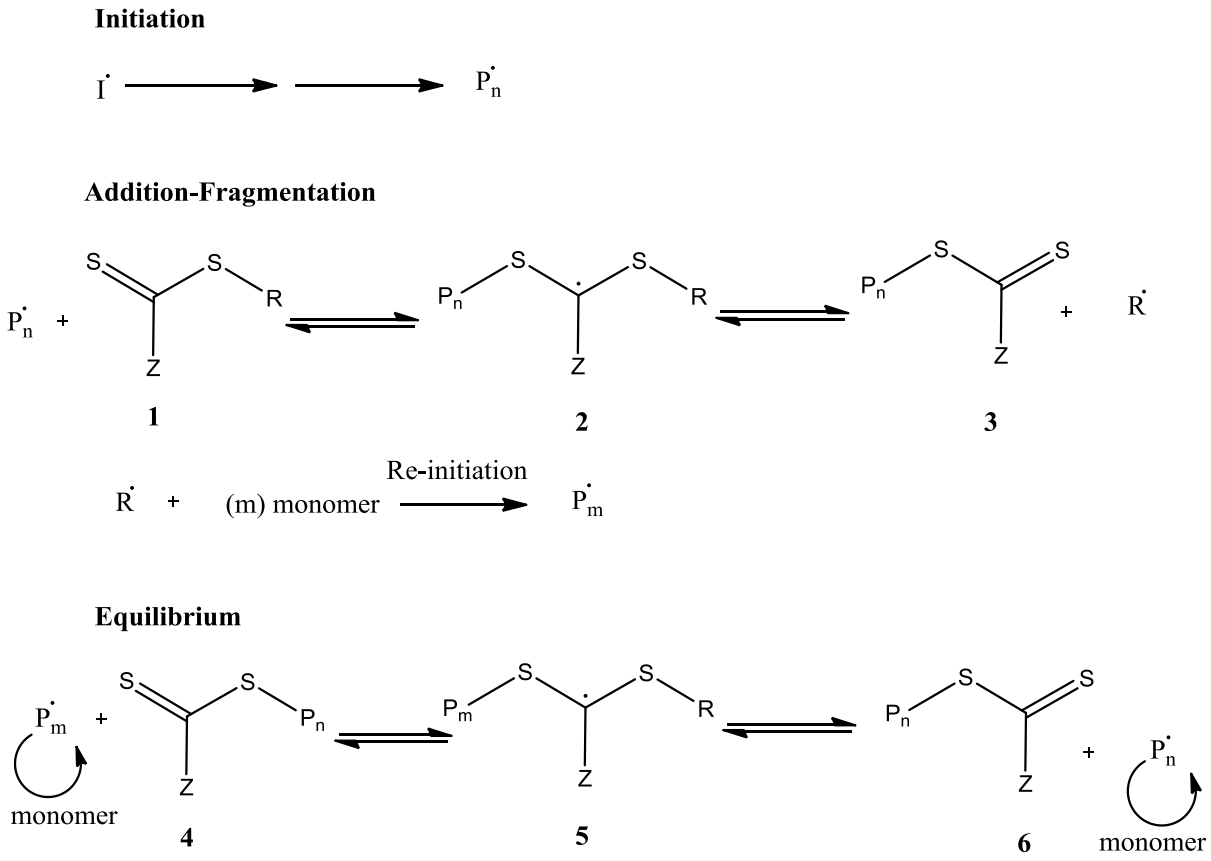

Figure 1.9 - Reaction scheme for RAFT mediated polymerisation[105]

The first step as with all radical polymerisations involves radical production by decomposition of the initiator followed by initiator reaction with monomer to produce a propagating species $P^{\cdot}_{n}$. This species will go on to react with (1) producing (2) which can rapidly fragment producing $R^{\cdot}$ and the polymeric thiocarbonylthio compound (3). $R^{\cdot}$ can then go on to react with monomer to produce a new propagating species $P^{\cdot}_{m}$. A rapid equilibrium between the $P^{\cdot}_{n}$ and $P^{\cdot}_{m}$ means that all chains have an equal probability to grow allowing narrow polydispersity polymers to be obtained. When the polymerisation stops most chains will have the thiocarbonyl chain end groups.[103]

A useful aspect of the RAFT mechanism is that thiocarbonyl groups are maintained at the chain ends of the polymer. This allows the addition of functionality to the polymer chain

ends. By using RAFT agents with carboxylic acid functionality this functionality can be added to the end groups. Two examples of such RAFT agents are shown in Figure 1.10. [106]

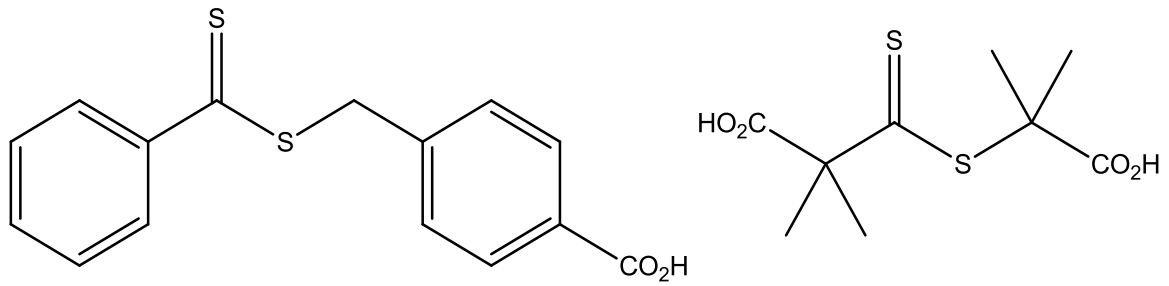

Figure 1.10 – Examples of structures of acid ended RAFT agents

However, the acid functional RAFT derived groups can be removed due to the labile dithioate ester. Therefore it may be difficult to carry out any further chemistry as the RAFT end groups can be readily cleaved.

The labile nature of the RAFT end group does allow modification *via* a 'Perrier' or 'radical bomb' mechanism.[107] A proposed mechanism for the modification of the RAFT end groups is shown in Figure 1.11.[108] A disadvantage of this mechanism is the large quantity of expensive azo initiator that is used to provide the radicals to displace the RAFT groups.

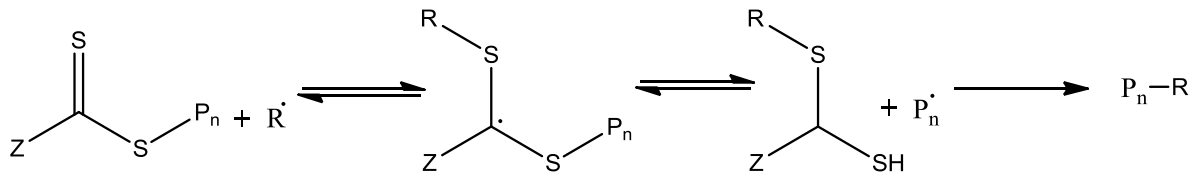

Figure 1.11 – A figure showing the proposed mechanism for the 'Perrier reaction'

A polymerisable RAFT agent containing not only the two subunits R and Z but also a polymerisable double bond shown in Figure 1.12 will form a polymer backbone which contains branch points from which further polymerisations can occur via transfer to the pendant dithioate. Consequentially a highly branched polymer is formed.[105] Functional materials prepared by this type of polymerisation will be the focus of this section and will be used to produce end functional polymers used in the following sections.

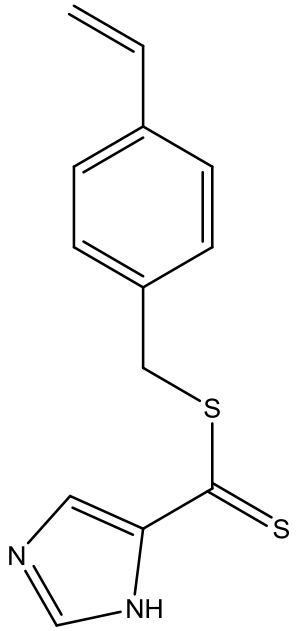

4-vinylbenzyl 1*H*-imidazole-5-carbodithioate

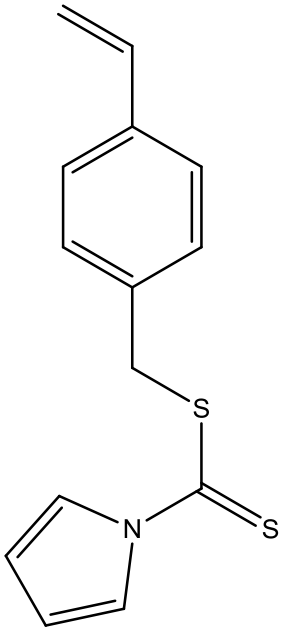

4-vinylbenzyl 1*H*-pyrrole-1-carbodithioate

Figure 1.12 - Branching RAFT agents for producing highly Branched polymers[105]

One of the characteristics of this type of RAFT polymerisation is the requirement for a constant flux of radicals generated by an initiator. This aspect makes the polymerisation very different to other controlled polymerisations including most RAFT polymerisations. A consequence of radicals being formed in this manner is that there is a significant amount of bimolecular termination. Thus, chain ends are functionalised with fragments from the initiator. This could be a problem in the synthesis of block copolymers as continuous initiation can produce homopolymer. However, in the synthesis of branched polymers this becomes a useful way to add functional endgroups.[109]

1.1.13 Lower Critical Solution Temperature (LCST)

The LCST of PNIPAM was first reported by Sarpa *et al.* in 1967. A polymer with a molecular weight of ≈200,000 g mol^{-1} was reported to precipitate from aqueous solution at 31°C.[110] However, a paper by Heskins and Guillet is often credited with the work. [111] Here the cloud point of the polymer is measured which is the most common method used for measuring the LCST. However, there are numerous alternative techniques. Such as DSC, turbidity, FTIR and NMR.

There are several theories which describe the coil to globule transition of PNIPAM: De Gennes's 'n-cluster' model [112] and and Winnik's 'string of pearls' model both of which have been widely adopted and essentially describe a similar process. Both theories describe localised collapse of the polymer coil forming n-clusters/pearls along the length of the coil. The coil to globule transition proceeds *via* aggregation of these clusters to the dehydrated globule. An aspect that is often overlooked in the literature is that the globule is a desolvated state rather than a fully hydrophobic state. Thus, the globular state will still contain significant amounts of water. This is explained in a Paper by P. Robert entitled, "Poly(N-Isopropylacrylamine) (PNIPAM) is never hydrophobic." [91]

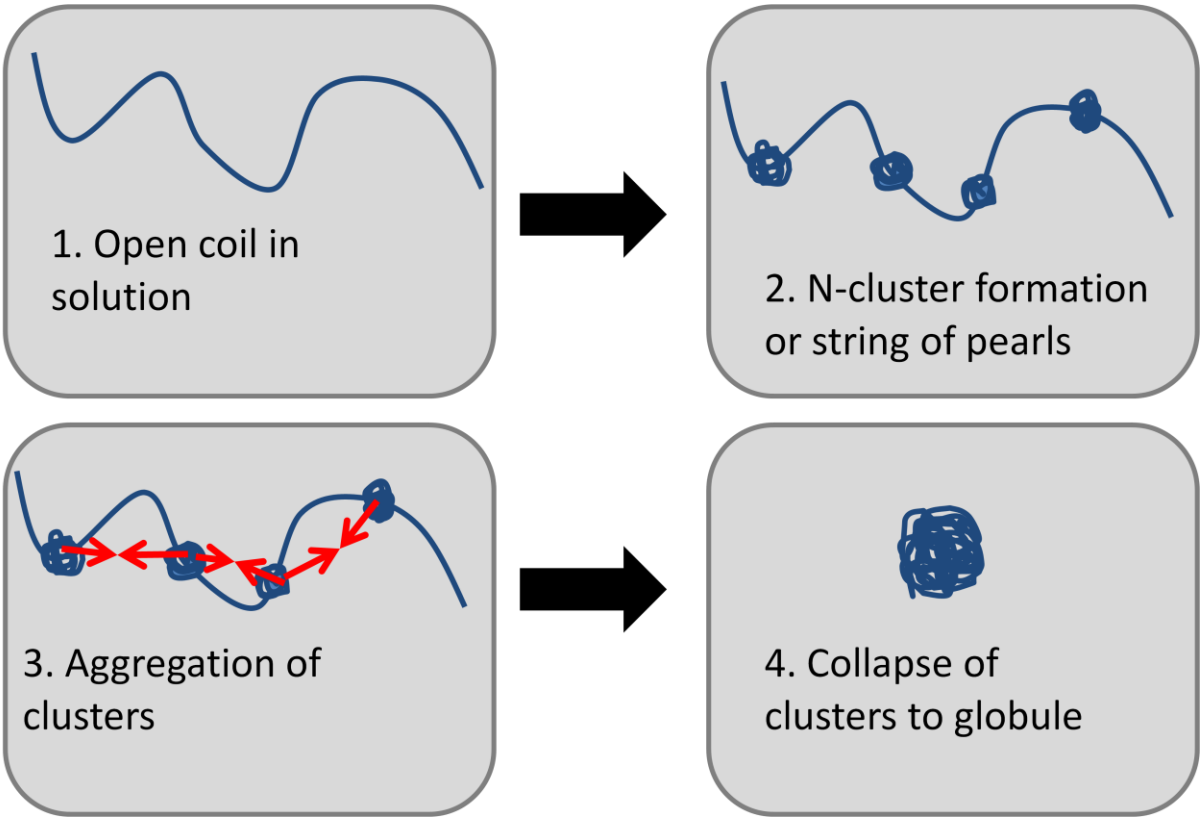

"

Figure 1.13 - Schematic diagram of coil to globule transition via n-cluster or string of pearls formation.

The LCST behaviour of PNIPAM can be explained by considering the Gibbs free energy (Equation 1.1).

$$\Delta G = \Delta H - T\Delta S$$

Equation 1.1

The dissolution of the PNIPAM is driven by the exothermic (negative) enthalpy of H-bond formation with polar amide groups. However, the entropy for the dissolution of the polymer chain into the highly ordered water is negative as water molecules reorganise around hydrophobic polymer chains. At higher temperatures the entropy term becomes dominant. At the LCST there is a switch where the ΔG becomes positive. The unfavourable entropy term becomes more important than the favourable enthalpic term and the polymer comes out of solution. [113]

At higher concentrations of polymer, polymer-polymer aggregates will form resulting in precipitation. Wu *et al.* described an intermediate state in the coil to globule transition when examining single chains in an extremely dilute solution.[114] This intermediate state is split into two parts crumpled coil and molten globule. Giving a total of 4 observable conformational states for Linear PNIPAM (Figure 1.14):L

1. A coil, which exists between θ and 31°C where θ is the temperature at which the polymer acts as ideal chains in a given solvent, here R_h (hydrodynamic radius) = R_g (radius of gyration). [114]
2. Crumpled coil, here the coil collapses slightly to form a crumpled coil. [114]
3. Molten globule, Each chain has collapsed into a globule, but there is a rough surface made from many chain loops.[114] Also observed in protein folding.[115].
4. Globule, R_g/R_h reaches a minimum value showing that the globule has fully collapsed.[114]

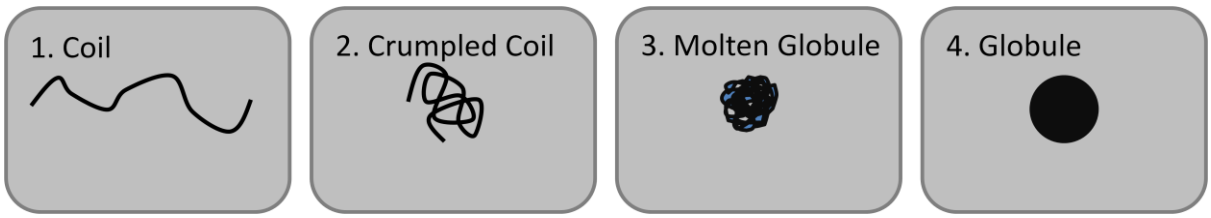

Figure 1.14 – A figure showing the four intermediate states of coil collapse described by Wu *et al.*[114]

1.1.14 Use of LCST in Tissue Engineering

The physiologically relevant LCST of PNIPAM (31°C), and its non-cytotoxic nature[84] has made it a good candidate for applications in the field of tissue engineering. PNIPAM surfaces have been used to culture cells above 37°C. which upon cooling releases the cells.[71-72] This can allow an intact cell sheet to be fully detached from a surface. This technology has multiple applications in tissue engineering of cell sheets.

Various modifications have been made to optimise these systems to specific tasks; copolymerisation of NIPAM with 2-carboxyisopropylacrylamide to increase the rate of cell detachment;[76] increasing the porosity of the membranes;[77] and altering the density of polymer chains adhered to a well plate.[78] This was shown to change the rate of cell sheet detachment and alter the detachment temperature and serum concentration within the media. Both of which effect the rate of detachment from these surface by influencing the metabolic rate of the cells.[75]

Biodegradable variants of PNIPAM based hydrogel scaffolds have been synthesised by including with 2-methylene-1,3-dioxepane and polycaprolactone dimethacrylate prepolymer in the polymerisation.[116] These hydrogels allow penetration of cells, are fully degradable and thermo responsive making them an attractive prospect for tissue engineering.

The thermal transition of loosely crosslinked PNIPAM hydrogels gives a change in viscosity allowing an injectable solution to stiffen above its LCST.[117-118] These polymers have had wide ranging applications in tissue engineering and they have removed the need for an *in vitro* polymerisation. Variations on this theme have produced similar polymers with degradable crosslinks.[119] This technology removes the need for post-operative surgery to remove the device.

The coil to globule transition of PNIPAM is increasingly adopted as a tool for sensing devices.[120-121] There have been significant advances in the binding of bacteria. This has become important as a result of recent problems with antibiotic resistance.[122-124] The development of new strategies to deal with bacterial infection is of key importance. Aggressive antibacterial agents such as silver compounds have been used as an alternative. However, they exhibit high cytotoxity as well as antibacterial properties and as a result will increase wound healing times.[125]

Linear PNIPAM with pendant glucose functionality, has been shown to interact with *Eschericha coli* below the LCST.[126-127] This interaction did not occur above the LCST, as the globule conformation buried the sugars within the coil preventing the interaction. Seemingly contradictory evidence has been shown where the functional polymer will only bind with its target above the LCST.[128-129] It is apparent from these results that the binding site can be either shielded or exposed by the globular conformation. This results in opposing data for the on/off binding response with the thermal transition

Branched PNIPAM polymers functionalised with antibiotics have been shown to reversibly to bind *S.aureus* bacteria above the LCST.[130] Binding of bacteria also modifies the LCST of the polymer, so the polymer must be cooled to a lower temperature to release these bacteria. This implies that the bacteria binding could drive the polymer through the LCST. These polymers have been used to remove bacteria as an insoluble polymer/bacteria complex from a tissue engineered human skin model.

1.1.15 Solvatochromic Dyes

The term solvatochromism was introduced by Hantz-Schlater,[131] it has since been claimed that these compounds would be termed perichromic, to account for their behaviour on solids, gasses and surfaces.[132] In solvatochromism the UV/Vis/IR spectrum of a compound in solution can be affected by the polarity of the solvent used. There are several types of solvatochromism which are characterised by an increase or decrease in intensity or a red or blue shift.[133] The different types of solvatochromism are shown in Figure 1.15. They are an increase or decrease in intensity, termed hyperchromism and hyposhromism respectively. Or an increase or decrease in wavelength, termed hypsochromism or bathochromism respectively.

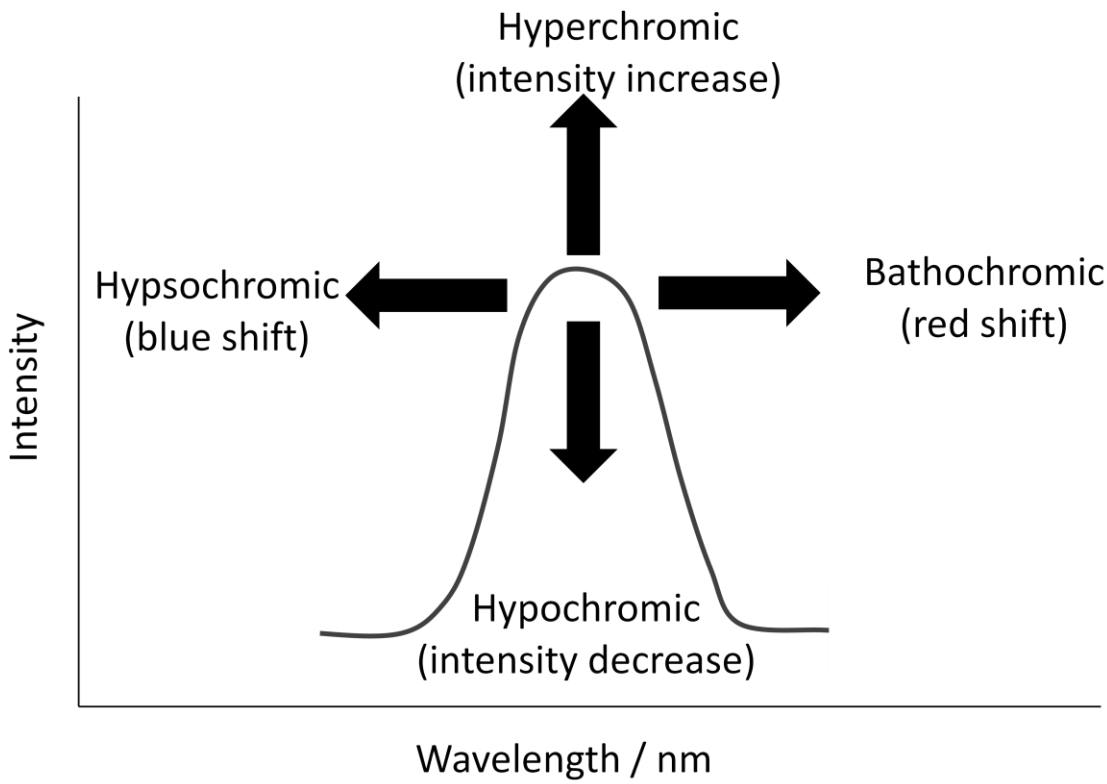

Figure 1.15 – A figure to give an explanation of solvatochromism.[133]

Nile Red and Nile Blue, the structures of which are shown in Figure 1.16, show an increase in wavelength of absorption when the polarity of the solvent is increased.[134-136] This change in solvatochromic properties can be used as a method of assessing the relative polarity of a solvent or solvent system.[137] In Chapter 2 Nile Red was shown to undergo a shift in peak emission at the LCST when dissolved within a temperature responsive polymer. This has also been shown in the paper published by Plenderleith *et al.[90]*

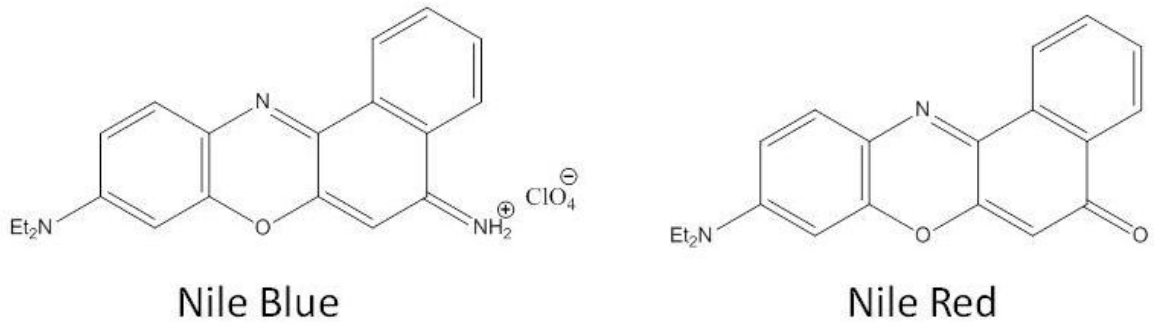

Figure 1.16 – A figure showing the structures of Nile Blue and Nile Red

Nile Red has been shown to undergo a shift in peak emission, with the coil to globule transition, when dissolved within a HB-PNIPAM polymer. However dissolution of a dye within a polymer is unlikely to be approved by medical governing bodies, as this would be a migratable species. Therefore, it is important that the dye should be covalently bonded to the polymer chain. Nile Blue has an amine group which can be easily utilised for addition to an activated carboxylic acid or to other functionalities.[138] Tethering a dye molecule to a temperature responsive polymer has been shown to change the microenvironment of the dye.[139] It is expected that bacteria binding triggered collapse of vancomycin functional HB-PNIPAM (HB-PNIPAM-van) will produce a similar effect in the solvatochromic dry Nile Blue. Solvatochromic dyes will be used to indicate the coil-to-globule transition and this will be an important part of the projects undertaken.

1.1.16 Interpenetrating Polymer Networks

An interpenetrating polymer network (IPN) is a combination of two or more polymers in network form, at least one of which is polymerised and/or crosslinked in the immediate presence of the others.[140] The IUPAC definition states that an IPN is 'A polymer comprising two or more networks which are at least partially interlaced on a molecular scale, but not covalently bonded to each other and cannot be separated unless chemical bonds are broken. A mixture of two or more preformed polymer networks is not an IPN.'[94]

Semi IPN's may contain a linear polymer entrapped in a polymer network. This is defined by IUPAC as 'a polymer comprising of one or more networks and one or more linear or branched polymer(s) characterised by the penetration of at least some of the linear or branched macromolecules.' [94] However, despite the inclusion of branched polymers in the IUPAC definition there are relatively few examples of branched polymers containing semi interpenetrating polymer networks.

When combining polymers in these ways it is possible to combine the respective properties of each individual polymer system in a favourable way. This maintains the advantages, whilst overcoming the disadvantages of both systems.[141]

There are several mechanisms by which an IPN can be manufactured, resulting in multiple outcomes. These are outlined by Figure 1.17, Figure 1.18, Figure 1.19 and Figure 1.20. Firstly,

simultaneous interpenetrating networks are created by mixing the components of two polymer systems together. The polymers are then both synthesised simultaneously by reaction mechanisms that do not interact. For example, this can be done by using a step and a chain growth mechanism.

Sequential IPNs are created by making one polymer, then swelling it in the monomer and crosslinker of the next. The second polymerisation creates an IPN, which is shown in Figure 1.17.[140]

Figure 1.17 – A schematic diagram showing the structure of an interpenetrating polymer network produced by simultaneous or sequential polymerisations.

A gradient IPN (Figure 1.18) can be made by relatively simple means. One system can be polymerised, subsequently the monomer and crosslinker of the second system is allowed to swell the first polymer. Before diffusion allows the monomer to be absorbed homogeneously throughout the network, polymerisation of the second monomer takes place. The timescale for this will be highly dependent on the dimensions, physical and chemical properties of the network and its interaction with the second monomer. This process results in a polymer (polymer 1) within a second polymer (polymer 2) which decreases in concentration moving through polymer 1, this type of IPN is shown in Figure 1.18. [140]

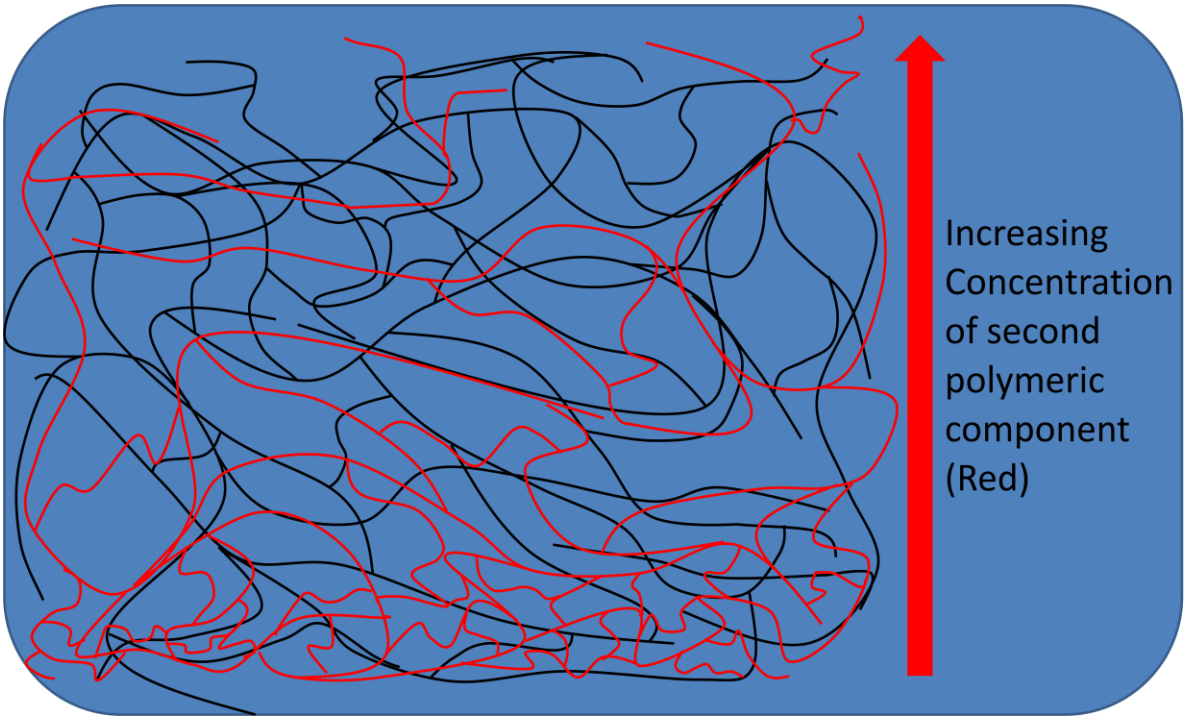

Figure 1.18 – A schematic diagram showing a gradient IPN. In this IPN the one polymer matrix is crosslinked then second monomer is soaked into the matrix and cured before the monomer diffuses evenly through the matrix. This results in a concentration gradient of the second polymer.

Thermoplastic IPNs are not chemically crosslinked. Instead the polymers are held together by physical crosslinking. The physical bonds may be broken by heating allowing the plastic to flow.[140]

Semi-IPNs are composed of a linear (Figure 1.20) or branched polymer (Figure 1.19) entrapped within a crosslinked polymer. In the case of a linear polymer (red) it may be easily washed out of the crosslinked polymer (black) as it is not held by physical interactions. However, when branching is introduced this will become more difficult as the polymer must take up many unfavourable conformations to untangle itself from the surrounding matrix.[140]

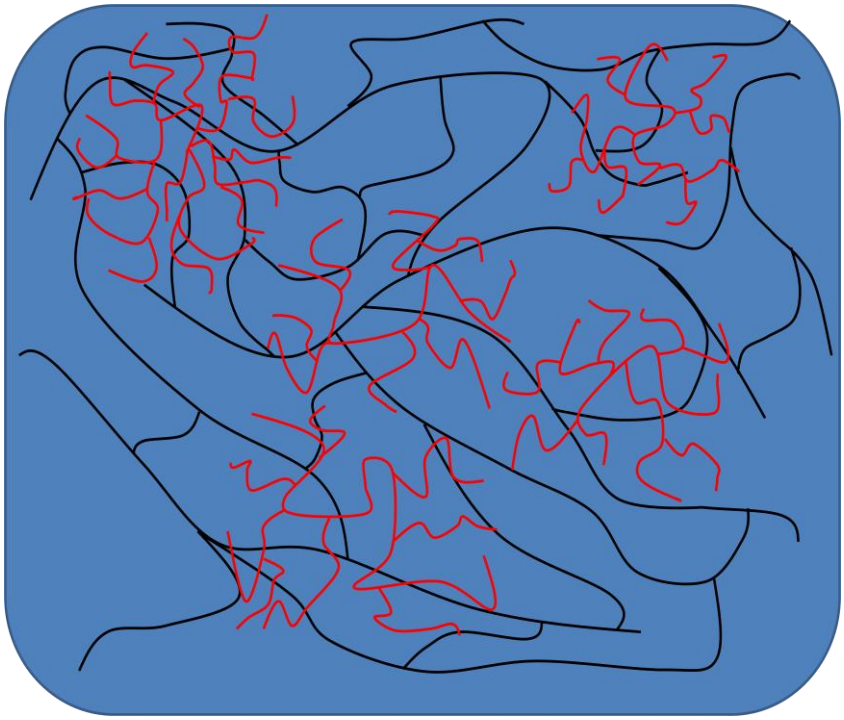

Figure 1.19 - A schematic diagram showing the structure of a semi-IPN with embedded branched polymer (BS-IPN).

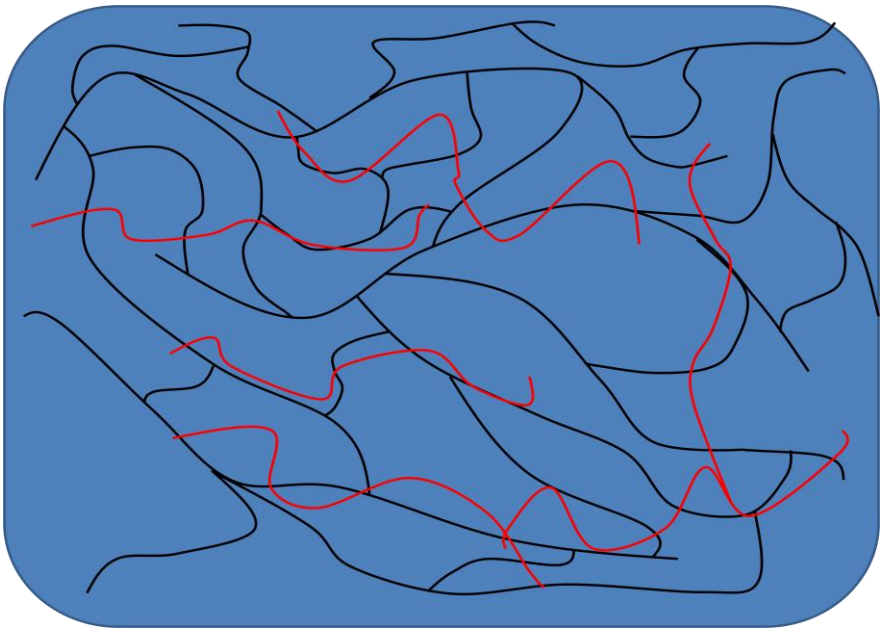

Figure 1.20 - A schematic diagram showing the structure of a semi-IPN with embedded linear polymer

Figure 1.19 and Figure 1.20 show the difference between a semi-IPN containing a linear polymer and a semi-IPN containing a branched polymer. Semi-IPNs containing branched polymer will be termed branched semi-interpenetrating polymer networks (BS-IPNs) to

distinguish them from a linear system. The characteristic difference between these systems is the extractability of the entrapped component. This can become important in a swollen hydrogel system where linear polymer that is not securely held by physical interactions of the surrounding matrix may be readily removed.

1.1.17 Interpenetrating Polymer Networks in Tissue Engineering

The following section outlines research carried out in field of tissue engineering regarding interpenetrating polymer networks and semi-interpenetrating polymer networks.

It has been hypothesised that by using a composite hydrogel composed of hydrophilic and hydrophobic polymer chains the natural properties of the extra cellular matrix (ECM) will be better imitated.[142] In addition the biological properties could be improved by introduction of peptide sequences or other bioactive agents. For example the incorporation of peptide sequences into an agarose-PEGDA IPN has been show to increase cell viability and proliferation.[142] There has also been significant evidence for the improvement of mechanical properties. Wen-Fu Lee *et al.* found that the IPN gels containing crosslinked chitosan displayed increased compression moduli due to a more compact structure.[143] Further evidence can be seen in the Weng *et al.* study into 'Double Network Photocrosslinked Hydrogels.' Here a sequential IPN was produced, Hyaluronic swollen in N-dimethylacrylamide produced a hydrogel with a compression modulus and a stress at failure of 0.5 MPa and 5.2 MPa respectively.[144]

An advantage of IPNs is that a composite material can be made that allows a compromise of the properties of both materials. Stile *et al.* synthesised semi-interpenetrating networks composed of poly(N-*iso*propylacrylamide-co-acrylic acid) P(NIPAM-co-AA) hydrogels containing linear poly(acrylic acid). At 22°C oscillatory shear rheometry data showed that the material was a soft lightly crosslinked solid. Only the highest concentrations of poly(acrylic acid) had an effect on the rigidity of the P(NIPAM-co-AA) semi-IPN's compared to the P(NIPAM-co-AA) hydrogels which contained no linear P(AA). At 37°C it was shown that the complex shear moduli of the P(NIPAM-co-AA) based semi-IPN's were significantly greater than the values for the P(NIPAM-co-AA) hydrogels. Furthermore the value of the complex shear moduli increased for the semi-IPN's as the concentration of PAA in the semi-

IPN increased. This could be used to tailor the mechanical properties of PNIPAM based scaffolds.[145] Further work from the Stile group using a similar system has shown that the properties of a semi-IPN system composed of PNIPAM hydrogel with linear PAA chains are affected by the amount of PAA within the IPN. It was found that the PAA affected the injectability, transparency, and phase transitions of the matrices. The effects observed were related to the amount of PAA present in the semi-IPN.[146] However, there is no cell work in this paper and no follow up paper.

Phillips and Kao synthesised IPN's of poly(ethylene glycol) (PEG) with PEGylated RGD-modified gelatine. Human macrophages were cultured on IPN's containing modified and unmodified gelatine and monitored at 2, 4, 24, 96, and 168 hours. The IPN's containing the PEGylated RGD were comparable to cells grown on tissue culture polystyrene in terms of cell density. There were significantly fewer cells on the unmodified gelatine or gelatine with triglycine.[147] Further work using a gelatine based IPN by Jaiswal *et al*. studied how cell proliferation was observed on a semi-IPN of polyacrylamide crosslinked with polycaprolactone diacrylate and gelatine by composition feed, degree of hydrophobicity and internal morphology. It was found that fibroblasts proliferated on the surface of the hydrogel scaffolds. Incorporation of a hydrophobic crosslinker regulates the degree of hydrophobicity, which in turn dictates properties of the matrix such as internal morphology, contact angle and protein absorption. These IPN's may serve as a potential scaffold for tissue engineering.[148]

Lui and Park have produced IPN scaffolds for tissue engineering. The IPN is composed of gelatine and dextran bifunctionalised with methacrylate and aldehyde. These dextran based gelatine containing IPN's not only supported the culture of endothelial cells but also allowed encapsulation of skeletal muscle cells to proliferate and spread through the bulk interior of the hydrogel. It is proposed that these materials could be used to create 3D scaffolds for tissue engineering.[149]

Pescosolido *et al.* carried out work where by IPN's based on hyaluronic acid and hydroxyethylmethacrylate derivatized dextran were structured by bioprinting to form 3D constructs. Photo-polymerisation of the system gave strong biodegradable IPN hydrogels with mechanical properties that could be tuned for the application. The system with the highest hyaluronic acid concentration was successfully printed by deposition of fibres which

were then photopolymerised. The structure formed had high porosity and well defined strand spacing. These parameters can be controlled by adjusting the process. The results show the suitability of hyaluronic acid hydroxyethyl-methacrylate derivatised dextran IPNs for bioprinting.[150] Hyaularonic acid systems have also been used by Suri and Schmidt.[151] IPN hydrogels of collagen and hyaluronic acid with and without laminin were used as nerve guidance conduits. When Schwann cells were encapsulated in the polymers the viability of the cells was not affected. The cells underwent spreading and proliferation. In some cases the cells lined up parallel to each other and also secreted nerve growth factor and brain-derived neutrophic factor. The use of laminin in the IPN caused the production these factors to increase. Furthermore, when co-cultured with neurones the neurones were able to extend neurites some of which were observed to follow the Schwann cells. These results show encapsulated Schwann cells hold promise for nerve repair.

Polycaprolactone diacrylate crosslinked biodegradable semi-IPNs of polyacrylamide and gelatine have been used by Jaiswal to produce a vehicle for controlled drug delivery.[152] A semi-IPN of polyacrylamide and gelatine was prepared using polycaprolactone diacrylate as a crosslinker. Curcumin was loaded onto the IPN by diffusion method. Fitting the drug release data to the Korsmeyer-Peppas model suggested that the drug was released for 10 days with a combination of a diffusion and an erosion mechanism. This research shows that biodegradable, porous and elastic IPN's could be ideal for drug release applications.

Wang *et al.* synthesised a semi IPN nanocomposite hydrogel of PNIPAM containing alginate. Fibroblasts, human lung adenocarcinoma epithelial cells and human cervical cancer cells were cultured on the polymers and all showed improved cell compatibility with increased alginate content.[153] On lowering the temperature a rapid cell sheet detachment was observed within 15 minutes without trypsin treatment. The roughness of the IPN sheet accelerated the cell sheet detachment by allowing faster water penetration. The detached cell sheet was seeded and proliferated again with good cell viability. This is an encouraging result for tissue engineering applications.

1.1.18 Biodegradable Polymers

Albertsson and Karlsson defined biodegradation as 'an event which takes place through the action of enzymes and/or chemical decomposition associated with living organisms (bacteria, fungi, etc.) or their secretion products.'[154] This does not take into account environmental degradation by oxidation, hydrolysis or photodegradation.[155] Albertsson and Karlsson went on to describe four methods for the development of biodegradable polymers;[154]

1. The use of cheap, synthetic, bulk polymers with the addition of a biodegradable unit.
2. Chemical modification of the main chain of synthetic polymers by the introduction of hydrolysable or oxidisable units.
3. The use of biodegradable polymers and their derivatives.
4. Tailor made new biodegradable polymers based on polyesters, polyanhydrides and polycarbonates.

These polymers have wide ranging applications, they are very important for tissue engineering and medical devices. They have been used to create polymers for surgical fixation,[156] controlled drug delivery,[157] and in many types on medical devices.[158-161] They are also important in waste management. Currently, non-degradable polymers used in packaging cause terrible environmental damage. Increases in recycling of plastics can help meet these targets. Widespread adoption of biodegradable polymers for packaging would help enormously with these environmental issues.

1.1.19 Biodegradable Polymers in Tissue Engineering

In tissue engineering, polymeric biomaterials are used in numerous areas,[162] including tissue replacement,[163-164] tissue augmentation,[165] tissue support [166] and drug delivery.[167] In most cases the biomaterial provides its function and is no longer needed. It is important to consider what will happen to the device in the long term to avoid a further surgery to retrieve the device. It is often beneficial to use a biodegradable system. Once the function is complete, the device will be digested/hydrolysed to soluble oligomers and carried away in the blood stream to be excreted.

Natural biodegradable polymers such as collagen,[163, 168-169] gelatine,[170-171] silk,[172-173] and alginate[174] are common in biomaterials. Although, batch to batch reproducibility, immunogenicy and pathogen transmission[160] have caused a move towards synthetic polymers which mimic the extra cellular matrix.

The most commonly used biodegradable polymers in tissue engineering are polyesters. Polylactide (PLA), polyglycolide (PGA) and their copolymer poly(lactide-co-glycolide) (PLGA). These polymers are widely used to make scaffolds for tissue engineering,[175-176] and are approved for medical use, in numerous devices, by the FDA.[160] They are thought to degrade to components that are eliminated via the Krebs cycle.[177] It is unlikely that these polymers will be degraded to monomer, It is more likely that they will degrade to soluble oligomers which can be eliminated by macrophages. The difference in structure of PLA and PGA causes a large difference in degradation rates enabling copolymers with tailored degradation rates.[178] Another commonly used polyester is poly(caprolactone) (PCL). Its rate of degradation is slow compared to PLA and PGA and this is favoured in many applications.

1.1.20 Trimethylene Carbonate (TMC) Biomaterials

The synthesis of trimethylene carbonate from diethyl carbonate and 1,3-propanediol has been patented by Boehringer Ingelheim Gmbh.[179] Small quantities of this monomer have not been made commercially available and as such academic study of its polymers has been limited until recently.

Much of the research on poly(trimethylene carbonate) (PTMC) has come from Grijpma *et al.* who have studied the polymerisation and properties of PTMC polymers in detail. It has been demonstrated that the rate of degradation is much higher *in vivo* than *in vitro*.[180] The high *in vivo* degradation was caused by surface erosion by cell mediated processes. PTMC polymers will lose mechanical properties *in* vivo within 5 months and are fully reabsorbed within 11 months, *in* vitro PTMC polymers can maintain their mechanical properties for over a year.[181] The degradation rate is also inversely proportional to the molecular weight. Lower molecular weight polymers degraded more slowly *in vitro* (with lipase solution) than *in vivo*.[182] It was suggested that this was caused by the more hydrophilic surface of the lower molecular weight polymers, which provides a poor substrate for the enzyme.

Grijpma *et al.* produced PTMC scaffolds for tissue engineering of cardiac muscle by leaching salt from within the polymer.[183] Using differing particle size allowed for a tuneable pore size and high flexibility in the physiological temperature. Porous, flexible poly(trimethylene carbonate) and poly(trimethylene carbonate-co-caprolactone) polymers were also made for the production of nerve guidance conduits.[184] Although, the title of this paper suggests that these polymers were used to make nerve guidance conduits, no structuring of the prepolymer was undertaken. The prepolymer was used to make porous polymer films which may have appropriate properties to use in a nerve guidance conduit. Unfortunately, there has been no follow up paper where the devices have been produced. However, PTMC copolymers have been used to culture human Schwann cells and did support adhesion and proliferation. [185]

PTMC microspheres have been added to calcium phosphate cement to introduce macroporosity into the cement after polymer degradation.[186] The addition of the polymer increased the elastic modulus but decreased the compressive strength of the material. In bones compressive strength is often a more important factor than elastic modulus, so the introduction of porosity by this method does come with this caveat.

1.2 Aims

The project aims to use HB-PNIPAM as a platform to introduce specific desirable functionalities to materials and scenarios.

1.2.1 Chapter 2 Aims

The aim of this project was to produce temperature responsive HB-PNIPAM polymers over a range of monomer feed ratios by RAFT polymerisation and to characterise these polymers by NMR, GPC, solution DSC and temperature dependant turbidity. This detailed characterisation will be important in taking these polymers forward to other applications in the following chapters. An alternative method of GPC analysis based on medians and quartiles will be used to analyse the characteristic bimodal molecular weight distribution. Traditional analysis was not appropriate, as this applies to only Gaussian distributions. This analysis is not intended to replace the existing analysis but can be used to enhance polymer molecular weight analysis when traditional methods are less appropriate. In order to probe the internal polymer structure a solvatochromic dye (Nile Red) dissolved within the polymer core and monitored by fluorescence spectroscopy across the LCST transition.

1.2.2 Chapter 3 Aims

The aim of this project was to produce a synthetic, temperature responsive, highly branched polymer by RAFT polymerisation with a high concentration of peptide end group functionality. This polymer was used to passage cultured cells from TCP. Trypsin (the enzyme typically used to carry out a passage) is aggressive and digests the extracellular matrix to 'lift' the cells. The aim is to use the synthetic polymers as a 'gentle' alternative for sensitive cell types. This has been demonstrated using primary human fibroblasts.

1.2.3 Chapter 4.1, 4.2 and 4.3

The aim of chapter 4.1 and 4.2 was to produce water swollen, composite systems with added biofunctionality, from a highly branched peptide functional polymeric additive (HB-PNIPAM-GRGDS) and a crosslinked polymer matrix. These materials were used to make 3d structured objects by microstereolithography. Typically hydrogels are non-adhesive due to their high water content so can perform badly in biomaterials applications where cell adhesion is desirable. Poly(vinyl pyrrolidone) (PVP) and poly(ethylene glycol) were

investigated as potential matrixes for the branched semi-interpenetrating polymer network systems.

1.2.4 Chapter 5 Aims

This work aimed to produce a resorbable polymer matrix which could be used in conjunction the peptide functional composite BS-IPN systems. Biodegradation of biomaterials is important in numerous applications and degradable biofunctoinal polymer systems will have many applications in scaffolds.

1.2.5 Chapter 6 Aims

The aim of this work was to produce a bacteria binding antibiotic functional polymer which would undergo a coil to globule transition upon binding of *gram negative* bacteria. Using solvatochromic dyes tethered to the polymer to detect the change in polymer conformation by the associated colour change a colour change bacterial detector could be made. This could be used as a colour change sensor for the presence of bacteria. Unfortunately this objective was not met due to the positioning of the dye at the polymer chain ends where no change in polarity of the environment was felt by the dye upon the coil to globule transition.

2. Effects of Degree of Branching on Highly Branched Poly(*N*-isopropylacrylamide)

2.1 Abstract

A range of highly branched PNIPAM polymers were synthesised by RAFT polymerisation with varying feed ratios of 4-VBPCD (the RAFT agent) initiator and NIPAM. The effects of this upon the properties of the resulting polymer was established. The bimodal molecular weight distributions were described using a alternative system based on quartiles and the median of the distribution. This method was used to avoid problems associated with non-Gaussian distributions using the traditional analysis. The inner structure of the polymer particles was probed by the introduction of a solvatochromic dye (Nile Red). This provided evidence for a core shell morphology where the core of the particle is collapsed and globular and the outer segments are solvated and in the coil conformation. This effect was found to be dependent on the degree of branching.

2.2 Experimental

2.2.1 Synthesis of 4-Vinylbenzyl Pyrrolecarbodithioate

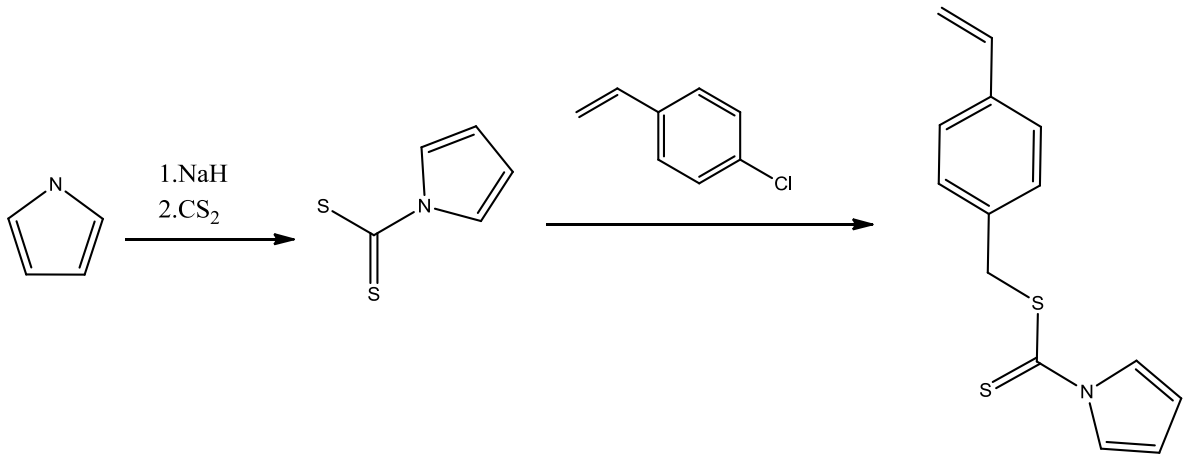

Figure 2.1 – A figure showing the reaction scheme for the synthesis of the 4-VBPCD RAFT agent.

Pyrrole (100 mL, 1.49 mol) was distilled (boiling point. 129°C). NaH (11.98 g, 0.497 mol) was added to a 3 neck flask under N_2, with stirring, as a suspension in DMF (240 mL). Pyrrole (20 g, 0.298 mol) in DMF (40 mL) was added dropwise to the reaction over 30 mins at 0°C. The solution was stirred at room temperature for 30 minutes. Carbon disulphide (22 g, 0.298 mol) in dimethylformamide (DMF) (40ml) was added dropwise over 10 minutes at 0°C. The solution was stirred at room temperature for 30 minutes. 4-vinylbenzyl chloride (45.48 g, 0.289 mol) in DMF (40 mL) was added dropwise over 20 minutes at 0°C with stirring. The solution was stirred at room temperature for 30 minutes. Deionised water (400 mL) was added to the reaction mixture and the product was extracted with diethyl ether (4 x 500 mL). The organic layers were combined dried with magnesium sulphate and evaporated yielding a dark coloured liquid which was purified by flash silica column in petroleum ether followed by recrystallisation at -20°C to give 51.78 g of a yellow solid with a yield of 7.48%.

The product was confirmed by elemental analysis, NMR and mass spectroscopy. A list of the measured and expected carbon, hydrogen, nitrogen and sulphur contents has been given below along with a list of NMR peaks and the splitting patterns associated with the peaks and details of the measured and calculated molecular ion by mass spectroscopy. The full spectrum has been given in Figure A.16.

Elemental analysis:

Expected Results: Carbon 64.9%, Hydrogen 5.1%, Nitrogen 5.4%, Sulphur, 24.7%. Actual Results: Carbon 65.3%, Hydrogen 5.1%, Nitrogen 5.3%, Sulphur 22.41%.

^{1}H NMR (400MHz, $CDCl_3$) (ppm): δ 4.61 (2H, s, RCH_2Ar), δ 5.81 (1H, m, RC=CH), δ 6.35 (1H, m, RC=CH), δ 6.76 (2H, m, Ar), δ 7.18 (2H, m, Ar), δ 7.45 (2H, d, Ar), δ 7.59 (2H, d, Ar).

MH^+ (HPLC-ESI) = 259, (calculated= 259.05 (100.0%), 260.05 (17.1%), 261.04 (9.0%), 262.05 (1.4%), 261.06 (1.1%))

2.2.2 Synthesis of Pyrrolecarbodithioate Ended HB-PNIPAM

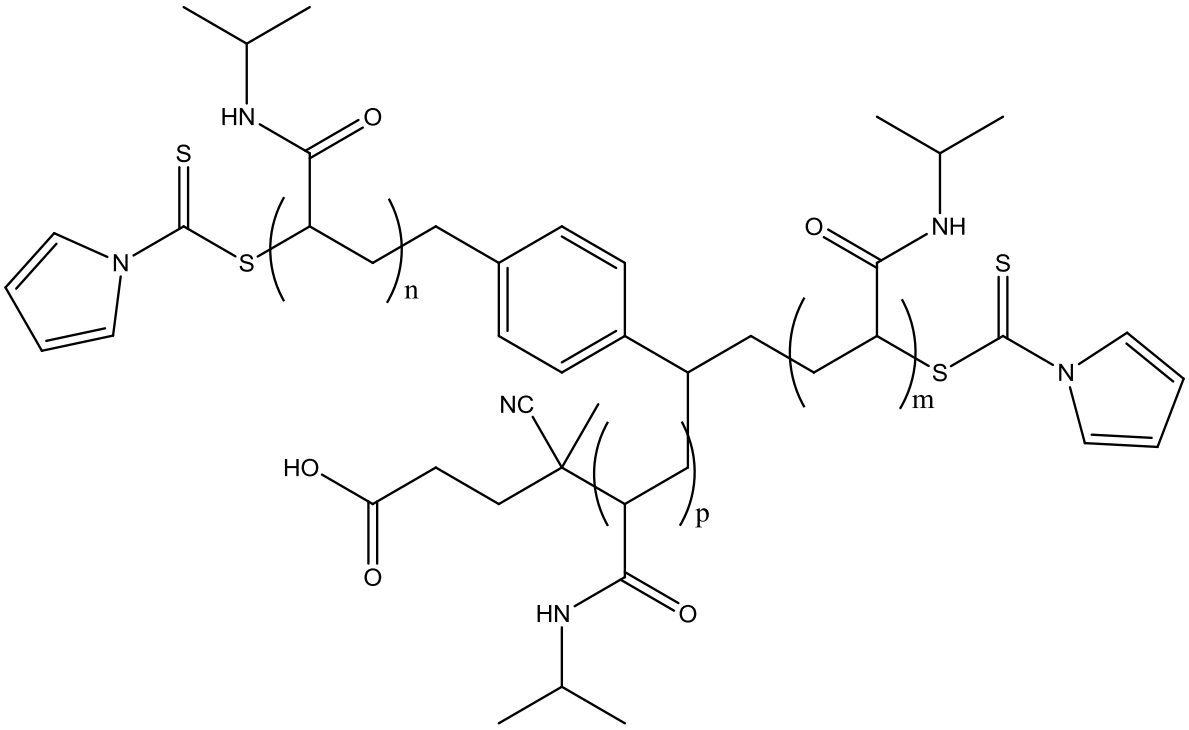

Figure 2.2- A figure showing the generic structure of HB-PNIPAM-pyrrole with one branch point.

N-isopropylacrylamide was recrystalised from 40:60 hexane:toluene. This was dissolved in dioxane (10 ml) with 4-vinylbenzyl pyrrolecarbodithioate and ACVA in the quantities shown in Table 2.1. The solution was transferred to a glass ampoule, 3 cycles of freeze, pump and thaw were carried out at high vacuum. The ampoule was flame sealed and reacted at 60°C

for 48 hours. The viscous solution was precipitated into diethyl ether and dried under vacuum. Precipitation was repeated three times to give an off white solid.

The polymer was characterised by NMR and a list of the peaks with associated splitting patterns are shown below. The NMR spectra for the polymers can be found in Section 8.1.

^{1}H NMR (400MHz, $CDCl_3$) (ppm): δ 0.9-1.3(6H,s,-N(CH_3)$_2$), δ 1.4-1.8 (2H, br m, -CH2-CH-Ar-), δ 1.9–2.2(2H, br m, -CH2-CH-CO-NH-) and (1H, br m, CH2-CH-CONH-), δ 4.0 (1H, br s, (CH3)2CH-), δ 6.3 (H2, br s, N-pyrrole-H), δ 6.6–7.2 (br m, -Ar-), δ 7.65 (2H, br s, N-pyrrole-H).

The data for GPC, elemental analysis, conversions cloud point and DSC LCST are shown in the results section.

Table 2.1 – A table showing the formulations of HB-PNIPAM systems used to make HB-PNIPAM polymers with varying feed ratios of 4-VBPCD and ACVA to NIPAM.

NIPPAM:RAFT	NIPAM moles	NIPAM mass / g	4-VBPCD moles	4-VBPCD mass / g	ACVA moles	ACVA mass / g
10:1	2.655	3.000	2.655	0.687	2.655	0.743
15:1	2.655	3.000	1.770	0.458	1.770	0.500
25:1	2.655	3.000	1.062	0.275	1.062	0.295
35:1	2.655	3.000	0.759	0.197	0.759	0.212
45:1	2.655	3.000	0.590	0.153	0.590	0.165
55:1	2.655	3.000	0.483	0.123	0.483	0.120
65:1	2.655	3.000	0.410	0.106	0.410	0.114
75:1	2.655	3.000	0.354	0.092	0.354	0.099
85:1	2.655	3.000	0.312	0.081	0.312	0.088

2.2.3 NMR Functionality Calculations

2.2.3.1 Conversions

Integrals of the isopropyl 6H and vinyl 2H were recorded from the NMR spectra of the reaction mixtures.

Table 2.2 - Integrals of unreacted NIPAM vinyl 2H and PNIPAM isopropyl 6H from reaction mixture in $CDCl_3$

NIPAM:RAFT	∫ vinyl	∫ Isopropyl
10:1	0.0036	1
15:1	0.0045	1
25:1	0.0043	1
35:1	0.0065	1
45:1	0.0048	1
55:1	0.0043	1
65:1	0.0043	1
75:1	0.0045	1
85:1	0.0047	1

The integrals were used to calculate the percentage conversion by dividing the isopropyl 6H by 6 and the vinyl 2H by 2 Equation 2.1 was used to calculate the percentage conversions.

$$\%\, conversion = \frac{1\text{H vinyl}}{1\text{H vinyl} + 1\text{H isopropyl}} \times 100$$

Equation 2.1

2.2.3.2 Functionalities and Degree of Branching

For ^{1}H NMR functionality calculations the integrals of the NIPAM isopropyl functional unit, the benzyl unit and the N-pyrrole hydrogens were compared, fixing the isopropyl NIPAM functionalities to RAFT functionalities (results shown in Table 2.3). The 1H values were calculated by using the isopropyl 1H and dividing the benzyl 4H by 4 and N-pyrrole 2H by 2. An example spectrum and the structures of the polymer components are given in Figure 2.3.

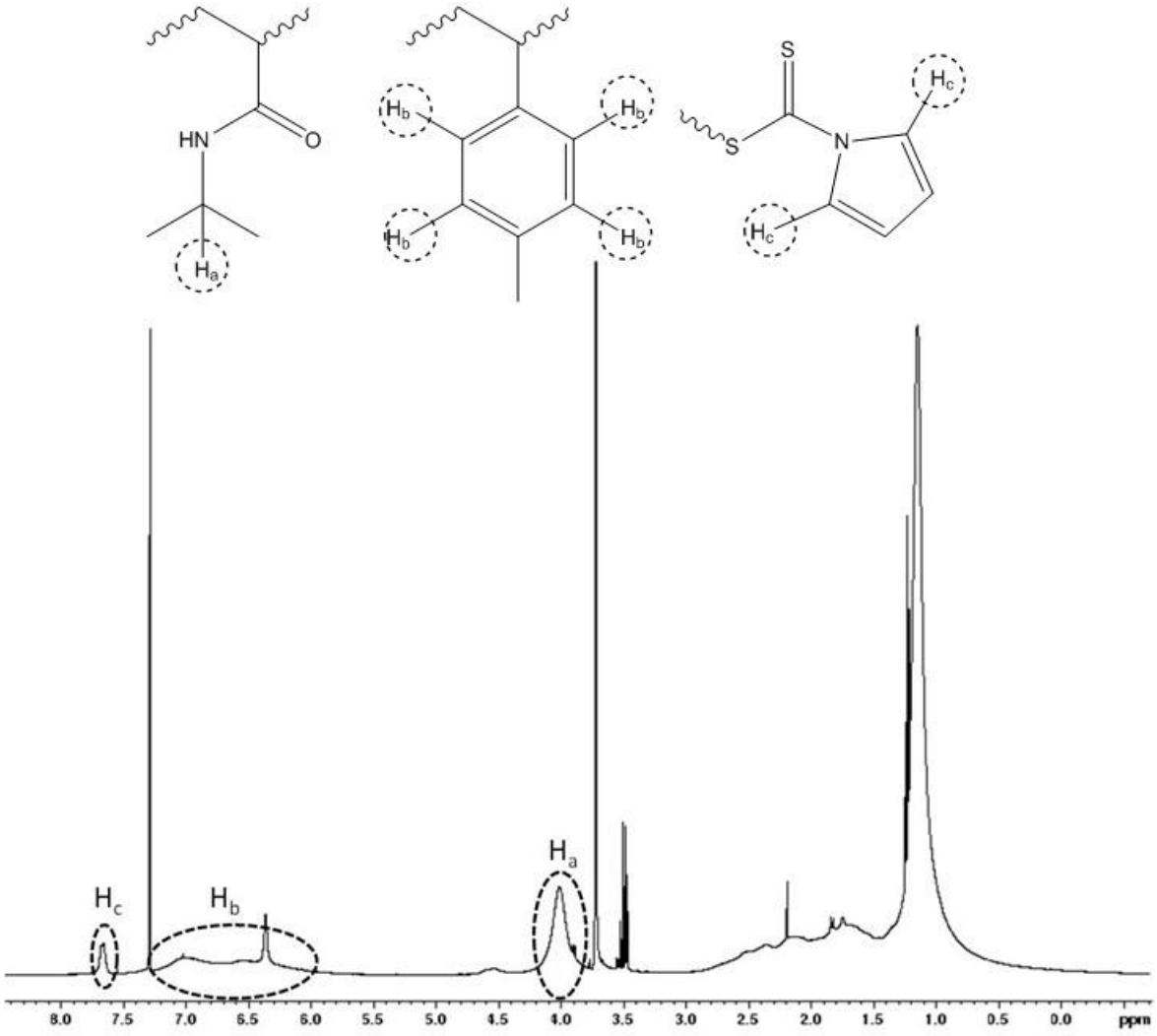

Figure 2.3 – An example ^{1}H NMR spectrum for 10:1 HB-PNIPAM in $CDCl_3$ with highlighted pyrrole 2H (H_c), benzyl 4H (H_b) and isopropyl 1H (H_a).

Table 2.3 – A table of the integrals from ^{1}H NMR spectra of the HB-PNIPAM polymers.

NIPAM:4-VBPCD	∫ Total benzyl	∫ Benzyl - Pyrrole	∫ Pyrrole	∫ Isopropyl
10:1	0.080	0.060	0.020	0.139
15:1	0.053	0.041	0.013	0.155
25:1	0.033	0.024	0.009	0.157
35:1	0.026	0.019	0.007	0.168
45:1	0.021	0.016	0.005	0.169
55:1	0.016	0.012	0.004	0.151
65:1	0.015	0.011	0.004	0.165
75:1	0.011	0.008	0.003	0.151
85:1	0.011	0.008	0.003	0.166

The NMR integrals were used to calculate the number of RAFT and acid (*via* TAI) chain ends per branch (% acid/pyrrole functionality), the degree of branching (number of branch points per number of monomers) and the pyrrole functionality (moles of pyrrole per gram of polymer).

$$\%\, PyrroleFunctionality = \frac{1H\ Pyrrole}{1H\ Benzyl} \times 100$$

Equation 2.2

$$Degree\ of\ Branching = \frac{1H\ Benzyl}{(1H\ NIPAM + 1H\ Benzyl + 1H\ Pyrrole)}$$

Equation 2.3

2.2.3.3 TAI Chain End Reaction

Concentration of acid chain ends was determined by reacting the sample with 200 µl trichloroacetyl isocyanate (TAI) with 50 mg of HB-PNIPAM in an NMR tube The reaction is given in Figure 2.4. The imide peak was found at 11.1 ppm and compared to the isopropyl integral of that spectra. The imide was confirmed by addition of D_2O causing exchange of deuterium with the labile imide proton. This removes the TAI imide peak from the spectrum. The integrals of the relevant peaks from the NMR are given in Table 2.4. The integrals were used to calculate the % pyrrole and % acid functionality using Equation 2.4 and Equation 2.5.

Table 2.4 – A table showing the ^{1}H NMR integrals for TAI and benzyl regions of NMR spectra.

NIPAM:4-VBPCD	∫ TAI	∫ Benzyl
10:1	0.052	1
15:1	0.026	1
25:1	0.033	1
35:1	0.053	1
45:1	0.064	1
55:1	0.052	1
65:1	0.078	1
75:1	0.052	1
85:1	0.060	1

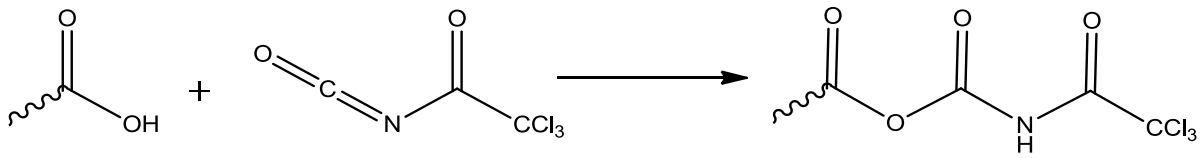

Figure 2.4 – A figure showing the reaction of TAI with acid end group of HB-PNIPAM. This reaction produces a distinctive imide peak which is detectable by NMR.

$$Functionality = 1 \,/\, (M_r\, NIPAM \times \frac{1H\ TAI}{1H\ NIPAM} + M_r\, RAFT\ )$$

Equation 2.4

$$\%\ Acid\ Functionality = \frac{1H\ TAI}{1H\ Benzyl} \times 100$$

Equation 2.5

2.2.4 DMF GPC Analysis

Samples were run on a system using a Polymer laboratories LC 1120 HPLC pump, a Polymer Laboratories ER3 3415, and three PLGEL™ 20 µm mixed A columns at 60°C, in series with a Viscotec 250 RI detector. Polymer samples were dissolved at 1 mg per mL in DMF with 0.1% LiBr and eluted at 1 mL per minute

The system was calibrated using Easivial poly(methyl methacrylate) standards. Three standards were used which each contained four polymers of known molecular weights. The molecular weights of the standards 'red', 'yellow', and 'green' are shown in Table 2.5. The retention times of these known polymers were measured (Figure 2.5) and were used to create a calibration plot. The resulting calibration plot is shown in Figure 2.6. This was used to give the relative molecular weight distributions of the analysed polymer samples.

Table 2.5 – A table showing the molecular weights of GPC standards used in the calibration of the GPC instrument.

Standard	Polymer Mp / g mol-1
Red	1944000
	332000
	30620
	1860
Yellow	679000
	144000
	13300
	875
Green	590000
	67400
	6830
	634

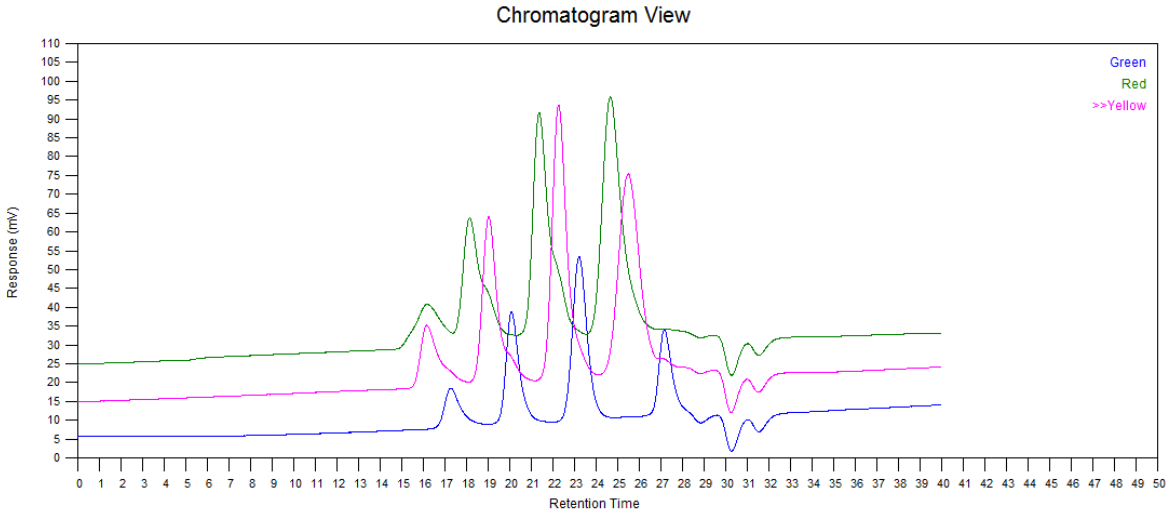

Figure 2.5 – A graph of detector response for three solutions of GPC standards each containing four polymers of known molecular weight.

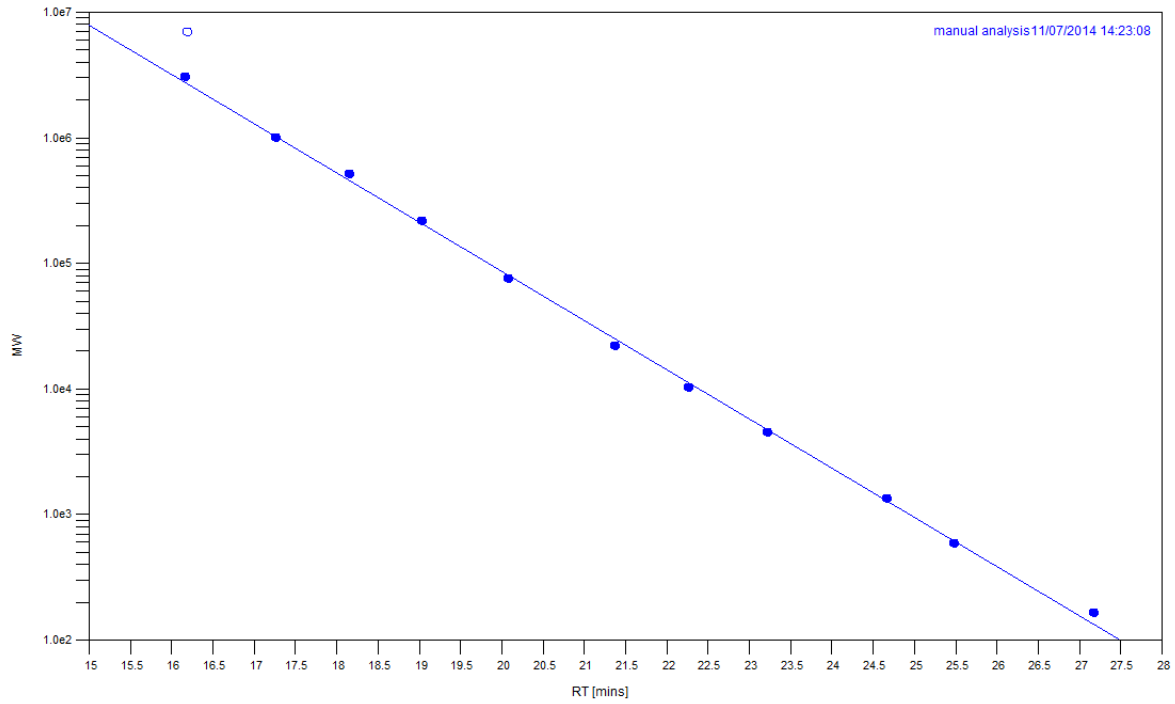

Figure 2.6 – A calibration plot made from the elution times of the GPC standards of known molecular weight.

2.2.5 Micro DSC

Polymer samples were dissolved in H_2O at 5 mg mL^{-1} and stored at 5°C for 24 hours prior to use to ensure complete dissolution. Samples were run on a Microcal inc VP-DSC over the temperature range 5-60°C with a heating rate of 1.5°C min^{-1} and cooling rate of 1°C per minute. The LCST was taken as the temperature at the thermograph peak maximum.

2.2.6 Integration of DSC Curves

The area under the curve was calculated using the trapezoidal rule using Graph_v2.exe programmed by Dr Lewis Williams.

2.2.7 Cloud Point

Polymer samples were dissolved in H_2O at 5 mg mL^{-1} and stored at 5°C for 24 hours prior to use to ensure complete dissolution. Samples were run on a Perkin Elmer UV spectrometer over the temperature range 10-60°C with a heating rate of 1.5°C min^{-1}. The turbidity of the

solution was measured by the absorbance at 500 nm. The LCST was taken as the onset of the increase in turbidity.

2.2.8 Nile Red Solutions

A stock solution of Nile Red was made up by adding Nile Red (2 mg) to solvents (99% water, glycerol, ethylene glycol, methanol, ethanol, DMSO butanol, isopropanol,dimethyl formamide and acetone) (25 cm^3). Measurements were made in 99% water by diluting the DMSO stock solution down to 10^{-7} mol dm^3 by further addition of water. This was necessary due to the insolubility of Nile Red in water. The fluorescence response of the label to solvent polarity was used to determine the relative polarity of the environment within the polymer.

2.2.9 Labelling Polymer Solution with Nile Red

A stock solution of Nile Red was made up by adding Nile Red (2 mg) DMSO (25 cm^3). The HB-PNIPAM polymers (11 mg) were dissolved in ultrapure water (7 mL). 100 µL of the Nile Red stock solution was added to the polymer solution and mixed well. The Nile Red polymer solution was then further diluted 1 part in 2 parts ultrapure water.

2.3 Results and Discussion

2.3.1 Conversions and Functionalities by ^{1}H NMR

HB-PNIPAM was synthesised by RAFT polymerisation with varying feed ratios of NIPAM to 4-VBPCD. The polymers were analysed by elemental analysis, ^{1}H NMR and GPC to find percentage conversions, functionality and degree of branching. The LCST was determined by VP-DSC and UV (turbidity).

Samples of reaction mixture were analysed by NMR to determine the percentage of unreacted NIPAM compared to reacted NIPAM. As shown in Table 2.6 the conversion was above 98% for all ratios of NIPAM to 4-VBPCD.

The purified polymer was also analysed by NMR and the spectra were used to calculate the pyrrole and acid functionality as a percentage and the degree of branching. The results of this are shown in Table 2.6.

Table 2.6 - Table showing the percentage conversions of PNIPAM as determined by ^{1}H NMR

NIPAM:4-VBPCDD	conversion / %	% Pyrrole Functionality / %	% Acid Functionality / %	Degree of Branching
10:1	98.9	50.9	23.4	0.091
15:1	98.7	47.6	11.3	0.059
25:1	98.7	53.5	14.1	0.036
35:1	98.1	50.5	22.2	0.027
45:1	98.6	49.7	26.5	0.023
55:1	98.7	51.1	21.2	0.019
65:1	98.7	52.2	32.2	0.016
75:1	98.7	50.5	21.3	0.013
85:1	98.6	52.6	24.6	0.012

Conversion, % acid functionality, % pyrrole functionality and degree of branching were calculated from, Equation 2.2, Equation 2.3, Equation 2.4 and Equation 2.5.

In all cases, conversions are over 98% indicating the reaction had reached completion.

The % pyrrole and % acid functionality calculated by Equation 2.2 and Equation 2.5. The sum of the % acid and pyrrole functionality will yield the total percentage of end groups accounted for. The highest concentration is 50.1% for the 10:1 polymer. This is evidence

that there must also be a significant amount of intramolecular bimolecular termination occurring. This will result in a 'loop' with no end groups.

The degree of branching measures the number of benzyl groups relative to the other components. Over the measured range this decreases from 0.091-0.012 (Table 2.6). These figures fit well with the concentrations that would be expected for the given feed ratios. For example, the 10:1 sample gives a degree of branching of 0.091. This is equivalent to 9% branch points. This close relationship between the expected number of branch points from the feed ratio and the measured branching from NMR is seen across the range of polymers synthesised

Table 2.7 - Measured elemental analysis compared to expected data

NIPAM : RAFT	Measured carbon content / %	Expected carbon content / %	Measured hydrogen content / %	Expected hydrogen content / %	Measured nitrogen content / %	Expected nitrogen content / %	Measured sulphur content / %	Expected sulphur content / %
10:1	58.72	64.92	8.76	7.28	9.90	23.77	3.57	4.03
15:1	59.23	67.25	8.92	8.03	10.41	21.63	2.53	3.10
25:1	58.45	69.69	9.45	8.80	10.45	19.39	1.67	2.11
35:1	58.72	70.95	9.71	9.21	10.45	18.23	1.18	1.61
45:1	58.93	71.73	9.42	9.46	10.49	17.52	1.05	1.29
55:1	57.85	72.25	9.58	9.62	10.56	17.04	0.79	1.08
65:1	57.48	72.63	9.62	9.74	10.47	16.70	0.80	0.93
75:1	57.52	72.91	9.75	9.83	10.84	16.43	0.55	0.82
85:1	57.24	73.14	9.72	9.90	10.51	16.23	0.53	0.73

The measured sulphur concentration shown by elemental analysis is consistently less than the expected value showing that the thioester pyrrole group is not incorporated fully. This result may be expected. The thioester is a labile group and is unlikely to be 100% attached at the end point of the reaction. Thus the reduced sulphur content is expected. However, the concentration of sulphur is 70-80% of the expected concentration. This is much higher than the concentration of RAFT end groups measured by NMR. This could imply that the thioester can remain, whilst the pyrrole is removed from the chain end.

2.3.2 Molecular Weights by GPC

A detailed description of the GPC method and method of calibration has been given in section 2.2.4.

The molecular weight averages Mn, Mw, Mz and Mz+1 of highly branched PNIPAM polymers are shown in Table 2.8. These averages have been calculated from the GPC chromatographs shown in Figure 2.7. Analysis of these molecular weight distributions in the traditional way to give the Mn, Mw, Mz and Mz+1 relies on the shape of the molecular weight distributions fitting a Gaussian distribution. However, Figure 2.7 shows that these highly branched polymers have broad, bimodal distributions and so this type of analysis becomes less insightful. For this reason an alternative analysis technique was sought. It must be remembered that this alternative method should be used when the traditional means are not appropriate; it is not intended as a replacement for the traditional method of analysis for Gaussian distributions.

The retention times of the polymers were measured and are shown in Figure 2.7 (A). These data were used to calculate the molecular weight distributions shown in Figure 2.7 (B) by using the measured standards and calibration plot shown in Figure 2.5 and Figure 2.6 respectively. Table 2.8 sets out the molecular weight averages calculated by traditional means.

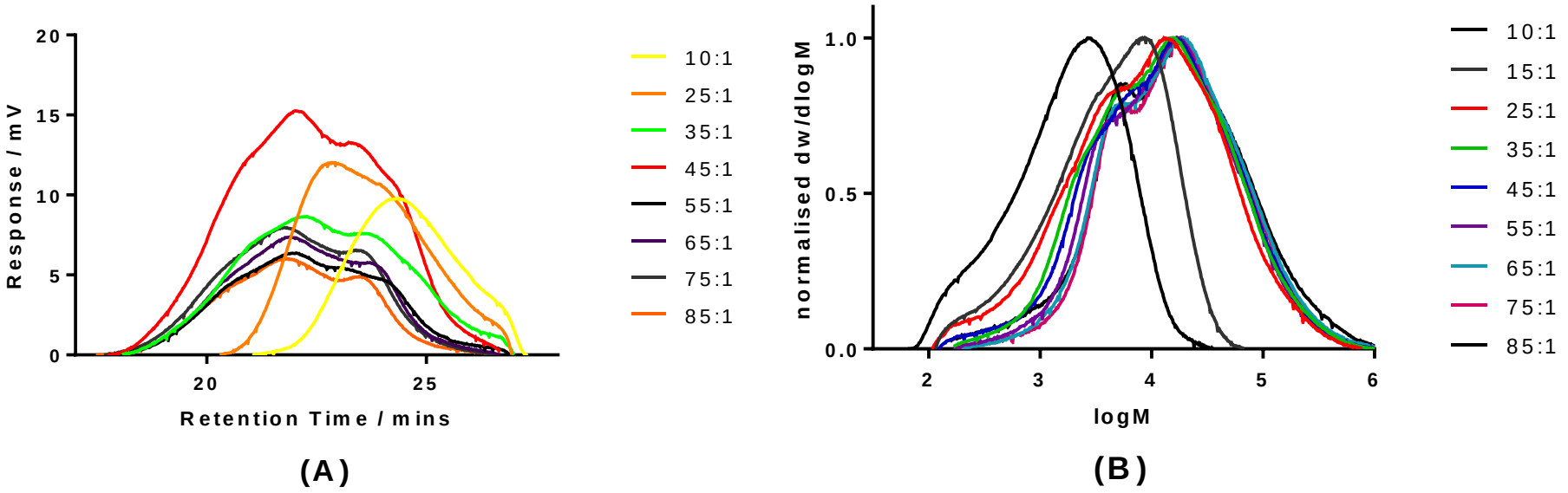

Figure 2.7 – A figure showing GPC chromatographs for RAFT HB-PNIPAM polymers. The raw data showing the elution time vs detector response is given by (A). This data was used to produce the logM vs normalised dw/dlogM via the calibration.

Table 2.8 - Table showing data calculated from GPC curves of pyrrole ended HB-PNIPAM with varying ratios of NIPAM to 4-VBPCD

NIPAM: 4-VBPCD	Mn / g mol^{-1}	Mw / g mol^{-1}	Mz / g mol^{-1}	Mz+1 / g mol^{-1}	Đ
10:1	1050	3350	6650	10500	3.2
15:1	2200	7650	14700	21600	3.5
25:1	3350	24850	103300	236300	7.5
35:1	5100	29250	123200	295200	5.7
45:1	4800	29800	121250	296650	6.2
55:1	6300	30100	115500	280750	4.8
65:1	7350	34750	143800	362350	4.7
75:1	7400	34400	142900	38750	4.6
85:1	7977	45000	251050	671100	5.6

The use of the traditional parameters of the distribution (Mn, Mw, Mz, Mz+1) has become well ingrained in polymer science. However, these parameters are related to standard deviations of symmetrical, Gaussian distributions of molecular weight. Hence, they may not be appropriate to describe the asymmetric bimodal distributions shown in Figure 2.7. Similarly, the dispersity (which relies on these parameters) is used as a measure of the width of the distribution and will also be compromised by asymmetric distributions. These statistics assumes that the distribution is Gaussian and that the variance on each side of the distribution are equivalent. The problem here is that the dispersity (Mn/Mw and Mw/Mz) only describes the distribution of the higher molecular weight side of the distribution. When the two sides of the distribution are significantly different in shape, such as in Figure 2.7, these numbers become meaningless. This issue has lead to the practice of including graphical data of the whole distribution.

The use of the traditional parametric descriptive statistics in polymer chemistry is the most appropriate means of analysis for parametric data but has evolved from a historic measurement of these values. For example, prior to the advent of GPC measurement colligative properties would provide Mn, light scattering and or sedimentation would give Mw and Mz and viscometry would provide Mv. Thus in the early days of the development of polymer science the only way to obtain the whole distribution was to fractionate the polymer and this was a very tedious process. Developments in instrumentation mean that it is now routine to find the whole distribution of a polymer using GPC. Therefore, it now

possible to reconsider how this data is described. Clearly a more appropriate description of the distribution could be found for non-Gaussian distributions. At this point it should be made clear that this analysis it intended for systems where traditional analysis is no longer appropriate. For parametric, Gaussian molecular weight distributions the traditional statistical description (using Mn, Mw, Mz, Mz+1) is still the most appropriate method.

The first step in this approach is to test the distribution to see if it is Gaussian. If the polymers are non-Gaussian they can be considered for this method of analysis. The molecular weight distributions of the polymers shown in Figure 2.7 have been tested by Kolmogorov-Smirnov normality test, D'Agostino & Pearson onibus normality test and Sharpirs-Wilk Normality test. The results are shown in Table A.1, Table A.2 and Table A.3 in the Appendix. These tests showed that all the polymers analysed were non-Gaussian and that this alternative method of analysis was appropriate. Once the non-Gaussian nature of the distribution is confirmed the parametric moments of the distribution become of little use. However, the traditional use of these descriptive statistics means that it will be wise to quote these as well as more appropriate non-parametrics.

In other fields the width of the distribution at half of the peak value is used. This can be a useful statistic to use provided it is possible to define the peak height but this maybe difficult if the distribution is multi-modal. A better and more general approach is calculate the percentiles from the cumulative distribution. The percentiles are completely free of any assumptions as to the form of the distribution and they more accurately describe each side of the distribution. It may also be possible to apply non-parametric tests to compare the percentiles but care should be exercised to ensure that the assumptions of the tests are not violated. For example, the Mann-Whitney or Willcoxan tests can be applied to test differences in the 50^{th} percentile (The median) of non-Gaussian distributions but the distributions must be of the same shape. Another approach would to use the Kolmogorov-Smirnov test to test differences between whole distributions but at this point it not clear how typical GPC data should be transformed into an appropriate form for this test. The approach used here is to determine the 25^{th}, 50^{th} and 75^{th} percentiles from the cumulative distributions.

The 25^{th} percentile (first quartile) is the point where 25% of the molecules are less than this value of molecular weight. Similarly, the 50^{th} (the median) and 75^{th} percentile (third quartile)

are the values of molecular weight where 50 or 75 % of the distribution is lower than the stated percentile. These statistics are trivially obtained from the cumulative distribution (Figure 2.8) and provide a robust basis for comparison of non-parametric distributions. Interquartile ranges have been calculated from normalised cumulative distributions were calculated from the data shown in Figure 2.7. The cumulative distributions are shown in Figure 2.8. From this, the 25th and 75th percentiles were taken along with a median value and the corresponding logM measured. The results of this are shown in Table 2.9. These data are not directly comparable to the traditional average molecular weight values but they could be seen as an alternative for this type of distribution.

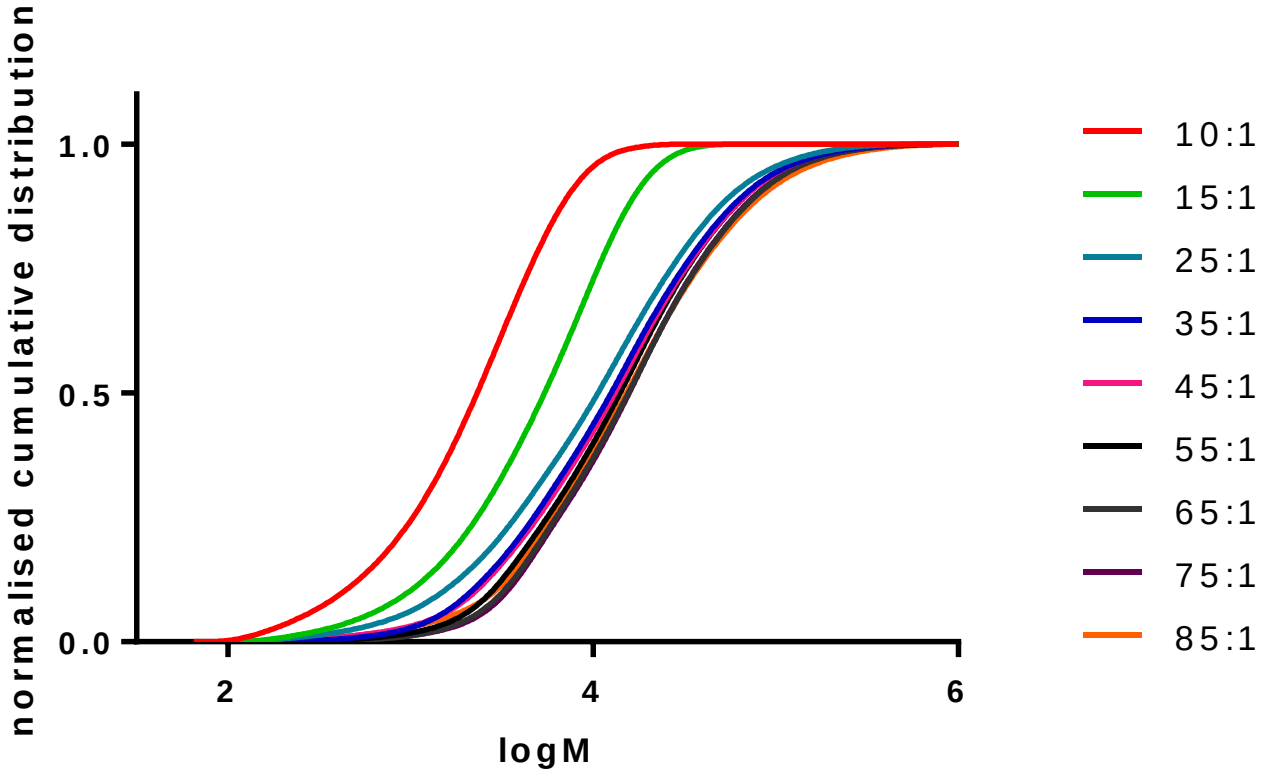

Figure 2.8 - Normalised cumulative distributions of 10:1, 15:1, 25:1, 35:1, 45:1, 55:1, 65:1, 75:1 and 85:1 RAFT HB-PNIPAM polymers.

Unlike the traditional parametric parameters of the distribution which are dependent on the type of distribution presented, these parameters show no such dependence. When using the traditional polymer molecular weight analysis four molecular weight distributions are

important; the number distribution, the weight distribution; the log number distribution and the log weight distribution. It is therefore important to define the type of distribution when using the percentiles to describe it. A useful symbolism could be:

i. Number distribution

$^{N}M_{25}$, $^{N}M_{50}$ and $^{N}M_{75}$ to indicate the 25^{th} , 50^{th} and 75^{th} percentiles

ii. Weight distribution

$^{W}M_{25}$, $^{W}M_{50}$ and $^{W}M_{75}$ to indicate the 25^{th} , 50^{th} and 75^{th} percentiles

Iii. Log Number distribution

^{N}lgM25 , $^{N}lgM_{50}$ and $^{N}lgM_{75}$ to indicate the 25^{th} , 50^{th} and 75^{th} percentiles

Iv. Log weight distribution

^{W}lgM25 , $^{W}lgM_{50}$ and $^{W}gM_{75}$ to indicate the 25^{th} , 50^{th} and 75^{th} percentiles

For example, in terms of the percentiles used in this way, the 25th the percentile of a number distribution is obtained by considering that 25% of the number of molecules have molecular weights below the percentile. On the other hand the 25^{th} percentile of a weight distribution can be obtained by considering that 25 % of the mass of the sample lies below a the molecular weight of the percentile.

The most appropriate distribution for GPC data that is wide use is the log weight distribution and that distribution is used solely in the following sections.

Once the percentiles, usually the quartiles and median are obtained distribution can be compared by stating the median and interquartile range (75^{th} percentile (3rd quartile) – 25^{th} percentile (1^{st} quartile)). These data are shown in Table 2.9.

Table 2.9 – A table showing the interquartile ranges of molecular weights calculated from the first and third quartiles from GPC.

Sample ID	Interquartile range logM	Median logM
10:1	1.28	3.42
15:1	1.28	3.64
25:1	1.66	4.02
35:1	1.66	4.14
45:1	1.70	4.09
55:1	1.62	4.11
65:1	1.65	4.18
75:1	1.71	4.19
85:1	1.70	4.17

In Figure 2.9 the interquartile range data (Table 2.9) is compared to the molecular weight averages from the traditional method of analysis. The M_n and M_w are given by the blue and red lines respectively. The box plot represents the first and third quartiles. The box plots demonstrate the usefulness of this technique; the traditional means of measuring M_n and M_w grossly underestimate the dispersity. The whiskers shown in Figure 2.9 show the extent of the data.

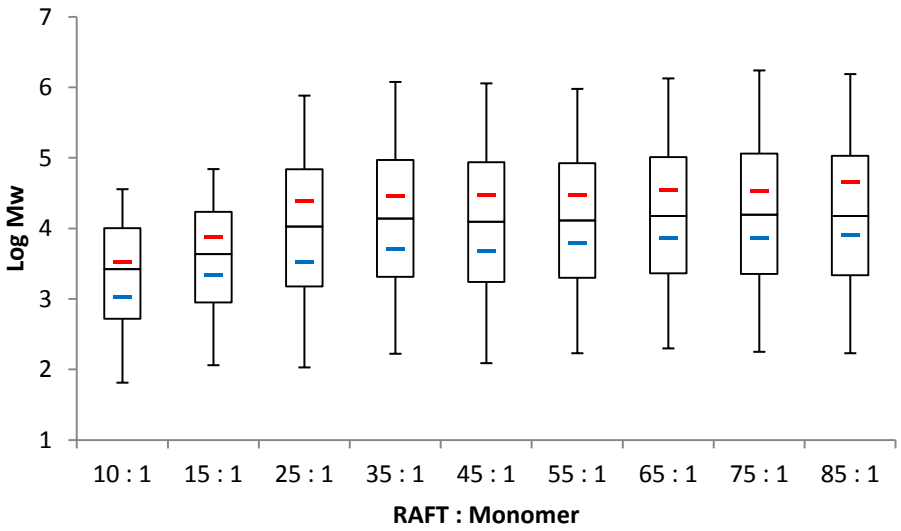

Figure 2.9 – GPC data represented by box plots, whiskers representing the limits of the data, the central black oblong gives the interquartile ranges, the central line gives the median of the data, the blue line gives the Mn and the red line gives the Mw as calculated by traditional means.

The data show that in general the interquartile range increases as branching decreases. Although, this effect seems to be shown most strongly from 10:1-25:1, it is not clear

whether the increases are significant. The same can be said for the median data. There is an increase in the interquartile range as branching decreases. However, it is not clear is this is a statistically significant change. Although, using interquartile and median comparisons it is currently not possible to carry out a full statistical analysis. Attempts have been made to analyse and compare distributions via statistical means, however, the tests were not appropriate for this type of data. Formal statistical testing has been adjourned until an appropriate method of analysis has been identified.

2.3.3 LCST of HB-PNIPAM Polymers

The LCST is a key feature of HB-PNIPAM polymers and has been shown to vary with branching. The LCST was measured by VP-DSC and cloud point (turbidity). The results of these experiments are tabulated in Table 2.10 and have been shown graphically in Figure 2.10.

Table 2.10 - A table showing the LCST of pyrrole ended HB-PNIPAM as measured by DSC and cloud point.

NIPAM:RAFT	cloud point /°C	DSC peak /°C
15.1	11.0	10.5
25.1	20.0	18.3
35.1	25.4	22.8
45.1	27.6	24.4
55.1	30.1	26.5
65.1	30.7	27.0
75.1	31.0	28.4
85.1	32.1	29.1

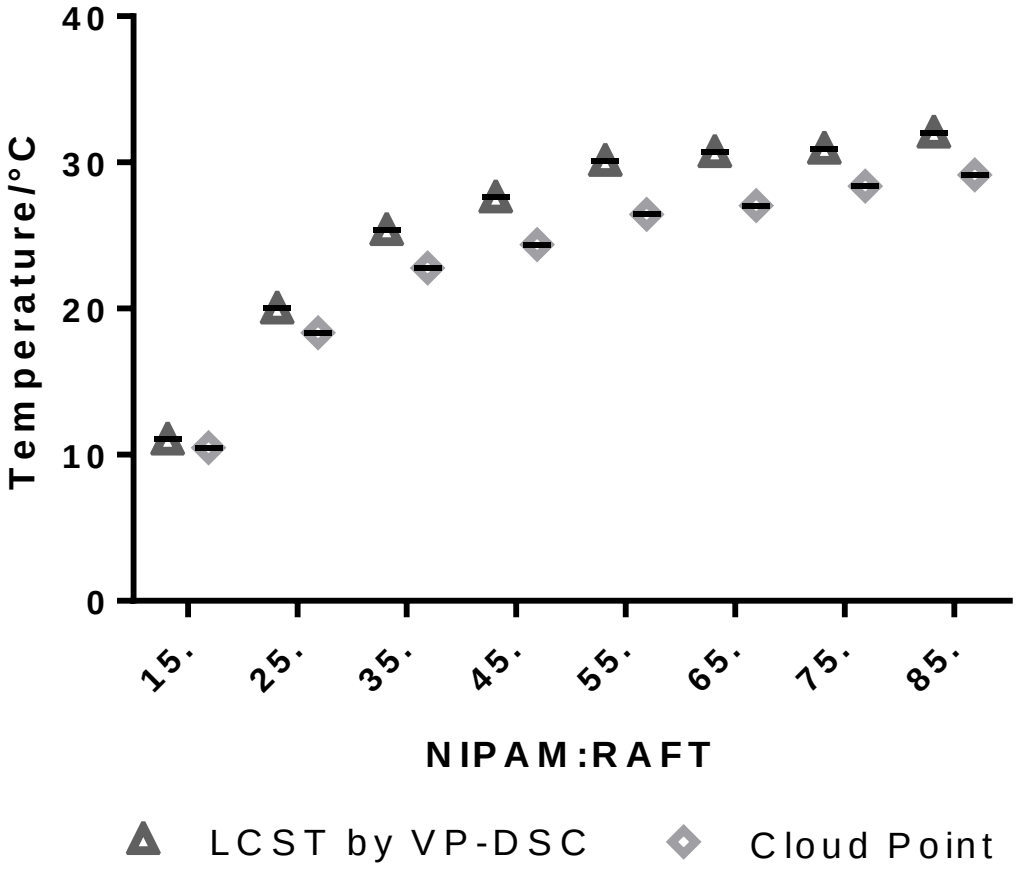

Figure 2.10 – Calorimetric LCST by VP-DSC and cloud point by onset of turbidity from UV-vis thermogram of HB-BNIPAM polymers. Standard error of mean shown.

The LCST by DSC are shown in Figure 2.12. The curves for cloud point section 8.4. THE LCST is shown to increase with increased branching. This is due to the increased incorporation of hydrophobic benzyl branching units from the RAFT agent (4-VBPCD). It has been widely reported that incorporation of a hydrophilic monomer unit or hydrophobic monomer unit will increase or decrease the LCST of PNIPAM respectively. [187] For the 10:1 sample a cloud point could not be measured as the polymer had already passed through to the globule state at 10°C

Figure 2.12 shows that a decreasing amount of the polymer mass is involved in the transition as the degree of branching increases. Between the 15:1 and 25:1 polymers there is a large step change in the amount of polymer undergoing a transition and the 10:1 polymer was insoluble in water at 5°C. It could be assumed that this is due to increased incorporation of benzyl branching units..

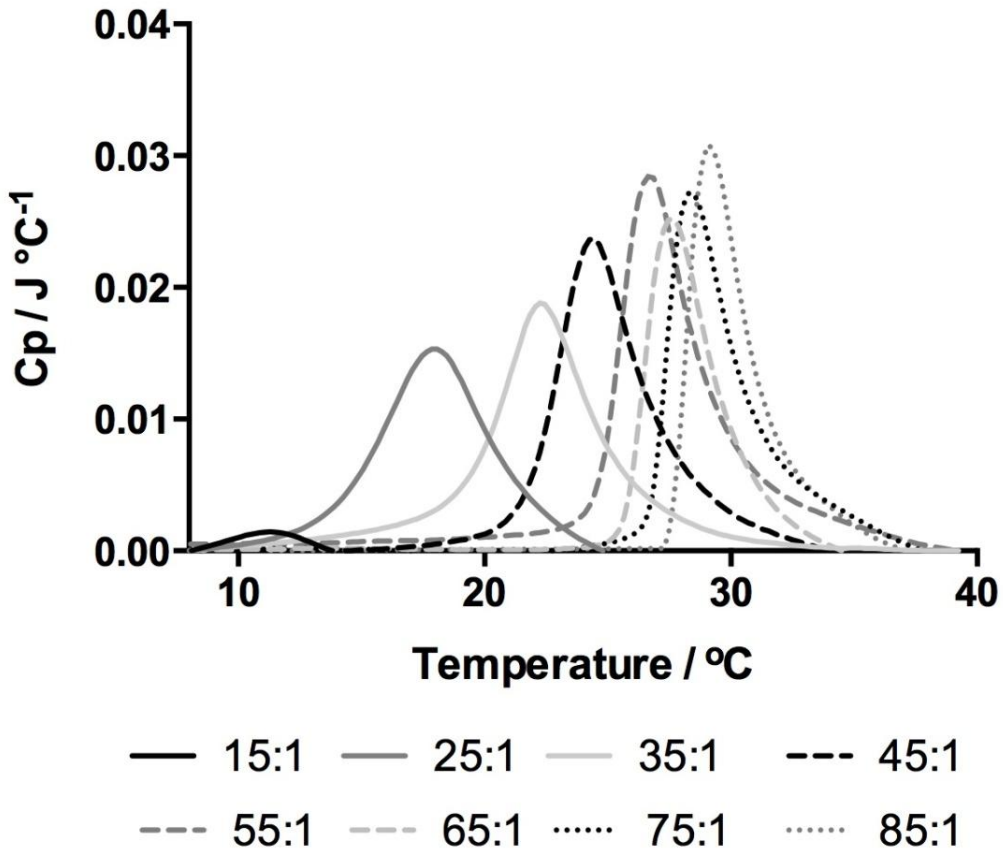

Figure 2.11 – A thermogram showing the endotherms for the LCST transition of HB-PNIPAM polymers in solution at a concentration of 5 mg ml^{-1}, as measured by VPDSC. The LCST is shown to decrease with increasing incorporation of the RAFT agent (4-VBPCD).

Further information about the structure of the polymer can be gained from analysis of the peak area of the VP-DSC thermograms. Figure 2.11 shows that the energy required (area under the curve) to cause the transition is dependent on the degree of branching. For a higher degree of branching the amount of energy for the transition is much lower. This effect is shown more clearly when the areas of the curves are plotted (Figure 2.12).

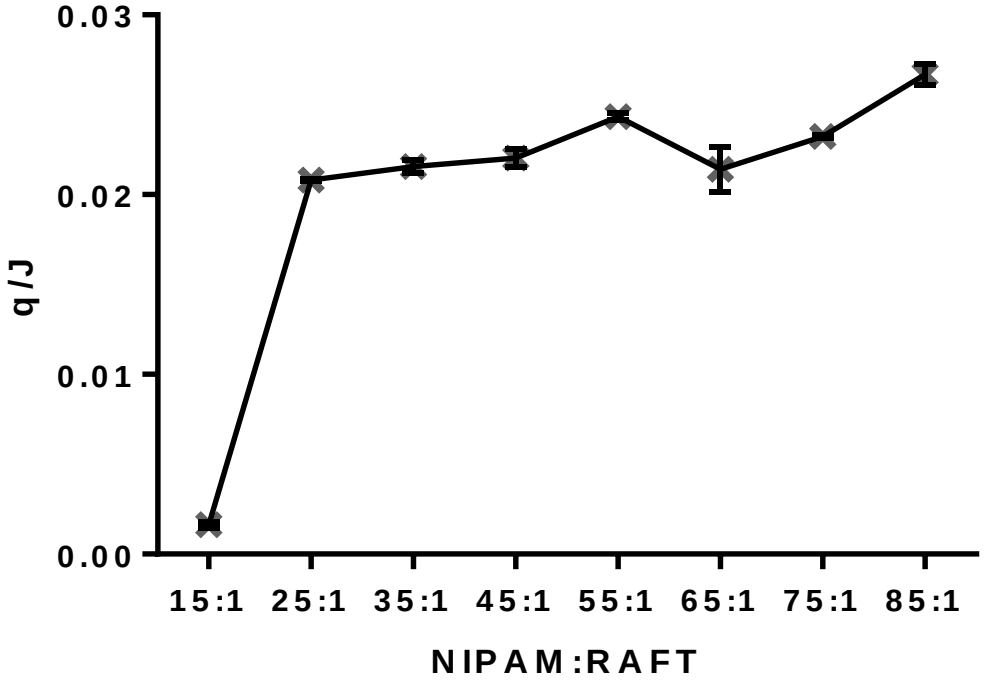

Figure 2.12 - Peak areas derived from micro-DSC measurements providing the heat released at the transition with errors bars showing standard errors of the mean

Additional hydrophilic ACVA should compensate for this effect to some degree. Furthermore, it has been shown that branching decreases the LCST independently from the effects of the hydrophobic branch points.[89] It must be considered that this is occurring *via* some other mechanism. By introducing more hydrophobic branching units to the core and more hydrophilic (ACVA) units to the polymer end groups. It is likely that a core-shell system. In this case, the inner core will be a dehydrated globule both above and below the observed LCST of the polymer. This area is not affected by temperature. The outer shell is a hydrated coil below the LCST, but will collapse into the globule above the LCST. This effect is dependent upon the degree of branching and becomes more prevalent with higher degrees of branching. A diagranm showing this effect is given in Figure 2.13. This will be further investigated using the solvatochromic dye Nile Red to probe the relative polarity within the polymer particles.

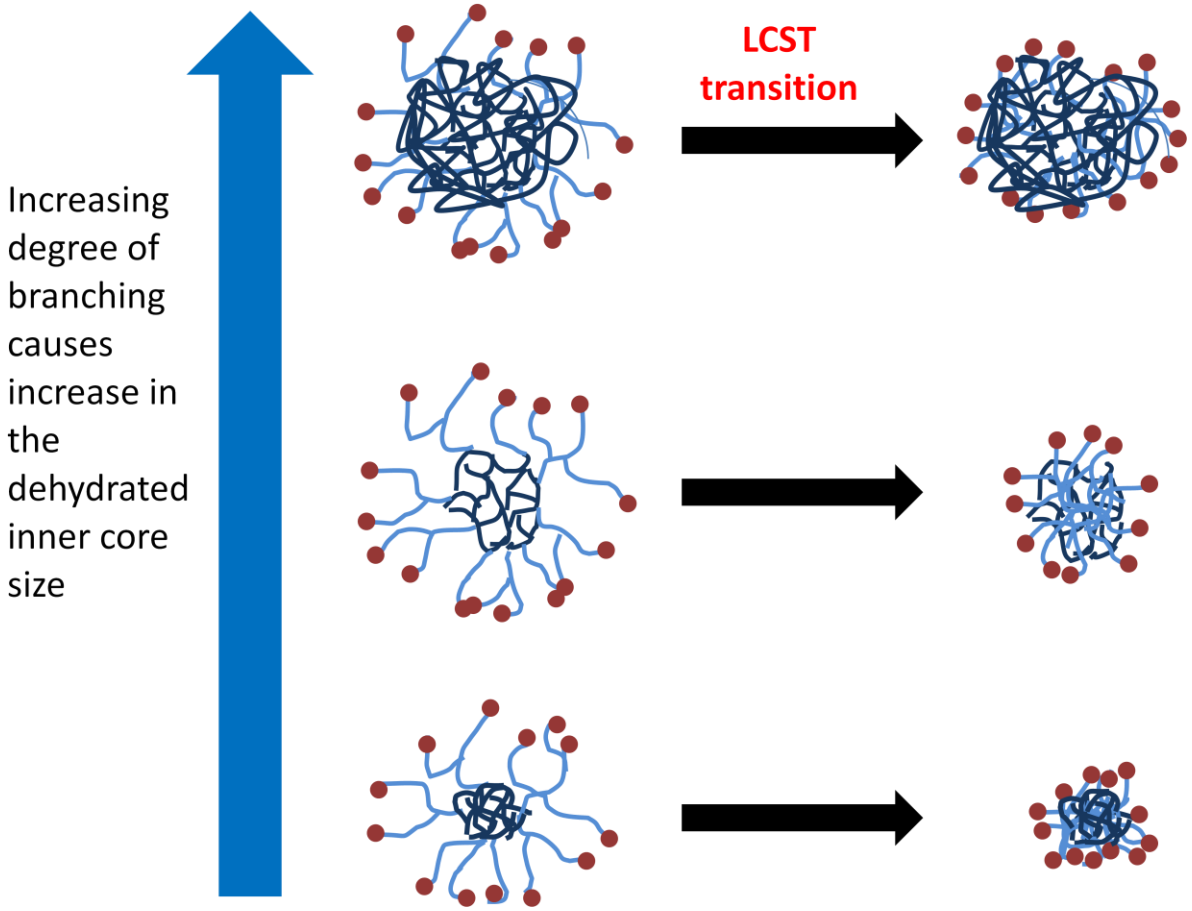

Figure 2.13 – A diagram showing how the increased degree of branching affects the relative size of the inner globular core and outer globular shell. A higher proportion of globular polymer in the core shell structure gives rise to a smaller energy for the transition for a given mass of polymer.

Figure 2.13 shows how the morphology of the core shell structure could change as a result of degree of branching. The increase in the proportion of the polymer that is in the globular state would result in a reduced energy requirement for the transition. As the relative amount of globular polymer increases, the amount of polymer going through the transition per unit mass of polymer decreases. Hence, the energy required for the transition decreases.

2.3.3.1 Use of a Nile Red to Probe LCST Behaviour

It has been shown that a great deal of control can be had over the LCST of the polymer. This opens up many potential applications of these polymers. Work has also been carried out using the fluorescent dye Nile Red, which has been dissolved inside the polymer using a

small amount of DMSO. The changing environment inside the PNIPAM nano-particles is manifested by the change in fluorescence intensity and wavelength of the Nile Red.

In order to give a comparison to the relative polarity experienced by the dye inside the polymer the Nile Red was dissolved into solvents of a range of polarities. The relative polarity of these solvents is known and can therefore be used as a comparison to polymer-Nile Red system. Figure 2.14 shows the fluorescence emission of Nile Red dissolved in various solvents, of known relative polarity, over a temperature range relevant to the LCST of HB-PNIPAM. The relative polarities of the solvents are given to the right of the curves.

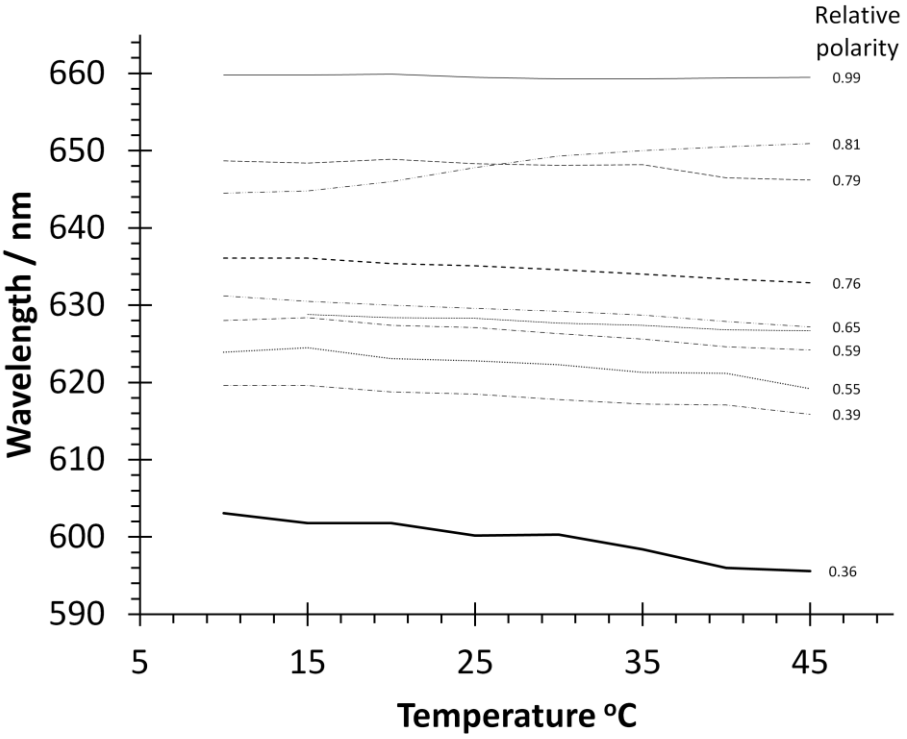

Figure 2.14 - Peak wavelength of fluorescence emission of dilute Nile Red in (from highest to lowest at 45°C) 99% water, glycerol, ethylene glycol, methanol, ethanol, DMSO, butanol, isopropanol, dimethyl formamide and acetone. The relative polarity of solvent shown by the numbers on right of each plot. *Data analysis courtesy of Thomas Swift from The University of Sheffield, Department of Chemistry.*

The calibration plot shown in Figure 2.14 was produced. This gave an emission for nile red in a system of known relative polarity. The polymers were then compared to Nile Red in these environments. This gives a relative environment that can be used to compare the changes observed in a PNIPAM system to the peak emission wavelength of Nile Red in a known solvent of known polarity.

The Nile red was then dissolved in the polymers using the method outlined in section 2.2.9. The Nile Red dye was then excited and its change in fluorescence emission was monitored. This was carried out across a temperature range so as to show the difference above and below the LCST. The results of this experiment are shown in Figure 2.15.

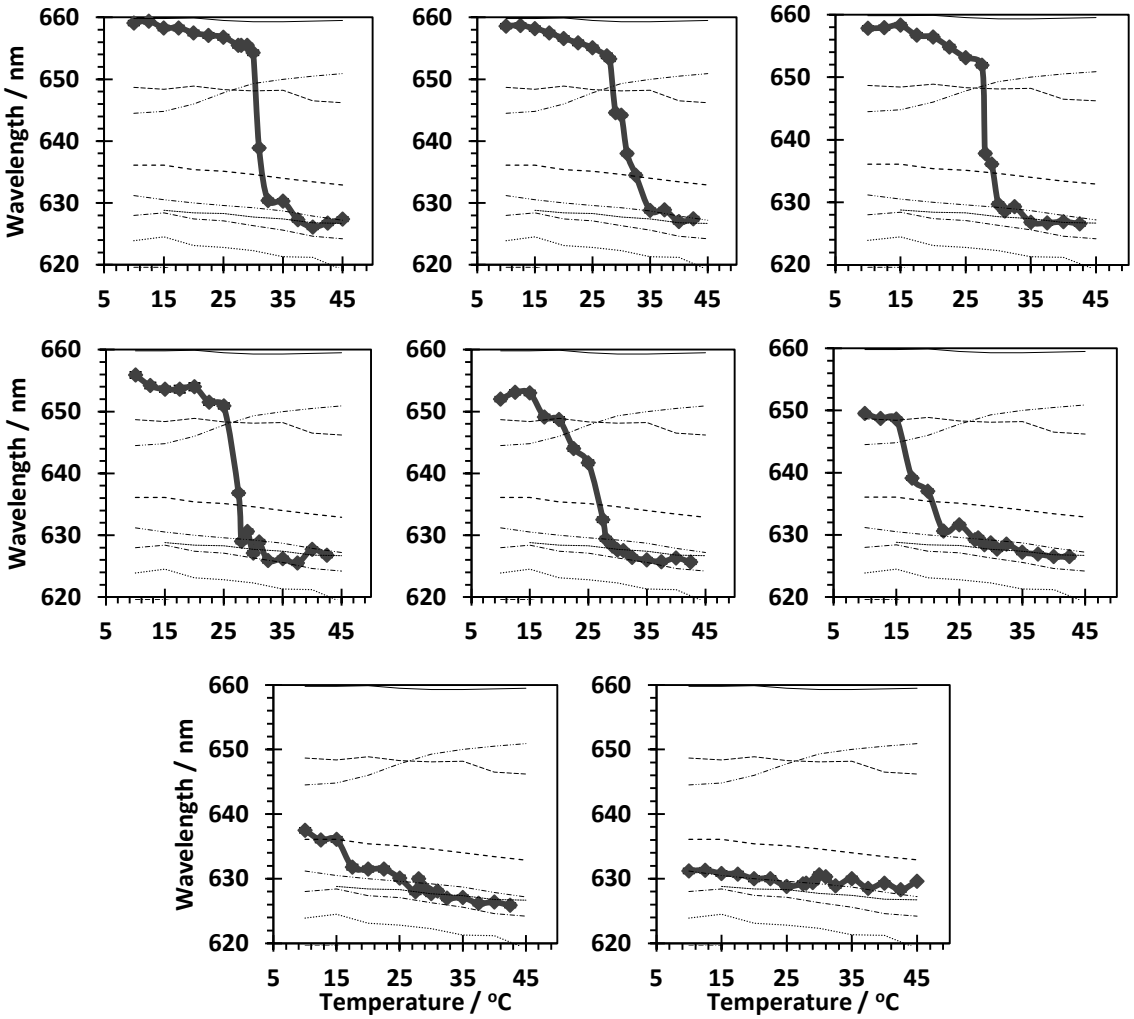

Figure 2.15 – A figure showing peak wavelength of fluorescence emission of dilute Nile Red / Polymer solutions following excitation at 580 nm displayed with comparative Nile Red / solvent shifts. Figure are in order 85:1, 75:1, 65:1, 55:1, 45:1, 35:1, 25:1, 15:1. The figure shows how the difference in the emission above and below the LCST is affected by the feed ratios of the polymers synthesised. This has important connotations for the structure of the polymers. *Data analysis courtesy of Thomas Swift from The University of Sheffield, Department of Chemistry.*

Figure 2.15 shows that the peak emission moves to lower wavelength as the polymer goes through its LCST. Using this as another measure of LCST, corroborates DSC and cloud point

data which shows as the degree of branching increases, the LCST shifts to lower temperature.

The largest changes in peak emission wavelength as the polymer undergoes the LCST transition are observed at a low degree of branching. For 85:1, 75:1 and 65:1 samples the wavelength falls from almost 660 nm to 525 nm. Comparing the emission wavelength of Nile Red within a polymer (Figure 2.15) to emission wavelength of Nile Red in a specific solvent (Figure 2.14) shows that at 10^{o}C the 85:1, 75:1 and 65:1 samples had a polarity only slightly lower than water (relative polarity 1). As the degree of branching increases the sub-LCST peak emission gradually decreased. The 35:1, 25:1 and 15:1 samples had peak emissions with relative polarity that corresponded to ethylene glycol (relative polarity 0.79), methanol (0.76) and ethanol (0.65) respectively. This suggests that below the LCST, with increased branching and increasing concentration of aromatic branching points the branched polymers provided an increasingly more hydrophobic environment in which the Nile Red was solvated.

When the polymers were above the LCST, all samples show a similar emission peak wavelength of approximately 628 nm. This suggests that the globular environment of all of the polymer systems is the same. The Nile Red solvated by the polymer globule had a relative polarity between that of ethanol and butanol (relative polarity 0.65 and 0.58). This is of key importance because in the 15:1 polymer there is no change in the fluorescence emission spectra above or below the LCST and there is very little change for the 25:1 polymer. These data indicated that there is no LCST transition for the 15:1 polymer. However, the VP-DCS and cloud point (turbidity) measurements show that this is not the case. The reason that the change in environment is not observed is that the Nile Red is dissolved by the polymer in the ‘core’. If this region of the polymer is collapsed above and below the LCST then no change will be observed by the solvatochromic dye. This has been outlined in Figure 2.13. In the 15:1 polymer this core region has become large enough that no change in environment is seen by the Nile Red. It is likely that this core-shell system will be present at other monomer feed compositions but to a lesser degree.

2.4 Conclusion

The traditional methods for polymer analysis assume a Gaussian distribution. Highly branched polymers may often have a bimodal distribution, but when analysed, this has often been ignored and the traditional method may be inappropriate for some polymer systems. An alternative means of analysis has been used to find measures of the average molecular weight and dispersity by using the first and third quartiles and median values.

Varying the degree of branching will have a wide ranging effect on PNIPAM properties. Most notably, the LCST which is highly dependent on the degree of branching. The more branching the lower the LCST. The reasoning for this is the incorporation of the hydrophobic benzyl branching unit. Incorporation of hydrophobic copolymer units into PNIPAM is known to decrease the LCST by nucleating the 'pearl necklace' structure before coil collapse.[86-87]

The degree of branching also has a substantial effect on molecular weights and the distributions of molecular weights observed for the polymer systems. At very high concentrations of 4-VBPCD the distribution loses the characteristic double peak in favour of single broad peak.

It has been shown in this work that the survival of the dithioate group (the number of pyrrole end groups per benzyl branching group, measured by NMR) appears to be relatively low. However, the sulphur concentration measured by elemental analysis is usually 70-80% of the expected value. It is suggested that a possible mechanism for this could be the loss of the pyrrole from the dithioester.

The data from VP-DSC and Nile Red fluorescence emission has shown existence of a core shell morphology below the LCST at some monomer feed ratios. This provided the first evidence for a polymer system where the central region is in the globular form with a hydrated outer shell.

HB-PNIPAM can be used to solvate Nile Red to produce an optical sensor. The change in polarity of the environment within the PNIPAM effects the peak emission of Nile Red in the same way as Nile Red would be effected by the polarity of its solvent.[134, 136-137] This gives a colourimetric measurement for the coil collapse. It has been shown that coil collapse can be driven by binding,[130] using the Nile Red in this manner would produce a visual confirmation of polymer binding.

3. GXGRGDS-HB-PNIPAM Polymers for Detachment of Human Cells from TCP

3.1 Abstract

GXGRGDS functionalised HB-PNIPAM polymers were synthesised and their suitability for detachment of cells from tissue culture plastic (TCP) was assessed. The ability of polymers to detach cells from the surface was highly dependent on the peptide sequence used. GVGRGDS and GGGRGDS were found to transfer the largest number of cells most consistently. HB-PNIPAM-COOH (acid ended HB-PNIPAM containing no peptide sequence) was found not to be significantly different from the control where no polymer was used. This demonstrated that the polymer alone does not bind strongly enough to the cells to detach them from TCP.

3.2 Experimental

3.2.1 Synthesis of 4-Vinylbenzyl Pyrrolecarbodithioate

The synthesis of 4-vinylbenzyl pyrrolecarbodithioate is covered in section 2.2.1.

3.2.2 Synthesis of Pyrrolecarbodithioate Ended HB-PNIPAM

The synthesis of pyrrolecarbodithioate ended HB-PNIPAM covered in section 2.2.2.

3.2.3 Carboxylic Acid Functionalisation of Pyrrolecarbodithioate Ended HB-PNIPAM

The concentration of pyrrole end groups was calculated from NMR. The pyrrolecarbodithioate ended HB-PNIPAM was dissolved in DMF (675 mL). ACVA (45 g, 20 eq) were reacted for 24 hours. The process was repeated twice, a total of 60 eq of ACVA had been added. The solvent was removed by rotary evaporation. The product was precipitated dropwise into diethyl ether, dried under vacuum then purified by ultrafiltration. The polymer (0.5 g) was dissolved in acetone:ethanol (9:1) (300 mL) The solution was concentrated to 50 mL by ultrafiltration. The solution was made up to 300 mL again and the process repeated three times. The remaining solvent was removed by rotary evaporation.

The polymer was characterised by NMR, GPC and cloud point. The cloud point was measured by turbidity of a 5 mg ml^{-1} solution in water. The cloud point was found to be 22°C.

A list of the peaks from NMR with their associated splitting patterns is shown below. The molecular weight averages and dispersity (Đ) of the polymer are detailed in the list below. The NMR spectrum is given in section 8.1.

1H NMR (400 MHz, CDCl3) (ppm): δ 0.9-1.3(6H, br, s, -N(CH_3)$_2$), δ 1.4–1.8 (2H, br, m, -CH2-CH-C_6H_4-), δ 1.9–2.2(2H, br, m, -CH_2-CH-CO-NH-) and δ (1H, br, m, CH_2-CH-CONH-), δ 4.0 (1H, br, s, (CH_3)$_2$CH-), δ 6.6–7.2 (br, m, -Ar-), δ 7.85 (br, s, -NH-CO-)

GPC (DMF 1%LiBr, 60°C): M_n -3350 g mol^{-1}, M_w - 24850 g mol^{-1}, M_z -103300 g mol^{-1}, M_{z+1}-236300 g mol^{-1}, Đ - 7.5

LCST (Cloud Point): – 22°C

3.2.4 Synthesis of GXGRGDS Peptide

The reaction scheme for peptide synthesis is indicated in Figure 3.1. Pre-loaded Serine-Wang resin was used. A programme written in '735 sampler software,' was run on a ChemSpeed® automated peptide synthesiser. Serine loaded Wang resin was swollen in DMF for 24 hours. The Fmoc protected amino acids were added sequentially. To couple each amino acid; 5 equivalents of each amino acid, 4.9 equivalents of the coupling agent PyBOP[i], 10 equivalent of the coupling agent DIPEA were added. The Fmoc protecting groups were removed by triple deprotection with 20% piperidine in DMF, and the peptide chain was built up from the resin bound Serine until the final Glycine was added.

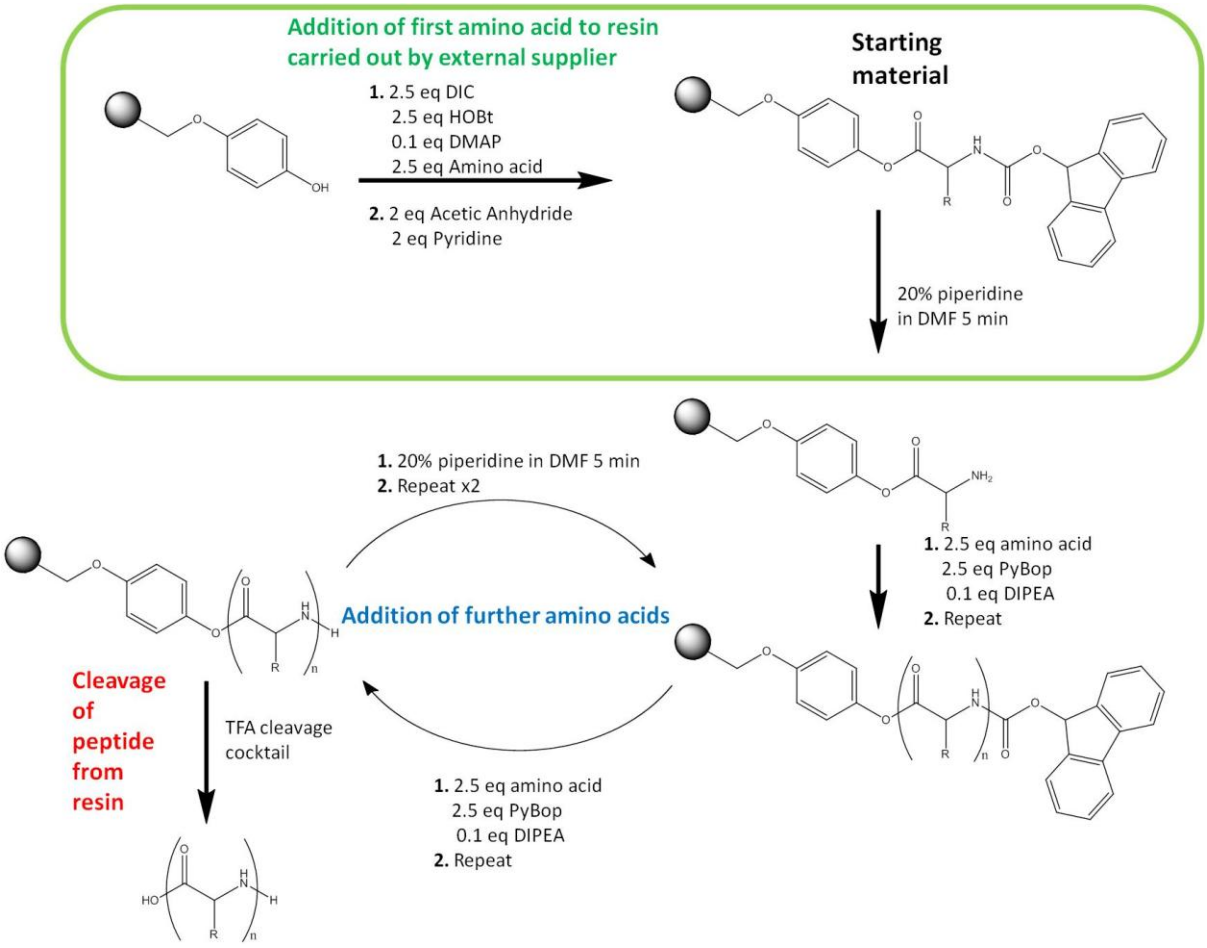

Figure 3.1 – A figure showing the reaction scheme for the synthesis of a polypeptide chain. The area within the green box shows the initial addition of the first peptide in the sequence to the resin. This is followed by repeated addition of further amino acids in a protection addition deprotection reaction. The final peptide sequence is removed from the resin by cleavage with TFA.

The process outlined in Figure 3.1 was carried out for each GXGRGDS peptide sequence to yield the nine peptide sequences shown in Figure 3.2. The resin was washed sequentially with DMF, DCM and methanol, dried and subsequently stored at -18°C.

Peptide Sequence	Structure
GDGRGDS	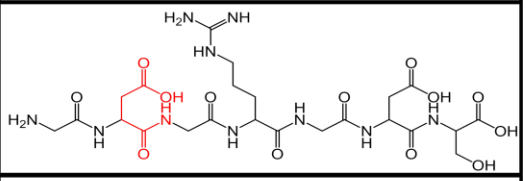
GGGRGDS	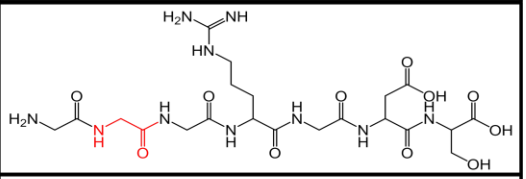
GPGRGDS	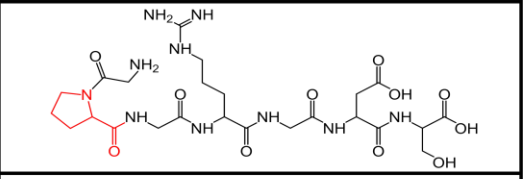
GQGRGDS	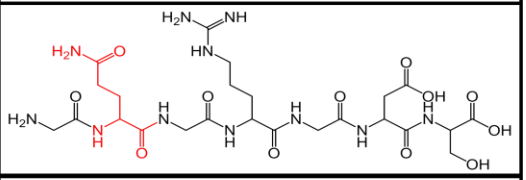
GRGDS	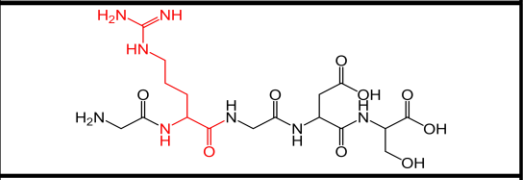
GRGRGDS	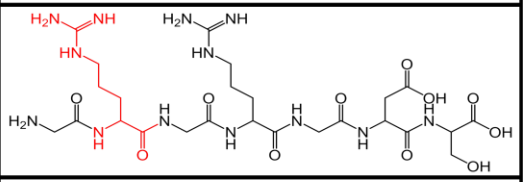
GSGRGDS	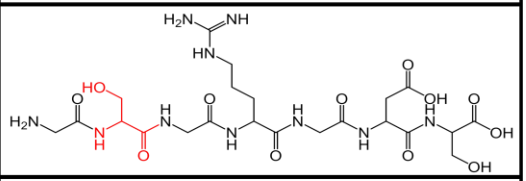
GVGRGDS	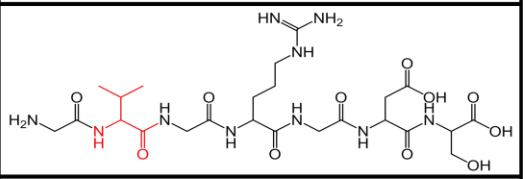
GYGRGDS	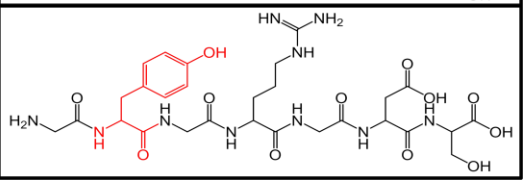

Figure 3.2 - Structures of the synthesised GXGRGDS peptide sequences.

3.2.5 Cleavage of Peptide from Resin

A TFA cleavage cocktail containing trifluoroaceatic acid (TFA), water, phenol and triisopropylsilane (TIPS) in the ratio 88:5:5:2 was added to the resin at 10 mL g^{-1} with stirring for two hours. The resin was filtered off and washed with cleavage cocktail and three times with TFA. The TFA was removed by rotary evaporation with two CO_2(s) and acetone cold traps in series to protect the vacuum pump. The remaining TFA was removed by triturating with five aliquots of diethyl ether. The remaining ether was removed by rotary evaporation and the product stored at -8°C.

The peptide was purified by prep HPLC and freeze dried, yielding a white fluffy solid.

The peptides were characterised by LC-MS using an electrospray ionisation detector. The data is shown in Table 3.1.

Table 3.1 – A table of the mess spectroscopy data for GXGRGDS peptides. The mass of the MH^+ molecular ion measured by electrospray mass spectroscopy is shown for each peptide along with its calculated (expected) mass

Peptide Sequence	Measured Mass	Calculated Mass
GDGRGDS	663.3	663.26
GGGRGDS	605.3	605.26
GPGRGDS	645.3	645.29
GQGRGDS	676.3	676.29
GRGDS	490.0	490.21
GRGRGDS	704.3	704.34
GSGRGDS	635.3	635.27
GVGRGDS	646.3	646.3
GYGRGDS	711.2	711.3

3.2.6 Synthesis of GXGRGDS-HB-PNIPAM

The reaction scheme for the addition of GXGRGDS peptides to the HB-PNIPAM-COOH is shown in Figure 3.3.

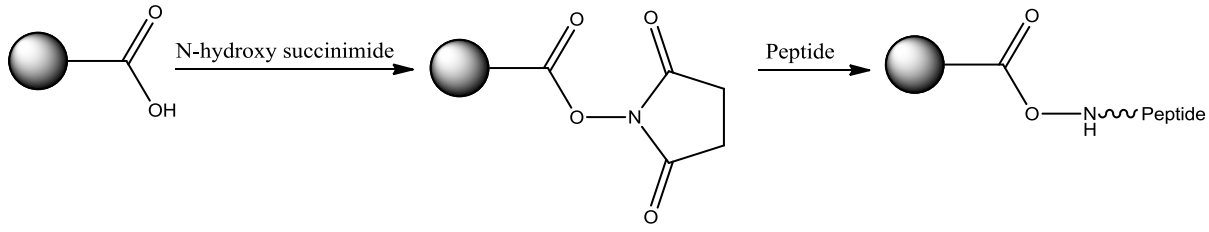

Figure 3.3 - A reaction scheme for the addition of peptide to the HB-PNIPAM-COOH by NHS activation.

200 mg of HB-PNIPAM-NHS was added to a flask at 0°C in 0.1 mol dm^{-3} pH 8.5 phosphate buffer under N_2 atmosphere with stirring. 5 molar equivalents of the appropriate peptide were added to the reaction. The reaction was allowed to warm to room temperature and the reaction continued for 48 hours. This procedure was repeated for each of the GXGRGDS peptide sequences.

The polymers were purified by ultrafiltration in ultrapure water (3x 300 mL). The purified products were freeze dried yielding white fluffy solids.

^{1}H NMR spectra were taken of the polymer and subsequently the concentration of peptide end groups was calculated from the NMR. The peaks of interest are shown in Figure 3.4. The integrals of these peaks were measured and are shown in Table 3.2. These integrals were used to calculate the concentration of peptide per gram of polymer using Equation 3.1. The spectra for the HB-PNIPAM-GXGRGDS peptides can be found in section 8.1.

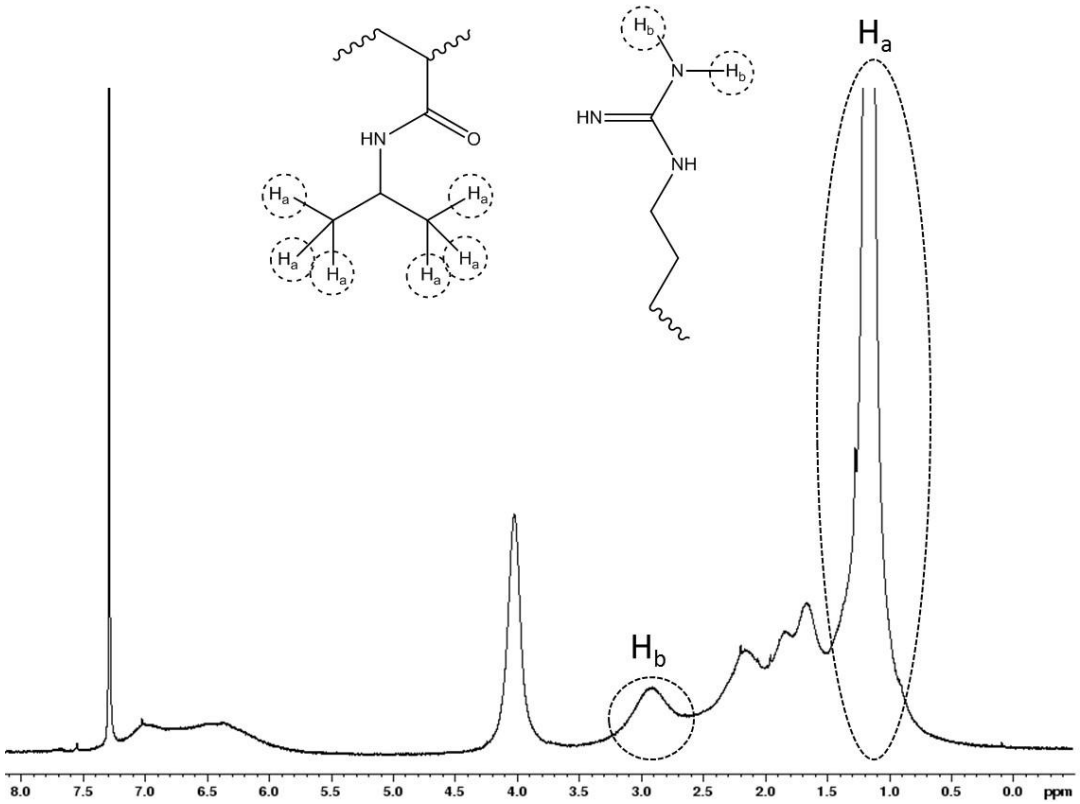

Figure 3.4 – An example of a ^{1}H NMR spectrum showing relevant peaks for NIPAM isopropyl protons and guanidine protons used for functionality calculations.

Table 3.2 – A table showing the integrals of isopropyl and guanidine peaks from NMR spectra of HB-PNIPAM polymers.

Sample ID	∫ NIPAM Isprpopyl	∫ Guanidine
GDGRGDS	1	0.1347
GGGRGDS	1	0.1184
GPGRGDS	1	0.1408
GQGRGDS	1	0.1667
GRGDS	1	0.2136
GRGRGDS	1	0.1987
GSGRGDS	1	0.1217
GVGRGDS	1	0.1203
GYGRGDS	1	0.1368

The integrals of the isopropyl and guanidine peaks measured from the NMR spectra (Table 3.2) were used to calculate functionality Equation 3.1

$$Functionality = 1 / (M_r\ NIPAM \times \frac{1H\ Guanidine}{1H\ NIPAM} + M_r\ RAFT)$$

Equation 3.1

3.2.7 Cell Lifting Protocol

The cell lifting protocol has been adapted from the method of S. Hopkins *et al*.[80] HDFs between passage 4 and 9 (P5, P7 and P8) were seeded into tissue culture well plates and cultured for 48 hours to allow the cells to adhere to the TCP surface. The polymers were dissolved in serum free DMEM (1% L-Gul, 1% PS, 1% fungizome) at 0.5 mg mL^{-1}. The polymer was stored at 5°C for 16 hours to ensure it had fully dissolved. Media was removed from the cultured cells and replaced with the polymer solutions. The cells were incubated at 37°C (5% CO_2) for 24 hours. The lifted cells were transferred to a new well plate, 1 mL of room temperature, polymer free, 10% FCS DMEM (1% L-Gul, 1% penicillin streptomycin, 1% fungizome) was added. Incubation of cells at room temperature for 45 minutes allowed the polymer to release the cells and the deposited cells to adhere to the TCP. The cells were washed with polymer-free, 10% FCS DMEM to remove remaining polymer, then incubated at 37°C.

3.2.8 Alamar Blue Assay Protocol

The standard AlamarBlue® protocol was followed.[188] A 1 mg mL^{-1} solution of resazurin was made up in PBS solution. This was diluted 1:10 in 10% FCS DMEM to make a stock solution of AlamarBlue®. 1mL of AlamarBlue® stock solution was added to each well. The cell plates were incubated at 37°C with 5% CO_2 for 4 hours. Absorbance was measured at 570 nm and 600nm.

3.2.9 Picogreen Assay

A Quant-iT™ PicoGreen® dsDNA Assay Kit from life technologies containing Quant-iT™ PicoGreen® dsDNA reagent, 20x TE, and Lambda DNA standard was used. The assay was carried out according to the Quant-iT PicoGreen dsDNA Reagent and Kits assay protocol by molecular probes invitrogen detection technologies.

The 20x TE buffer was diluted 20 fold in distilled water. The TE buffer was used to make a x200 dilution of the concentrated Quant-iT™ PicoGreen® reagent. This was covered with foil and stored at 5°C

A calibration curve was made up using the supplied 100 µg mL^{-1} dsDNA standard. The formulations are shown in Table 3.3.

Table 3.3 – A table showing volumes of reagents for preparing standard curve which will be used in the PicoGreen® assay for double stranded DNA.

Volume (µL) of TE	Volume (µL) of 2 µg ml^{-1} DNA Stock	Volume of Quant-iT™ PicoGreen® Reagent	Final DNA concentration in Quant-iT™ PicoGreen® assay / ng mL^{-1}
0	1000	1000	1000
900	100	1000	100
990	10	1000	10
999	1	1000	1
1000	0	1000	0

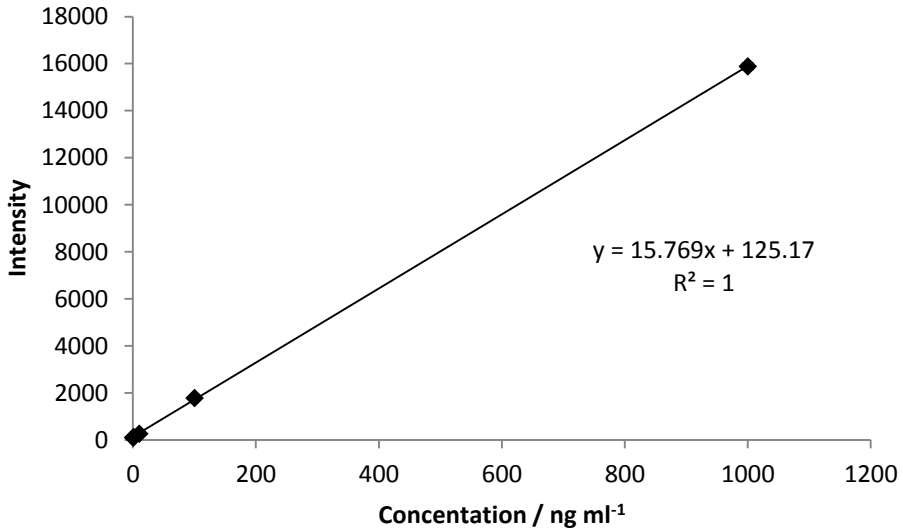

Figure 3.5 – A figure showing the calibration curve produced for dsDNA quantification with Quant-iT™ PicoGreen® Reagent.

1 mL of TE buffer was added to the test samples and the cells were lysed by 3x freeze thaw process. 1 mL dilute Quant-iT™ PicoGreen® reagent was added to each well and incubated for 5 minutes. Fluorescence emission was measured by exciting at 485 nm and fluorescence intensity was measured at 520 nm.

3.2.10 Analysis of Variance (ANOVA)

The name ANOVA comes from the Analysis of Variance. This is a statistical test that is used to compare variance within a group of measurements to the variance between groups of measurements. This is shown in Figure 3.6. This statistical test is similar to the t-test but it can be used for two or more sets of data where the t-test can only be used to compare two sets of data. In the ANOVA statistical test it is assumed that the variance within a group is a measure of the error associated with the measurement (within a group there should be no change in the independent variable. These are repeat measurements). Therefore, if there is more variation between the groups of measurements than within the groups, then the groups are said to be statistically different. In this case the null hypothesis would be rejected. The raw experimental data Figure 5.6 has been used to illustrate the point in Figure 3.6.

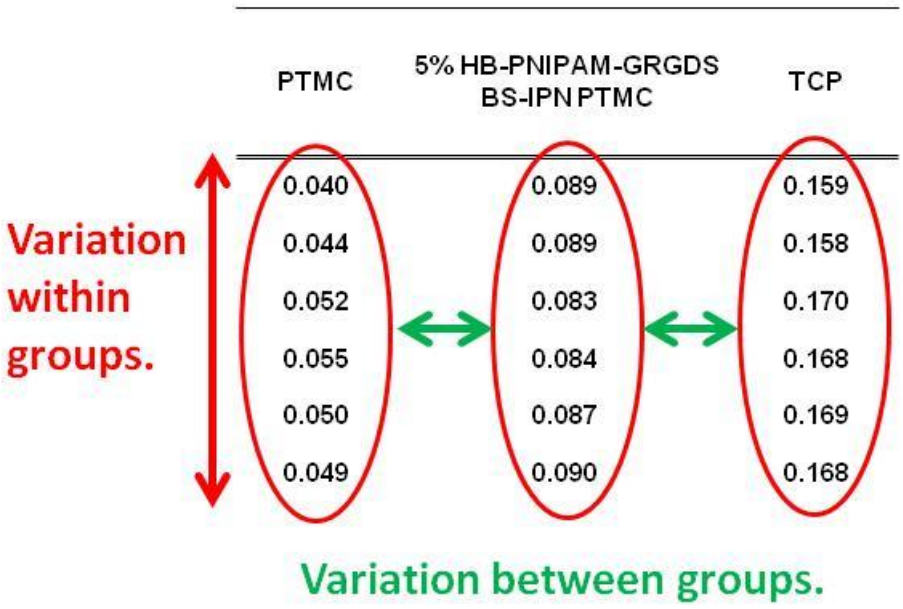

Figure 3.6 - A figure showing the 'within groups' and 'between groups' data which will be compared using an ANOVA analysis.

Figure 3.6 shows repeated measurements for the viability of cells measured by MTT assay. Six repeat measurements are shown for three surfaces on which the cells were grown (PTMC , 5% HB-PNIPAM-GRGDS BS-IPN PTMC and TCP). The data show that within a group there is little spread across the measurements. However, between groups there is a big difference in the measurements. In this case the ANOVA statistical test shows that each set

of experimental conditions gives a statistically different result on the cell viability. The ANOVA calculations were carried out using ‘GraphPad Prism6’ software.

3.3 Results and Discussion

When assessing the effectiveness of each HB-PNIPAM-GXGRGDS polymer it was important to consider the concentration of each peptide end group. This was assessed by NMR using the method described in section 3.2.4 Synthesis of GXGRGDS Peptide. Calculations from NMR data in Table 3.4 shows that the concentration of peptide per gram of polymer was consistent for the polymers. Therefore, direct comparisons can be made between the polymers provided they are used at the same weight concentration.

Table 3.4 - Concentrations of GXGRGDS peptide expressed in GXGRGDS per branch point and functionality measured in moles of GXGRGDS per gram of polymer.

Sample ID	Functionality / mmol g^{-1}
GDGRGDS	3.55
GGGRGDS	3.58
GPGRGDS	3.54
GQGRGDS	3.48
GRGDS	3.39
GRGRGDS	3.42
GSGRGDS	3.58
GVGRGDS	3.58
GYGRGDS	3.54

The cell GXGRGDS-HB-PNIPAM polymers were used to lift cells and deposit them into new well plates. After 16 hours the cells were imaged showing the difference in cell number for the GXGRGDS polymers. Phase contrast images showing the control samples, HB-PNIPAM-COOH (negative control), control (no polymer) (negative control) and trypsin (positive control) are shown along with three of the best performing test samples, GGGRGDS, GSGRGDS and GVGRGDS-HB-PNIPAM in Figure 3.7. Phase contrast images of all of the tested samples can be found in the Appendix.

Remaining cells
Deposited cells
Before polymer addition
Control. No polymer
HB-PNIPAM-COOH
Trypsin

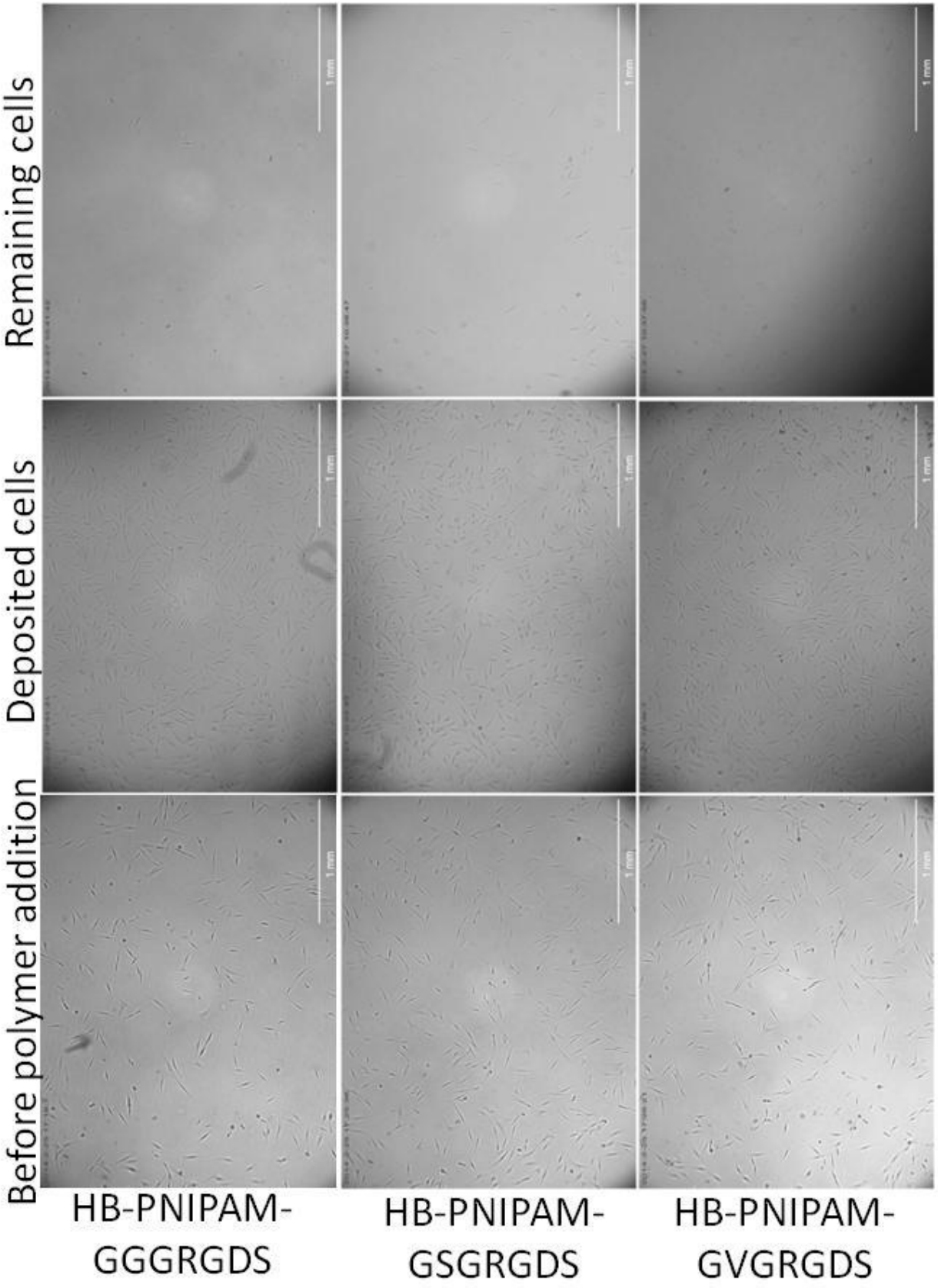

Figure 3.7 - Phase contrast images, using x4 objective lens, of normal human dermal fibroblasts grown on tissue culture plastic before addition of peptide functional HB-PNIPAM, 24 hours after being reseeded on TCP, after being lifted by peptide functional

HB-PNIPAM and remaining cells 24h after HB-PNIPAM lifting. Three controls and three of the best performing GXGRGDS-HB-PNIPAMs shown.

Qualitative examination of the images shows a clear difference in the performance of the GXGRGDS peptide functional polymers. GGGRGDS, GSGRGDS, GSGRGDS and GVGRGDS-HB-PNIPAM seem to have deposited a large number of cells. The AlamarBlue® and PicoGreen® assays that measure cell viability and DNA concentration respectively substantiate the cell density estimate from phase contrast images.

3.3.1 Cell Viability by AlamarBlue® Assay

The cells were lifted from TCP before redepositing into new tissue culture plastic wells. Figure 3.8 shows the data for AlamarBlue® assay of the deposited and remaining cells.

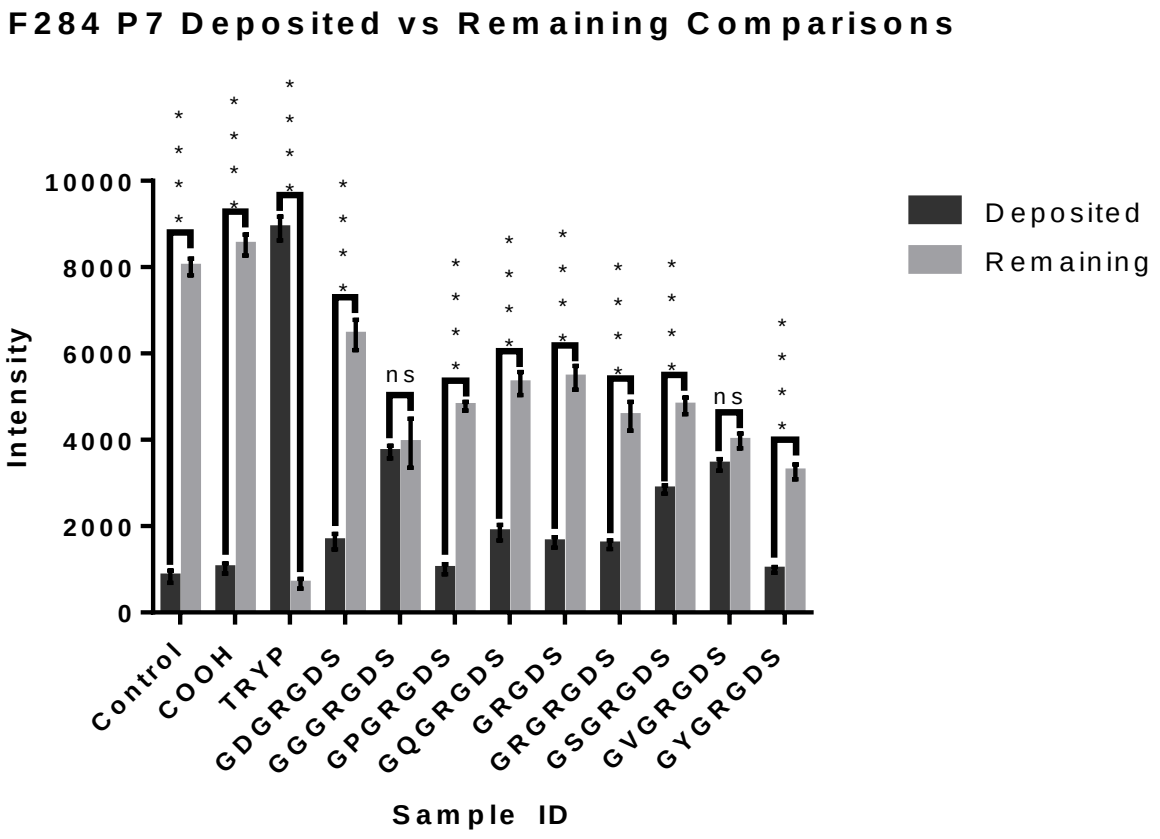

Figure 3.8 - Histogram of AlamarBlue® assay on HB-PNIPAM-GXGRGDS fibroblast transfer experiment with normal human dermal fibroblasts showing comparison of deposited and remaining cells. Statistical significance measured by one way ANOVA, level of significance indicated by asterisks (P<0.0001).

The AlamarBlue data in Figure 3.9 shows that the HB-PNIPAM polymers are able to transfer cells from TCP. These data have been compared to the negative control with no polymer, the positive control with trypsin and the acid ended polymer with no peptide attached.

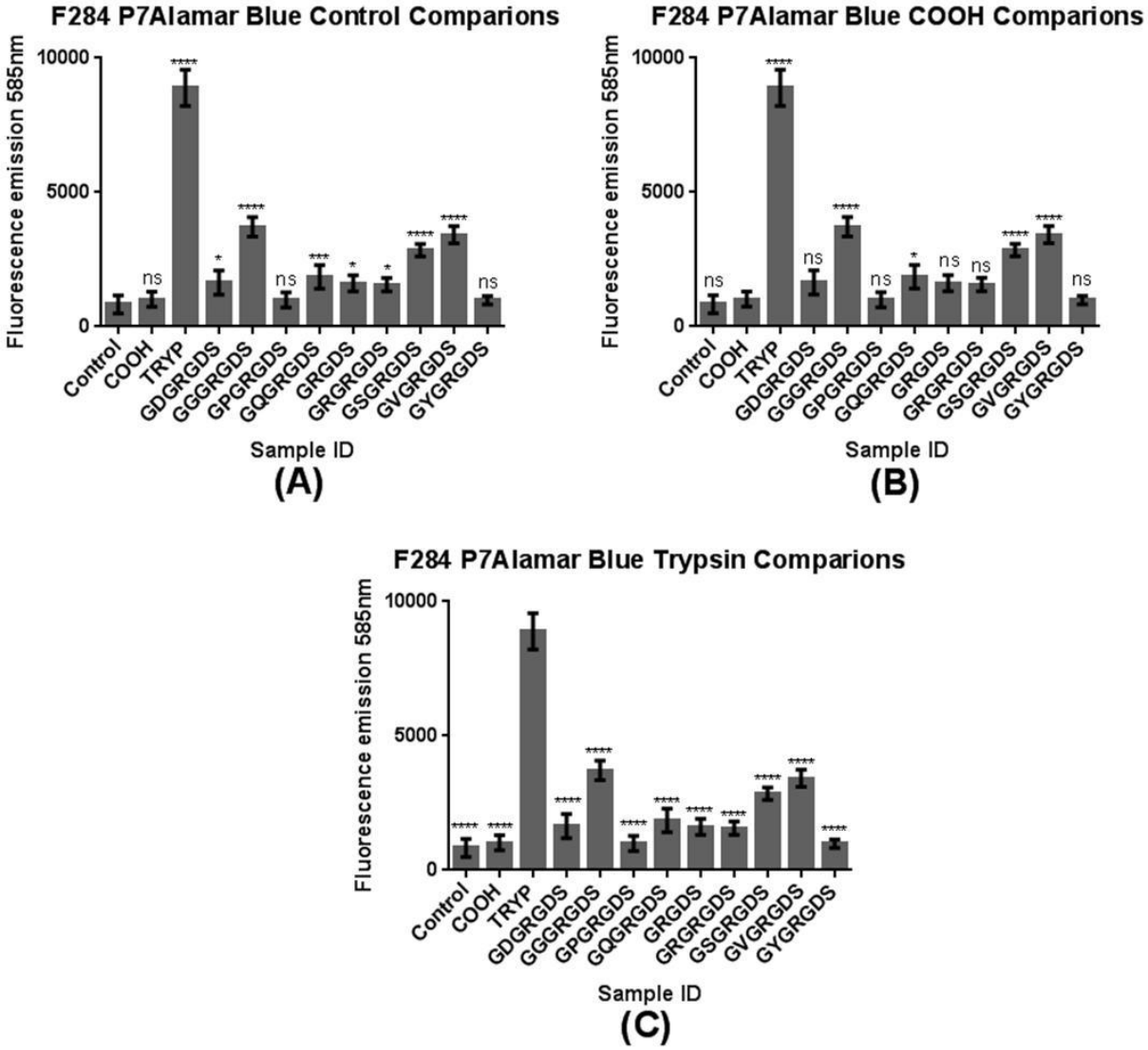

Figure 3.9 - Histogram of AlamarBlue® assay on HB-PNIPAM GXGRGDS fibroblast transfer experiment with normal human dermal fibroblasts. Statistical significance measured by one way ANOVA with multiple comparisons. Level of significance indicated by asterisks above. (A) - ANOVA comparisons to the no polymer control (negative control), (B) – ANOVA comparison with COOH functional HB-PNIPAM (HB-PNIPAM-COOH) (negative control) and (C) – ANOVA comparison to Trypsin (positive control).

In order to perform this effectively they must not only lift the cells at 37°C, but they must also release the cells on cooling allowing the cells to reattach to the new substrate. These data also demonstrated that both the transferred and remaining cells are still viable. Thus, the polymer has no cytotoxic effect at the experimental concentration.

One way ANOVA tests of the data in Figure 3.8 showed that the HB-PNIPAM GXGRGDS polymers deposited fewer cells than trypsin. In all cases the metabolic activity, by AlamarBlue® assay, was proven to be statistically lower than for the trypsin passaged cells. Indicating that fewer cells were transferred.

Compared to the negative controls GGGRGDS, GSGRGDS and GVGRGDS were shown to be statistically different from both 'no polymer' control and the HB-PNIPAM-COOH control. The peptide functional polymers did not perform as well as trypsin. This result is to be expected as the polymer does not digest the extra cellular matrix to remove the cells. Therefore it is likely that some cells will not be removed but will remain trapped in the matrix.

From the AlmarBlue® data, it appears that the HB-PNIPAM-GXGRGDS have performed similarly although HB-PNIPAM-GYGRGDS seems to show low metabolic activity, whilst GVGRGDS, GSGRGDS and GGGRGDS seem to have the highest metabolic activity. Whilst carrying out the experiment it was noted that GYGRGDS had lifted the cells but was unable to deposit them. This is shown in the phase contrast images in

Figure 3.7 where no cells are present on the deposited or remaining images. It is likely that the interaction of the peptide here is too strong and does not allow the cells to be released.

To give an accurate indication of cell number rather than metabolic activity (which could be altered by the addition of the polymers) a PicoGreen® DNA quantification assay was used. The PicoGreen® assays in

Figure 3.10 shows that GGGRGDS, GRGRGDS and GVGRGDS have transferred more cells than the other polymers. Although there are inconsistencies in the results this can be accounted for by biological variability between batches of primary human cells. The general trend shown within the deposited polymers remains fairly consistent especially between F284 P7 and F283 P5 experiments. There is a change in the relative fractions of deposited cells for the F284 P8 cells. However, this could be due to the fact that these cells are nearing the end of their lifetime as they are typically used until P9.

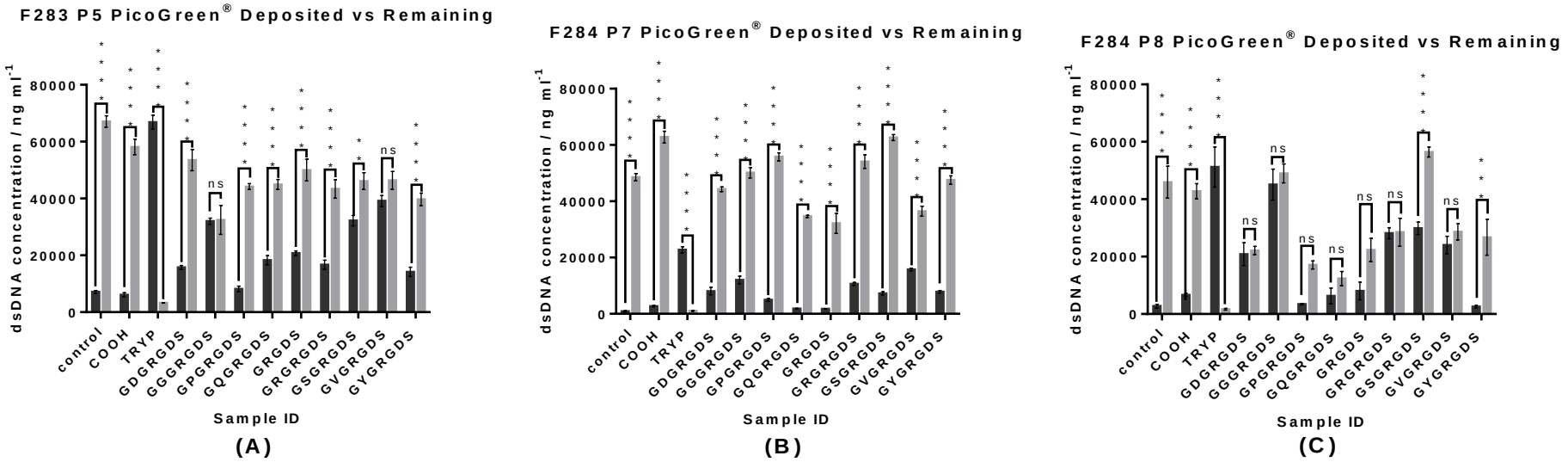

Figure 3.10 – A figure showing histograms of Picogreen ds-DNA quantification assay on HB-PNIPAM GXGRGDS fibroblast transfer experiment with normal human dermal fibroblasts at P5 (A), P7 (B) and P8 (C). Statistical significance was determined by one way ANOVA with multiple comparisons. The level of significance is indicated by the asterisks above. Deposited cells dark grey, remaining cells light grey. These data show that the polymers are able to transfer cells and that the peptide sequence on the polymers has a significant effect on their ability to do this.

Further statistical analysis of the results was carried out by means of ANOVA. Although these systems do not have any direct comparison in the literature, they can be compared to peptide functional PNIPAM surfaces used to produce cell sheets. RGD concentration has been observed to have a significant effect rate of detachment of cell sheets.[79] The endothelial cells used did detach more slowly with increasing RGD concentration, but did reach 100% detachment. Whereas, the most effective HB-PNIPAM-GXGRGDS particles transfer of approximately 50% of the cells. The amount of cells transferred by PNIPAM surfaces is much higher than in the HB-PNIPAM-GXGRGDS system, however, the specialised tissue culture wells are not required and centrifuging a cell suspension is unnecessary.

Further analysis of the deposited cells was carried out to determine which peptide functional polymer could transfer the most cells. One way ANOVA was used to compare the concentration of DNA from the lysed deposited cells.

GXGRGDS functional HB-PNIPAM polymers have been compared to the control samples by one way ANOVA in Figure 3.11, Figure 3.12 and Figure 3.13.

The data show that GGGRGDS, GRGRGDS, GSGRGDS and GVGRGDS are consistently better than the polymer free control and the HB-PNIPAM-COOH control. The peptide functional polymers do not perform as well as the trypsin with the exception of HB-PNIPAM-GGGRGDS, which is not significantly different from trypsin in F284 P8 experiment.

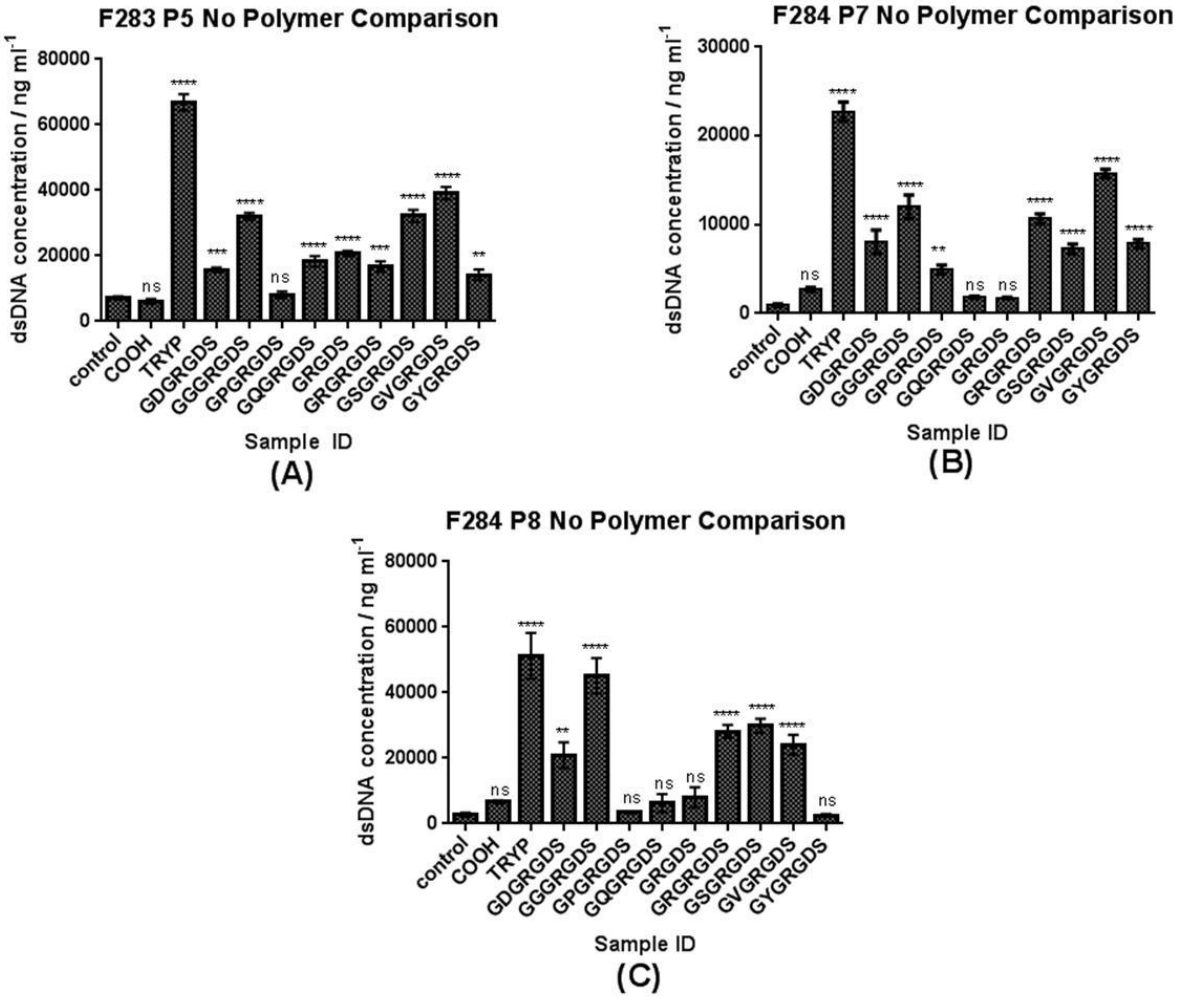

Figure 3.11 – Histogram of PicoGreen® assay on HB-PNIPAM-GXGRGDS deposited primary human fibroblasts from cell transfer experiment. Statistical significance measured by one way ANOVA with comparisons to the negative control with no polymer. Level of significance indicated by asterisks above. (A) – P5 primary human fibroblasts, (B) – P7 primary human fibroblasts (C) – P8 primary human fibroblasts.

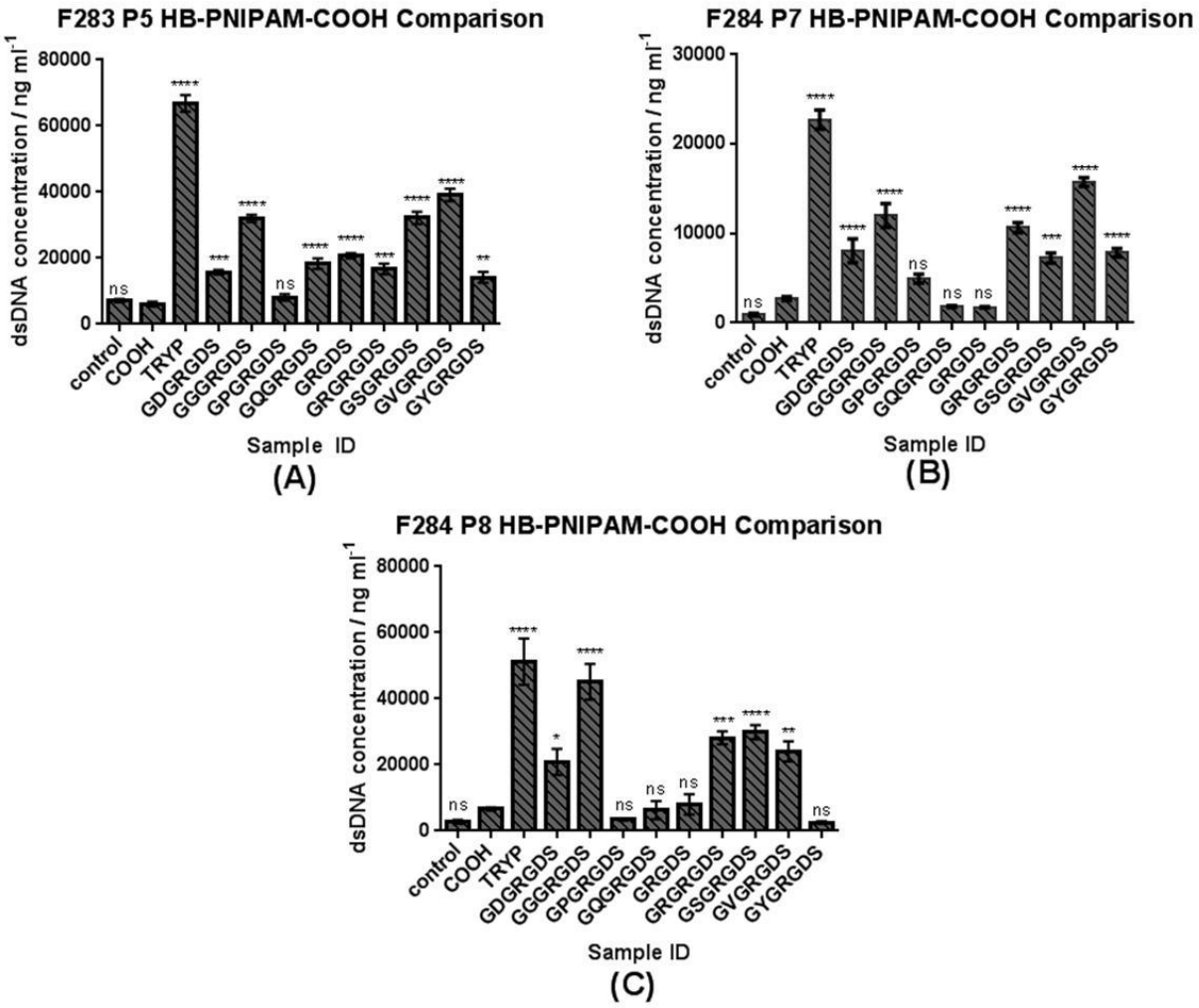

Figure 3.12 - Histogram of PicoGreen® assay on HB-PNIPAM-GXGRGDS deposited primary human fibroblasts from cell transfer experiment. Statistical significance measured by one way ANOVA with comparisons to the negative control with non-peptide-functional HB-PNIPAM (HB-PNIAM-COOH). Level of significance indicated by asterisks above. (A) – P5 primary human fibroblasts, (B) – P7 primary human fibroblasts (C) – P8 primary human fibroblasts.

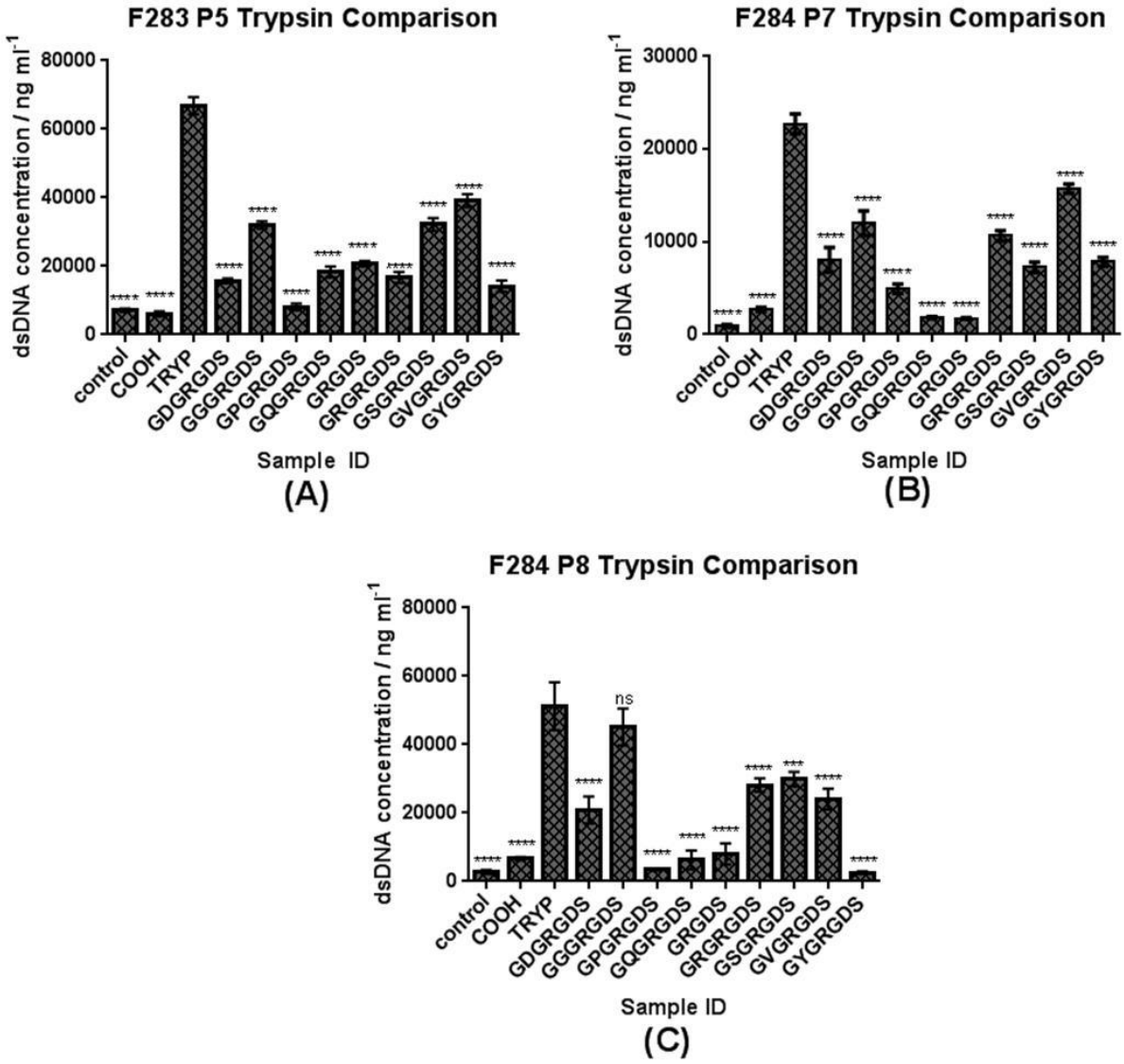

Figure 3.13 - Histogram of PicoGreen® assay on HB-PNIPAM-GXGRGDS deposited primary human fibroblasts from cell transfer experiment. Statistical significance measured by one way ANOVA with comparisons to the positive control trypsin. Level of significance indicated by asterisks above. (A) – P5 primary human fibroblasts, (B) – P7 primary human fibroblasts (C) – P8 primary human fibroblasts.

GGGRGDS, GRGRGDS, GRGRGDS and GVGRGDS consistently show the highest level of cell transfer with good statistical difference from the negative controls (no polymer and HB-PNIPAM-COOH).The GDGRGDS, GPGRGDS, GQGRGDS and GYGRGDS polymers did not show high levels of cell transfer. They were not significantly different or displayed a low level of significance when compared to the negative controls. When compared to the positive control (Trypsin) these samples transferred far fewer cells and the difference displayed a high level of significance. This showed that these polymers did not perform as well as trypsin.

The differences in cell number are likely to be due to increases in binding affinity caused by changes in the peptide sequence. Changes in the sequence influence electrostatic interactions between the peptide and the receptor or cause conformational changes which can also have a significant effect on binding interactions. It was demonstrated by Kostidis *et al.* that the flanking groups influence three factors which can have a large effect on binding.[50] These are; "(i) the distance between the charged centres, (ii) the distance between the Arg Cβ and Asp Cβatoms and (iii) the pseudo-dihedral angle defining the Arg and Asp side-chain orientation formed by the Arg Cζ, Arg Cα, Asp Cα and Asp Cγ atoms."

From the work by Kostidis *et al* outlined above, it can be inferred that the improvements seen by GRGRGDS and GSGRGDS are likely to be as a result of an increase in hydrogen bonding from the charged and polar residues of arginine and serine. Whereas, in GGGRGDS and GVGRGDS, which contain no charge, the improvements seen must arise from increased van der Waals bonding or beneficial change in the conformation of the peptide in a beneficial way. The distance of the peptide from the substrate can also have an effect. Reduced steric hindrance will improve binding. It is noteworthy that the RGD sequence is closer to the sterically hindering substrate in GRGDS compared to GXGRGDS peptides and this may be partly responsible for the reduced activity of GRGDS. Although there is no direct (crystallographic) evidence for the conformation of the peptides, it is likely that the GPGRGDS peptide displays a much different conformation to the other peptides because of the cyclic proline residue. This does not appear to have had a positive effect on the binding affinity of the peptide to the integrins as only low cell numbers are transferred. The deposited cell numbers have also been compared to the positive control, trypsin. The cell number is always lower than the trypsin control. Although, in the F284 P8 experiment the HB-PNIPAM-GGGRGDS was shown to be statistically similar to the trypsin positive control. It appears that these polymers do not transfer as many cells as trypsin but they may provide an alternative in situations where trypsinisation is not desirable. A possible mechanism for the cell detachment and redeposition is shown in Figure 3.14.

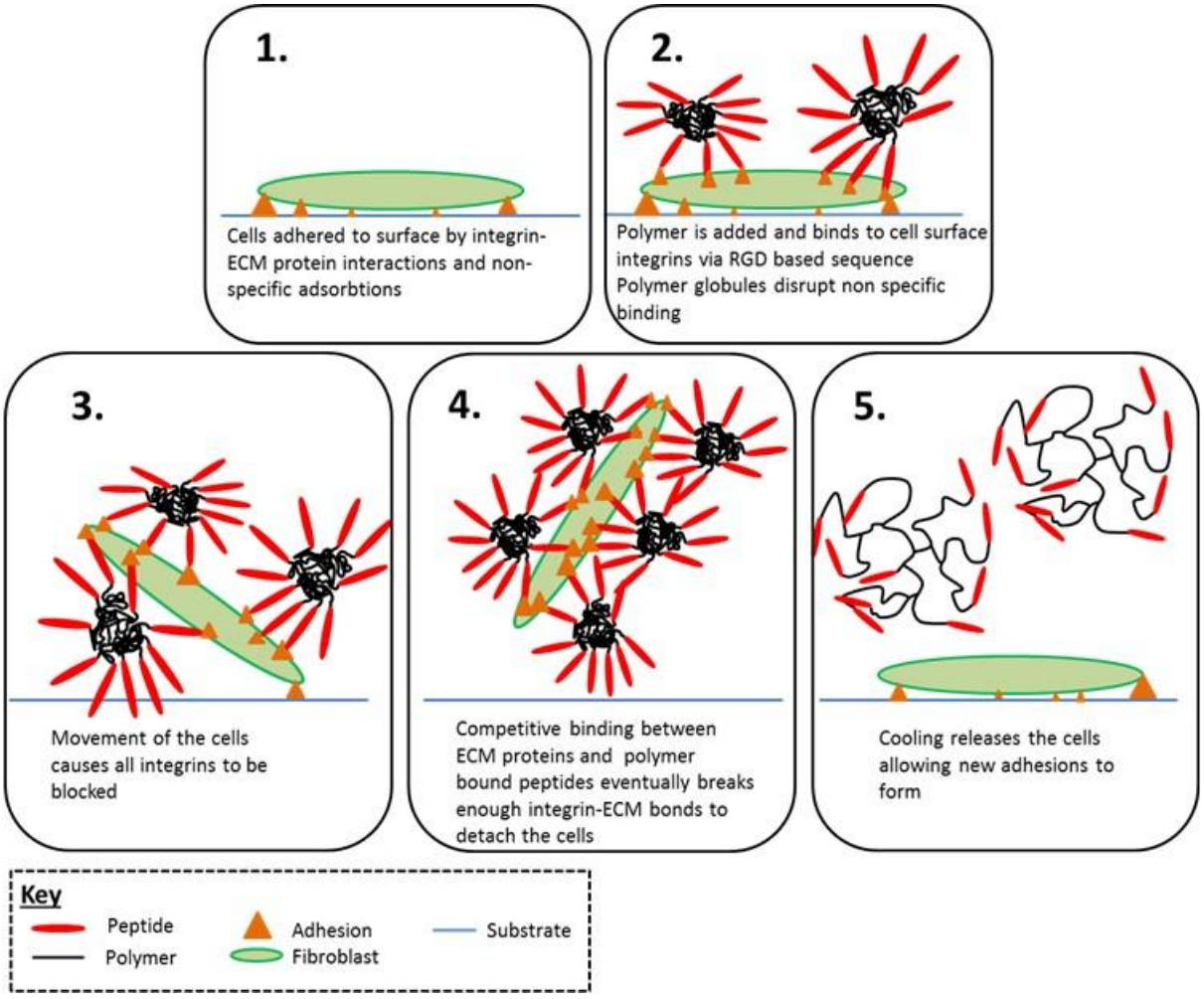

Figure 3.14 – Interactions of polymer particles with fibroblasts.

Figure 3.14 shows the mechanism for detachment of cells from a tissue culture plastic surface. The proposed mechanism had been broken down into 5 steps.

1. In the first step the cells are adhered to tissue culture plastic by bonds between cell surface integrins and ECM proteins such as fibronectin and virtonectin.
2. Peptide functional PNIPAM particles bind to the cells and start to block integrin sites on the cell surface. The high concentration of RGD functionality at the surface of a polymer particle means it is unlikely that all binding interactions will be broken simultaneously. The polymer particles therefore compete for binding sites more effectively than extracellular matrix proteins.
3. Movement of the cells causes further blocking of integrin sites, which were previously inaccessible to the polymer particles.

4. All integrin-fibronectin/vitronectin bonds are broken and the cells detach from the surface
5. The suspension is transferred to a new tissue culture plastic well plate and cooled to below the LCST of the polymer. The open coil conformation of the polymer is not conducive to integrin binding and the cells are released. The cells are now free to form new attachments with the well plate.

3.4 Conclusion

HB-PNIPAM-COOH was shown to be ineffective and not statistically different from the control which contained no polymer. HB-PNIPAM-COOH had no integrin binding RGD sequence and will not compete with fibronectin and vitronectin for binding sites.

The peptide functional HB-PNIPAM polymers investigated were effective for lifting and redepositing NHDFs. The concentration of cells deposited was dependent on the peptide sequence used. The most successful polymers were GGGRGDS, GRGRGDS, GSGRGDS and GVGRGDS containing HB-PNIPAMS. One way ANOVA demonstrated statistically that these polymers transfered more cells than the negative controls and in one instance, GGGRGDS functional polymer was shown to deposit a similar number of cells to trypsin.

Significant variation in the number of cells transferred was observed between experiments. This variation was attributed to a biological difference in primary cells from different patients at different passages numbers.

The polymers which consistently transferred high cell numbers were GGGRGDS and GVGRGDS peptides. In all cases these polymers performed better than the negative controls. GDGRGDS, GPGRGDS, GQGRGDS and GYGRGDS functionalised polymers were shown to perform similarly to the negative controls. These polymers did not show a statistically relevant significant difference from the negative controls or displayed a difference at a low level of significance. It can be concluded that these polymers were ineffective. It can also be concluded that there is a clear effect of the flanking groups around the RGD functionality on the ability of the peptide sequence to bind to cell surface receptors.

4. Branched Semi-Interpenetrating Polymer Networks (BS-IPNs) with a Poly(N-Vinylpyrrolidone) (PVP) and Poly (Ethylene Glycol) matrices

4.1Branched Semi Interpenetrating Polymer Networks with a Poly(Vinylpyrrolidone) Matrix

4.1.1 Abstract

Highly branched PNIPAM has blended into NVP monomer before curing to form a PVP polymer matrix with an entrapped HB-PNIPAM component. This formed a branched semi-interpenetrating polymer network (BS-IPN). The term BS-IPN has been used to differentiate these branched systems from semi-interpenetrating polymer networks containing a linear polymer (S-IPNs). Physical interactions from the matrix prevent the branched component from being fully extracted. The permenant entrapment of the HB-PNIPAM component has been demonstrated and quantified by FTIR. This created a platform for the introduction of peptide functional branched additives (HB-PNIPAM-GRGDS) to hydrogel formulations which have been used to control specific cell behaviours. A composite material with hydrogel mechanical properties and improved cellular adhesion properties was made. *In vitro* cell testing was used to determine the effectiveness of the additive, demonstrating its positive effect on cell adhesion, proliferation and migration. It was possible to structure the hydrogel system by projection microstereolithography. Tube type structures have been used in peripheral nerve repair and it was proposed that these polymers could be added to existing formulations to improve cell behaviour. Tube type structures have been fabricated from BS-IPNs with a PVP matrix and could be used to make nerve guidance conduits with improved biological properties.

4.1.2 Experimental

Synthesis of HB-PNIPAM derivatives was taken from previous work by Rimmer *et al*.[80, 85]

4.1.2.1 Synthesis of 4-Vinylbenzyl Pyrrolecarbodithioate

A detailed description of the synthesis of 4-vinylbenzyl pyrrolecarbodithioate can be found in section 2.2.1.

4.1.2.2 Synthesis of Pyrrolecarbodithioate Ended HB-PNIPAM

A detailed description of the synthesis of pyrrolecarbodithioate ended HB-PNIPAM can be found in section 2.2.2.

4.1.2.3 Carboxilic Acid Functionalisation of Pyrrolecarbodithioate Ended HB-PNIPAM

A detailed description of the synthesis of carboxylic acid functionalised HB-PNIPAM can be found in section 3.2.3

4.1.2.4 Peptide Synthesis

The ChemSpeed automated peptide synthesiser was used with 735 sampler software. Serine loaded Wang resin was swollen in DMF for 24 hours. The amino acids were added sequentially. To couple each amino acid; 1.1 equivalents of each amino acid, 1.1 equivalents of the coupling agent PyBOP, 2.2 equivalents of the coupling agent DIPEA were added. The Fmoc protecting groups were removed by triple deprotection with 20% piperidine in DMF and the peptide chain was built up from the Serine on the resin to the final Glycine. This gave the desired peptide sequence GRGDS. The resin was washed with DMF then DCM then methanol, dried and stored at -18°C.

A cleavage cocktail containing trifluoroaceatic acid (TFA), water, phenol and triisopropylsilane (TIPS) in the ratio 88:5:5:2 was added to the resin at 10 mL g^{-1} with stirring for two hours. The resin was filtered off and washed with cleavage the cocktail and three

then times with TFA. The TFA was removed by rotary evaporation with a cold trap containing CO_2(S). The remaining TFA was removed by triturating with five aliquots of diethyl ether. The remaining ether was removed by rotary evaporation and the product stored at -8°C.

The peptide was purified by prep HPLC and freeze-dried yielding a white solid.

The product was confirmed by NMR and mass spectroscopy. A list of NMR peaks and the splitting patterns associated with the peaks has been included below. This is supported by the Mass spectroscopy data which showed molecular ion peak at 490 as was predicted by the calculated mass.

^{1}H NMR (400 MHz, $CDCl_3$) (ppm): δ 0.9-1.3(6H, br, s, -N(CH_3)$_2$), δ 1.4–1.8 (2H, br, m, -CH_2-CH-C6H4-), δ 1.9–2.2(2H, br, m, -CH_2-CH-CO-NH-) and (1H, br, m, CH_2-CH-CONH-), δ 3.0-3.4(2H, br,s –CH_2-NH-C(NH)-NH_2 arginine), δ 4.0 (1H, br, s, (CH_3)$_2$CH-), δ 6.6–7.2 (b,r m, -Ar-), δ 7.85 (br, s, -NH-CO-).

MH^+ (HPLC-ESI) = 490 g mol^{-1}, (calculated = 490.21 g $mol^{-1.}$).

4.1.2.5 GRGDS Functionalisation of HB-PNIPAM

A detailed description of the synthesis of N-hydroxysuccinimide functional HB-PNIPAM can be found in section 3.2.4.

N-Hydroxysuccinimide ended HB-PNIPAM (1.5g) was dissolved in phosphate buffer (0.01 M, pH 8.5, 0°C). This was added to a 3 neck flask with GRGDS peptide, (380 mg, 5 eq) and cooled to 0°C and stirred under nitrogen for 48 hours. The resulting product was purified by ultrafiltration and freeze dried yielding a white fluffy solid.

The product was confirmed by NMR. A list of NMR peaks and the splitting patterns associated with the peaks has been included below.

^{1}H NMR (400 MHz, $CDCl_3$) δ/ppm: 0.9-1.3(6H, br, s, -N(CH3)2), 1.4–1.8 (2H, br, m, -CH2-CH-C6H4-), 1.9–2.2(2H, br, m, -CH2-CH-CO-NH-) and (1H, br, m, CH2-CH-CONH-), 3.0-3.4(2H, br,s –CH_2-NH-C(NH)-NH_2 arginine), 4.0 (1H, br, s, (CH3)2CH-), 6.6–7.2 (b,r m, -Ar-), 7.85 (br, s, -NH-CO-).

4.1.2.6 Production of Interpenetrating Polymer Networks

4.1.2.6.1 Formulations

The formulations shown in Table 4.1 and Table 4.2 were made up in glass vials without the initiator, 2-hydroxy-2-methyl-1-phenyl-1-propanone (HMPP). The contents of the vials was stirred in the absence of light until the highly branched polymer had dissolved in the monomer and solvent. The samples were then degassed by bubbling with N_2 before the initiator was added. The monomer/polymer solution was then ready to use.

Table 4.1 - Formulations for HB-PNIPAM PVP-co-DEGDA semi IPNs at 10% crosslinker

Sample	NVP / g	DEGDA / g	isopropanol / g	HB-p(NIPAM) / g	HMPP / g
5% HB-p(NIPAM)	4.5	0.5	3	0.25	0.05
10% HB-p(NIPAM)	4.5	0.5	3	0.5	0.05
20% HB-p(NIPAM)	4.5	0.5	3	1.0	0.05
30% HB-p(NIPAM)	4.5	0.5	3	1.5	0.05

Table 4.2 - Formulations for HB-PNIPAM PVP-co-DEGDA semi IPNs at 40% crosslinker

Sample	NVP / g	DEGDA / g	isopropanol / g	HB-p(NIPAM) / g	HMPP / g
5% HB-p(NIPAM)	3	2	3	0.25	0.05
10% HB-p(NIPAM)	3	2	3	0.5	0.05
20% HB-p(NIPAM)	3	2	3	1.0	0.05
30% HB-p(NIPAM)	3	2	3	1.5	0.05

4.1.2.6.2 Production of Semi-IPN Coated Cover Slips

When preparing samples for cell culture, 13 mm coverslips were methacrylate functionalised by cleaning with piranha solution, followed by thorough washing with methanol. The cover slips were added to a 5% solution of 3-Methacryloxypropyltrimethoxysilane in toluene, where they were stored until required.

A drop of the polymer monomer blend was applied to a clean microscope slide, and a clean methacrylate functionalised cover slip was placed on top. This was cured by UV and the BS-IPN coated coverslip removed from the microscope slide as shown in Figure 4.1.

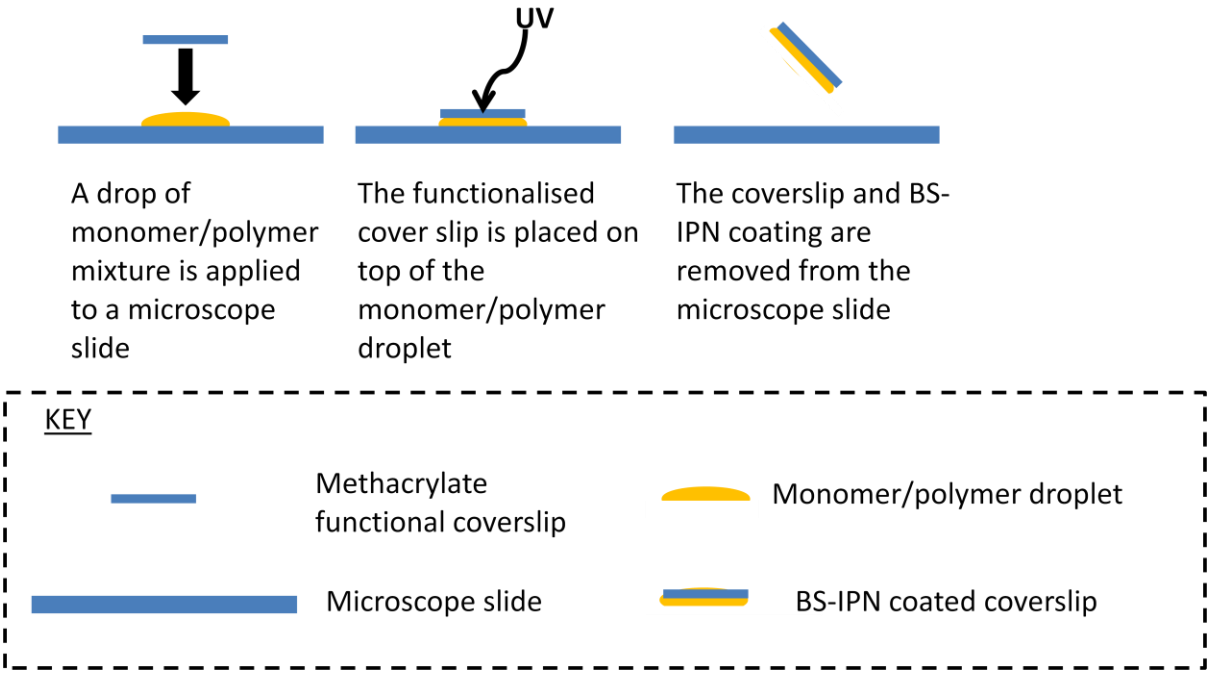

Figure 4.1 – A diagram showing the technique for making BS-IPN coated coverslips.

4.1.2.6.3 Production of Branched Semi-IPN Sheets

100 µm thick BS-IPN sheets were synthesised by injecting polymer/monomer blends into a quartz mould before curing with UV light. The process for injecting the polymer into the mould is shown in Figure 4.2. The samples were removed from the quartz mould. A small sample of the membrane (≈3 cm^3) was retained for analysis before the remaining membrane was subjected to a soxhlet extraction in isopropanol for 48 hours.

Figure 4.2 - A photograph showing the process of injecting the monomer/polymer mixture into a quartz mould. The mould consists of two quartz plates with an inner lining of PET. A PTFE spacer was used to create a 100 µm void within the mould into which the monomer could be injected. The apparatus was held in place with bulldog clips.

4.1.2.7 Extraction of HB-PNIPAM

The hydrogel sheets were subjected to a 48 hour Soxhlet extraction in isopropanol. HB-PNIPAM-COOH which was not held securely by the crosslinked hydrogel system was washed out by this process.

4.1.2.8 Measuring the Concentration of Remaining HB-PNIPAM in BS-IPNs by FTIR

FTIR spectra of samples were measured before and after extraction. Partial least squares analysis was carried out using TQ analyst to determine the concentration of HB-PNIPAM within the system after extraction compared to a calibration of known standards made up of samples before extraction. Samples of the BS-IPN membranes containing 0, 5, 10, 20, 30 and HB-PNIPAM and 100% HB-PNIPAM were used to create a calibration curve. The calibrations, with correlation coefficients, from the PVP systems at 10% and 40% crosslinker

and the PEG based system are shown in section 8.5.1 of the appendix. The spectral region used for analysis was 1480 - 1760cm^{-1}.

4.1.2.9 Determination of LCST of HB-PNIPAM within BS-IPNs by FTIR

All FTIR spectra were collected using a temperature controlled single reflection diamond ATR sampling accessory (Specac) coupled to a Thermo Nexus FTIR spectrometer with the clean ATR crystal at the same temperature as a background using Omnic 6.1 software. Collected spectra were the result of an average of 128 scans at a spectral resolution of 2 cm^{-1}. The BS-IPN samples were swollen in D_2O for 1 week prior to analysis to ensure full hydration of the entrapped HB-PNIPAM. The samples were loaded onto an ATR crystal in an air-tight chamber (1 cm^3 volume) and sealed using beeswax. The sample allowed to equilibrate at 25°C overnight to allow the D2O/H2O to reach a constant concentration at the ATR crystal interface. To determine the LCST spectra were collected at increments of 2°C from 25°C to 55°C, allowing 7 minutes for the system to equilibrate between each temperature change. Raw spectra of the amide carbonyl region can be found in section 8.5 of the appendix

4.1.2.10 Equilibrium Water Contents of BS-IPNs

Samples were cut from BS-IPN membranes using a cock borer. The dry weights were recorded for each sample before swelling the samples in water. Once the sample reached equilibrium excess water was removed gently with tissue and the sample was reweighed. From this data, the equilibrium water content was calculated as the percentage of water making up the total equilibrium mass.

For temperature dependant measurements samples were incubated at the required temperature in sealed vials before measuring the mass of the swollen sample at equilibrium. The water contents were carried out in the same way as for the ambient measurements.

4.1.2.11 Primary Human Fibroblast Cell Culture on BS-IPN samples

Human fibroblasts were obtained under local ethical permission and consent from female patients undergoing abdominoplasty or breast reduction operations. The method for the isolation and culture of fibroblasts is described in the literature.[189] The dermis was separated from the epidermis initially by removing subcutaneous tissue and cutting it into 0.5 cm^2 pieces. Fibroblasts were obtained from the dermis after trypsinisation of the skin. The dermis was then washed in PBS, finely minced with a scalpel and placed in 0.5% collagenase A overnight at 37°C. The collagenase digest obtained was centrifuged (1000g / 5 minutes) and supernatant discarded. The fibroblast cell pellet was re-suspended in 4 mL of fibroblast culture medium: DMEM supplemented with 10% (v/v) neonatal calf serum, $2x10^{-3}$ mol L^{-1} glutamine, 0.625 μg mL^{-1} amphotericin B, 100 IU mL^{-1} penicillin and 100 μg mL^{-1} streptomycin. Samples were placed in a T25 flask in an incubator (37°C / 5% CO_2) until confluent and passaged when 80-90% confluent (using a 1 mL 1:1 mixture of 0.1%w/v trypsin and 0.02% w/v EDTA per T25 flask) transferring to a T75 flask. Cells were used for experimentation between passages 4 and 9.

4.1.2.12 Imaging of Primary Human Fibroblasts on BS-IPN Samples

Samples were fixed in 3.7% formaldehyde and labelled for vinculin, actin and nuclei. Samples containing cultures of primary human dermal fibroblasts were washed three times with PBS and fixed with 4% (v/v) paraformaldehyde for 20 min, permeabilised with 0.1% Triton X-100 for 20 min followed by washing with PBS (x3). Unreactive binding sites were blocked with 10% (v/v) goat serum in PBS for 1 hour. The primary antibody (mouse monoclonal anti-vinculin from Sigma Aldrich) was diluted (1:150) in 1% (v/v) goat serum in PBS and fibroblasts incubated for 1 hour at room temperature. The antibody solution was removed and cells were washed twice with PBS. The secondary antibody (rabbit biotinylated anti-mouse IgG) was diluted (1:1000) in 1% goat serum in PBS. Fibroblasts were incubated with secondary antibody for 1 hour at RT. The cells were washed twice with PBS before adding a tertiary fluorescein-conjugated streptavidin label (diluted 1:100 v/v in 1% goat serum in PBS) and incubated for 1 hour. The tertiary label was removed and cells washed three times with PBS before adding phalloidin-TRITC (1:1000) and 4',6-diamidino-2-phenylindole dihydrochloride (DAPI) (300 nM) (Sigma Aldrich) in PBS, to label actin filaments

and nuclei, respectively. Cells were incubated for 30 minutes at room temperature before removing the labels and washing a further 3 times in PBS prior to imaging. Fibroblasts were imaged using an upright Zeiss LSM 510 confocal microscope using an argon ion laser (488 nm) for FITC excitation (λex = 495 nm / λem = 521 nm). Nuclei were visualized by two photon excitation using a Ti:Sapphire (Coherent Ultra III) laser (716 nm) for DAPI (λex = 358 nm λ em = 461 nm). Image acquisition was conduction using the Kroto Imaging Facility, University of Sheffield, U.K.

4.1.2.13 Migration Study of Primary Human Fibroblast Cultured on BS-IPN samples

The samples were placed into individual wells on a 12 well plate. Samples were held in place with cell crowns. HDFs were seeded at a density of 10,000 per well in 1 ml of culture medium. The plates were incubated at 37°C with 5% CO2 for 24 hours to allow the HDFs to adhere.

HDF were imaged using a AF6000 Time-lapse (Leica, Milton Keyes) with LAS AF software. The incubation chamber of the microscope was set to 5% CO_2 and 37°C the plate was allowed to equilibrate within the chamber to avoid focal drift. Set positions were found using the 2-dimensional multi-position stage. Images were taken at each set position every 15 minutes.

Time lapse videos produced in LAS AF were analysed in Image J using the manual tracking plugin to track cell movement. The Chemotaxis tool was used to convert the cell tracking data into a speed and accumulated distance and Euclidean distance for the cells was tracked.

4.1.2.14 MTT Assay

Cells were seeded onto test samples and positive and negative controls and cultured at 37°C and 5% CO_2. At the required time point the cells were removed from the incubator and the cell culture medium was removed. The cells were washed with PBS before adding 1 mL of 3,4,5-dimethylthiazol-2,5-diphenyl tetrazonium bromide (MTT) (0.5 mg mL^{-1}). The samples were incubated at 37°C with 5% CO_2 for a further 45 minutes before removal of the MTT solution and addition of 300 µL of acidified isopropanol. The resulting purple solution was

pipetted into a 96 well plate and the absorbance measures at 540 nm with a 630 nm reference.

4.1.2.15 3D Structuring by Stereolithography

The basic setup of the stereolithography system has been outlined in the annotated photograph in Figure 4.3.

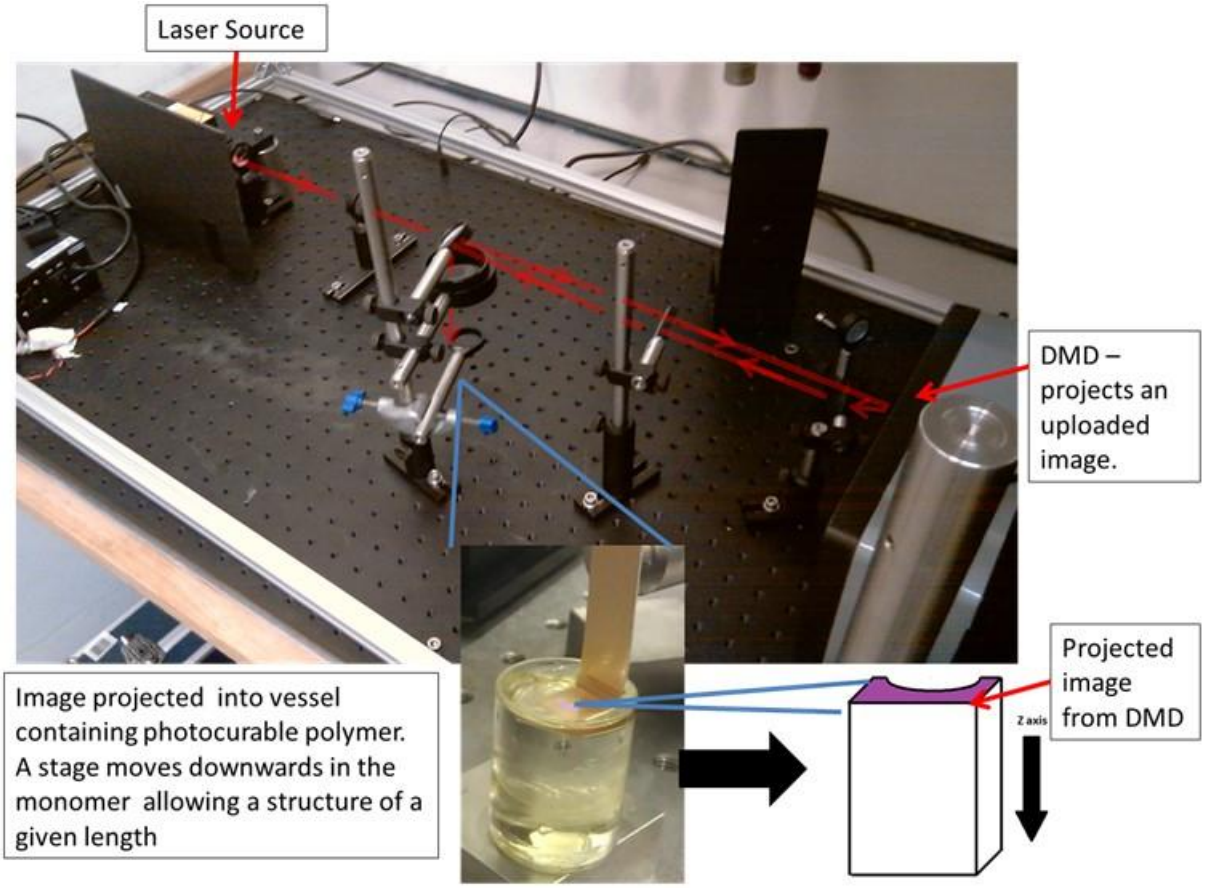

Figure 4.3 – An annotated diagram showing set up of the DMD projection microstereolithography setup. The path of the laser has been highlighted with the red line. An enlarged image showing the monomer and z-stage has been shown with a diagram of possible structure and the direction of polymerisation.

A colour-inverted image was created in MS paint and uploaded to the digital micro-mirror device (DMD) software (ALP-3 basic version 1.0.03). A power tunable, 100 mW 405 nm laser (Vortran Laser Technologt Inc.) was beam columnated before the resulting columnated beam directed onto the DMD. The reflected beam pattern from the DMD was directed via several mirrors and lenses to the surface of the monomer where the pattern was focused to

give a single sharp image. The z-stage (Thor Labs) was moved in a downwards direction using the control software (APT Software by Thor Labs) allowing the polymerisation to continue at the surface of the monomer, thus building up a structure of given length. A schematic showing the setup is shown in Figure 4.3. BS-IPN structures were made from NVP and PEG-DA based systems. The formulations can be found in Table 4.1 and Table 4.2.

4.1.2.16 Analysis of Variance

An explanation of the ANOVA statistical test has been given in section 3.2.10

4.1.3 Results and Discussion

4.1.3.1 Extractability of HB-PNIPAM from BS-IPNs

When producing semi-IPN from hydrophilic components for use in aqueous media, it is possible that the entrapped polymer can be extracted. For this application the entrapped polymer is used to add biofunctionality to the scaffold. It is therefore essential that the entrapped polymer cannot be extracted from the system. The use of a highly branched polymer allows a stable polymer system to be formed that will reduce/prevent leaching of the entrapped component. If the functionalised polymer can be fully extracted by this process then it will leach out from the sample and the benefit of using this additive will be completely lost. This demonstrated the usefulness of BS-IPNs compared to liner S-IPNs in swollen systems. The following experiments were carried out to determine the extractability of the polymer. Ideally large portions of functionalised polymer will remain after vigorous extraction using a good solvent for both the matrix and the entrapped functional polymer.

Formulations (Table 4. and Table 4.2) of HB-PNIPAM-COOH were blended with NVP and DEGDA and polymerised by UV light. The BS-IPN samples were then subjected to rigorous soxhlet extraction in isopropanol. The concentrations of HB-PNIPAM remaining after extraction are shown in Figure 4.4. Figure 4.4 (A) and (B) show the data obtained using feeds of 10 and 40 wt% crosslinker (relative to polymerisable monomers). Both sets of data show that these BS-IPN systems are unlike conventional S-IPNs as large quantities of the branched polymer are permanently entrapped. In a conventional S-IPN which uses a linear polymer, the linear component would be fully extracted because diffusion of the linear polymer chain through the network is possible[190-191] When a branched component is used in the BS-IPNS the movement of the branched polymer is severely restricted and the polymer cannot diffuse out of the system.

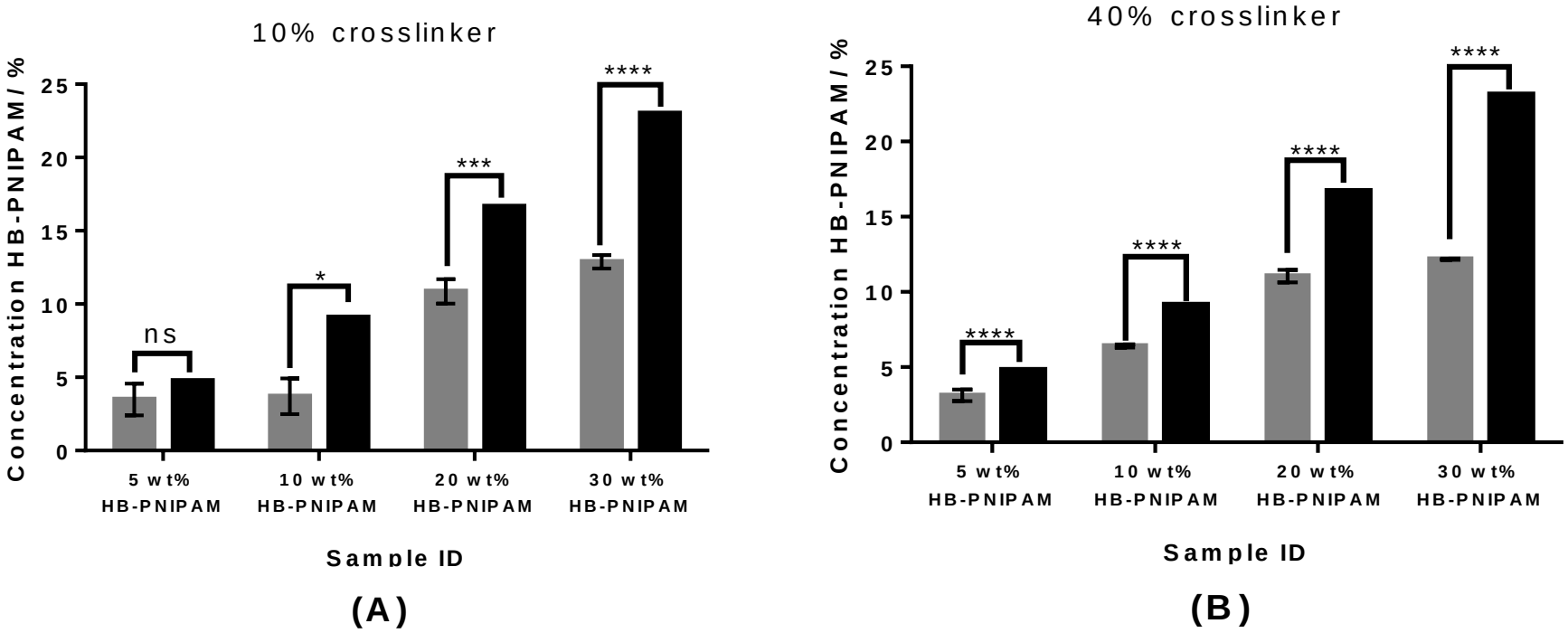

Figure 4.4 - Composition of the networks prior to and after Soxhlet extraction with 2-propanol: (A) 10 wt% DEGDA in the monomer feed and (B) 40wt% DEGDA in the monomer feed. The level of significance between initial concentration of HB-PNIPAM (black) and the measured post Soxhlet extraction concentration (grey) (measured by FTIR) are shown by one way ANOVA with multiple comparisons [(A) - ($p<0.0001$), (B) - ($P<0.0001$)].

It is important to note the significance of the data, at lower concentrations the change in concentration is much smaller and for the 10% HB-PNIPAM sample the difference is not significant. However, as the wt% of HB-PNIPAM increases the amount that can be extracted increases. For the 10% crosslinker system, which was studied most extensively, the level of significance between the feed and extracted values increases.

It was assumed that the HB-PNIPAM is entrapped by the polymer matrix in such a way that it cannot be removed. To remove the polymer, the chains would be forced to take up many unfavourable conformations. It could be that the extracted fraction of HB-PNIPAM was exposed HB-PNIPAM at the membrane surface. In this position it is possible that the HB-PNIPAM could be insecurely held by the PVP matrix when compared to HB-PNIPAM bound within the inner regions of the membrane. This is different from an S-IPN containing a linear polymer as in a swollen system this linear polymer could be easily extracted.

4.1.3.2 SEM of BS-IPN Surfaces

Further evidence of the entrapment of the HB-PNIPAM within the matrix of the BS-IPN was demonstrated by SEM (Figure 4.5). A change in the surface topography was shown by small 'wrinkles' or 'worm' like structures being formed on the hundreds of nanometres scale length. Examples of the images are shown in Figure 4.5. The SEM of an X-PVP hydrogel showed a smooth featureless surface, whereas the HB-PNIPAM containing BS-IPNs showed worm like surface structures of ≈200 nm (measured by SEM) feature width. These surface features are completely absent when X-PVP is imaged. Interestingly, these features are a similar size to the radii of the HB-PNIPAM particles in solution (136± 10 nm) as measured by DLS. It can be speculated that these features are a nano scale aggregations of polymer chains and that the two polymers are actually partially phase separated on the scale of individual polymer chain dimensions.

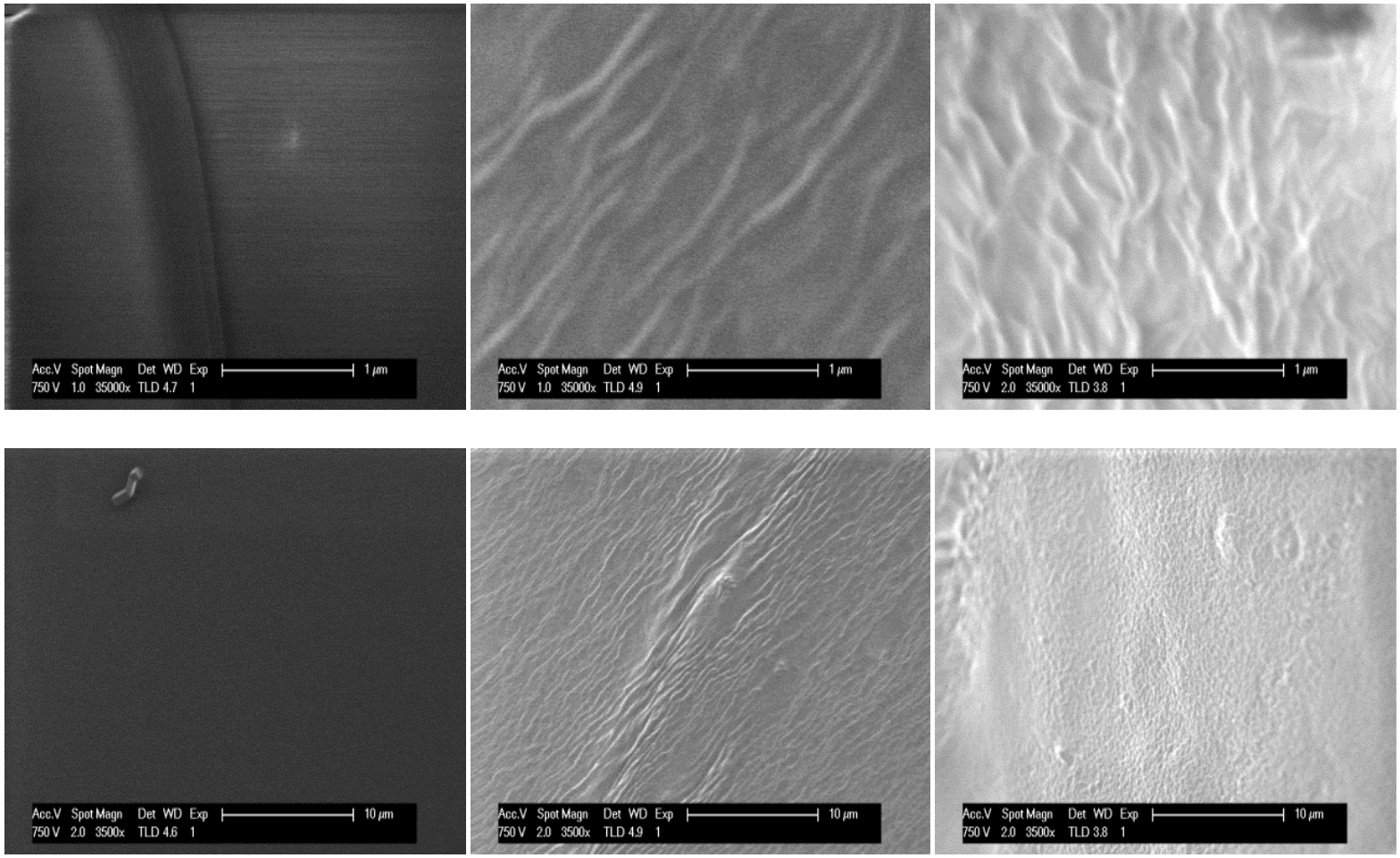

Figure 4.5 – High resolution electron micrographs of polymer surfaces x35000 (top row), x3500 (bottom row).The images show X-PVP hydrogel (left), 10% HB-PNIPAM/X-PVP S-IPN (centre), 20% HB-PNIPAM/X-PVP S-IPN (right). The images show that on the nm length scale the BS-IPNs display a phase separation which is not present in X-PVP.

The fine degree of phase separation demonstrated by the SEM imaging is what would be expected in a BS-IPN system. When producing a full IPN where both polymers are fully integrated, it is unlikely that these nano-structures would be observed. This observation suggests that polymer-polymer interactions between like polymers are favoured over polymer-polymer interactions between non-similar polymers during the BS-IPN formation. However, because the phase separation is at such fine length scale, it is likely that the core of the HB-PNIPAM does not interact significantly with the polymer matrix. The outer regions of the HB-PNIPAM particles are well integrated with the PVP matrix.

Detailed analysis of the SEM images using an auto correlation function (ACF) by C. Rodenburg in a paper by Plenderleith *et al.* showed that the average width of the worm like structures was 139 nm.[192] This correlated almost exactly with the measured particle size of the HB-PNIPAM in aqueous solution (≈136 nm). This is a very strong indication of molecular scale interpenetration.

4.1.3.3 LCST Behaviour of HB-PNIPAM BS-IPNs

PNIPAM has attracted much academic interest due to the fact that it exhibits a LCST transition at ≈33°C (for linear polymer). The temperature at which this occurs makes it of great interest due to its proximity to physiological temperature.

The HB-PNIPAM polymers created by RAFT polymerisation do indeed show the same temperature coil to globule transition. However, due to the incorporation of hydrophobic benzyl branching groups from the RAFT agent the LCST has been lowered to 26°C. The position of the LCST in these polymers is complex because branch points from the hydrophobic aryl groups drive the LCST down whereas the hydrophilic carboxylic acid/peptide end groups push the LCST up. In a network the LCST is manifested as a step change in deswelling but the HB-PNIPAM BS-IPNs produced here did not show this behaviour. This has been demonstrated by water content measurements, DSC and FTIR. The data can be seen in Figure 4.6, Figure 4.7 and Figure 4.8.

4.1.3.4 The Effect of Temperature Equilibrium Water Contents

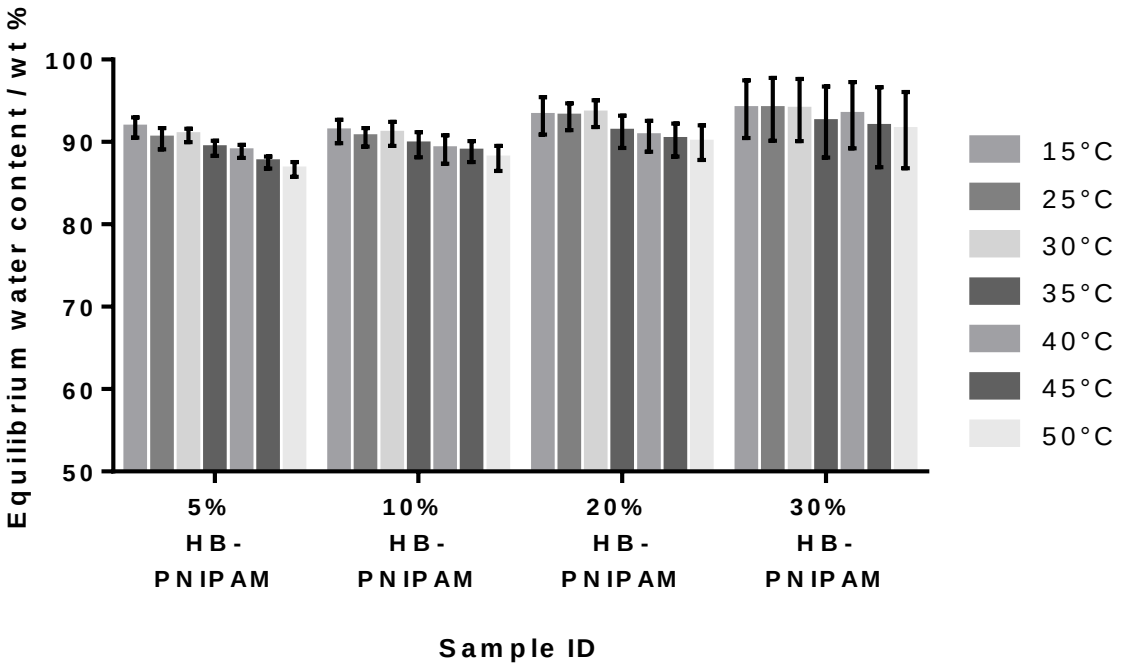

Figure 4.6 – A figure showing the equilibrium water contents for 5, 5, 10, 20 and 30% HB-PNIPAM BS-IPNs with PVP matrix over a range of temperatures. Level of significance determined by one way ANOA. No significant difference was found between any values (P<0.0001).

The equilibrium water content (by weight, in deionised water) was 85 to 95 wt% for all samples with no significant decrease on raising the temperature (Figure 4.6). The very high water contents of these polymers (caused by the matrix which does not show a temperature response in this range) coupled with in some cases the relatively low weight percentages of HB-PNIPAM relative to PVP and H_2O, meant the change in the H_2O content would likely be small and difficult to observe. This technique is crude by nature and may not be appropriate for such a fine measurement. Other avenues were explored to investigate the LCST however no stepwise LCST transition was observed.

4.1.3.5 DSC of BS-IPN Samples

The endothermic LCST transition can be observed by differential scanning calorimetry (DSC). However, Figure 4.7 shows an example of a typical featureless thermogram derived from a BS-IPN. No endothermic transitions were observed in any of DSC thermograms of the BS-

IPNs. However S-IPNs containing linear polymers did show an LCST endotherm. This observation shows that the linear and branched S-IPNs/BS-IPNs are structurally different at the molecular scale. For BS-IPNs there are interactions between polymer chains of the two components and molecular scale interpenetration which prevents the LCST transition. In linear S-IPNs the movement of the linear polymer is not restricted and the LCST transition is possible.

A series of variants were produced with linear polymers and the matrix component switched from X-PVP to X-PNIPAM. In Figure 4.7, conventional S-IPNs (containing a linear polymer) composed of either crosslinked PVP (X-PVP) with linear PNIPAM or crosslinked PNIPAM (X-PNIPAM) with linear PVP and an X-PNIPAM hydrogel were analysed by DSC. Note that the amount of PNIPAM in the linear PNIPAM/X-PVP S-IPN (10 wt%) was chosen to be equivalent to the amount of HB-PNIPAM in the extracted HB-PNIPAM/X-PVP BS-IPN (Figure 4.4), which provided the data in Figure 4.7. The data show that both of the conventional S-IPNs display endothermic events that can be assigned to LCST behaviour as does the X-PNIPAM hydrogel. The data indicate that the absence of an endotherm that could be associated with a LCST appears to be a feature of the BS-IPN structure.

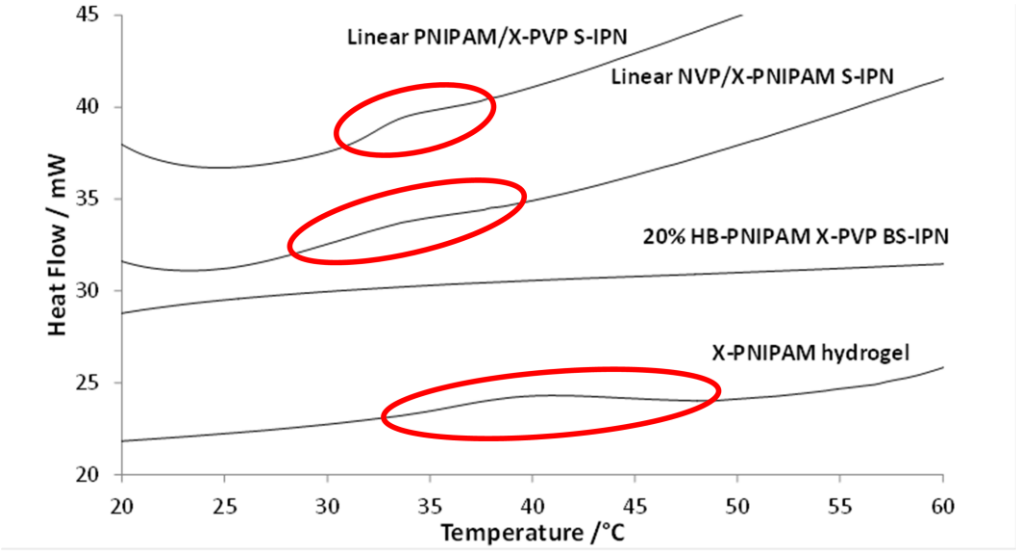

Figure 4.7 – A figure showing the DSC data of IPN systems. The peak associated with the desolvation of PNIPAM between 30 and 45°C for: 10wt% linear PNIPAM/X-NVP S-IPN (circled in red), 10wt% linear PVP/X-PNIPAM S-IPN (circled in red) and a X-PNIPAM hydrogel (circled in red). In the 20wt% HB-PNIPAM/X-PVP BS-IPN system the desolvation peak is a not observed due to the interpenetrated structure of a BS-IPN.

4.1.3.6 LCST Transition in BS-IPNS measured by FTIR

The suppression of the HB-PNIPAM LCST by the PVP hydrogel matrix can also be shown by FTIR spectroscopy. The LCST can be measured in FTIR by observation shifts in the peak centres of amide functional groups such as amide I (≈1630-1640 cm^{-1}), amide II (≈1560 cm^{-1}) and v(CH3) (≈2930 cm^{-1}). Figure 4.8 shows that in a set of BS-IPN materials, there was no observed step change in the vibrational frequency of the peak centres the amide I carbonyl with increasing temperature. There is a frequency shift with temperature but this was restricted to a change of less than 4 cm^{-1} for all systems investigated (at a resolution of 2 cm^{-1}) for all test samples.

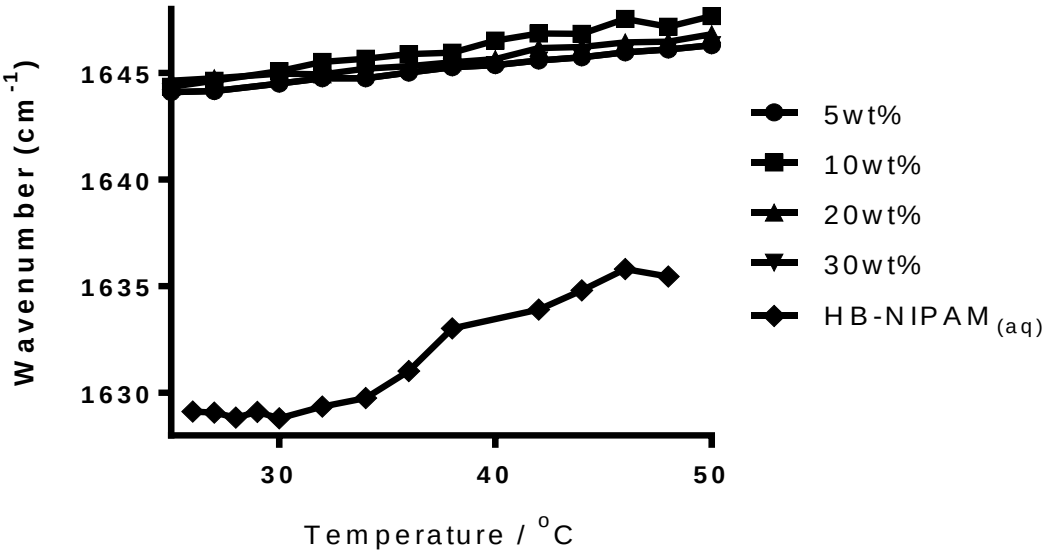

Figure 4.8 - Vibrational frequency of the amide carbonyl of HB-PNIPAM-COOH of BS-IPN systems with increasing concentration of HB-PNIPAM (5, 10, 20 and 30 wt% HB-PNIPAM-COOH in a PVP matrix) compared to HB-PNIPAM$_{(aq)}$ vs. temperature. A step change in the wavenumber of the amide 1 carbonyl was observed for the HB-PNIPAM in solution. This is indicative of the LCST. This was not observed for the BS-IPN samples where no step change was observed.

When the BS-IPN data is compared to HB-PNIPAM(aq) a step change in the amide 1 peak position (from ≈1630 to ≈1635 cm^{-1} between 32 and 34°C) is observed. This is the profile that would be expected to an LSCT transition of PNIPAM. The size of this change and the speed of the onset is compared to BS-IPNs with 10% crosslinker in Figure 4.8. The starting

position for the peak is much lower and even in the collapsed state the wavenumber of the peak maximum is still ≈8 cm^{-1} lower than the in the BS-IPNs at their most hydrated. This can be partially explained by the convolution of the amine I peak with the water bending mode δ(OH) in the system. Although convolution of these peaks lowered the measured wavenumber position δ(OH) has been shown not to vary with temperature.[193] As such the change in the peak centre can be fully attributed to the change in the amide I peak. It is likely that the small systematic increase in wavenumber with temperature in the BS-IPN samples was caused by lower strength of hydrogen bonds between D_2O and the amide at elevated temperature.[194]

The lack an observable LCST could be caused by an unexpectedly high or low LCST transition. However, comparing the amide I peak position of BS-IPNs (≈1646 cm^{-1}) to literature values for PNIPAM homopolymer LCST (≈1635 cm^{-1}) indicates that the HB-PNIPAM may have passed through its LCST. This provides further evidence that the HB-PNIPAM could be in a dehydrated state at much lower temperatures than we would have predicted from its solution behaviour. This could be explained by the high hydrophilicity of the PVP matrix. The high osmotic potential of the PVP matrix may be drawing water away from the HB-PNIPAM phase. A schematic diagram demonstrating this effect is shown in Figure 4.9.

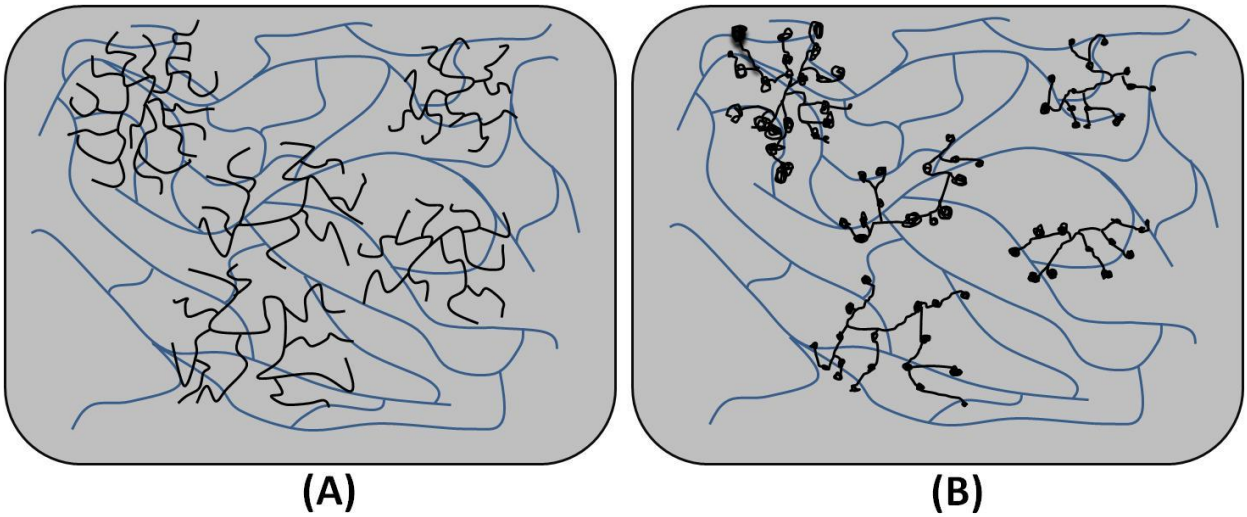

Figure 4.9 – A schematic diagram showing possible structures of a BS-IPN; A shows fully hydrated HB-PNIPAM particles whereas B shows HB-PNIPAM particles partially collapse to form n-clusters which cannot aggregate to form a globule because of the constraints of the polymer matrix.

The current model of the coil-to-globule transition (the n-cluster model) introduced by DeGennes [112] states that, intramolecular clusters form from an open coil. The aggregation of these n-clusters drives the formation of the 'desolvated globule'. It could be assumed that the interwoven structure of the matrix with the HB-PNIPAM prevents n-cluster formation and thus prevents coil collapse. This could explain the absence of the LCST from the FTIR and DSC data. However, taking into account FTIR data of the HB-PNIPAM in solution, it seems that in the BS-IPNs, n-clusters may already be formed due to the relative affinities for water of the two components. It is likely that the high affinity of the PVP for water draws the water away from the HB-PNIPAM particles forcing them through the LCST at a much lower temperature than expected. Whilst the conflicting physical forces exerted by the matrix on the HB-PNIPAM prevent these n-clusters from aggregating to form a globule. More work is required to substantiate this claim but in context of the n-cluster model one might expect in certain formulations of BS-IPNs to not observe a LCST.

4.1.3.7 The Effect HB-PNIPAM-GRGDS in BS-IPNs on *In Vito* Cultured ells

It has been shown previously that the polymer can be permanently incorporated into the hydrogel matrix. This provides a platform to introduce useful, polymer bound, biological factors into biomaterials. The advantage of this is that existing approved materials can be easily adapted by the simple addition of these functional polymers.

4.1.3.8 Comparison of PVP, HB-PNIPAM-COOH PVP BS-IPN, HB-PNIPAM-GRGDS PVP BS-IPN and TCP as Surfaces for *In Vitro* Cell Culture

Human Dermal Fibroblasts (HDFs) were used as these are a robust cell type which are often used to give an initial insight into the cytocompatibility of a biomaterial. The HDFs used in these experiments are primary cells which have been isolated from a human donor. Primary cells are more likely to give a result which will reflect *in vivo* testing better than immortalised cell lines as primary cells are typically more sensitive. Fibroblast cells are a very common extracellular matrix producing cell type which are found in many tissues in the

body. A good biological interaction with this cell type would be desirable for many biomaterials. This means that fibroblasts are typically widely available in many laboratories and are often the first cell type used for proof of principle work.

A cell adhesive peptide has been introduced to the system by blending the HB-PNIPAM-GRGDS into a PVP hydrogel. The GRGDS sequence has been shown to bind the $\alpha 5\beta 1$ cell surface integrin, increasing cell adhesion to non-adhesive substrates, and has been widely reported upon in biomaterials and polymeric systems.[195] Most non-charged hydrogels, such as PVP, are highly resistant to cell adhesion.[196] However, hydrogels have advantages as scaffolds in tissue engineering: nutrients and waste products can freely diffuse; they are resistant to general biofouling and their physical and mechanical properties can be tuned by controlling swelling and crosslinking.

Three materials were prepared: X-PVP and BS-IPNs composed of either HB-PNIPAM-COOH and GRGDS-BS-IPN. HDFs were cultured for 24 hours on the prepared materials using TCP as the positive control. The images from confocal microscopy are shown in Figure 4.10 and the corresponding MTT cell viability data in Figure 4.11. Actin filaments were labelled with phalloidin-TRITC (red) and nuclei were stained using 4',6-diamidino-2-phenylindole (DAPI, blue). The cells were cultured on each of the three materials for 24 hours before being fixed and labelled. From Figure 4.10 it can be seen that the cells adhere equally well to TCP (the positive control) and HB-PNIPAM-GRGDS BS-IPN. In both cases the cells reached confluence in over the experimental timescale. Although cell activity was shown to be significantly lower in HB-PNIPAM-GRGDS compared to TCP by one way ANOVA of MTT viability data (Figure 4.11). The characteristic morphology of strongly adhered cells was observed in the HB-PNIPAM-GRGDS BS-IPN and TCP samples. These cells were observed to have orthogonal actin filaments within most cells and convergent actin filaments at the points of focal adhesions. In the high magnification images (Figure 4.10 lower left and right) focal adhesion contacts can be seen which are co-located with convergent filaments. This is indicative of good cellular adhesion. In this instance the focal contacts have not been imaged directly by vinculin staining but are implied by the convergence of actin filaments.

This was not observed in the HB-PNIPAM-COOH BS-IPN or the X-PVP hydrogel (negative controls). These materials supported low cell numbers shown by confocal microscopy are echoed by MTT viability assay. These cells did not have the characteristics of adherent cells

observed previously. Instead, the cells which remained had atypical rounded morphologies with a low density of focal contact adhesions. The actin filaments were present but did not show any orthogonal organisation or convergence at the membrane. This is consistent with the lack of focal adhesions. These data indicate that the addition of HB-PNIPAM-GRGDS can improve the cell adhesive properties of a typically non adhesive hydrogel matrix.

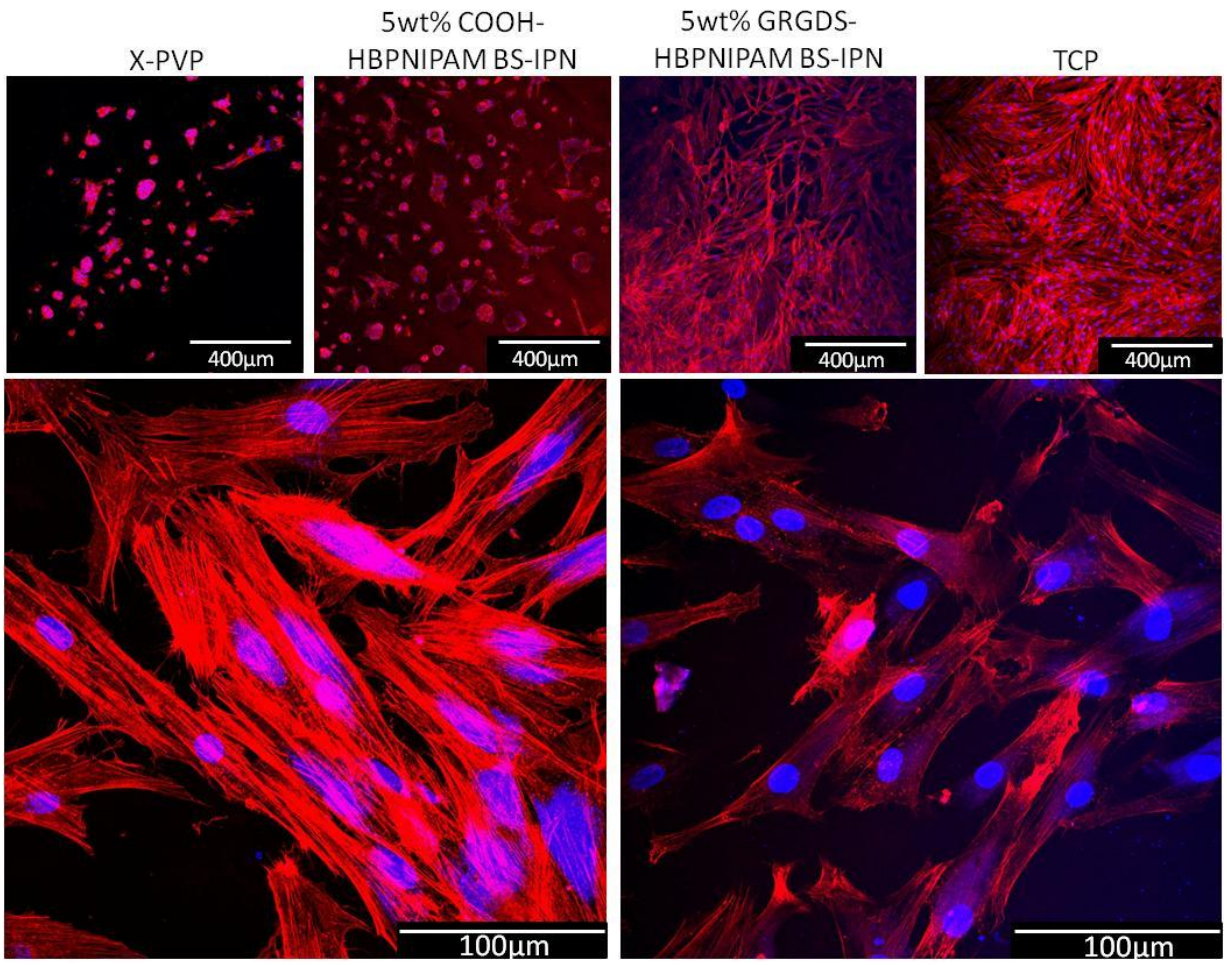

Figure 4.10 - (Top) Fluorescence micrographs by confocal microscopy with x10 objective lens (400 µm scale bars) of normal human dermal fibroblasts grown on PVP control (left), 5 wt% HB-PNIPAM-GRGDS/X-PVP BS-IPN (central left), 5 wt% HB-PNIPAM-COOH/X-PVP BS-IPN (central right), TCP (right). (Bottom) Micrographs with x40 objective lens (100 µm scale bars) of normal human dermal fibroblasts on TCP (left) and 5 wt% HB-PNIPAM-GRGDS/X- PVP BS-IPN (left). Images taken after 48 hours culture. Actin filaments labelled with phalloidin-TRITC (red), nuclear staining with DAPI (blue). The images show that cells grow well on TCP and on the HB-PNIPAM-GRGDS BS-IPN but display poorly adhered rounded morphologies and low cell numbers on X-PVP and a HB-PNIPAM-COOH BS-IPN.

The improvement in the cell viability and proliferation shown in Figure 4.10 is corroborated by the MTT data shown in Figure 4.11. This gives an indirect measurement of cell number as samples with a higher cell number will give a higher absorbance.

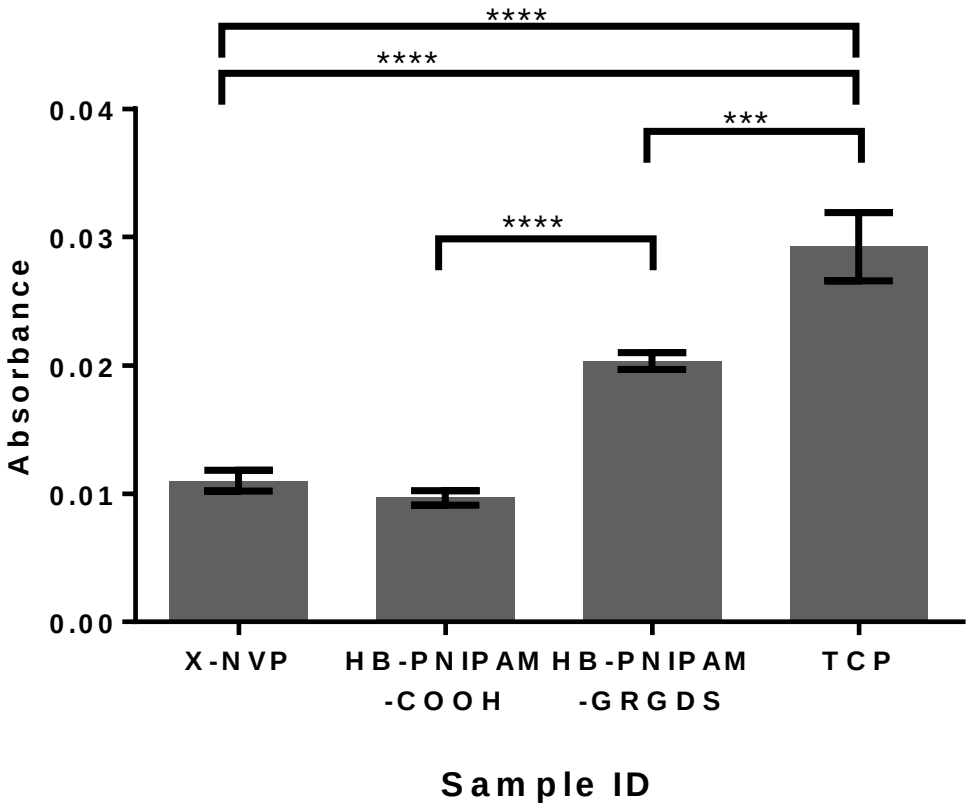

Figure 4.11 - MTT assay for cell viability for X-PVP hydrogel, HB-PNIPAM-COOH BS-IPN, HB-PNIPAM BS-IPN and TCP. Level of significance assessed by one way ANOVA with multiple comparisons shown by asterisks (P<0.0001). These data show that the addition of HB-PNIPAM-GRGDS can have a significant effect on the ability of cells to proliferate on a hydrogel surface.

The cell viability data in Figure 4.11 corroborates what has been shown by the cell imaging. There is no significant difference between the X-PVP and HB-PNIPAM-COOH samples, which both showed low cell number and viability. However, there was a significant difference between the X-PVP and HB-PNIPAM-COOH BS-IPN (negative controls) compared to the HB-PNIPAM-GRGDS and the TCP (positive control).

4.1.3.9 Effect HB-PNIPAM-GRGDS Concentration on Cell Viability

The effect of varying the amount of HB-PNIPAM-GRGDS was investigated. Images of the cells on BS-IPNs containing 0% to 2.5%, 5% and 10% GRGDS-PNIPAM are shown in Figure 4.12. The confocal imaging shows that the number of cells increases as the weight percentage of HB-PNIPAM-GRGDS increases. This resulted in a typically highly adherent morphology. The cells had organised actin filaments, orthogonal orientation and convergence at the cell membrane, with the formation of highly distinct focal adhesions. The fibroblasts were found to be confluent on the 10% HB-PNIPAM-GRGDS samples. Co-labelling of vinculin was undertaken in parallel (using anti-vinculin IgG, green), which showed a relatively high level of expression of this protein on 2.5%, 5% and 10% HB-PNIAPM-GRGDS BS-IPN samples. Vinculin is a protein present in adhesion plaques, labelling for this protein should help identify the adhesion plaques prescent at focal contacts. This protein was found to be co-localised with actin filaments on the 2.5% and 5% GRGDS surfaces, the expression of red and green yielded the yellow colour. This effect was prevalent at the point of focal adhesion contact formation where vinculin was expressed with convergent actin filaments. The cells presented the typical morphology of well adherent cells and were well spread. The formation of large adhesion plaques were less prevalent on the 10% GRGDS surface. Here, HDFs displayed a nearly confluent cell density which resulted from the higher density of GRGDS adhesion peptides. The cells are adherent but have proliferated to a higher degree which means they have less space per fibroblast. The lack of space prevents large adhesion plaques from forming. So these plaques are not observed at a high concentration of GRGDS.

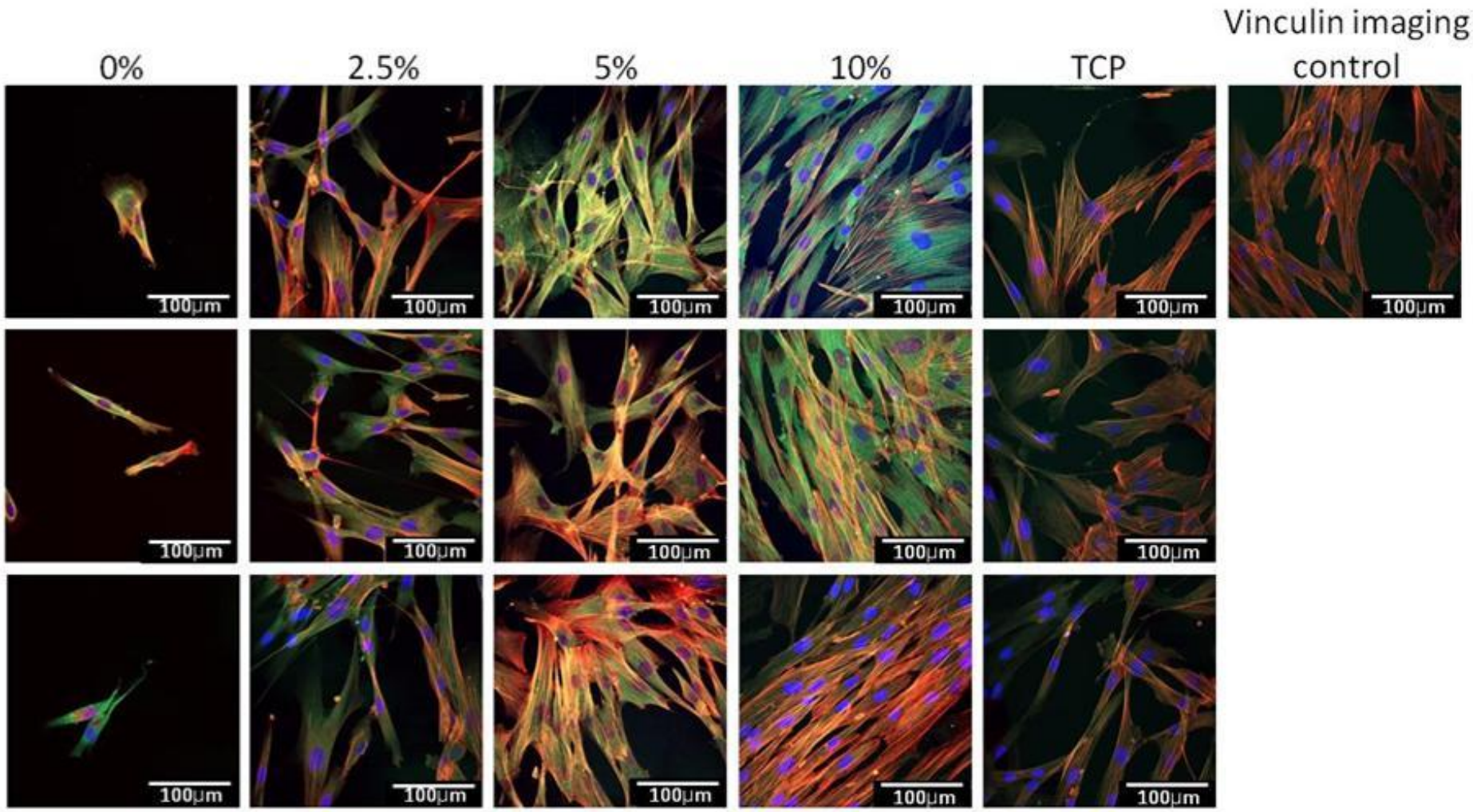

Figure 4.12 - Fluorescent micrograph images by confocal microscopy of human dermal fibroblasts after 24 hours culture on HB-PNIPAM X-PVP BS-IPNs containing 0, 2.5, 5 and 10 wt% of HB-PNIPAM-GRGDS with x40 objective lens with 100µm scale bars. Actin filaments labelled with Phalloidin-TRITC (red), nuclear staining with DAPI (blue) and vinculin labelled green.

The data were corroborated by MTT cell viability data (Figure 4.13), which showed higher overall viability on the peptide functionalised polymers.

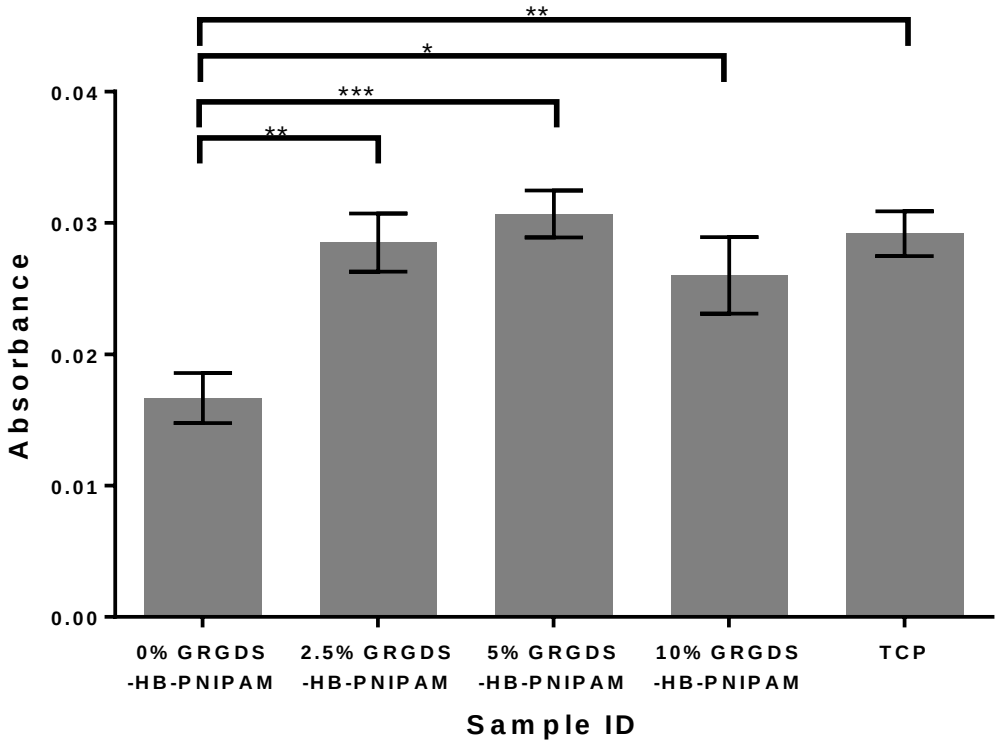

Figure 4.13 - MTT data for human dermal fibroblasts on BS-IPNs containing 0, 2.5, 5 and 10 wt% of HB-PNIPAM-GRGDS. Level of significance by one way ANOVA with multiple comparisons shown by asterisks above (P=0.0008). These data show that the addition of HB-PNIPAM to the membranes has a positive effect on the proliferation and viability of cells cultured on these surfaces.

Many reports have been provided that show that PNIPAM above the LCST supports cell adhesion but cooling to below LCST releases the cells.[81] Previous work by Rimmer *et al.* found PNIPAM grafted to a hydrogel supported the adhesion of chondrocytes at 37°C without the requirement of a cell adhesive peptide [197] and that the sub-micron HB-PNIPAM GRGDS particles lift cells from TCP above their LCST.[80] In both cases as the materials were cooled to below their LCST, the cells were released.

In this case the cells were not released from the substrates upon cooling. This is consistent with the DSC and FTIR data all of which suggest that the HB-PNIPAM is in a collapsed conformation. The BS-IPN is formed, and the crosslinked hydrophillic PVP matrix from the

BS-IPN drives the HB-PNIPAM through its LCST by drawing water away from the PNIPAM. The LCST or these materials is likely much lower than would be expected of an unrestrained polymer in solution. Therefore, it was not possible to cool them sufficiently to release the cells.

4.1.3.10 Migration Data NHDFs

It has been demonstrated theoretically and practically that the migration of cells on a surface will directly affect proliferation.[59-60] The concentration of peptide expression must be used for optimal migration. Low concentrations of peptide may not give the required cell adhesive properties.[57] Whereas, high concentrations can cause a "locking down" effect on the cells, inhibiting cell migration.[58] The migration of cells on an implanted medical device can be very important characteristic for biomaterial applications and thus was studied in detail. In a peripheral nerve repair application cells with a higher rate of migration could traverse a larger gap more readily allowing the nerve to heal with the aid of a nerve guidance conduit. HDF were imaged every 15 minutes. The cells were tracked and the Euclidean distance also known as the displacement (a vector quantity), accumulated distance (a scalar quantity) and speed were calculated from the data. A visual explanation of these terms is given in Figure 4.14. The data is shown in Figure 4.15.

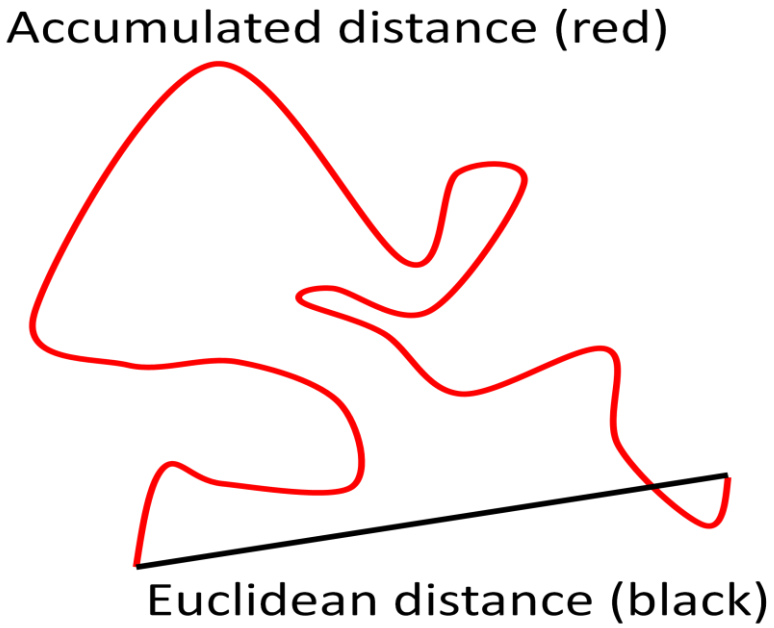

Figure 4.14 – A schematic diagram showing the path of a cell over time (red), the Euclidean and accumulated distances are shown in black and red respectively.

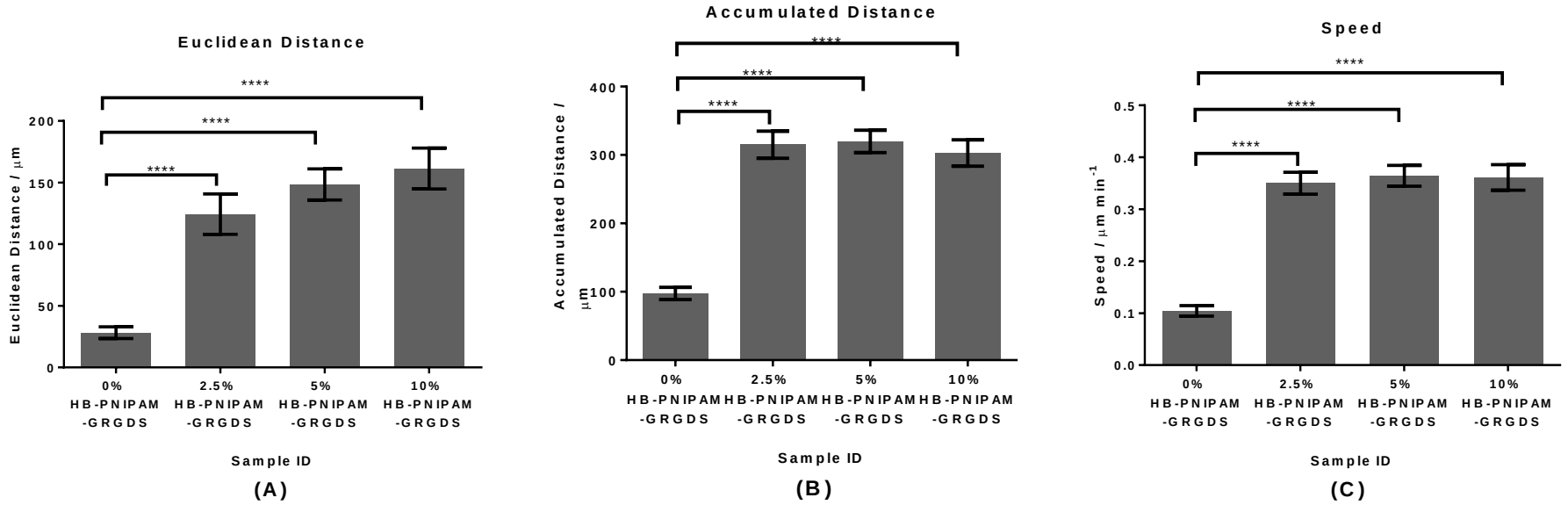

Figure 4.15 - Cell migration data for HDFs on X-PVP BS-IPN samples. Euclidean distance (A), accumulated distance (B) and Speed (C). Level of significance between 0% HB-PNIPAM and other concentrations by one way ANOVA with multiple comparisons. No significant difference between 2.5, 5 and 10% was observed [(A) – ($P<0.0001$), (B) – ($P<0.0001$), (C) ($P<0.0001$). These data show that the measured migratory parameters all increase upon addition of HB-PNIPAM GRGDS to the BS-IPN system.

Notably, the accumulated distance is much larger than the Euclidean distance. This is to be expected as the movement of the cells has no specific directionality. This difference is therefore indicative of the 'random walk' behaviour of cells caused by cycling through process of adhesion, spreading, migration and division. The non-fouling nature of the X-PVP matrix makes it a good negative control allowing it to show the effects of adding HB-PNIPAM-GRGDS to the system. One concern is that the X-PVP sample may overestimate some of the measured cell behaviours as the poorly adhered cells 'roll' around on the surface, which can give an artificially high reading. In these cases, cells often adhered to other cells in preference to PVP. The movement of cell clusters had to be tracked, as opposed to individual cells, which were tracked in the HB-PNIPAM-GRGDS containing BS-IPN samples. All three measurements show a significant change (by ANOVA) in the behaviour upon addition of 2.5 wt% GRGDS HB-PNIPAM. As reported by Hubbell *et al.* an RGD spacing of 440 nm is sufficient for integrin mediated cell spreading and 140 nm is sufficient for focal contact adhesion.[56] The 2.5 wt% HB-PNIPAM-GRGDS sample corresponds roughly to the 440 nm RGD spacing, at this concentration cells are adherent and able to spread. At higher concentrations of HB-PNIPAM-GRGDS the focal adhesions plaques observed by vinculin staining appeared to reduce in size (Figure 4.12) but no increase in cell migration was observed. Although, the number of available RGD sites provided by the polymer increases and a change was observed in the morphology of the cells (Figure 4.12), there was no significant change in the measured migration parameters. This suggests that the $\alpha 5\beta 1$ integrin receptors were saturated. However, no reduction in cell migration was observed with increased RGD concentration.

4.1.3.11 *In Vitro* Culture of Primary Schwann Cells on X-PVP BS-IPNs

The samples were also tested using rat derived primary Schwann Cells. This cell type was chosen as it was hoped that these materials could be used to produce improved nerve guidance conduits to be used in peripheral nerve repair. Schwann cells are an important cell type in the environment of a peripheral nerve injury. In this environment the Schwann cells release signalling factors which help guide the growth of neural cells to repair the damaged nerve. As these cells are very important to the repair of a peripheral nerve then a good interaction with this cell type would be highly desirable for this type of biomaterial. As the

cells used are primary cells we would expect that these cells would give a result more representative of a result in the body.

Rat-derived primary Schwann cells were cultured on HB-PNIPAM-GRGDS X-PVP BS-IPN samples for 4 days. The MMT data for cell viability are shown in Figure 4.16. The data corroborated what has been shown with NHDFs: there was an increase in cell viability with the introduction of the HB-PNIPAM-GRGDS. However, the dose dependent increase in cell viability was not observed. A significant difference was observed between the 0% HB-PNIPAM-GRGDS sample and the HB-PNIPAM GRGDS containing samples. However, all of the HB-PNIPAM-GRGDS samples were statistically similar.

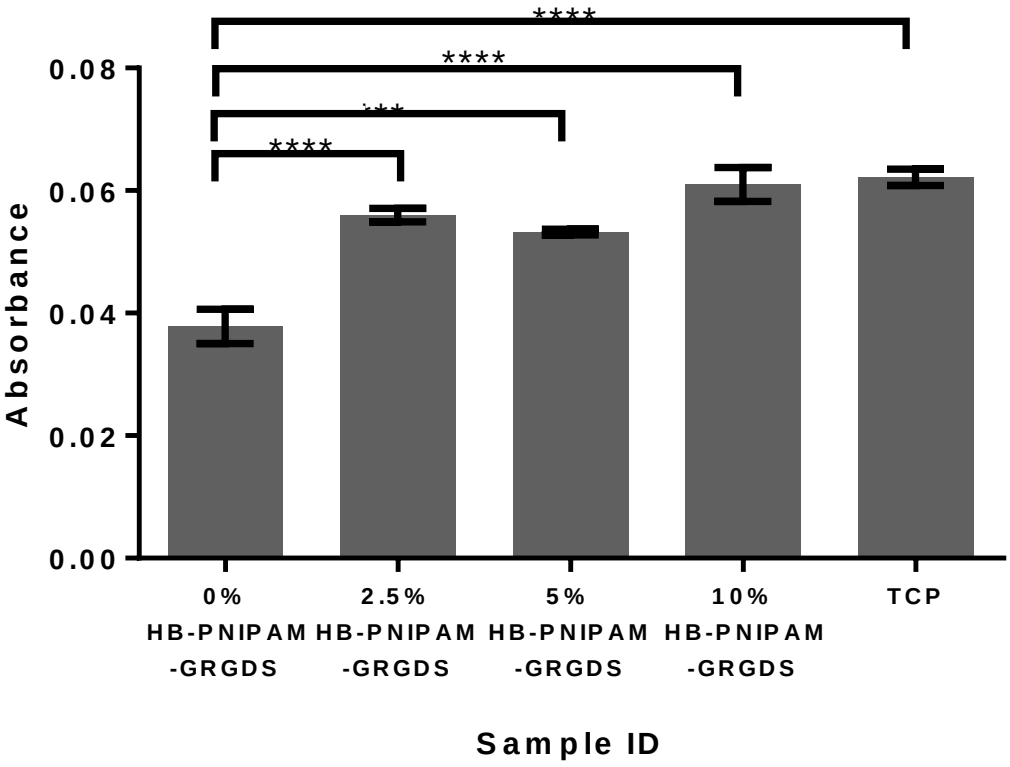

Figure 4.16 - MTT data from rat derived primary Schwann cells on HB-PNIPAM-GRGDS PVP BS-IPNs after 72 hours culture, with error bars showing standard error. Level of significance calculated by one way ANOVA with multiple comparisons shown by asterisks above (P< 0.0001). These Data show an increase in viability and proliferation of cells on addition of the HB-PNIPAM-GRGDS additive the BS-IPNs.

Although there is no dose-dependent increase in the cell viability by MTT, there does appear to be an increase in the cell density and a change in the cell morphology as shown in Figure

4.17. The change in cell morphology is typical of a more adherent cell. Cells appear flatter with multiple projections as the HB-PNIPAM-GRGDS concentration is increased.

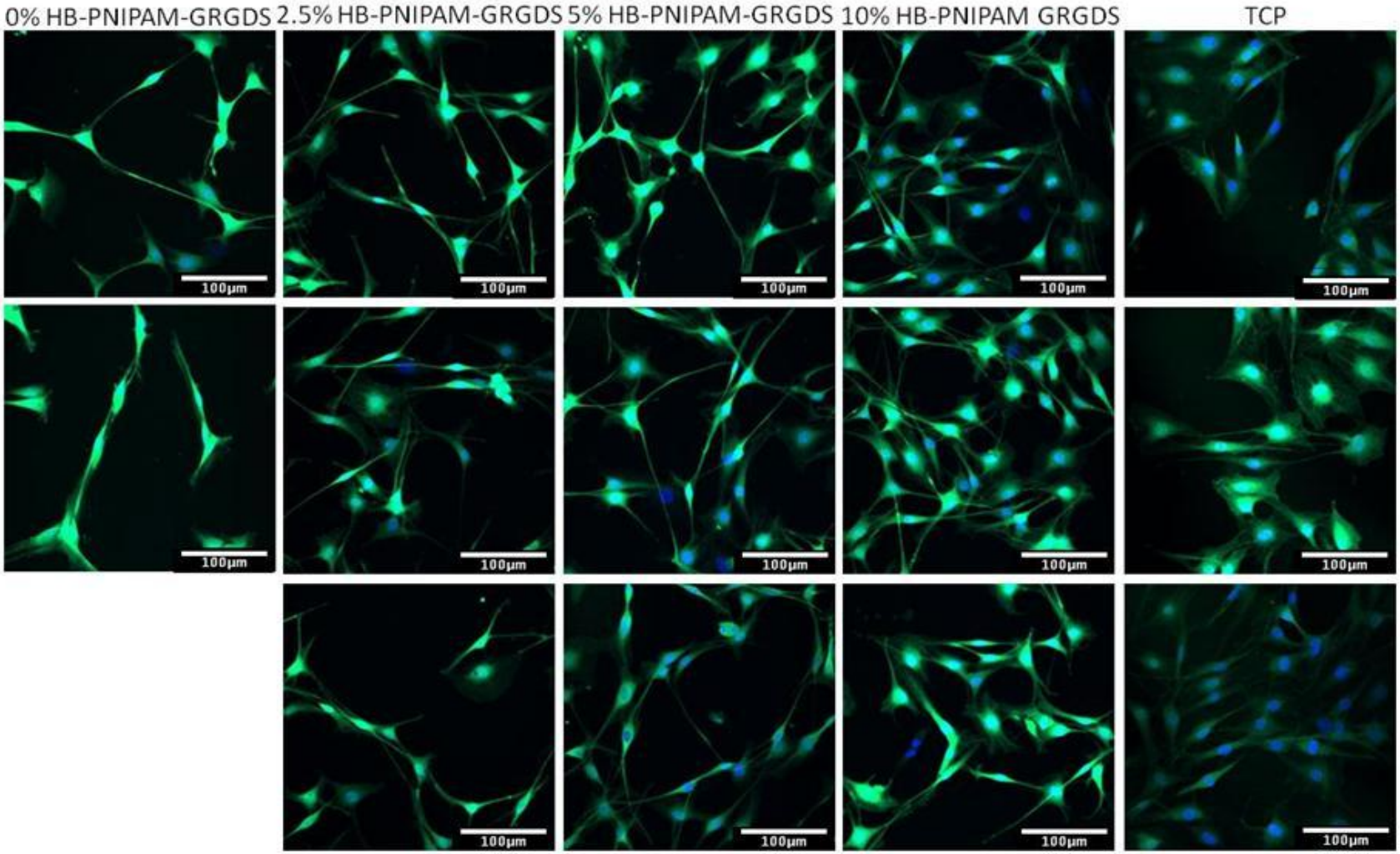

Figure 4.17 - Fluorescence micrographs by confocal microscopy of rat derived primary Schwann cells after 5 days culture on HB-PNIPAM-GRGDS X-PVP BS-IPN surfaces at. Images taken with x40 objective lens (100µm scale bars). Nuclei stained with DAPI (blue) and S100 labelled with TRITC (green). The images show an increase in cell density with increasing concentration of the HB-PNIPAM-GRGDS additive.

4.1.3.12 Projection Microstereolithography

Previous work by Pateman *et al* used stereolithography to produce nerve guidance conduits from a PEG based monomer system.[198] This system was an unmodified PEG which could be improved by the addition of HB-PNIPAM-GRGDS additive. This X-PEG system will be used in 4.2.6.7 where it will be functionalised with HB-PNIPAM-GRGDS. In this section the X-PVP matrix will be used to create BS-IPNs. Traditional methods of producing nerve guidance conduits rely on producing a product which is often available in a limited range of dimensions. The nature of peripheral nerve injury often meant that great flexibility is required in the dimensions of the conduit. This makes stereolithography a good choice for production of customised nerve guidance conduits. Although, the PEG based system used previously did achieve good results,[198] the incorporation of the HB-PNIPAM-GRGDS additive could be used to increase cell viability and proliferation within the conduit which would allow a greater gap to be bridged.

The photocurable nature of these materials makes them suitable for the manufacture of devices by projection microstereolithography. The structures in Figure 4.18 have been manufactured using a 405 nm laser with DMD. The image of a triangle, circle or square is projected into the monomer, and a stage moved downwards allowing the tubes to build up the polymerised structure. These circular tubes are routinely used as nerve guidance conduits. The triangular and square tubes have been made to illustrate the flexibility of this system with respect to creating structures of varying shaped and complex architectures. BS-IPN systems could be incorporated to create advanced biofunctional copolymer variants. This could help bridge larger gaps between the proximal and distal ends of the severed nerves. Current nerve guidance conduits can bridge gaps of >3cm, they are made via a range of techniques and with a multitude of biomaterials.[159] It is proposed that adding such functionalities will allow larger gaps to be bridged.

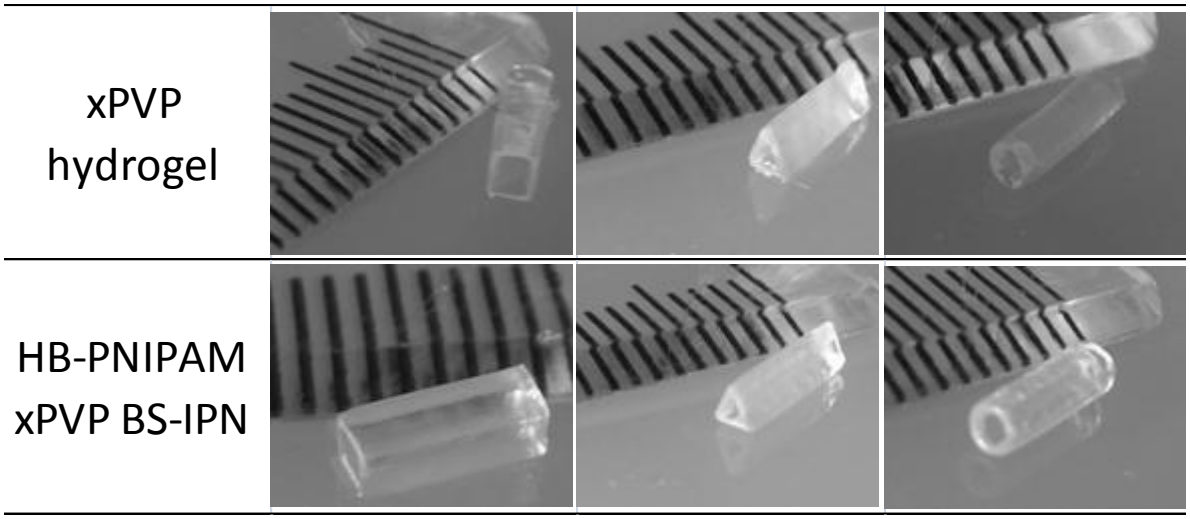

Figure 4.18 - Images of HB-PNIPAM X-PVP BS-IPN and X-PVP structures created by stereolithography. Ruler with 1mm increments used for scale. Circular tube type structures could be used in peripheral nerve repair. The square and triangular structures have been fabricated to demonstrate that alternative complex architectures are possible and this system could be used for many medical device types.

The samples produced are stable crosslinked hydrogels, based on data in section 4.1.3.4 it can be assumed that these polymers had a high equilibrium water content. The high degree of swelling of these samples did lead to large deformations of sample dimensions on drying. This was problematic for imaging by SEM, as dried samples did not represent their original shape or dimensions. To avoid problems with shrinkage upon drying, images were taken using swollen samples. Images of fully hydrated samples were taken using a camera with a macro lens. This gave an accurate indication of the shape and dimensions of the structure. Although the high water content is problematic for imaging, it allows high permeability of oxygen and nutrients through the walls of the structure, which is beneficial for the healing process and prevents the accumulation of waste products.

4.1.4 Conclusion

A significant proportion of the HB-PNIPAM incorporated into a BS-IPN can be permanently entrapped. It was hypothesised that this polymer becomes entrapped due to an entangling effect of the polymer matrix. To remove the branched component would require the polymer chains to take up highly unfavourable conformations.

Once incorporated into a BS-IPN, the osmotic pressure of the X-PVP matrix causes water to be drawn away from the HB-PNIPAM. This results in an LCST transition that is significantly lower than expected. Hence the transition could not be observed. From DSC, FTIR and extractability data it is assumed that the HB-PNIPAM is entrapped within the PVP matrix with a partially collapsed morphology. Here n-clusters may form and aggregate to some degree. However, physical interactions from adjacent polymer chains prevent the full collapse to the globular HB-PNIPAM.

HB-PNIPAM-GRGDS has been shown to have a positive effect on cellular adhesion when permanently entrapped within a PVP matrix forming a BS-IPN. HDFs will adhere more strongly to this substrate when compared to an X-PVP hydrogel or a BS-IPN containing HB-PNIPAM-COOH. When the concentration is increased from 2.5 to 5 to 10% HB-PNIPAM-GRGDS there is a dose dependent increase in the adhesion of cells to these surface. This increase in cellular adhesion and morphology has been correlated with the results of Hubbell *et al.*[56] This showed an RGD spacing of 440 nm was required for cellular adhesion and a 140 nm spacing was required for cells with fully adherent normal morphology and spreading.

These results were corroborated by the Schwann cell imaging data and by migration of HDFs on BS-IPN surfaces. A similar dose dependent increase was observed in migratory parameters leading to the conclusion that the 2.5% system roughly corresponded to a 440 nm spacing and the 10% system roughly corresponded to a 140 nm RGD spacing.

These materials could be used in medical devices, and as such were structured by projection microstereolithography to create tube type structures that could be used for peripheral nerve repair.

4.2 Branched Semi-Interpenetration Polymer Networks with a Poly(ethylene glycol) (PEG) Matrix

4.2.1 Abstract

Following on from section 4.1, BS-IPNs have been synthesised using PEG-DA to form the polymer matrix. It was found that PEG-DA could retain around 100% of the HB-PNIPAM within the membrane after 48h of rigorous soxhlet extraction. As with X-PVP BS-IPNs the X-PEG BS-IPNs did not exhibit the LCST normally associated with PNIPAM. This was demonstrated by DSC, and equilibrium water contents. The inclusion of the peptide functional branched polymeric component (HB-PNIPAM-GRGDS) improved the cytocompatibility of the membranes allowing greater proliferation, adhesion and a higher rate of migration of relevant cell types.

4.2.2 Experimental

4.2.2.1 Synthesis of 4-Vinylbenzyl Pyrrolecarbodithioate

A detailed description of the synthesis of 4-vinylbenzyl pyrrolecarbodithioate can be found in section 2.2.1.

4.2.2.2 Synthesis of Pyrrolecarbodithioate Ended HB-PNIPAM

A detailed description of the synthesis of pyrrolecarbodithioate ended HB-PNIPAM can be found in section 2.2.2.

4.2.2.3 Carboxilic Acid Functionalisation of Pyrrolecarbodithioate Ended HB-PNIPAM

A detailed description of the synthesis of carboxylic acid functionalised HB-PNIPAM can be found in section 3.2.3

4.2.3 Peptide Synthesis

A detailed description of the synthesis and isolation of the GRGDS peptide sequence can be found in 3.2.4 and 3.2.5.

4.2.4 GRGDS Functionalisation of HB-PNIPAM

A detailed description of the synthesis HB-PNIPAM-GRGDS is described in section 3.2.6.

4.2.4.1 Production of Interpenetrating Polymer Networks

4.2.4.1.1 Formulations

The formulation shown in Figure 4.3 was made up in a glass vial without the initiator, 2-hydroxy-2-methyl-1-phenyl-1-propanone (HMPP). The contents of the vials was stirred in the absence of light until the highly branched polymer had completely dissolved in the

monomer and solvent. The samples were then degassed by bubbling with N_2 before the initiator was added. The monomer/polymer solution was then ready to use.

Table 4.3 – A table showing the formulations for HB-PNIPAM PEG-DA (Mn~250) semi-IPN.

Sample	PEG-DA/g	GRGDS-HB-PNIPAM/g	HMPP/g	DMSO/g
0% GRGDG-HB-PNIPAM	1	0	0.02	0.5
2.5% GRGDG-HB-PNIPAM	1	0.035	0.02	0.5
5% GRGDG-HB-PNIPAM	1	0.05	0.02	0.5
10% GRGDG-HB-PNIPAM	1	0.1	0.02	0.5

4.2.4.1.2 Production of Branched Semi-IPN Coated Cover Slips

A detailed description of the production of BS-IPN coated cover slips can be found in section 4.1.2.6.2.

4.2.4.1.3 Production of Branched Semi-IPN Sheets

A detailed description of the production of BS-IPN sheets can be found in section 4.1.2.6.3.

4.2.4.2 Soxhlet Extraction of BS-IPN Sheets

A detailed description of the Soxhlet extraction of BS-IPN Sheets can be found in section 4.1.2.7.

4.2.4.3 Concentration of Remaining HB-PNIPAM in BS-IPNs by FTIR

A detailed description of the measurement of HB-PNIPAM within a membrane by FTIR can be found in section 4.1.2.8.

4.2.4.4 Equilibrium Water Contents of BS-IPNs

A detailed description of the measurement of equilibrium water contents for BS-IPN samples can be found in section 4.1.2.10.

4.2.4.5 Cell Culture and Imaging of Primary Human Fibroblast on BS-IPN Sample

A detailed description of cell culture and imaging of HDFs can be found in 4.1.2.11 and 4.1.2.12.

4.2.5 Migration Study of Primary Human Fibroblast on BS-IPN samples

A detailed description of the method used in the migration study of HDFs can be found in 4.1.2.13.

4.2.5.1 Culture of Dorsal Root Ganglion Explants on BS-IPNs

Male Wistar rats were sacrificed by cervical dislocation in accordance with the Animals (Scientific Procedures) Act 1986.[199] The skin was removed to allow the spine to be removed cleanly. The spine was cut longitudinally and the DRGs were extracted. Excess flesh was removed from the DRGs before placing them onto the test samples. The excess liquid around the DRG was removed with a pipette. The test samples were fixed in place with cell crowns (manufactured in house) and the tissue culture plate was incubated at 37°C with 5% CO_2 for 15 minutes to allow the explant to adhere to the surface. Supplemented DMEM (1 mL): 10% (v/v) neonatal calf serum, 0.25 µg mL^{-1} amphotericin B, 2 mM glutamine, 100 units mL^{-1} penicillin and 100 µg mL^{-1} streptomycin, was added to the well, covering the DRG. Samples were incubated at 37°C with 5% CO_2 for 14 days.

4.2.5.2 Imaging of Dorsal Root Ganglia on BS-IPN Samples

Cells were fixed using a 3.7% (w/v) formalin solution for 20 minute. The formalin solution was removed and the samples were washed with PBS before permeablising the cell membranes with 0.1% (w/v) Triton X100 in PBS. The samples were then incubated at room temperature in a 5% (w/v) solution of bovine serum albumin (BSA) for one hour. The cells were then labelled with the primary antibodies, anti-β tubulin primary mouse monoclonal antibody (Promega Corporation, Southampton, UK) (1:500) in 1% (w/v) BSA in PBS and anti-S100 β rabbit polyclonal IgG (Dako.UK Ltd, Cambridge UK) (1:250) in 1% BSA in PBS. The samples were incubated for 24 hours at 5°C. The samples were washed then incubated with the secondary antibodies, horse anti-mouse IgG conjugated Texas Red (Vector Labs, Peterborough, UK) (1:250) in 1% (w/v) BSA in PBS and fluorescein conjugated goat anti-rabbit IgG (Vector Labs, Peterborough, UK) (1:250) in 1% (w/v) BSA in PBS. The samples were incubated at room temperature for 1 hour before addition of 4,6-diamidino-2-

phenylindole dihydrochloride (DAPI) (nuclear stain) (300 nM) (1:1000) in 1% BSA in PBS which was incubated at room temperature for a further hour.

Images were collected using a Zeiss LSM 510 META confocal microscope and Zeiss LSM Imager software with a tunable 2-photon Ti-saphire laser (Chamelion Ultra II, Coherent Inc.), set to 750 nm, a 543 nm laser and a 488 nm laser. DRGs were imaged using a x10 magnification Zeiss W Plan Achromat objective lens. 543 nm light was used to excite the Texas Red label, the emission was observed at 576 nm. FITC was excited with 488 nm light and the emission was observed at 525 nm. The DAPI label was excited with 750 nm light and the emission was observed at 480 nm.

4.2.5.3 MTT Assay

Cells were seeded onto test samples and positive and negative controls and cultured at 37°C and 5% CO_2. At the required time point the cells were removed from the incubator and the cell culture medium was removed. The cells were washed with PBS before adding 1 mL of 3,4,5-dimethylthiazol-2,5-diphenyl tetrazonium bromide (MTT) (0.5 mg mL^{-1}). The samples were incubated at 37°C with 5% CO_2 for a further 45 minutes before removal of the MTT solution and addition of 300 µL of acidified isopropanol. The resulting purple solution was pipetted into a 96 well plate and the absorbance measures at 540 nm with a 630 nm reference.

4.2.5.4 3D Structuring by Stereolithography

A detailed description of the stereo lithography set up and the procedure used to manufacture 3D structures is given in section 4.1.2.15

4.2.5.5 Analysis of Variance

An explanation of the ANOVA statistical test has been given in section 3.2.10

4.2.6 Results and Discussion

4.2.6.1 Concentrations of HB-PNIPAM Within Extracted BS-IPN Samples

BS-IPN samples were subjected to 48 hours of Soxhlet extraction in isopropanol. The analysis was carried out using 'TQ analyst' software by Thermo Scientific. FTIR spectra of unextracted samples were used to create a calibration curve, of known concentrations, which had a correlation coefficient of 0.998. The concentration data, calculated from FTIR spectra of the unknown extracted samples, were compared to the calibrations curve using the 'TQ analyst' software. The concentrations of each component was calculated and the data are shown in Figure 4.19.

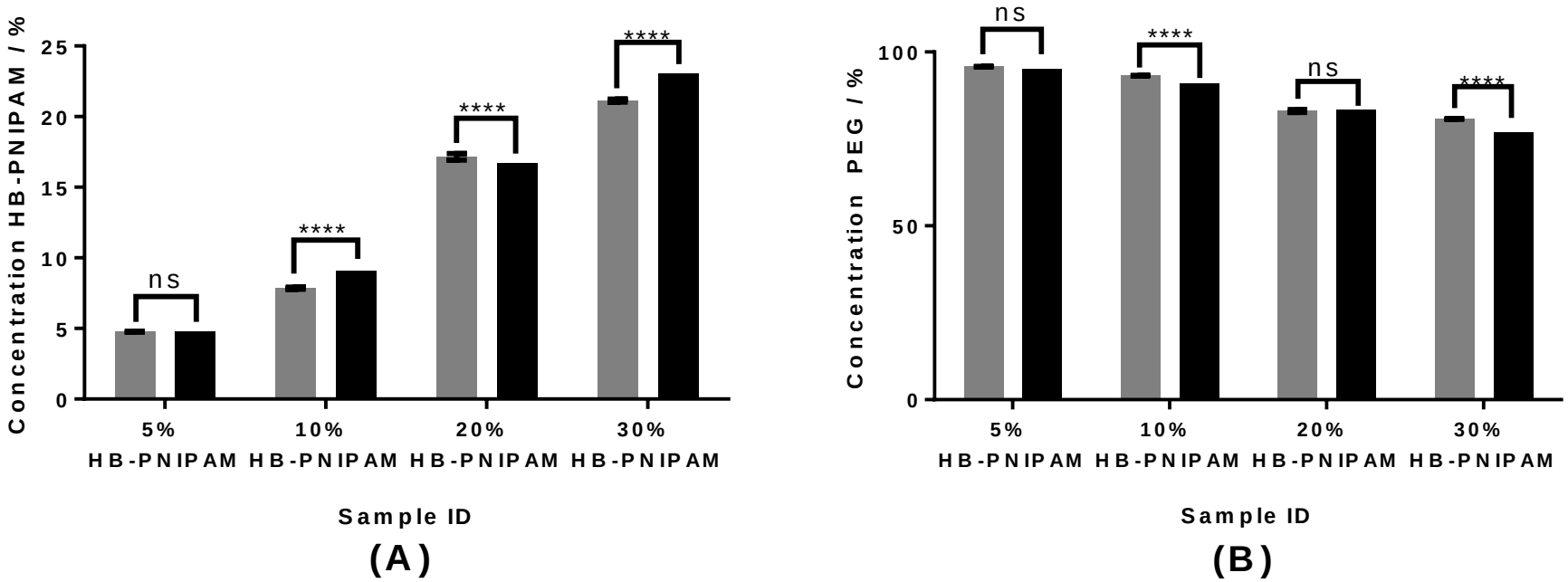

Figure 4.19 - Concentrations of components in HB-PNIPAM BS-IPN X-PEG measured data shown in light grey expected data shown in dark grey. PEG concentration with standard error (A), HB-PNIPAM concentration with standard error bars (B). Significance measured by one way ANOVA with multiple comparisons, the level of significance is indicated by asterisks above [(A) – (P <0.0001), (B) – (P<0.0001)]. These data show that there is little variation in the relative concentrations of X-PEG and HB-PNIPAM within the polymer matrix before and after Soxhlet extraction.

Figure 4.19 shows that there is very little change in the concentration of HB-PNIPAM between the extracted samples and expected values from the feed values. In X-PEG BS-IPNs a very high proportion of the HB-PNIPAM has been retained, compared to the X-PVP BS-IPN system previously investigated. It is apparent in both systems that within the concentrations investigated the proportion of HB-PNIPAM retained is proportional to the amount added to the system. There does not seem to be a plateau after which more HB-PNIPAM will not be retained.

Interestingly the extracted 20% HB-PNIPAM BS-IPN sample contains a higher concentration of HB-PNIPAM than the expected concentration. The ANOVA statistical test shows that this difference is statistically significant. When the PEG concentrations are scrutinised, it can be seen that in the 20% HB-PNIPAM BS-IPN sample there is no significant difference between the extracted and the feed concentration of PEG. This is not the case for the extracted 10 and 30% HB-PNIPAM BS-IPN samples which have a significantly higher PEG percentage than the feed. This shows that in the 10 and 30% HB-PNIPAM BS-IPN samples have had a small amount of HB-PNIPAM extracted and probably a smaller amount of unreacted PEG-DA. In the case of the 20% HB-PNIPAM BS-IPN sample it is possible that a greater proportion of the PEG has been extracted relative to the HB-PNIPAM. This gives the impression of an increase in the HB-PNIPAM concentration as the relative concentration of X-PEG has been reduced. By ANOVA there is no statistical difference in the concentrations of HB-PNIPAM or PEG before or after extraction for the 5% HB-PNIPAM sample. The 5% HB-PNIPAM BSIPN sample seems to be unchanged by the soxhlet extraction process.

The histograms in Figure 4.19 show that for the samples 5, 10 and 30% HB-PNIPAM the measured PEG concentration is higher than the expected PEG concentration. This validates the theory that the PEG matrix is fully cured and the HB-PNIPAM is preferentially extracted. However, this is not the case for the 20% HB-PNIPAM sample. This implies that PEG could also have been extracted, which could account for the unexpected result in the HB-PNIPAM concentration for this sample.

A disadvantage of this technique it that it is internally calibrated, so only relative proportions of each component can be calculated. This can lead to a level of uncertainty in the data. For example, is the same proportions of both components (the matrix and the

branched polymer) were extracted from the matris this would appear as though nothing had been extracted as the relative concentrations of the two components within the membrane unchanged.

4.2.6.2 DSC of Water Swollen BS-IPN Samples

It was previously show that a HB-PNIPAM BS-IPN in X-PVP showed no measurable LCST transition in the temperature range measured. This effect has also been observed in X-PEG BS-IPN systems, as shown in Figure 4.20. When measured by DSC, there was no observable peak corresponding to the LCST. The results from FTIR, DSC and equilibrium water content for the X-PVP BS-IPN system allowed us to from a theory that the polymer was in a partially collapsed state where n-clusters had formed but the constraints of the matrix prevented the transition to the globule. This meant that the polymer could not be extracted as it was entangled but dehydration of the polymer chains was evident from the FTIR data. The featureless curves shown in Figure 4.20 are evidence that the HB-PNIPAM within the X-PEG BS-IPNs may be in a similar partially collapsed state as in the X-PVP BS-IPN systems.

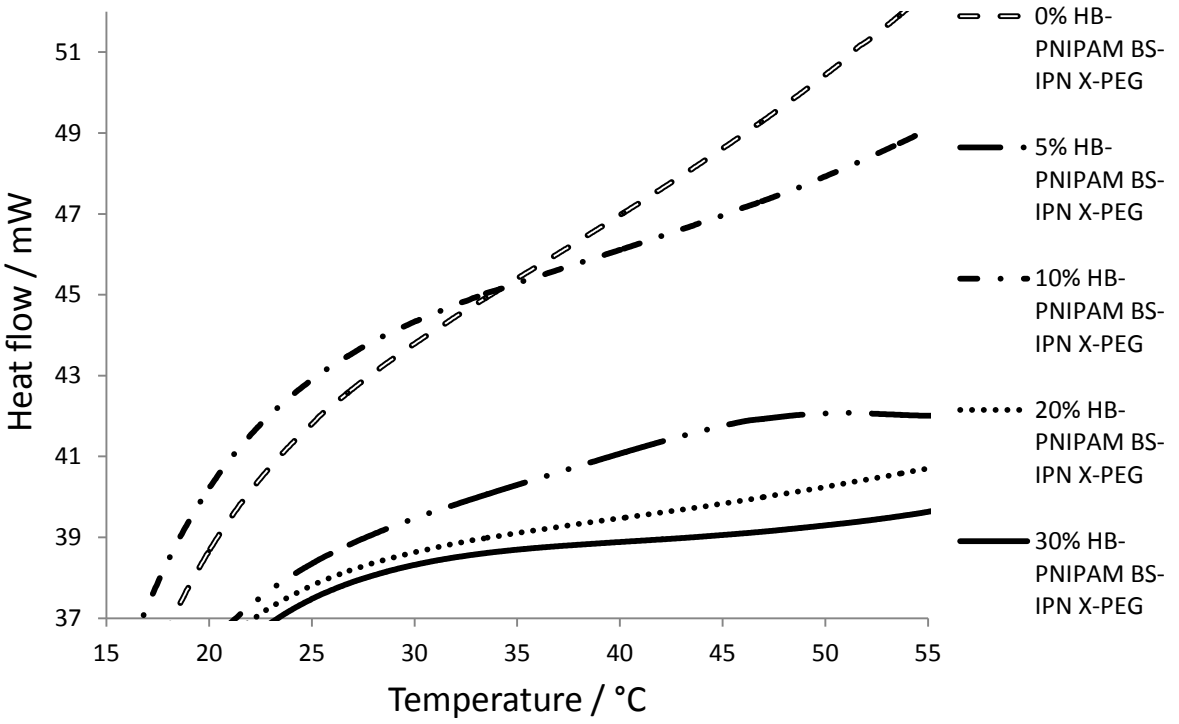

Figure 4.20 – A figure showing DSC curves for 0, 5, 10, 20 and 30% HB-PNIPAM BS-IPN samples showing lack of observable endotherm for the HB-PNIPAM LCST.

4.2.6.3 Equilibrium Water Content of Swollen BS-IPN Samples

The equilibrium water content for X-PEG based BS-IPNs are shown in Figure 4.21. It was expected that measurement of equilibrium water contents over a temperature range relevant to the LCST of HB-PNIPAM would provide insight into the presence or absence of an LCST transition. The ANOVA statistical test was applied to the data in Figure 4.21 and it shows that there is no significant change in the swelling of BS-IPN samples with temperature. This corroborates the data for PVP BS-IPNs where no stepwise change in swelling was observed. The changes in water content in both systems can be put down to evaporation at high temperature. Hence the large experimental error and lack of statistical significance in the results.

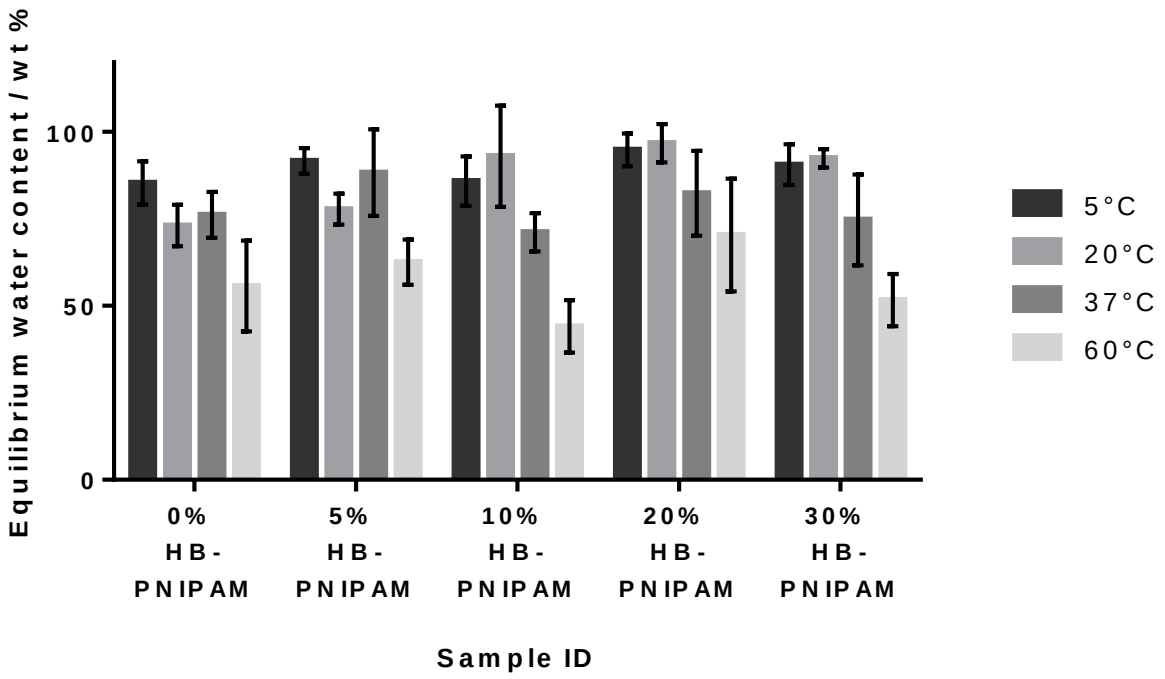

Figure 4.21 - Equilibrium water contents for 0, 2.5, 5, 10, 20 and 30% HB-PNIPAM BS-IPNs with PEG at 5, 20, 37 and 60°C. Level of significance determined by one way ANOA. No significant difference was found between any values (P<0.0001). As no significant difference was found between any of the samples it was concluded that there is no LCST transition.

With the equilibrium water content data there is a large error. This makes interpreting the data difficult. It is important to use this method in conjunction with other methods such as

the DSC. As no LCST transition was observed by DSC (Figure 4.20) and the dehydration shown by equilibrium water contents (Figure 4.21) was shown to be insignificant by ANOVA, it is likely that the partially collapsed HB-PNIPAM observed in the X-PVP BS-IPN is present in the X-PEG BS-IPN systems as well.

4.2.6.4 Cell Culture Rat Derived Primary Schwann Cells on BS-IPN Samples

Schwann cells are an important cell type in the environment of a peripheral nerve injury. In a peripheral nerve injury they will release chemical signalling factors which guide the growth of neural cells which will aid the repair of the nerve. Therefore increasing the adhesion and proliferation of these cells will improve the healing in a peripheral nerve injury. A good result with this cell type is therefore highly desirable in a biomaterial used for peripheral nerve repair.

HB-PNIPAM-GRGDS has been incorporated into PEG BS-IPN and used to culture rat derived primary Schwann cells. The Schwann cells showed a dose dependent response to the concentration of HB-PNIPAM-GRGDS with higher cell viability recorded by MTT assay being observed at higher HB-PNIPA-GRGDSM loading (Figure 4.22).

The MTT assay gives a measure of the cell density and how well the cells have proliferated over the time period tested. The results of the MTT assay are shown in Figure 4.22. One way ANOVA of the MTT data shows that the 0% HB-PNIPAM (X-PEG) sample is statistically different from all of the HB-PNIPAM-GRGDS containing BS-IPN samples. So it can be concluded that adding the HB-PNIPAM-GRGDS has a beneficial effect on cell behaviour at all concentrations investigated. There is also a significant difference between 2.5/5% and the 10% HB-PNIPAM-GRGDS samples. This demonstrates that for rat derived primary Schwann cells increasing the HB-PNIPAM concentration to 10% has an increasingly beneficial effect on cell viability. 5 and 10% HB-PNIPAM-GRGDS are not significantly different from the positive control, TCP.

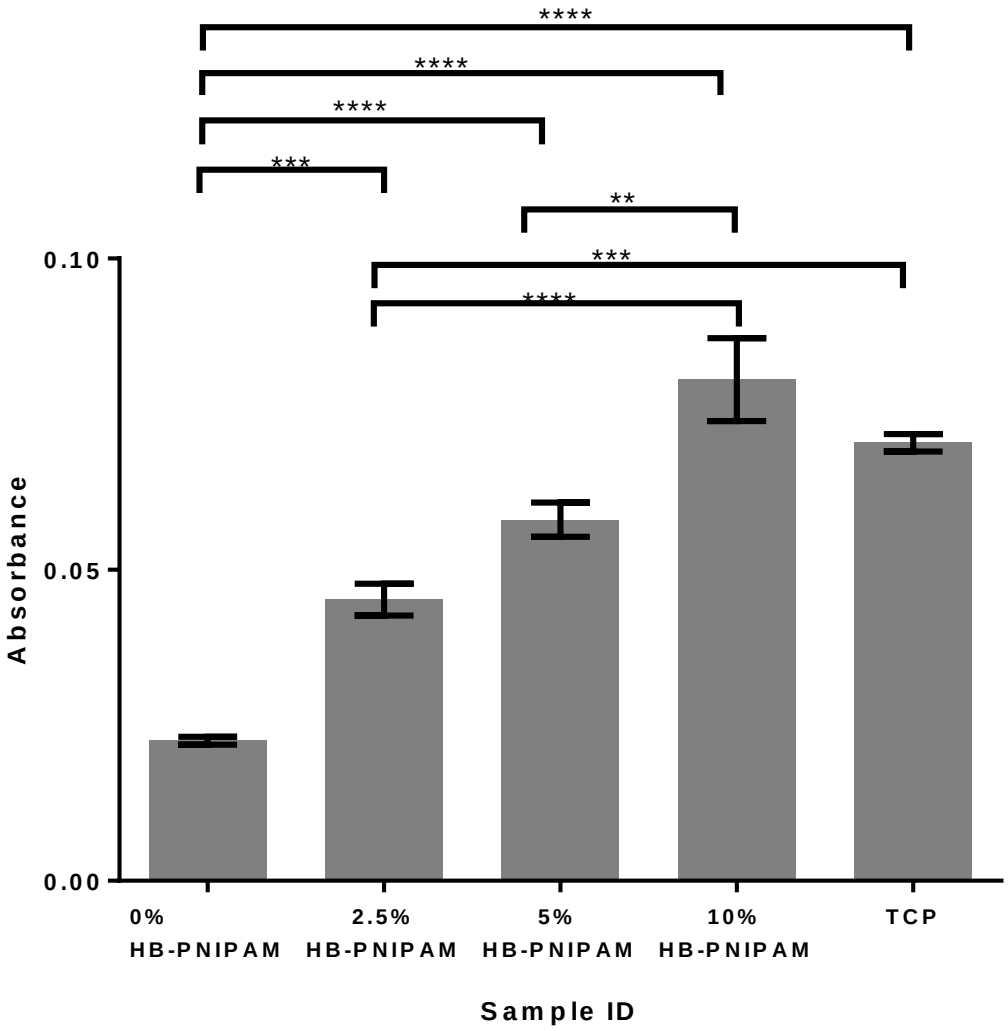

Figure 4.22 - MTT of primary rat derived Schwann cells after 5 days culture on HB-PNIPAM-GRGDS PEG BS-IPNs containing 0, 2.5, 5 and 10% HB-PNIPAM-GRGDS compared to TCP. with error bars showing standard error. Level of significance determined by one way ANOVA with multiple comparisons and indicated above by asterisks (P<0.0001). The data show that the addition of HB-PNIPAM-GRGDS to the X-PEG system improves cell viability and proliferation.

Fluorescence micrographs were used in conjunction with the MTT data to assess the Schwann cells (Figure 4.23). More evidence was provided for the dose dependent effect on increasing cell viability and proliferation. Cells on 0% HB-PNIPAM-GRGDS samples displayed poorly adherent rounded morphologies with low cell density. As the HB-PNIPAM-GRGDS concentration was increased the Schwann cells displayed a spinodal geometry typical of Schwann cells in 2D culture with some adhesion. At 10% HB-PNIPAM-GRGDS, the cells showed a higher cell density with highly adherent flattened morphology.

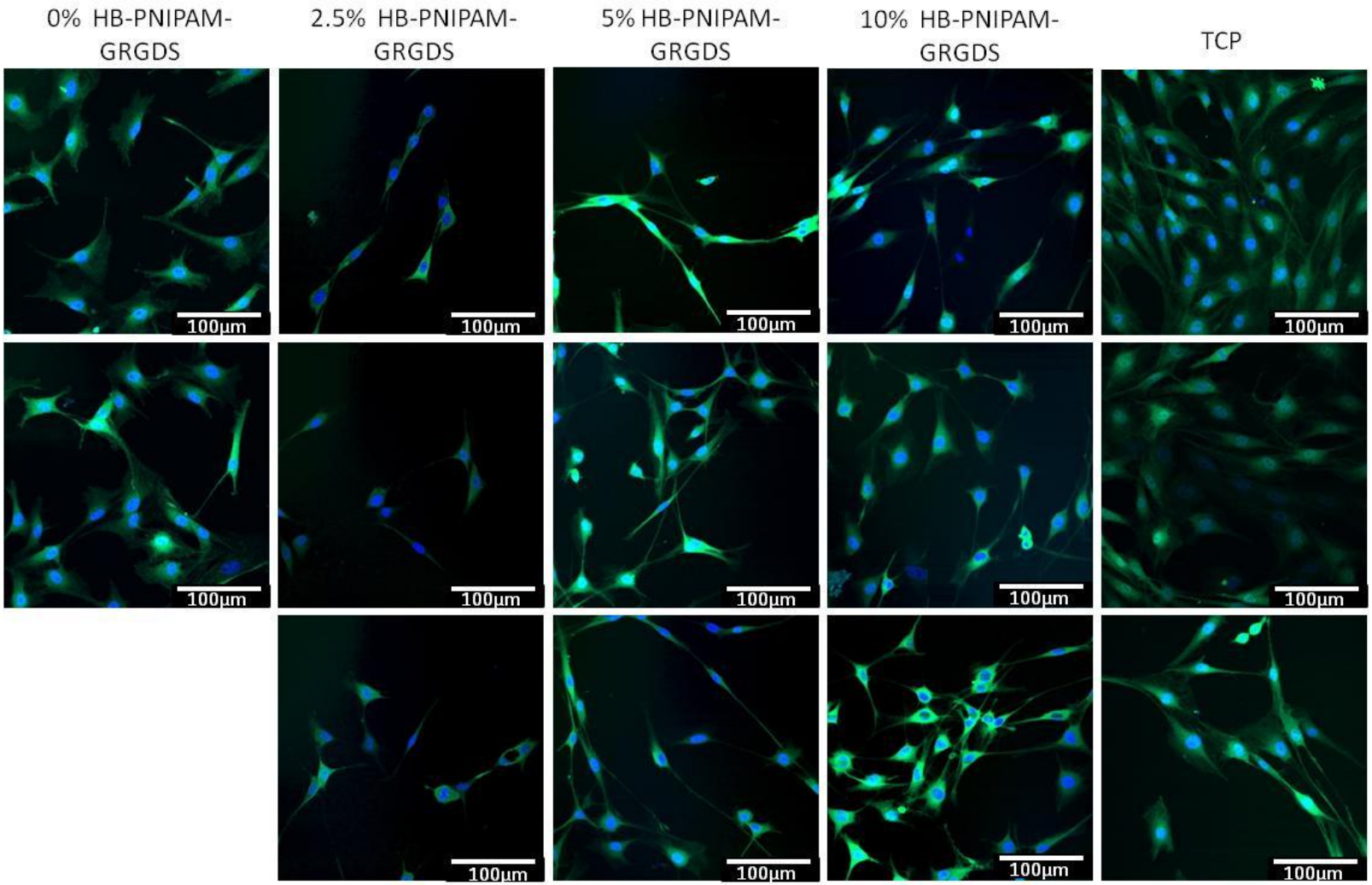

Figure 4.23 – Fluorescence micrographs of rat derived primary Schwann cells after 5 days culture on 0%, 2.5%, 5% and 10% HB-PNIPAM-GRGDS X-PEG BS-IPN samples with TCP as a positive control. Images taken with x40 objective lens (100µmscale bars). Nuclei stained with DAPI (blue) and S100 labelled with TRITC (green).

4.2.6.5 Migration of HDFs on BS-IPN Surfaces

Data from MTT assay and fluorescence micrographs were further corroborated by cell migration data. This is shown in Figure 4.24. Samples were seeded with a low density of cells (10,000 cells). This was done to reduce the chances of cell-cell interactions which complicate measurements. Six regions were selected on each sample and the cells in the region were tracked. No significant difference was observed in the 0, 2.5 and 5% HB-PNIPAM-GRGDS for the accumulated distance, Euclidean distance or speed. However, there was a large increase in all three measured variables for the 10% HB-PNIPAM-GRGDS system. This showed that the 10% HB-PNIPAM=GRGDS system has a statistically significant positive effect on the migration of the cells.

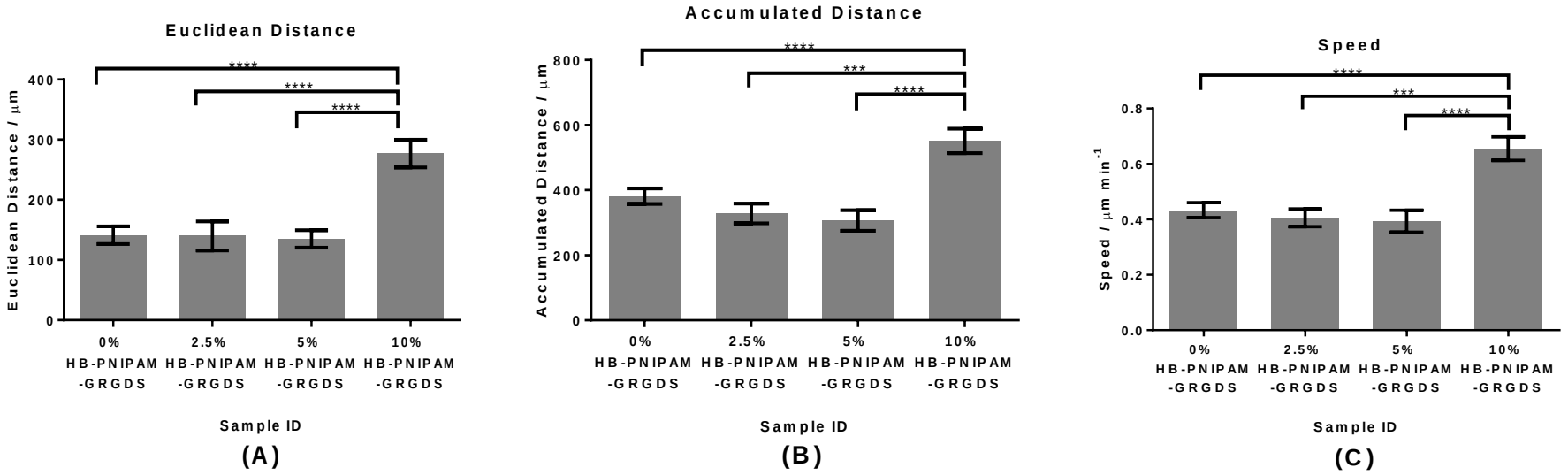

Figure 4.24 - Cell migration data for HDFs on X-PEG (Mn~250) BS-IPN samples. Euclidean distance (A), accumulated distance (B) and Speed (C), with error bars showing standard error. The level of significance was analyses by one way anova with multiple comparisons and is indicated by the asterisks above [(A) P<0.0001, (B) P<0.0001, (C) P<0.0001)]. These data show that at 2.5 and 5 wt% the effect on Hb-PNIPAM-GRGDS is not notsignificant in a X-PEG system. However a large increase in the migratory parameters is observed for the 10 wt% HB-PNIAM-GRGDS system.

Figure 4.24 shows that Euclidean distance accumulated distance and speed all showed no significant difference between the 0, 2.5 and 5% HB-PNIPAM-GRGDS. There was a significant increase between 0, 2.5 and 5% HB-PNIPAM-GRGDS and the 10% HB-PNIPAM-GRGDS. This appears to differ from the PVP sample which showed an increase from the 0% to 2.5% HB-PNIPAM-GRGDS. However, PEG-DA will produce a much more cell adhesive surface than PVP. This is demonstrated by the initial values. For X-PEG (0% HB-PNIPAM PEG BS-IPN) the initial values for the three measured variables are all significantly higher than for X-PVP (0% HB-PNIPAM PVP BS-IPN). There are other (non-integrin based) interactions which allow cells to adhere to surfaces. The increases functionality provided by the PEG-DA allows adhesion of proteins to the surface of the membrane which gives the initial increase in speed and distance moved. The highly crosslinked nature of the PEG-DA also means that is it less swollen. Therefore cells can adhere to these membrane more easily.

4.2.6.6 Primary Dorsal Root Ganglia (DRG) Explants Cultured on X-PEG BS-IPNs

DRGs are clusters of nerve cell bodies found in the vertebral column of the spine. When these pieces of tissue are extracted from the spine all of the primary cell types that are present in a peripheral nerve injury will be present in the explants. This makes experiments using DRGs very good for modelling the repair of a peripheral nerve injury for particular biomaterials. Good results using DRG explants is a strong indication that the biomaterial is a good candidate.

Computational modelling and practical experimentation have been used to demonstrate that the rate migration of cells on a surface directly correlate with proliferation.[59-60] The concentration of peptide should be optimised for the high rates of cell migration.[56-58] The observations for migration of fibroblasts and proliferation of Schwann cells and fibroblasts indicate that there will be a dose dependant increase in outgrowth. The recorded observations for DRG explants outgrowth are shown in the phase contrast and fluorescence micrographs in Figure 4.25. Figure 4.25. These figures show that there is a significant increase in the amount of cellular outgrowth from the DGR after 8 days on BS-IPNs

containing HB-PNIPAM-GRGDS. This is not the case for the X-PEG system which has no outgrowth. This has been highlighted with red arrows and circles in Figure 4.25. The dark shadow in the centre of these images is the DRG. Cells can be seen around these dark shadows and the amount of cellular outgrowth increases as the concentration of HB-PNIPAM-GRGDS increases.

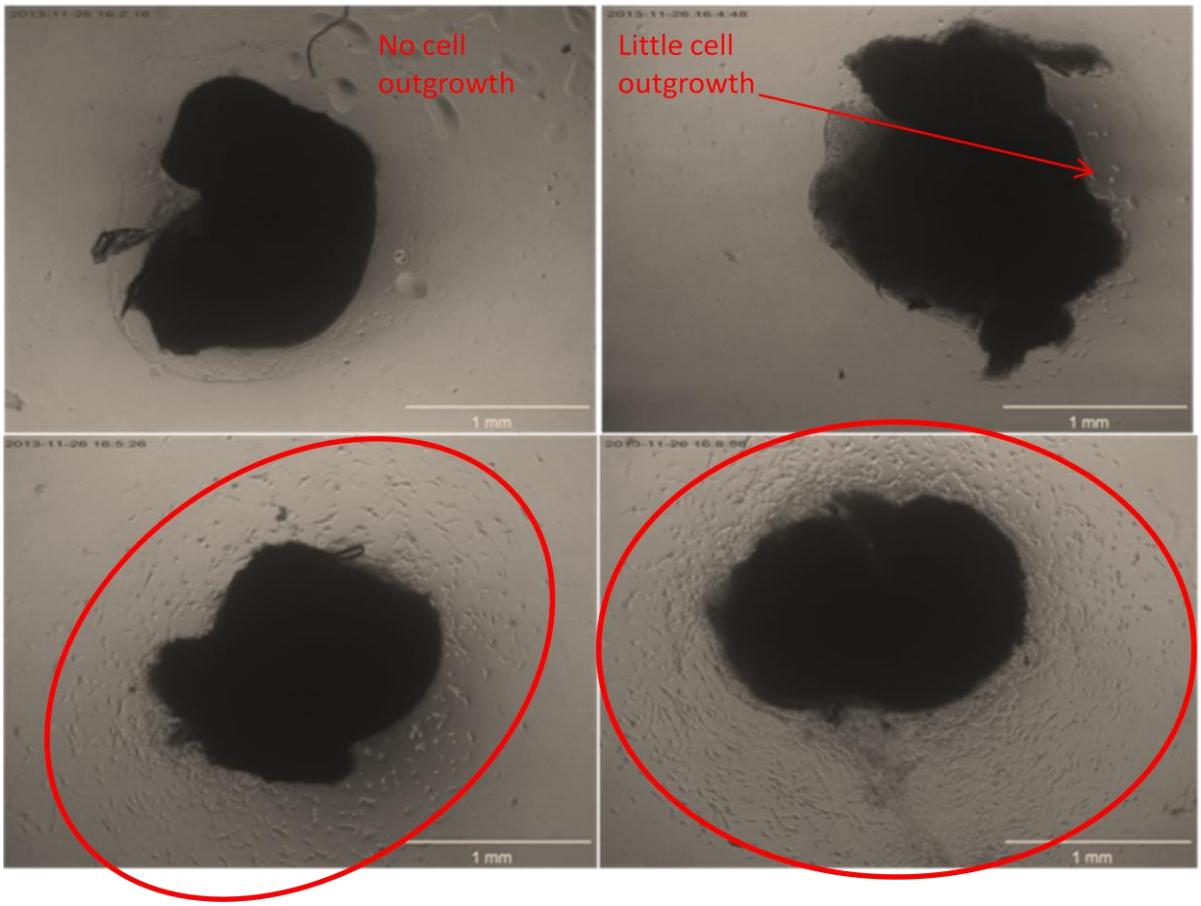

Figure 4.25 - Phase contrast micrographs of DRGs on HB-PNIPAM-GRGDS S-IPNs with PEG-DA matrix after 8 days culture. 0% HB-PNIPAM S-IPN in PEG-DA (top left), 2.5% HB-PNIPAM S-IPN in PEG-DA (top right), 5% HB-PNIPAM S-IPN in PEG-DA (bottom left) and 10% HB-PNIPAM S-IPN in PEG-DA (bottom right). The number of cells 'growing out' from the DRG explants is shown to increase in the order top left < top right < bottom left < bottom right. This matches with the dose of HB-PNIPAM-GRGDS present in the BS-IPN. The amount of cell outgrowth has been indicated qualitatively with the red circles and arrows. The black shadow in the centre of the images is the DRG.

Figure 4.26 shows that at 2 weeks the difference in the samples becomes even greater. There is still very little outgrowth on the 0 and 2.5% HB-PNIPAM-GRGDS. However, there is more outgrowth on the 5% HB-PNIPAM-GRGDS sample and a great deal more on the 10%

HB-PNIPAM-GRGDS sample. This has been highlighted by the red arrows and circles used to indicate where the outgrowth has reached (Figure 4.26)

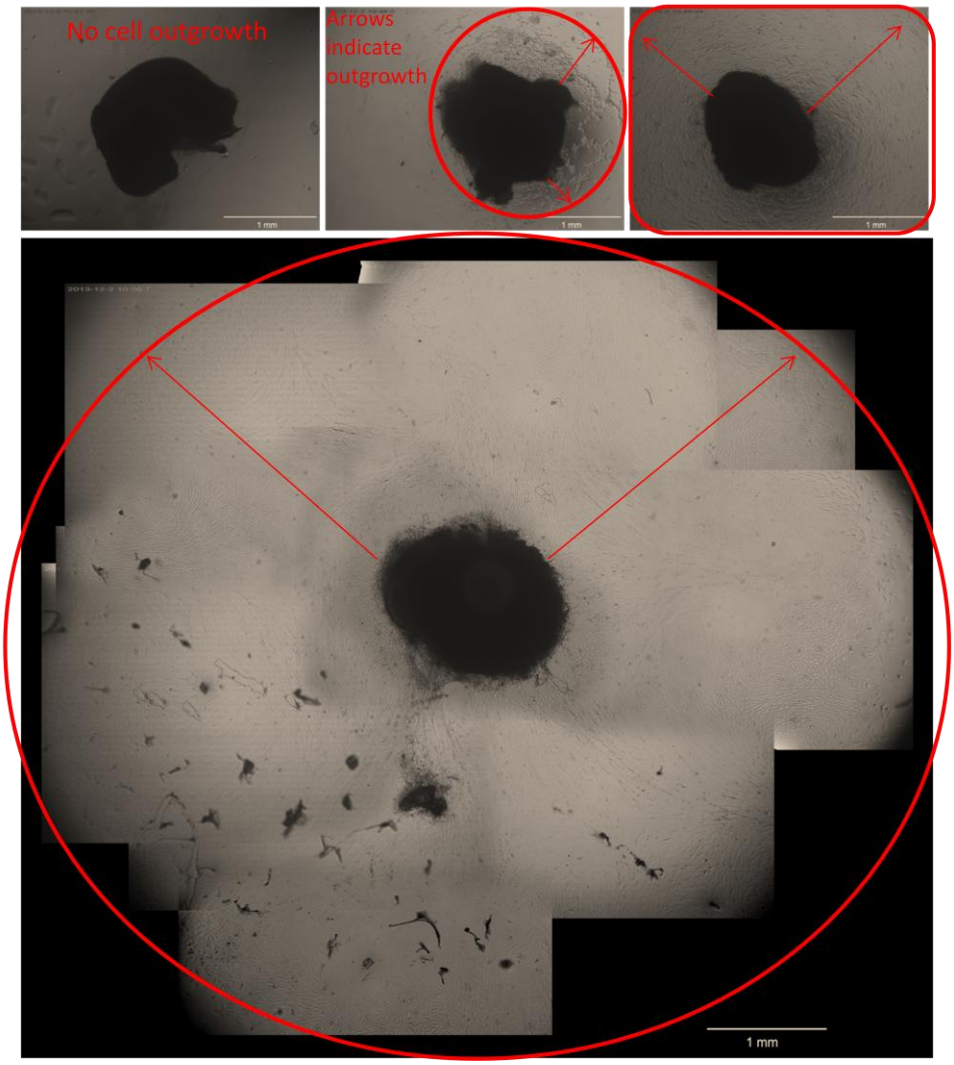

Figure 4.26 - Phase contrast micrographs of DRGs on HB-PNIPAM-GRGDS S-IPNs with PEG-DA matrix after 14 days culture. 0% HB-PNIPAM S-IPN in PEG-DA (top left), 2.5% HB-PNIPAM S-IPN in PEG-DA (top centre), 5% HB-PNIPAM S-IPN in PEG-DA (top right) and 10% HB-PNIPAM S-IPN in PEG-DA (merged image) (bottom). The number of cells 'growing out' from the DRG explants is shown to increase in the order top left < top right < bottom left < bottom right. This matches with the dose of HB-PNIPAM-GRGDS present in the BS-IPN. The amount of cell outgrowth has been indicated qualitatively with the red circles and arrows. The black shadow in the centre of the images is the DRG.

The results from the phase contrast micrographs are confirmed by the fluorescence micrographs of the DRGs on the HB-PNIPAM-GRGDS X-PEG BS-IPNs. Figure 4.27 demonstrate that increasing the concentration of HB-PNIPAM-GRGDS has a dramatic effect on the cell density with the 10% HB-PNIPAM-GRGDS sample out performing all other

samples by a significant margin. The dramatic increase of cell density and length of outgrowths is a good indication that the materials with HB-PNIPAM-GRGDS additive are having a beneficial effect on proliferation as predicted. In Figure 4.27 and Figure 4.28 the DRGs have been stained for neuronal cells (green), Schwann cells (red) and cell nuclei (blue) The blue stain for cell nuclei will stain all cell types. A substantial proportion of these cells will be fibroblasts.

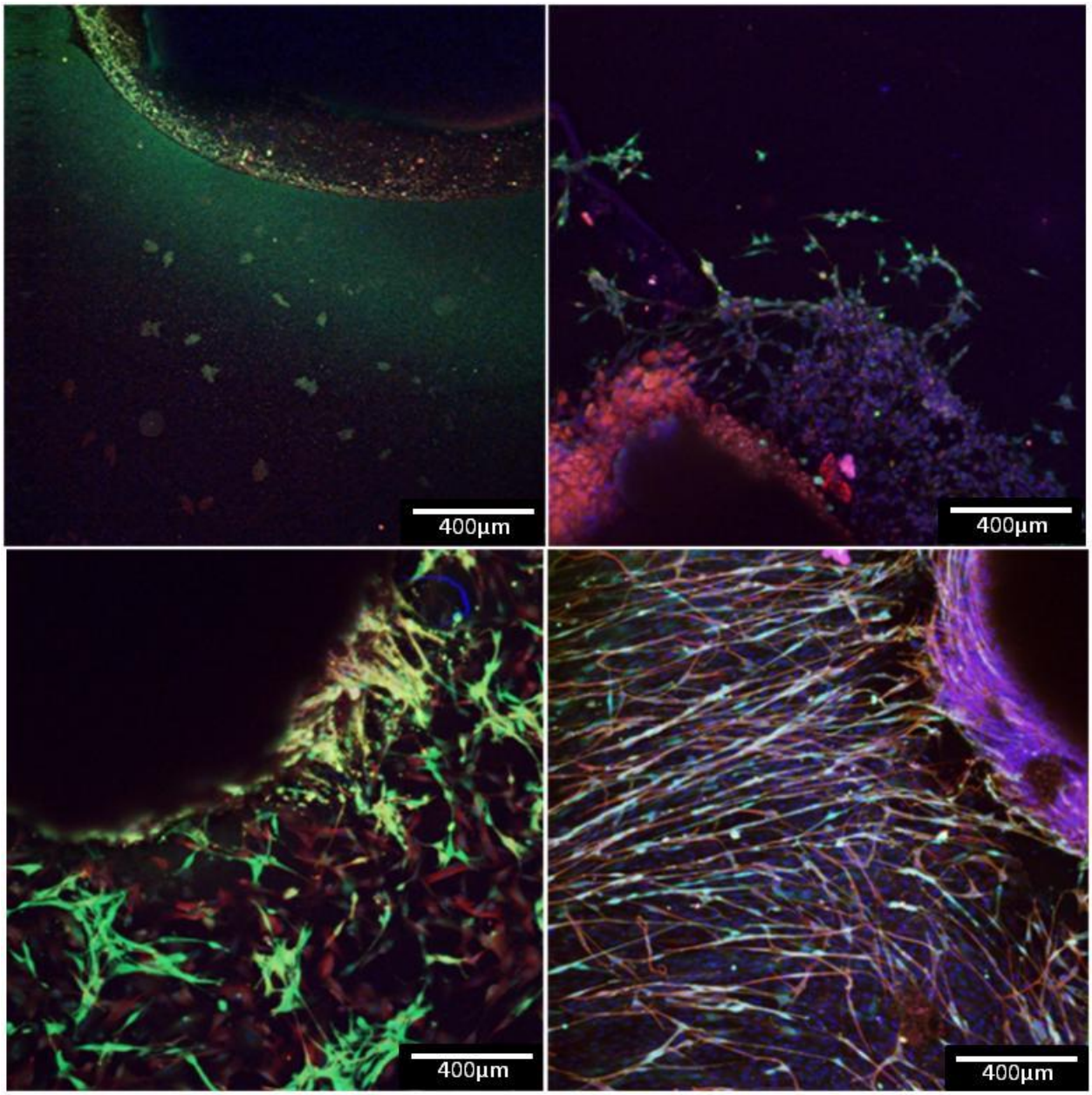

Figure 4.27 - Fluorescence micrographs showing DRGs grown on HB-PNIPAM-GRGDS S-IPNs with PEG-DA matrix after 14 days culture. PEG-DA matrix (left), 2.5% HB-PNIPAM S-IPN in PEG-DA (central left), 5% HB-PNIPAM S-IPN in PEG-DA (central right) and 10% HB-PNIPAM S-IPN in PEG-DA (right).

Figure 4.27 shows that as the concentration of HB-PNIPAM-GRGDS increases in the BS-IPN samples the density of all cell types growing out from the DRG increases. As DRGs represent a good *in vitro* model for peripheral nerve repair it is likely that the addition of the HB-PNIPAM-GRGDS additive would be a good candidate for producing improved biomaterials for peripheral nerve repair.

Figure 4.28 shows further images of DRGs on the 10% HB-PNIPAM-GRGDS X-PEG BS-IPN samples show the extent of the increase in outgrowth. The images show the top bottom and both sides of a DRG. It can be seen that there is a high density of outgrowth of all cell types all the way around the explants. This high density of outgrowth was not observed at lower concentrations of HB-PNIPAM-GRGDS as shown in Figure 4.27 and no outgrowth was observed when the HB-PNIPAM-GRGDS was not present.

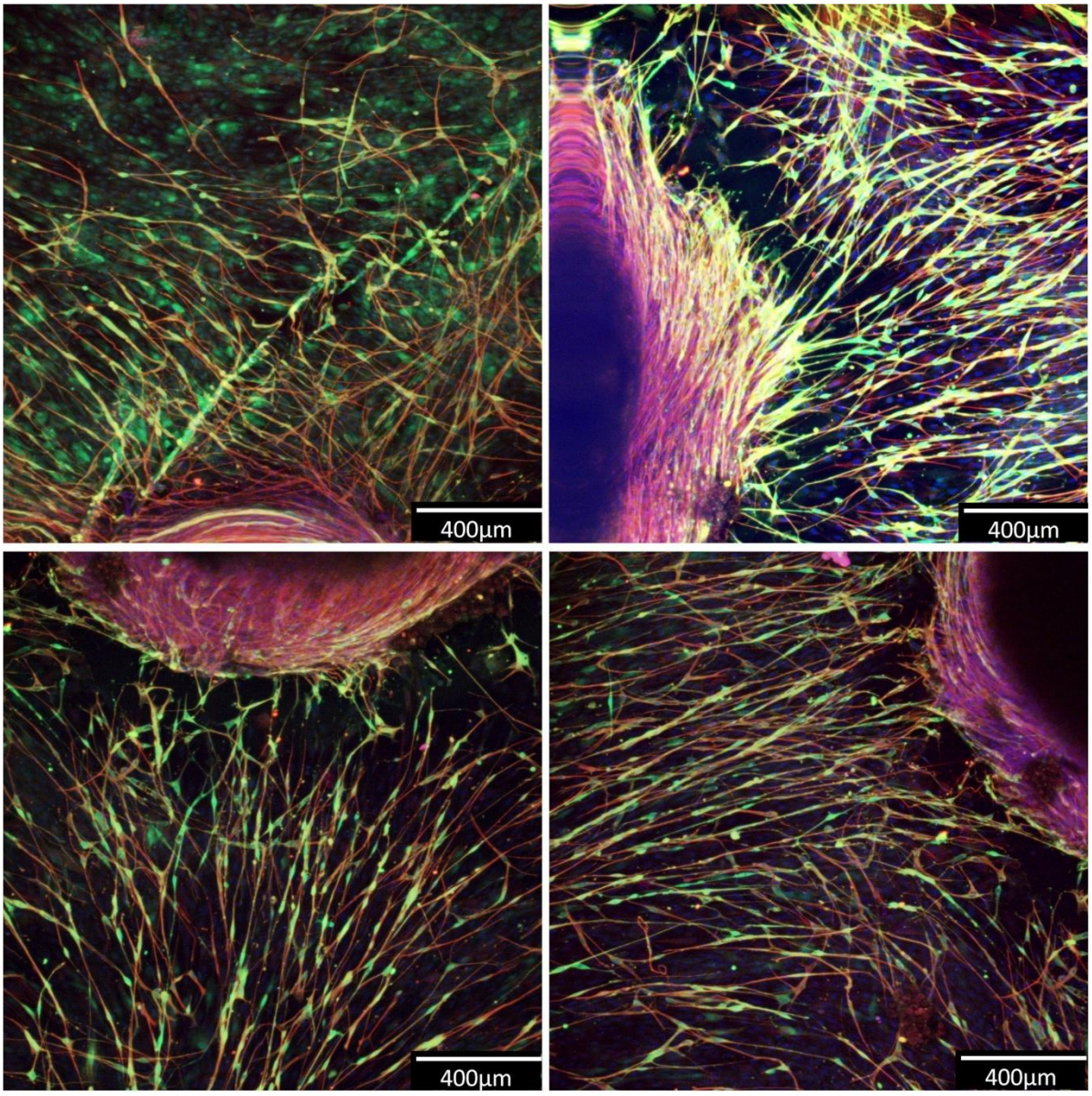

Figure 4.28 – Fluorescence micrographs from confocal microscopy of Dorsal Root Ganglia on 10% HB-PNIPAM-GRGDS XPEG BSIPN surfaces at x10 magnification with 400 µm scale bars. The images show a high density of cellular outgrowth from the 10% HB-PNIPAM-GRGDS BS-IPN in all directions.

The images shown in Figure 4.27 and Figure 4.28 show that there is a definite increase in the cell density for outgrowths from DRGs when the HB-PNIPAM-GRGDS concentration is increased. In Figure 4.28 it can be seen that the high density of cells growing out from the DRG is present in all directions.

4.2.6.7 Microstereolithography

Previous work has used a photocurable PEG to produce tailored nerve guidance conduits to be used in peripheral nerve repair.[198] Traditional methods of producing nerve guidance conduits rely on producing a product which is often available in a limited range of dimensions. The nature of peripheral nerve injury often meant that great flexibility is required in the dimensions of the conduit. This makes stereolithography a good choice for production of customised nerve guidance conduits. Although, the PEG based system used previously did achieve good results,[198] the incorporation of the HB-PNIPAM-GXGRGDS additive could be used to increase cell viability and proliferation within the conduit which would allow a greater gap to be bridged.

The BS-IPN samples can be easily blended into formulations used in microstereolithography. This makes adapting an established process then used without any need for adjustments to setup of formulation. They have been combined with PEG-DA and polymerised using a 477nm laser with DMD. This method could be used to make complex medical devices with intricate physical features and specific biofunctionalities. Figure 4.29 shows that introduction of the HB-PNIPAM additive to the PEG system did not affect the structural integrity of the shaped produced and did not appear to have any nefarious effects on the curing. Figure 4.29 shows that with the X-PEG BSIPNs more complex structures can be fabricated. The complexity of these shapes was not possible with the PVP system.

The X-PEG based systems used here are very hard and have lower water contents than the X-PVP systems shown in Figure 4.18. However, this hardness does allow for more accurate structuring of the monomer. The intricate shapes produced in Figure 4.29 would not be possible with the X-PVP monomer system.

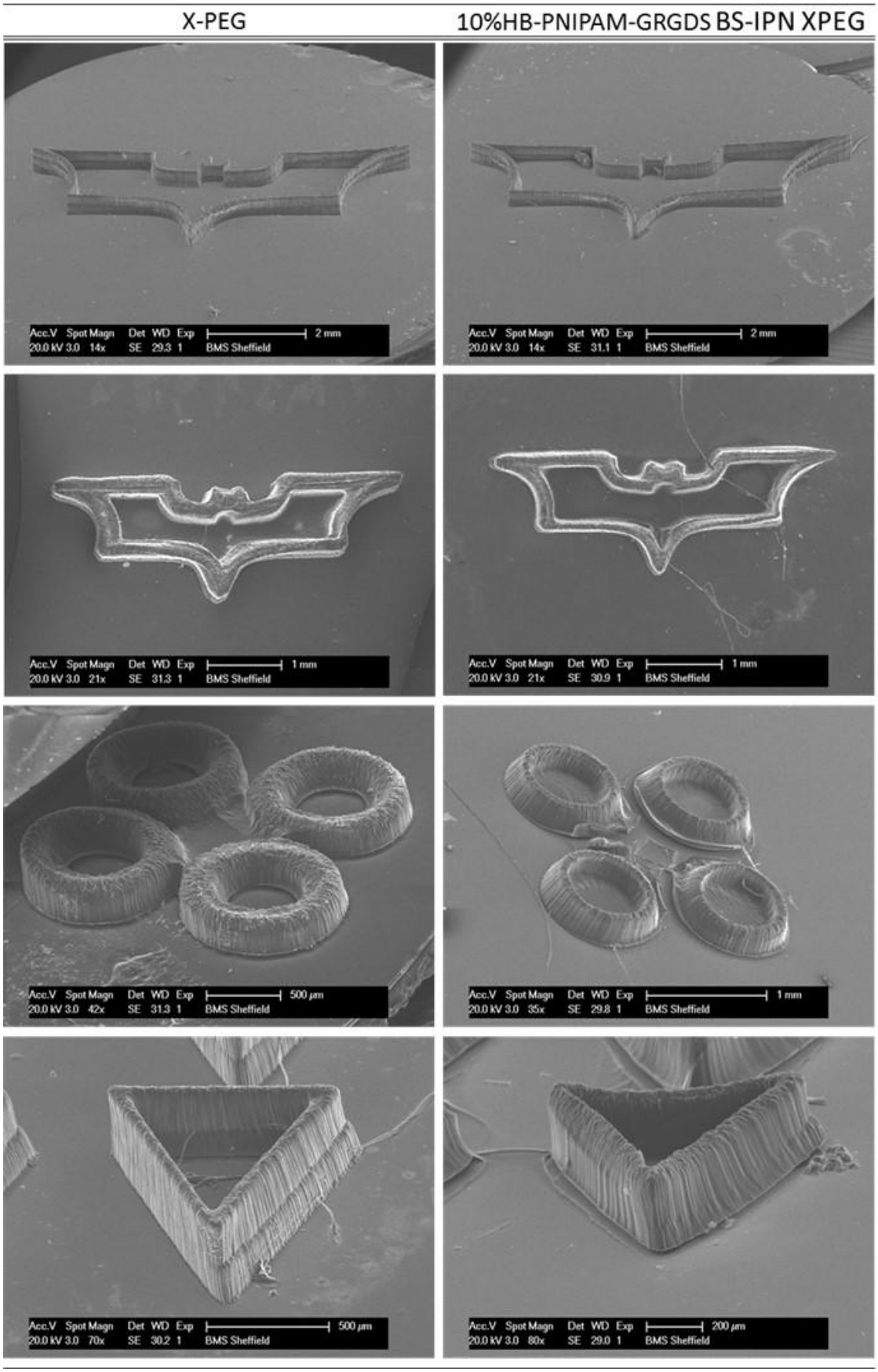

Figure 4.29 - Images of 3d structures samples of PEG-DA and HB-PNIPAM-GRGDS BS-IPNs X-PEG

4.2.7 Conclusions

BS-IPNS with X-PEG have been shown to permanently incorporate a much larger fraction of the branched component into the BS-IPN matrix. It was concluded that this is likely due to the increased crosslink density of the crosslinked polymer and the increased compatibility of the PEG-DA and resultant matrix with the HB-PNIPAM. These factors allow almost 100% of the polymer to be retained within the BS-IPN.

Similarly to the PVP system these X-PEG BS-IPNs have been shown not to exhibit an LCST. In this case the measurements were taken by DSC and equilibrium water content measurements. However no change in water content or observable peak (DSC) was observed at any concentration of HB-PNIPAM. Therefore, it must be concluded that the PEG based BS-IPNs do not display an LCST within the temperature range investigated.

HB-PNIPAM BS-IPNs in X-PEG have been shown to increase cell viability and proliferation and increase the rate of migration of *in vitro* cultures. These results support previous data using a PVP BS-IPN system and data on RGD density published by Hubbell.[56]

PEG-DA is a widely used monomer for producing medical devices in stereolithography groups.[200-201] However, the non-fouling nature of the resulting crosslinked membranes leads to low cellular adhesion.[37] Addition of a highly branched biofunctional polymeric component to an existing stereolithography formulation could be a valuable asset for producing medical devices. The improved biological properties make BS-IPNs an ideal material for the additive manufacture of medical devices. These materials can be accurately structured by stereolithography at high concentrations (10 wt%) of HB-PNIPAM without major change to setup or formulation.

4.3 Comparison of X-PEG and X-PXP BS-IPN Systems

As similar work has been carried out with the X-PEG and XPVP BS-IPN systems a comparison of the two materials will now be made.

The first piece of analysis carried out on these systems was the extraction of HB-PNIPAM from the BS-IPN. This experiment was carried out by Soxhlet extraction of the cured BS-IPN samples which were then analysed by FTIR to find the HB-PNIPAM concentration within the membranes. Figure 4.4 and Figure 4.19 and show how the relative concentrations of HB-PNIPAM within the membranes differ after extraction. In the X-PEG BS-IPNs around 50% of the HB-PNIPAM is lost from the material. Whereas, in the X-PEG BS-IPNs the material retains almost 100% of the HB-PNIPAM within the BS-IPN. This increase in retention of the HB-PNIPAM has been put down to the high crosslinking in the X-PEG system which prevents the polymer from being extracted. This could also be down to an improved compatibility of the HB-PNIPAM with the X-PEG matrix compared to the X-PVP matrix.

This interaction of the HB-PNIPAM with the X-PEG and X-PVP matrix also means that there is no observable LCST for the HB-PNIPAM in these materials. In both cases the LCST was probed by DSC (Figure 4.7 and Figure 4.20) and equilibrium water content (Figure 4.7 and Figure 4.21). In both cases there was no LCST displayed by the BS-IPN materials. In Figure 4.7 a range or materials were made up which included samples of S-IPN with a linear PNIPAM polymer, a X-PNIPAM hydrogel and a S-IPN with X-PNIPAM matrix. All of these systems displayed a LCST in the expected region. It must therefore be assumed that the lack of an observable LCST in the X-PEG and X-PVP systems is a feature of the BS-IPN system. The use of a branched polymeric component instead of a linear component means that the polymer is held in position within the matrix and polymer motion will be restricted or stopped. This prevents the coil to globule transition of the entrapped branched polymer within these systems.

As these materials are to be used in biomaterials they were subjected to *in vitro* cell testing with various cell types. A direct comparison can be made with the cell migration study using HDF cells. Here three parameters were measured. The Euclidean distance, the accumulated distance and the speed of the migration. The BS-IPNs with a X-PVP matrix showed a dose dependant increase in these parameters with increasing HB-PNIPAM-GRGDS content. This

was not the case for the X-PEG system. Here there was no significant increase in the parameters from 0-5% HB-PNIPAM-GRGDS. At 10% HB-PNIPAM-GRGDS there was an increase in all three parameters. These results are shown in Figure 4.15 and Figure 4.24. However it must be noted that Figure 4.15 and Figure 4.24 show that X-PEG and X-PVP with no added HB-PNIPAM-GRGDS show quite different results. With X-PEG giving much higher initial values for speed (≈0.4 μm min^{-1}), accumulated distance (≈300-400 μm) and Euclidean distance (≈130 μm) compared to X-PVP initial values for speed (≈0.1 μm min^{-1}), accumulated distance (≈100 μm) and Euclidean distance (≈20 μm). This difference is due to the ability of cells to form adhesions to these substrates. As the X-PEG has a lot of crosslinks formed from the reaction of the methacrylate groups. There are many more functional sites where cellular proteins can adhere and allow proliferation of cells. However the use of the X-PVP system which is very non-fouling surface highlights the usefulness of this HB-PNIPAM-GRGDS additive and shows how effective it can be. Further testing was carried out using HDFs on the X-PVP BS-IPN system. Figure 4.10 and Figure 4.12 shows increasing cell density and improved cell morphology for HDFs cultured on X-PVP BS-IPNs. It can be assumed from the migration data that a similar pattern would be seen for the X-PEG BS-IPN system but with higher cell density and improved cell morphology on the samples with low HB-PNIPAM-GRGDS contents.

As it was hoped that these materials could be used as biomaterials for peripheral nerve repair it was important for Schwann cells to show a good response to these materials. Culture of Schwann cells on both of these materials showed positive results with increased metabolic activity (higher cell number) measured but MTT as the concentration of HB-PNIPAM-GRGDS increased (Figure 4.16 and Figure 4.22). The increase in cell density with increasing HB-PNIPAM-GRGDS concentration can also be seen in the fluorescence micrographs in Figure 4.17 and Figure 4.23.

The X-PEG and X-PVP BS-IPN systems were structured by stereolithography. Stereolithography was chosen as the method of fabrication as this allows greater flexibility in the dimensions of the finished product. Custom made devices can be fabricated by this methodology to find a specific injury. The fabricated structures made from the X-PVP BS-IPN were highly swollen and as such were not possible to image by SEM. Hence these structures had to be imaged in the water swollen state as dehydration caused large deformations. This

was not the case for the X-PVP BS-IPNs. These devices maintained their shape when swollen or dehydrated. However these structures were hard to the tough and as such do not have mechanical properties which are well suited to this soft tissue engineering applications. Although the X-PVP structures were hard these devices have been used previously in *in vivo* testing with positive results. However, it is likely that the softer X-PVP material would give improved result in this scenario due to increased flexibility and improved diffusion of waste products and nutrients from the injured site. Images of the structures made by stereolithography can be seen in Figure 4.18 and Figure 4.29.

5. Biodegradable Photocurable Trimethylene Carbonate Based Prepolymers for Tissue Engineering Applications

5.1 Abstract

Trimethlyene carbonate was successfully synthesised from diethylcarbonate and propanediol, and was used to synthesise oligomers of varying molecular weights. These polymers were methacrylate functionalised with methacrylic anhydride yielding photocurable prepolymers. As the molecular weight of the polymers increased the methacrylate density decreased and the prepolymers became less reactive. The highest molecular weight polymers could not cure to form a solid gel. Polymer membranes made from the prepolymers supported cell adhesion and proliferation and the adhesion and proliferation could be further improved by addition of HB-PNIPAM-GRGDS. The change in molecular weight of the prepolymers gave resulting membranes with a range of mechanical properties suitable for a different tissue engineering applications.

5.2 Experimental

5.2.1 Synthesis of Trimethylene Carbonate from Diethylcarbonate and Propanediol

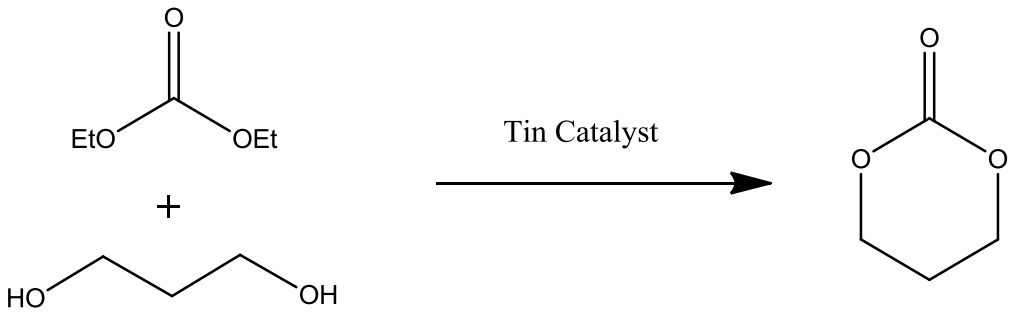

Figure 5.1 – A reaction scheme for the synthesis of trimethylene carbonate from diethycarbonate and propanediol

Diethylcarbonate, (1477 g, 12.5 mol) propanediol (761 g 10.0 mol) and tin powder (50 g) were added to a 3 litre 3 neck round bottom flask with a condenser at 80°C.[179] A heating mantle set to 150°C was used to heat the reaction. Ethanol produced by the reaction was allowed to leave via the 80°C condenser and was collected by condensing with a condenser at 23°C and collecting in a round bottom flask. The temperature of the reaction was monitored with a temperature probe the highest point was 130°C.

The reaction was complete when ethanol was no longer evolved. When the reaction was complete the mixture was vacuum distilled to yield the crude product.

The crude product was recrystallised from ether to give 485 g of pure TMC. The yield of reaction was 47.5%

The melting point of the compound was measured and was found to be 46-48°C compared to a literature value of 45-47°C.[202] This result matches well with the literature value and shows that the compound had been synthesised in high purity.

Mass spectroscopy, FTIR and NMR were used to fully characterise the molecule. The measured molecular ion and calculated mass are shown below along with a list of peaks observed by FTIR and a list of peaks with associated splitting patterns for NMR. The NMR and FITR spectra can be found in section 8.1 and section 8.2respectively.

MH^+ (ESI) = 103.0 [calculated: m/z: 102.03 (100.0%), 103.04 (4.5%)]

FTIR (ATR) ῡ/cm^{-1} 2980(sp^3 C-H), 1800(-O-**(C=O)**-O- stretch), 1750(C=O stretch)

^{1}H NMR (400 MHz, $CDCl_3$) δ/ppm: 1.8 (2H, quin, -O-CH_2-C**H$_2$**-CH_2-O-), 4.1 (4H, t, -O-C**H$_2$**-CH_2-C**H$_2$**-O-)

5.2.2 Polymerisation of TMC

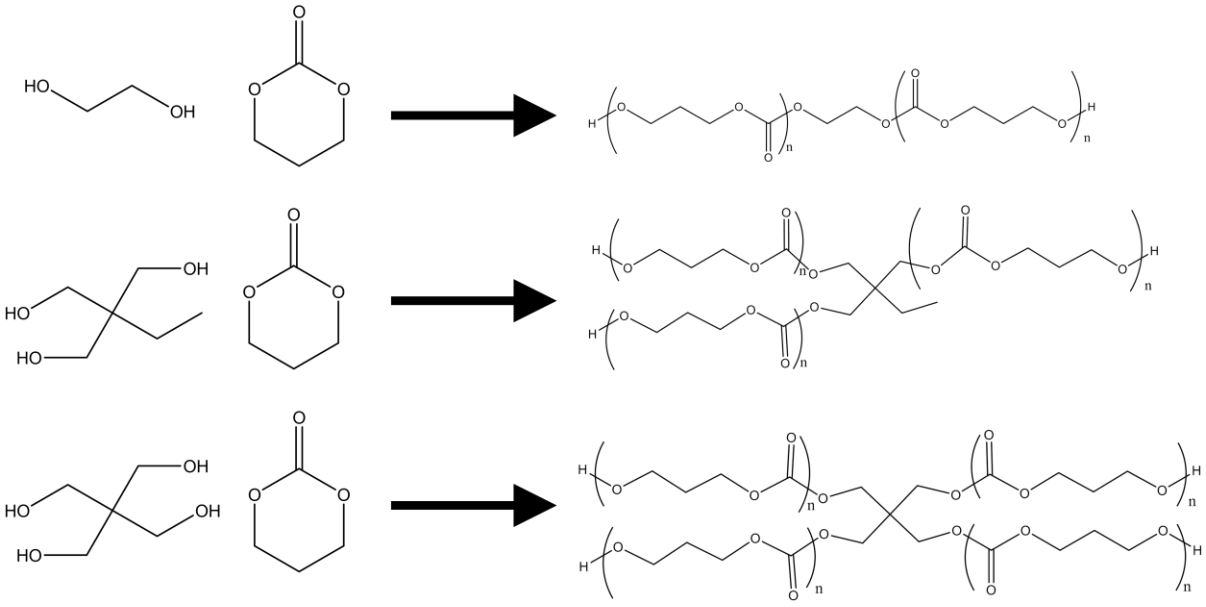

Figure 5.2 – A figure showing the reaction scheme for the formation of 2,3 and 4 are TMC polymers

Trimethylene carbonate and an initiator (ethylene glycol, trimethylolpropane or pentaerythritol) were added to an ampoule and evacuated for 6 hours to remove water. Stannous octanoate catalyst was added to the sealed ampoule by syringe through a suba seal. The polymerisation was carried out at 130°C with stirring for 6 hours.

The polymers were characterised by FTIR and NMR. A list of peaks for FTIR and NMR has been included below. The NMR and FITR spectra can be found in section 8.1 and section 8.2respectively.

FTIR (ATR) ῡ/cm^{-1} 2980(sp^3 C-H), 1806(-O-**(C=O)**-O- stretch), 1730(C=O stretch) 1640(conjugated C=C-C=O stretch), 1220(C-O stretch), 1030(C-O stretch),

^{1}H NMR (CDCl3, rt, 250 MHz): δ/ppm 2.03(O=C-C(C**H$_3$**)=CH2, 3H, s) 2.061(O=C-O-CH2-**CH$_2$**-CH2-O-C=O, 2H, quin), 4.25(O=C-O-**CH$_2$**-CH$_2$-**CH$_2$**-O-C=O, 4H, t), 4.50(initiator O-**CH$_2$-CH$_2$**-O, 4H, t)

5.2.3 Methacrylate Functionalisation of TMC Polymers

The polymers were dissolved in DCM and cooled to -78°C. 2eq of methacrylic anhydride and triethylamine were added dropwise under nitrogen with stirring. The reaction was allowed to warm to room temperature and reacted for 16 hours.

The polymers were purified by removal of the DCM followed by dissolution in methanol at room temperature. The mixture was cooled to -80°C to precipitate the polymer. The liquor was decanted off and the process repeated three times.

The resulting polymers were characterised by FTIR and NMR. A list of the peaks for FTIR and the peaks with associated splitting patterns is shown below. The spectra can be found in section 8.1 and 8.2 respectively.

FTIR (ATR) ῡ/cm^{-1} 2980 (sp^3 C-H), 1730 (C=O stretch) 1640 (conjugated C=C-C=O conjugated stretch), 1220 (C-O stretch), 1030 (C-O stretch), 730 (=C-H bend)

^{1}H NMR (CDCl$_3$, rt, 250 MHz): δ/ppm: 2.03 (O=C-C(C**H$_3$**)=CH$_2$, 3H, s), 2.06 (O=C-O-CH2-**CH$_2$**-CH2-O-C=O, 2H, quin), 4.25 (O=C-O-**CH$_2$**-CH$_2$-**CH$_2$**-O-C=O, 4H, t), 4.50 (O-**CH$_2$-CH$_2$**-O, 4H, t) 5.60 (O=C-C(CH3)=C**H$_2$**, 1H, s), 6.14 (O=C-C(CH$_3$)=C**H$_2$**, 1H, s)

5.2.4 Analysis of PTMC Prepolymers by GPC

Samples were run on a system using a Waters 515 pump, Gilson 238 auto-sampler, Polymer Laboratories ERC 2415 degasser, a PL-Gel™ 10 µm guard column, and 3 PL-Gel™ 10 µm columns connected in series with an Erma RI detector. Samples solutions at 1 mg per mL in THF with 1% LiBr were injected with a flow rate of 1 mL per minute.

5.2.5 Preparation of Samples for Mechanical Testing

A silicone mould with a 30 mm x 9 mm x 1 mm cavity was prepared in order to produce samples for mechanical testing. The PTMC-MA polymers were mixed with 1% initiatior, then

injected into the mould. A microscope slide was placed on top of the open surface of the mould and the samples were exposed to UV light for 1 minute on each side. The cured polymers were removed from the mould, and stored at room temperature prior to testing.

5.2.6 Mechanical Testing of Crosslinked PTMC Sheets

Mechanical testing was carried out on a Lloyd instruments TA 500 tensometer with a 500 N load cell. The samples were preloaded at a force of 0.1 N and extended at a rate of 1 mm per minute. The load deflection from initial length were used to calculate the stiffness of the material.

5.2.7 Preparation of Samples for *In Vitro* Cell Work

13 mm coverslips were methacrylate functionalised by cleaning with piranha solution, followed by repeated washes with methanol. The cover slips dried then added to a 5% solution of 3-methacryloxypropyltrimethoxysilane in toluene, where they were stored until required.

A droplet of the prepolymer was added to a clean microscope slide and a methacrylate functionalised cover slip was placed on top of the polymer droplet. The sample was exposed to UV light and the coverslip with bound crosslinked PTMC was removed from the microscope slide. The samples were stored in ethanol until required.

5.2.8 Fibroblast Cell Culture on X-TMC and X-TMC BS-IPN

Human fibroblasts were obtained from female patients undergoing abdominoplasty or breast reduction operations. Ethical approval and consent were obtained for the use of human fibroblasts. The method for the isolation and culture of fibroblasts as described in the literature.[189] Cells between passage 4 and 9 were used in experimentation. The cells were seeded at a density of 20,000 cells per well into 12 well plates containing the PTMC coated coverslips described in 5.2.7. The cells were incubated at 37°C with 5% CO_2 for 24 hours. The cell number was assessed by MTT assay.

5.2.9 RN22 Cell Culture on X-TMC and X-TMC BS-IPN

RN22 cells were seeded at a density of 20,000 cells per well into 12 well plates containing the PTMC coated coverslips described in 5.2.7. The cells were incubated at 37°C with 5% CO_2 for 24 hours. The cell density after 24 hours was assessed by MTT assay.

5.2.10Analysis of Variance

An explanation of the ANOVA statistical test has been given in section 3.2.10

5.3 Results and Discussion

5.3.1 Molecular Weight Analysis of PTMC by GPC

The molecular weights of the PTMC polymers were measured by GPC, the chromatograms shown in Figure 5.3 and the molecular weight averages are given in Table 5.1. GPC chromatograms were compared to demonstrate the change in molecular weight with initiator concentration.

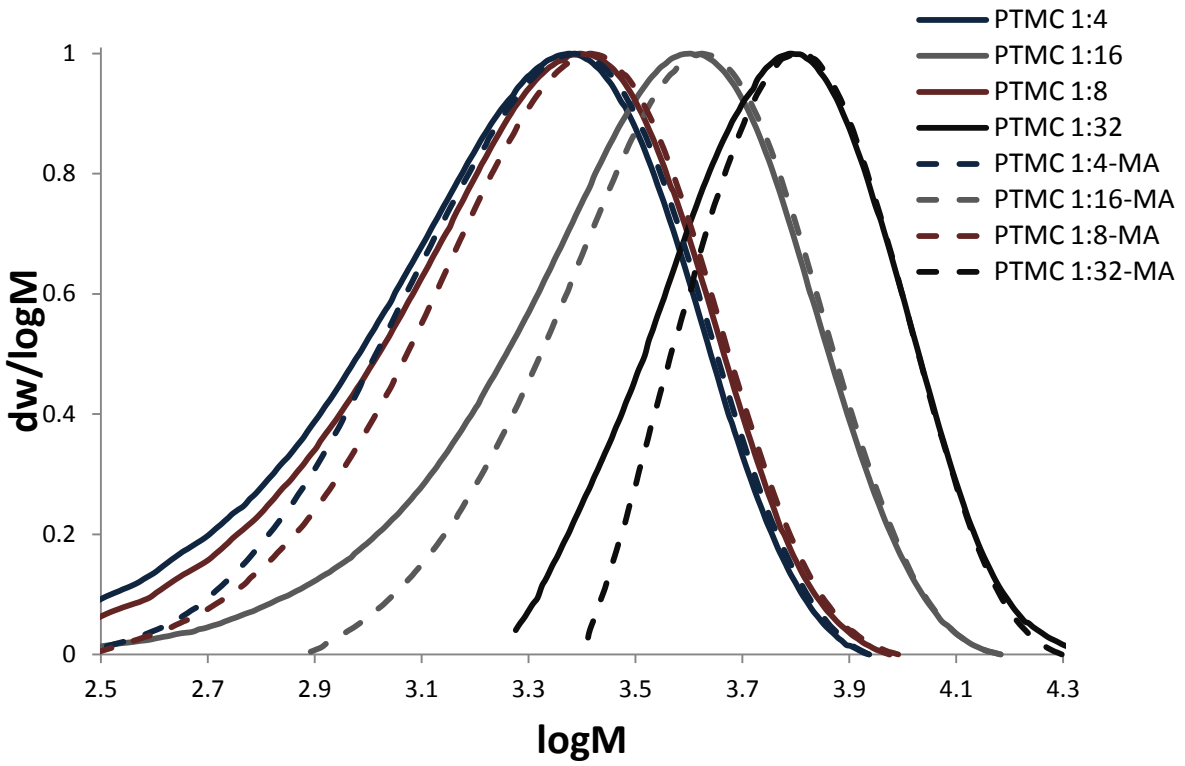

Figure 5.3 – A figure showing the GPC data for ethylene glycol initiated PTMC and PTMC-MA at various initiator to monomer ratios.

The GPC data in Figure 5.3 and Table 5. show that there is an increase in the molecular weight as the concentration of initiator decreases.

Table 5.1 - GPC data taken from THF GPC showing Mn, Mw and Mz for 1:4, 1:8 1:16 and 1:32 ethylene glycol initiated PTMC prepolymers.

Initiator:monomer ratio	Mn / g mol^{-1}	Mw / g mol^{-1}	Mz / g mol^{-1}	Đ
1:4	4100	5600	7700	1.37
1:4-MA	4600	6100	8100	1.31
1:8	4400	6000	8300	1.38
1:8-MA	4700	6400	8690	1.35
1:16	6500	10000	14700	1.53
1:16-MA	8200	11400	15600	1.37
1:32	14000	18800	25200	1.35
1:32-MA	16400	20500	2570	1.25

Table 5.1 shows that these polymers have low dispersities of between 1.25-1.53. This is probably due to the ring opening polymerisation mechanism used to make these polymers. This range for dispersity seems to be corroborated by literature values. [184, 203-204] The dispersity seems to decrease upon addition of the methacrylate. This is caused repeated precipitation to purify the polymers. The low molecular weight reagents and side products are preferentially removed by this process, causing the amount of low molecular weight material to be reduced. This can be seen in the GPC chromatograms (Figure 5.3), by the low molecular weight side of the chromatogram shifting to the right after addition of the methacrylate functional group.

5.3.2 Curing of Methacrylate Functional PTMC Polymers

The methacrylate functional polymers were exposed to UV light to investigate their ability to form a solid membrane. After UV exposure the polymer cure was assessed qualitatively by inspecting the tackiness of the surface and the bulk properties of the film. The results can are shown in Figure 5.2. This simple test was carried out by putting a small drop of polymer with 1-2 wt% initiator onto a microscope slide. The sample was exposed to UV light for 1 minute. It was noted whether or not the samples had cured. Only the highest molecular weight sample PTMC 1:32-MA did not cure.

Table 5.2 – A table showing the qualitative assessment data on curing of prepolymers.

Initiator:monomer ratio	Cure
PTMC 1:4-MA	✔
PTMC 1:8-MA	✔
PTMC 1:16-MA	✔
PTMC 1:32-MA	✘

Here, the polymer cured to the point where elastic strings could be drawn from it but even after long periods of exposure (+5 minutes) it did not form a gel. This is because there is a relatively low concentration of methacrylate functional group compared to lower molecular weight polymers. Here, the crosslink density is not high enough to form a solid gel.

5.3.3 Mechanical Properties of Crosslinked PTMC Membranes

The polymers had been made at three different molecular weights by manipulating the initiator concentration the difference in mechanical properties. The molecular weight of the prepolymer will affect the mechanical properties of the resulting crosslinked film was investigated. Figure 5.4 (A) shows that as molecular weight of the prepolymer increases or crosslink density of the resulting membrane decreases the stiffness of the membrane is reduced. The same trend is shown for the Young's Modulus (Figure 5.4 (B)).

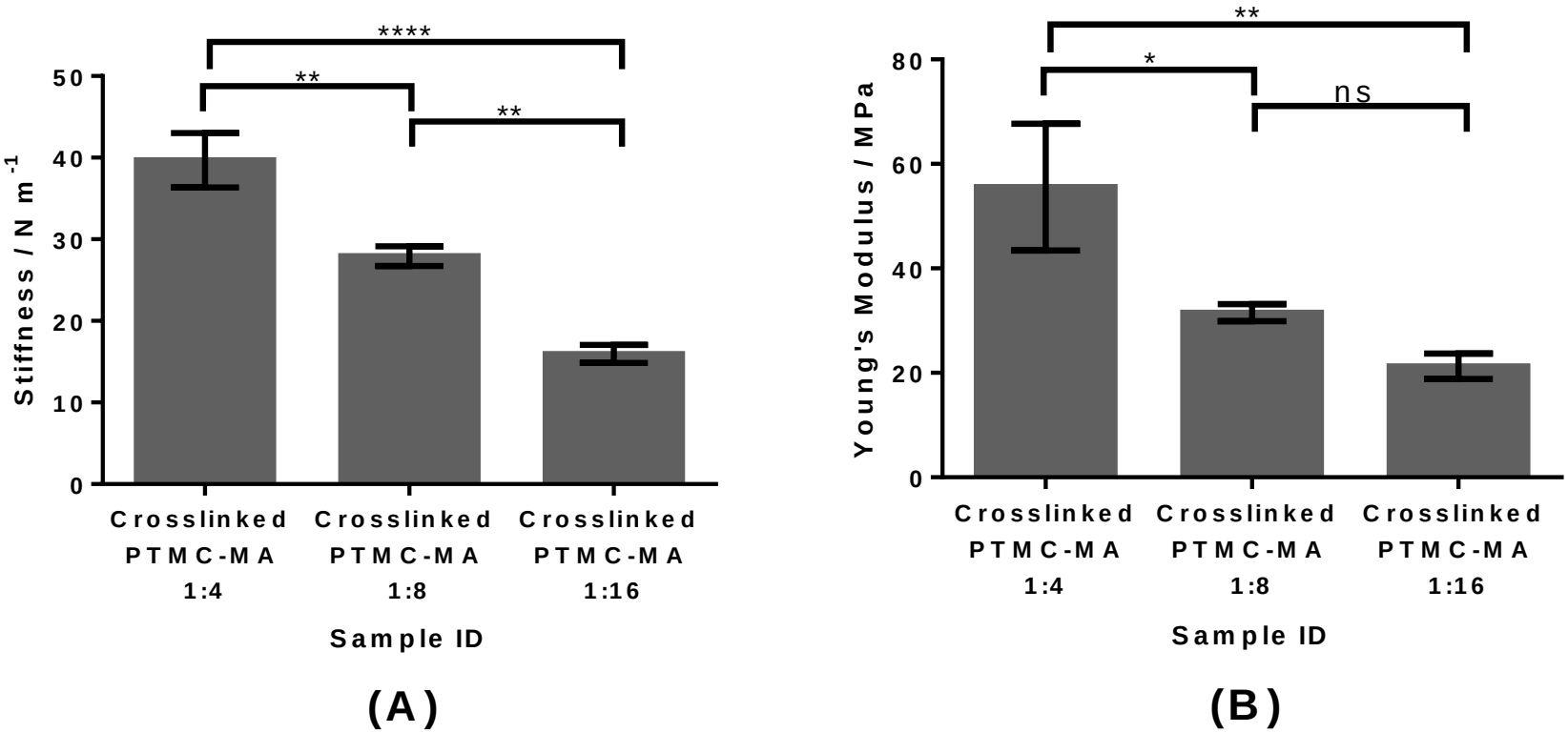

.

Figure 5.4 - Variation in stiffness with molecular weight of prepolymer. Statistical significance assessed by one way ANOVA with Tukey's multiple comparisons. Level of significance indicated by asterisks above (P<0.0001). These data show that as the molecular weight of the prepolymer increases the modulus and stiffness of the resulting membrane decreases.

The stiffness of the resulting three X-PTMC membranes was measured and compared by ANOVA (Figure 5.4 (A)) A distinct stiffness was observed for each set of polymers, which were shown to be statistically different by ANOVA. The ANOVA statistical test has also been used on the Young's Modulus data (Figure 5.4 (B)) and shows that there is no statistical difference in the modulus of the 1:16 and the 1:18 polymers once crosslinked. The modulus it a measure of stiffness but this is independent from the measurements of the sample. For the 'Stiffness the dimensions have not been taken into account. A stiff polymer is ineffective as a scaffold for soft tissue engineering, so it is important that the scaffold be flexible. As molecular weight of the prepolymer increases, the flexibility of the scaffold increases. Higher molecular weight prepolymers will therefore give more effective scaffold for soft tissue engineering. However, this introduces a trade-off between advantageous mechanical properties and ease of curing. As previously discussed, the higher the prepolymer molecular weight, the lower the methacrylate functional group density. This low methacrylate density will make curing more difficult.

The maximum load at break was also measured and the data is shown in Figure 5.5. The general trend of these data is that the X-PTMC polymers with the higher crosslink density have a higher maximum load at break than the polymers with a lower crosslink density. The crosslink density decreases X-PTMC-MA 1:4 > X-PTMC-MA 1:8 > X-PTMC-MA 1:16. This data supports what is shown by the stiffness and Young's Modulus data.These mechanical properties will be highly important in a biomaterial application. The fact that these properties are tuneable via the molecular weight of the prepolymer will allow the membranes to be well suited to various applications.

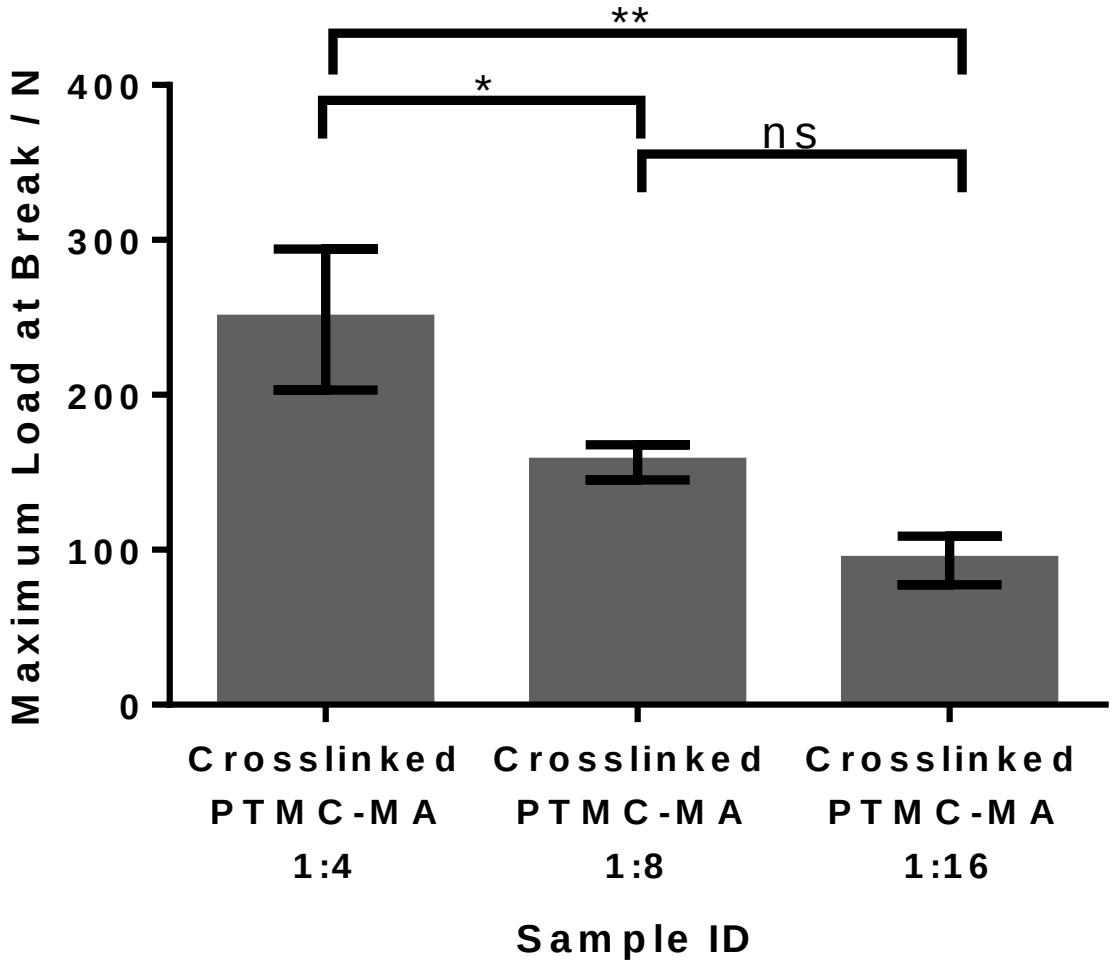

Figure 5.5 - A histogram showing the maximum load at break for X-PTMC samples. Statistical significance assessed by one way ANOVA with Tukey's multiple comparisons. Level of significance indicated by asterisks above (P<0.0001).

5.3.4 *In Vitro* Cell Culture

To assess the suitability of these materials for use in biomaterials, the samples were used for *in vitro* testing with HDF and RN22 cells. HDFs were chosen as fibroblast cells are a very common extracellular matrix producing cell and are found in many tissues throughout the body. As fibroblasts are so common it is likely that a biomaterial for implantation will come into contact with fibroblasts. Thus, it is highly desirable to have a biomaterial which will support adhesion and proliferation of fibroblasts. These cells are easily cultured and give a good indication of the cytocompatibility of a biomaterial. In this case Primary human cells have been used which means that they have been taken directly from a human donor.

These cells are likely to give more representative results than a cells from an immortalised cell line as they may be more sensitive.

The RN22 cells are a more specialised cell line. These cells are an immortalised cell line of rat Schwann cells. These cells can give information on how primary Schwann cells likely to grow on these biomaterials. Schwann cells are very important in peripheral nerve repair. These cells release chemical signalling factors, which guide the growth of neural cells. A positive result with a Schwann cell will be highly desirable for a biomaterial to be used in peripheral nerve repair. This could be important for the peripheral nerve repair applications. The data for these tests are shown in Figure 5.6 A and B respectively.

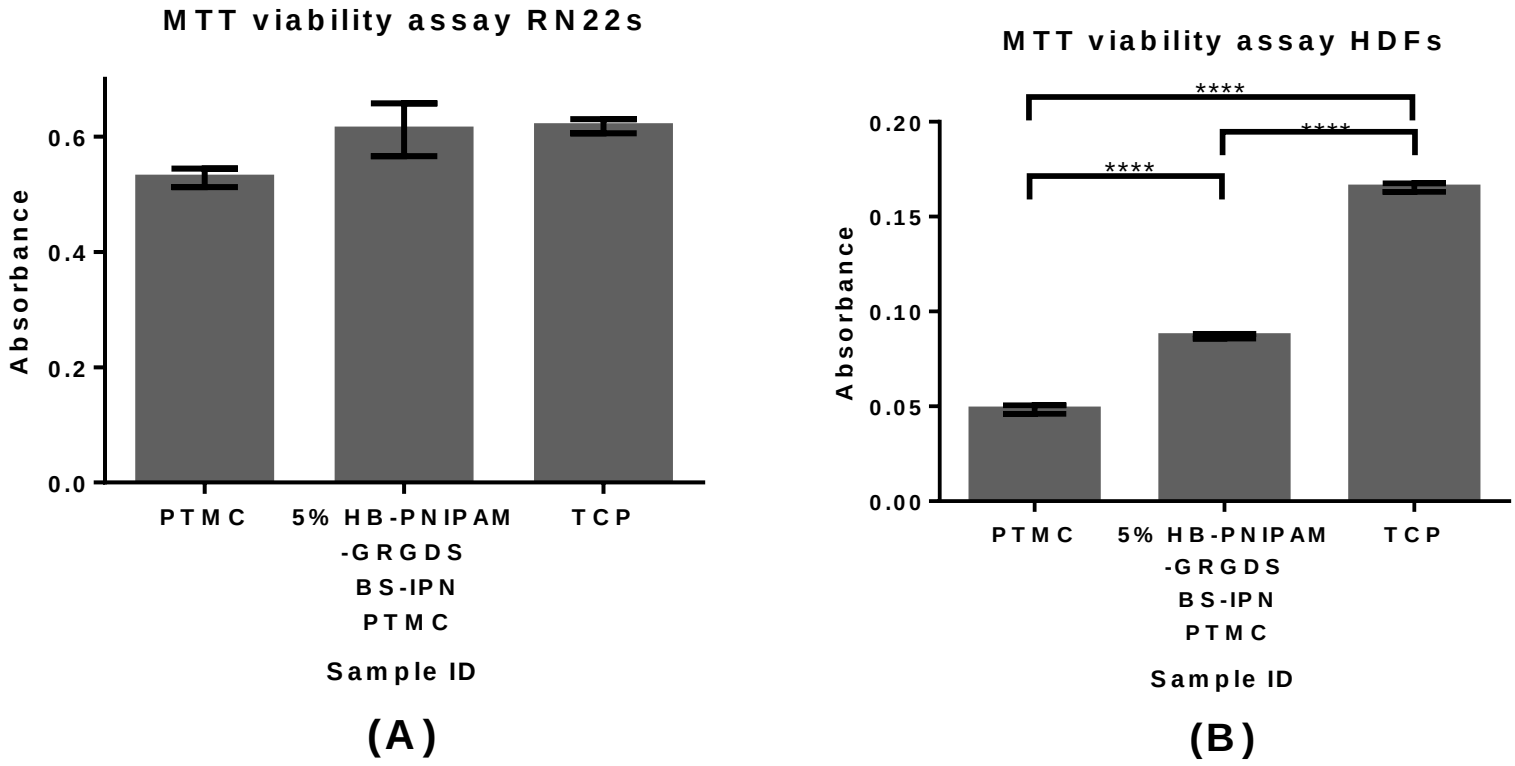

Figure 5.6 – A figure showing the MTT data from NHDFs and RN22s after 24 hours culture on PTMC 5% HB-PNIPAM-GRGDS and TCP. Level of significance determined by one way ANOVA with Tukey's multiple comparisons (P<0.0001).

N22s and NHDF cultured on PTMC showed good adhesion and proliferation on PTMC surfaces. The addition of HB-PNIPAM improved the proliferation of the HDFs but the effect was not significant for RN22s. From our previous research we would expect the HB-PNIPAM-GRGDS additive to have a positive effect on proliferation of cells on the biomaterial.[192] This is the case however, cells grow reasonably well on PTMC without the addition of the HB-PNIPAM GRGDS additive. This is supported by evidence in the literature, which shows PTP can be a good substrate for cell culture.[185]

5.4 Conclusion

TMC monomer was synthesised and characterised by NMR, FTIR, melting point and mass Spectroscopy. This was used to synthesise PTMC by ring opening polymerisation. The polymers were synthesised at a range of molecular weights with narrow dispersity. The addition of methacrylate to these polymers was possible and was demonstrated by the observation of the relevant peaks in NMR.

The methacrylate functional polymers are photocurable, and can be used to create biodegradable surfaces for tissue engineering. At higher molecular weight the crosslinked membrane formed from these polymers becomes flexible and elastic and would be well suited to soft tissue engineering applications. However, with increasing molecular weight the polymers become more difficult to cure due to a decreased methacrylate density. This creates a trade-off in favourable mechanical properties and ease of curing. The surfaces support cell adhesion and proliferation, and the biological properties of these surfaces can be further improved by the addition of HB-PNIPAM-GRGDS. The cell viability and proliferation data is in support of HB-PNIPAM GRGDS BS-IPN data from previous chapters. However, in the Case of PTMC the biomaterial will support a higher degree of cellular adhesion and proliferation without the aid of the HB-PNIPAM-GRGDS additive.

6.Vancomycin Functionalised HB-PNIPAM Containing the Solvatochromic Nile Blue Dye

6.1 Abstract

Previous research has shown that vancomycin functionalised HB-PNIPAM (HB-PNIPAM-vanc) could be used to bind to bacteria creating bacteria/polymer aggregates that formed self-supporting 'mats.'[130, 205] The bacteria binding induced coil collapse has been proven by Förster resonance energy transfer.[206] The solvatochromic dye, Nile Blue was attached to the end of the HB-PNIPAM in addition to the vancomycin (HB-PNIPAM-vanc/NB). The reaction was carried out by activating the carboxylic acid end group with N-hydroxy succinumide then attaching the Nile blue via the amine functionality. The colour of the dye is dependent on its environment, thus, the dye was expected to change colour upon binding to the bacteria. The expected colour change was monitored visually and by fluorescence spectroscopy. The colour change effect was not observed and no change in the fluorescence emission was seen upon coil to globule transition. The most likely reason for this is that there is no change in the environment of the dye as it remains on the outside of the globule (in contact with the solvent) after the coil to globule transition.

6.2 Experimental

6.2.1 Synthesis of 4-Vinylbenzyl Pyrrolecarbodithioate

A detailed description of the synthesis of 4-vinylbenzyl pyrrolecarbodithioate can be found in section 2.2.1.

6.2.2 Synthesis of Anthryl Methyl Methacrylate (AMMA)

The synthesis of AMMA was taken from Hargreaves and Webber.[207] 9-anthracenemethanol (3g) was dissolved in Grubbs THF (12 mL) under dry N_2 with stirring and cooled to 0°C. Dry metharyloyl chloride (3 mL) and pyridine dry Grubbs pyridine were added dropwise to the reaction mixture whilst maintaining the temperature below 0°C. Following the addition the mixture was warmed to 25°C and stirred for one hour. Water was added to the reaction and the product was extracted with diethyl ether before an acid base workup. The solvent was removed by rotary evaporation and the product recrystalised from methanol yielding a yellow crystalline solid with a melting point of 81-84°C (literature value[207]: 82-83°C).

The product was characterised by NMR. A list of the peaks with the associated splitting patterns has been given below.

^{1}H NMR (400MHz, $CDCl_3$) δ/ppm: 1.80(3H, s, R-CH_3), 4.05(1H, s, C=CH_2), 6.00(1H, s, C=CH_2), 6.15(2H, s, (C=O)-O-CH_2), 7.00-8.50 (9H, m, aromatic)

6.2.3 Synthesis of HB-P(NIPAM-co-AMMA) Pyrrolecarbodthioate Chain Ends

N-isopropylacrylamide (14.56 g, 0.13 mol), recrystalised from 40:60 hexane:toluene, and 4-vinylbenzyl pyrrolecarbodithioate (1.29 g, $4.9x10^{-3}$ mol), anthryl methyl methacrylate (AMMA) (0.36 g, $1.29x10^{-3}$ mol) and ACVA (1.391g, $4.9x10^{-3}$) were dissolved in dioxane (50ml). The solution was transferred to a glass ampoule, 3 cycles of freeze pump thaw were carried out. The ampoule was sealed and to reacted at 60°C for 48 hours. The viscous solution was precipitated into diethyl ether and dried under vacuum. Precipitation was repeated three times to give 14.7g an off white solid. This was equal of a conversion of 83%.

The polymer was characterised by GPC and NMR. The molecular weight averages from GPC have been given below along with a list of NMR peaks and associated splitting patterns. The NMR spectrum can be found in section 8.1.

GPC (DMF 0.1% LiBr): Mn – 23000, Mw – 243840, Mz –1615000, Đ – 10.45

^{1}H NMR (400MHz, $CDCl_3$) δ/ppm: 0.9-1.3(6H,s,-N(CH_3)$_2$), 1.4-1.8 (2H, br m, -CH2-CH-Ar-), 1.9–2.2(2H, br m, -CH_2-CH-CO-NH-) and (1H, br m, CH_2-CH-CONH-), 4.0 (1H, br s, (CH_3)2CH-), 6.3 (H2, br s, N-pyrrole-H), 6.6–7.2 (br m, -Ar-), 7.65 (2H, br s, N pyrrole-H).

6.2.4 Carboxilic Acid Functionalisation of Pyrrolecarbodithioate Ended HB-P(NIPAM-co-AMMA)

The concentration pyrrole end groups was calculated from NMR. The pyrrolecarbodithioate ended HB-(PNIPAM-co-AMMA) was dissolved in DMF (675 ml). ACVA (26 g, 20 eq) were reacted for 24 hours. The process was repeated twice, so that a total of 60 eq of ACVA had been added. The solvent was removed by rotary evaporation. The product was precipitated dropwise into diethyl ether, dried under vacuum then purified by ultrafiltration in acetone:ethanol (9:1).

The product was characterised by NMR. A list of the peaks with the associated splitting patterns has been given below. The NMR spectrum can be found in section 8.1.

1H NMR (400 MHz, CDCl3) δ/ppm: 0.9-1.3(6H, br s, -N(CH_3)2), 1.4–1.8 (2H, br m, -CH_2-CH-C_6H_4-), δ 1.9–2.2(2H, br m, -CH_2-CH-CO-NH-) and (1H, br m, CH_2-CH-CONH-), δ 1.9–2.2(2H, br m, -CH_2-CH-CO-NH-) and (1H, br m, CH_2-CH-CONH-), 4.0 (1H, br s, (CH_3)2CH-), 6.6–7.2 (br m, -Ar-), 7.85 (br s, -NH-CO)

The concentration of acid ends was calculated from NMR and found to be 2.92x10^{-4} mol g^{-1}.

6.2.5 Synthesis of Nile Blue/ Vancomycin ended HB-P(NIPAM-co-AMMA)

HB-P(NIPAM-co-AMMA)-COOH (2.72 g) was dissolved in DMF (20 mL). *N,N*′-Dicyclohexylcarbodiimide (1.626 g, 7.88x10^{-3} mol, 5 eq) and N-hydroxysuccinimide (0.909 g, 7.88x10^{-3} mol, 5 eq) were added to the reaction vessel and stirred under nitrogen for 24

hours at room temperature. The DMF was removed by rotary evaporation and the product was purified by ultrafiltration in acetone with 10% ethanol. Once purified the solvent was removed by rotary evaporation yielding 1.5 g of a buff coloured solid.

1.5 g of HB-PNIPAM-NHS ended HB-PNIPAM was dissolved at 0°C in 0.01M pH 9.5, phosphate buffer. Vancomycin (0.9 eq, 0.253 g) was added along with Nile Blue (0.1 eq, 0.014 g). The reaction mixture was maintained at 0°C and stirred under nitrogen for 48 hours. The resulting product was purified by ultrafiltration in 1:10 ethanol:acetone mix until the eluting solvent was colourless. The solution was rotary evaporated the product was dissolved in water and freeze dried yielding a blue fluffy solid (0.85g). This gave a yield of 84%.

6.2.6 Steady State Spectroscopy

Emission and excitation scanning measurements 'steady state spectroscopy' to determine wavelength of fluorescence absorption and emission were carried out on a fluoromax 4. Samples were prepared at 1 mg ml concentration in ultrapure water and examined using quartz cuvette with a 1 cm path length.

6.2.7 Steady State Lifetime Measurements

Steady state lifetime measurements were carried out on an Edinburgh 999 - with fixed excitation and emission wavelengths corresponding to peak absorption / emission. Samples were prepared at 1 mg ml concentration in ultrapure water and examined using quartz cuvettes with a 1 cm path length.

Fluorescence excited state lifetimes were calculated from the flurescence intensity decays using equation 6.1. Here, the initial fluorescence intensity is given by I_o, the fluorescence excited state lifetime is given by τ_f, the time is represented by t, and the background noise is given by A.

$$I(t) = A + I_o \exp\frac{-t}{\tau_f}$$

Equation 6.1

6.2.8 Analysis of Variance

An explanation of the ANOVA statistical test has been given in section 3.2.10

6.3 Results and Discussion

6.3.1 Cloud Point

In this chapter the HB-PNIPAM polymers used previously have been be functionalised with vancomycin. These polymers have been shown to bind to bacteria and the binding can trigger the coil to globule transition.[130, 206] It is proposed that a correctly positioned solvatochromic dye could be used to detect the change. This had been shown previously with Nile Red dissolved within the polymer core.[90] Nile Blue has amine functionality that can be used to attach it to the polymer chain end. Utilising the environment dependent emission of Nile Blue a colour change should be observed upon coil collapse provided the hydrophobic Nile blue dye can penetrate into the polymer core. When coupled to the bacterial binding coil collapse this can be used as a sensor for bacteria binding. The LCST of HB-P(NIPAM-co-AMMA)-NB/vanc was measured by cloud point, the onset of the increase in turbidity was observed as 25°C. This is shown in Figure 6.1.

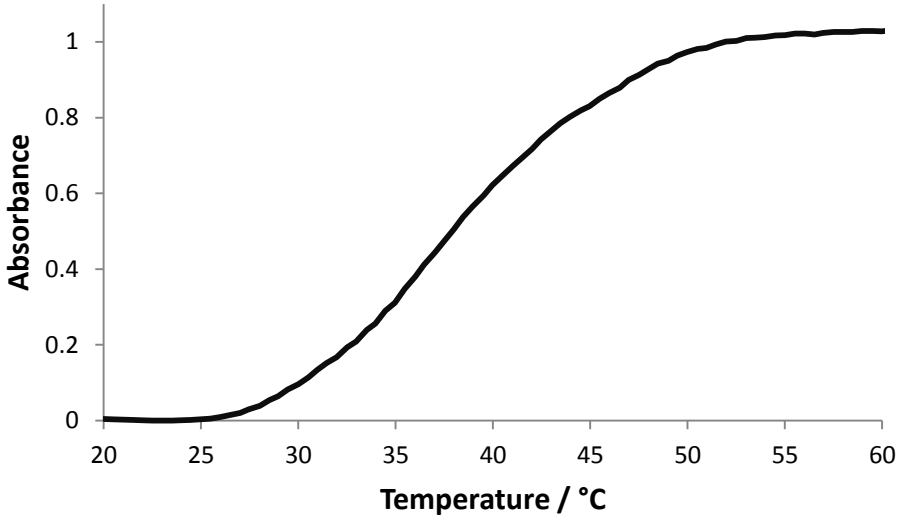

Figure 6.1 – A figure showing the cloud point of HB-P(NIPAM-co-AMMA)-NB/vanc by change in turbidity.

The observation of a cloud point at 25°C (Figure 6.1) is important because at room temperature the polymer will be in the coil state. If the binding of the bacteria triggers the coil collapse then this transition will be observed at room temperature it may be possible to detect this with a solvatochromic dye if it can be positioned in an appropriate manner.

6.3.2 Observation of a Colour Change Over the LCST

The colour change was assessed by heating one solution of HB-PNIPAM-NB/vanc (20 mg mL^{-1}) through its LCST and cooling another to below its LCST. A side by side comparison was then made as shown in Figure 6.2. This would give an indication of the colour change to be expected when binding bacteria. An obvious change in the colour could be seen in Figure 6.2.

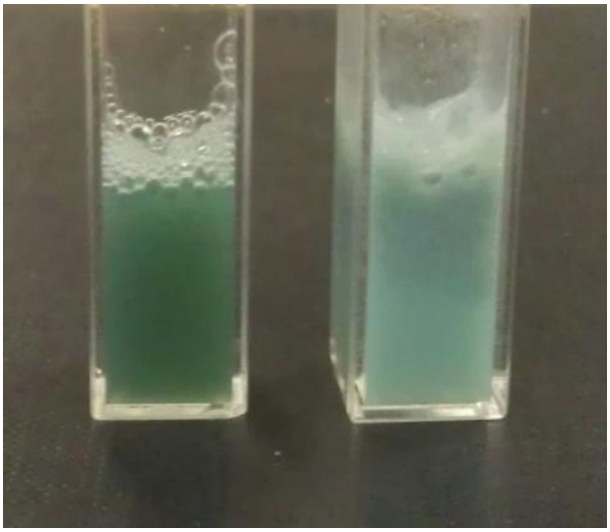

Figure 6.2 - Image showing Nile Blue/vancomycin functional HB-P(NIPAM-co-AMMA) in aqueous solution 20mg ml^{-1} below its LCST (left) and above its LCST (right). The image highlights the difference I colour of the polymer above and below its LCST. It is likely that this difference is caused by light scattering from the particles above the LCST.

This was probably caused by the increased scattering of light caused by the 'desolvated' HB-PNIPAM particles in dispersed in the solution. This will have had the effect of masking the blue colour from the Nile Blue and which was so prominent in the system below the LCST. To investigate further, fluorescence measurements were used.

6.3.2.1 Steady State Experiments

In these steady state spectroscopy excitation and emission processes are used to investigate a polymer sample with an attached fluorescent probe. Labels covalently attached to the polymer backbone have been shown to be good reporters of stimuli responsive polymer conformational change. The sample is irradiated with a specific wavelength this excites the fluorescent probe causing it to emit light at a higher wavelength due to the loss of energy

between excitation and emission. This emitted light is detected at 90° to the probe so as to avoid interference from the excitation beam.

A scanning spectrum can be run across a range of excitation wavelengths. The emission spectrum is measured for each excitation wavelength. This can be used to find unknown excitation and emissions. If a slovatochromic label (such as Nile Blue) is used then changes in the wavelength or intensity of these excitation and emission spectra can give information on the conformation of the polymer. Figure 6.3 shows how the conformation of a polymer can change the environment of the AMMA probe bound in the polymer chain. This change in environment can have an effect on the dyes fluorescent profile and thus be measured directly from the fluorescence spectra of the probe.

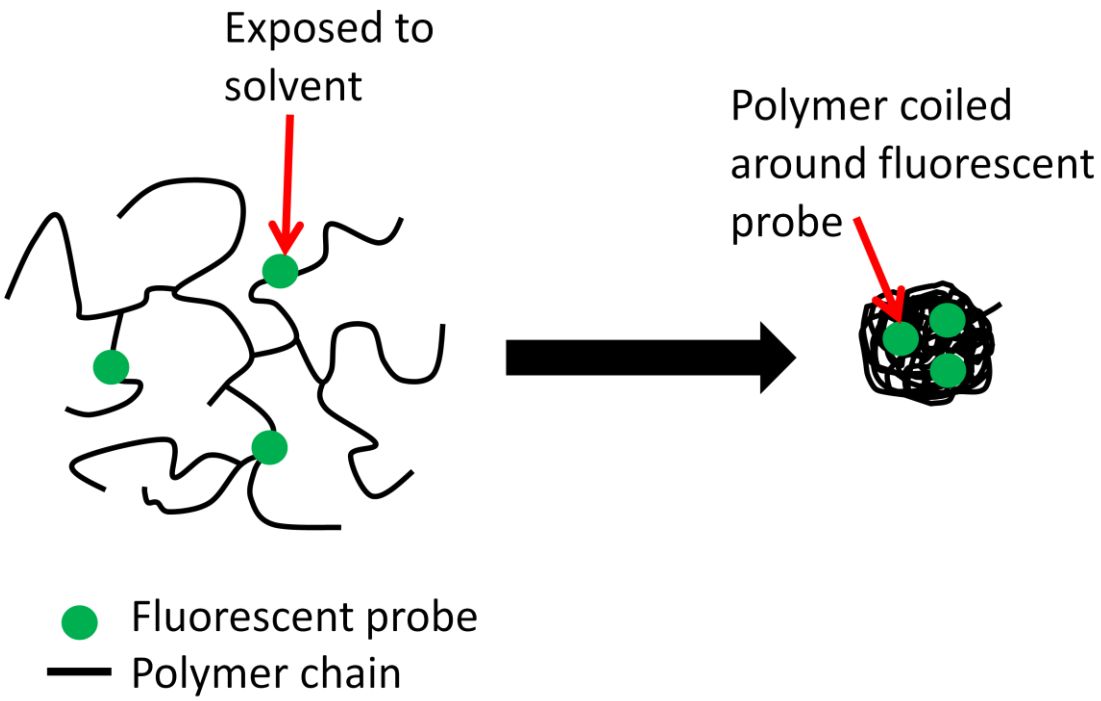

Figure 6.3 - A Schematic diagram showing how the conformation of a polymer around a fluorescent probe can affect the environment of the probe. Left shows the probe in a solvated coil where it is exposed to interactions from the solvent. Right shows the fluorescent probe buried within the collapsed globular polymer. This protects the probe from interactions with solvent.

3D steady state experiments at 10 and 40°C confirmed the presence of both Nile Blue and AMMA labels; with an apparent increase in intensity of emission from the Nile Blue at 40°C (above the LCST) compared to below the LCST. The temperature dependant change in environment of the HB-PNIPAM may cause a shift in the emission of Nile Blue. This was not

observed in these spectra. Although, the intensity of the Nile Blue did seem to increase at 40°C compared to 10°C. This is shown qualitatively in Figure 6.4.

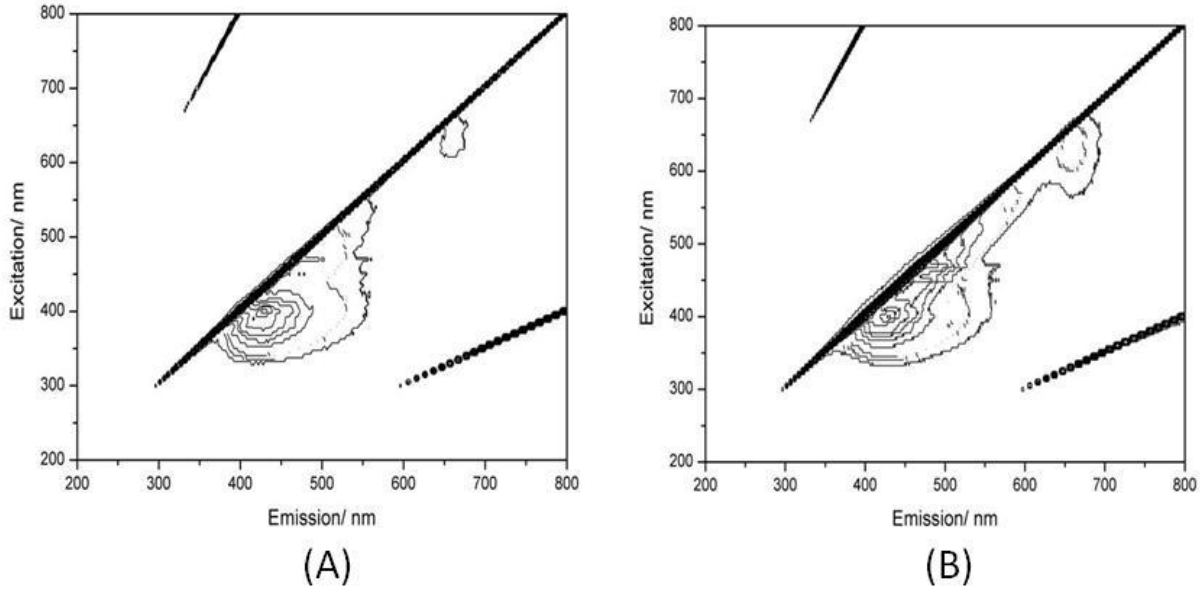

Figure 6.4 - 3D steady state excitation emission spectra of HB-P(NIPAM-co-AMMA)-NB/vanc showing integer increases intensity (photons per second) from $1x10^4$ to $1x10^7$ with integer spacing of $1x10^4$. *Data analysis courtesy of Thomas Swift from The University of Sheffield, Department of Chemistry.*

In order to assess the presence of a colour change a control sample was made which contained Nile Blue dissolved in the polymer core (not covalently attached). It has been previously observed that the peak emission of Nile Red will change with temperature when dissolved within HB-PNIPAM. Nile Blue should behave in a similar way. A schematic of the two modes of inclusion of the Nile Blue are shown in Figure 6.5. A difference in the environments and thus, the peak emission wavelengths may be expected due to the change in the relative positions of the Nile Blue.

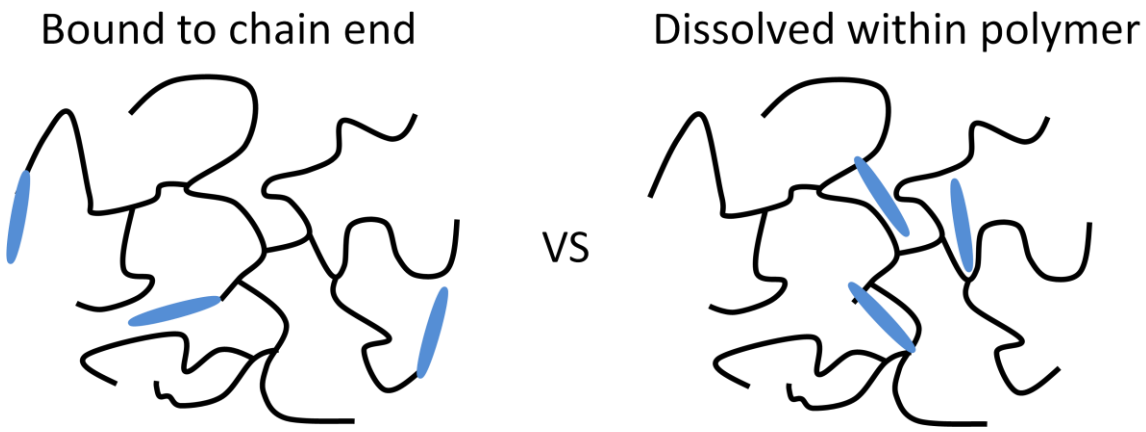

Figure 6.5 - Schematic showing the difference between Nile Blue chemically bound at the chain ends (left) and Nile Blue dissolved within the polymer (right).

From the 3D steady state experiments (Figure 6.4) it can be seen that 620 nm will give the optimum excitation for the Nile Blue dye. Figure 7.6 shows that at 10°C there is a large difference between peak emission for the chain end bound Nile Blue compared to the dissolved Nile Blue. However, the temperature dependent change in peak emission observed for the dissolved Nile Blue is not observed with a chain end bound Nile Blue. As the decrease in wavelength is caused by a change in the environment of the solvatochromic dye, this is further evidence that end groups do not penetrate into the core. The solvatochromic dye dissolved in the polymer perceive the coil to globule transition but this is not reflected by the dye on the chain ends.

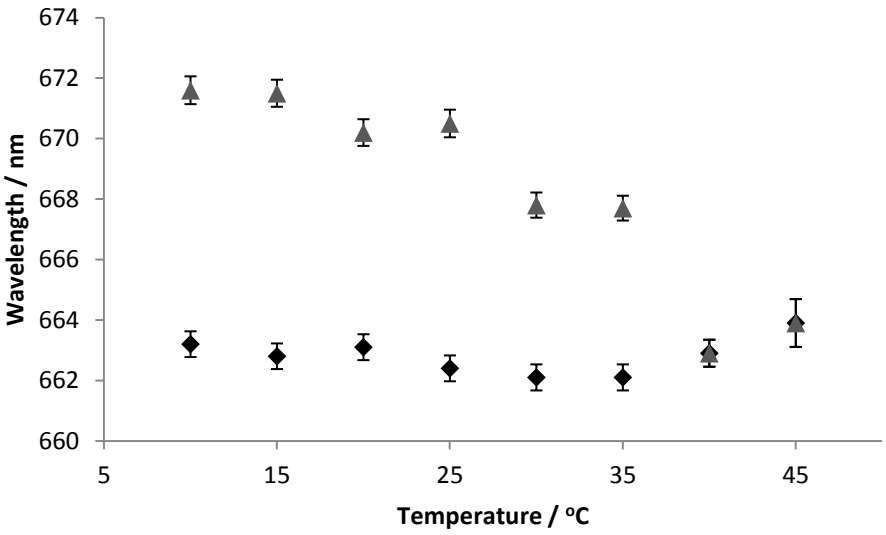

Figure 7.6 - Comparison of wavelength of peak emission for Nile Blue bound to the chain in HB-P(NIPAM-co-AMMA)-NB/vanc end (black diamonds) and Nile Blue dissolved in the polymer (grey triangles), over the temperature range 10-45°C, using a excitation wavelength of 620nm. ***Data interpretation courtesy of Thomas Swift from The University of Sheffield, Department of Chemistry.***

6.3.2.2 Fluorescent Lifetimes

The fluorescence lifetime is a measure of the number of photons emitted from an excited sample over a period of time. This does not measure the changing wavelength of these dyes but the stability of the excited state prior to photon emission. The lifetime of this excited state can give important information on the conformation of stimuli responsive polymers. [208] Depending upon the conformation of the polymer the fluorescent probe within the polymer can be quenched at different rates. If the polymer is in the extended conformation the probe will be more exposed to quenching species and will have a shorter fluorescent lifetime. In the globular conformation the fluorescent probe will be shielded from the quenching species and will have longer excited state lifetimes. This is shown in Figure 6.7.

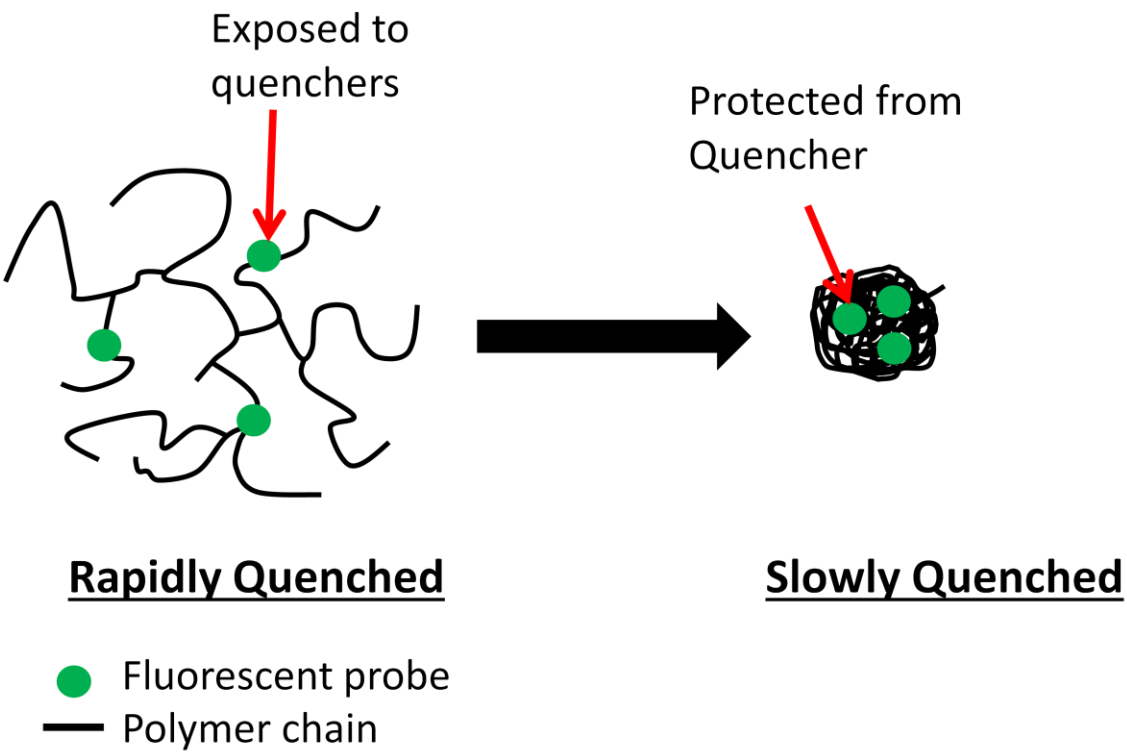

Figure 6.7 - A schematic diagram showing how polymer conformation can affect quenching of a fluorescent probe. When in the coil conformation the fluorescent probe is exposed to quenching and as a result will have a short fluorescence lifetime. In the globular conformation the fluorescence probe if protected from interactions with quenching species and will have longer fluorescence lifetimes.

The fluorescence decays of AMMA within HB-(PNIPAM-co-AMMA) and HB-(PNIPAM-co-AMMA)-NB/vanc are shown in Figure 6.8. The fluorescence decay can be used to indicate the lifetime of the excited states as shown in Figure 6.9, a shorter decay indicating a shorter lifetime. The samples were excited at 340 nm and emission monitored at 440 nm.

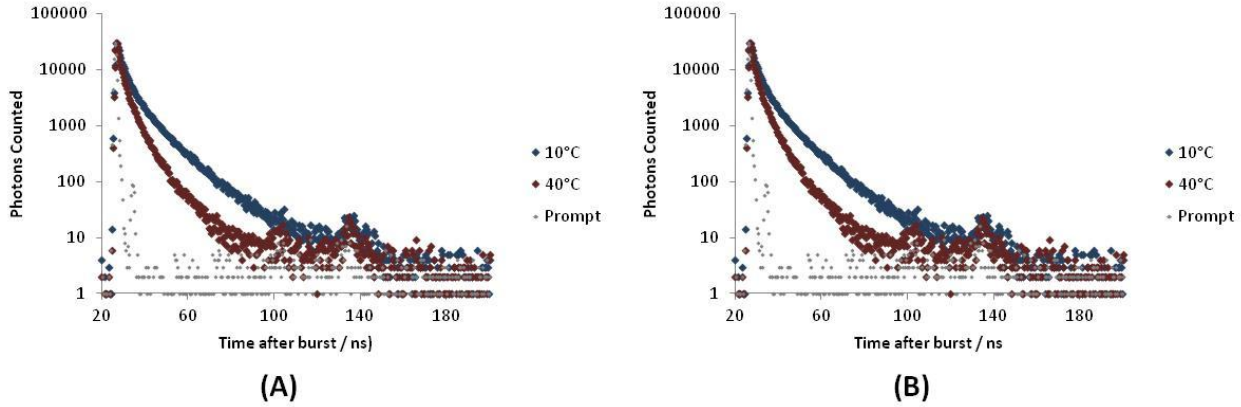

Figure 6.8 - Fluorescence decays of HB-P(NIPAM-co-AMMA) (A) and HB-P(NIPAM-co-AMMA)-NB/vanc (B) at 10 and 40°C. ***Data analysis courtesy of Thomas Swift from The University of Sheffield, Department of Chemistry.***

The fluorescence lifetimes of both systems are increased at 40°C compared to 10°C. The collapse of the coil to a globule reduces solvent quenching of the label, and increases the fluorescence lifetime. This is shown in Figure 6.9. It should be noted that the Nile Blue/vancomycin end functionalised polymer has an increased fluorescence lifetime compared to the polymer without Nile Blue and vancomycin (AMMA alone). The increase in fluorescent lifetime is usually associated with reduced quenching upon coil collapse. This morphological change causes polymer chains shield the fluorescent label from quenching (by solvent) thus increasing the lifetime. The addition of Nile Blue and vancomycin to the chain ends could inhibit the coil collapse. If the polymer chains were packed less tightly within the globule, quenching could be more prevalent compared to the HB-P(NIPAM-co-AMMA) without Nile Blue and vancomycin.

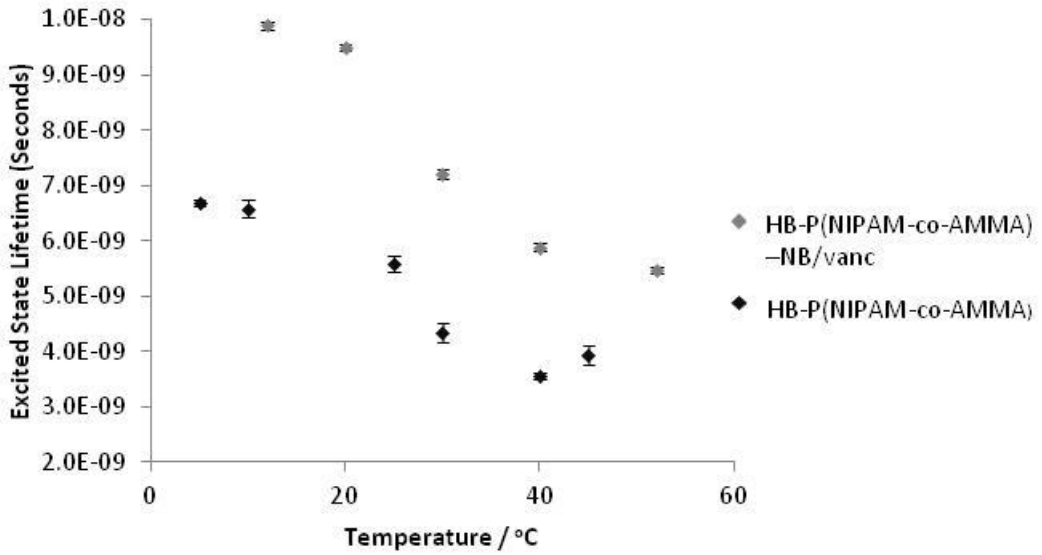

Figure 6.9 - Excited state lifetime of HB-P(NIPAM-co-AMMA) and HB-P(NIPAM-co-AMMA)-NB/vanc over the LCST. *Data courtesy of Thomas Swift from The University of Sheffield, Department of Chemistry.*

6.3.3 Bacteria Binding

Figure 6.10 shows that there is no visible difference in the colour of the polymer with bacteria and without bacteria at any of the concentrations used. As the polymer is the same as previously used it is fair to assume that the bacterial binding is still occurring.[130, 205]

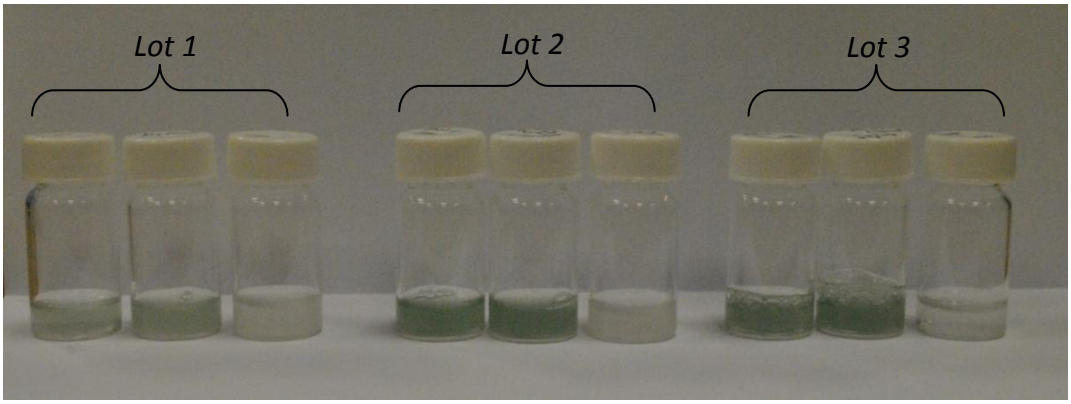

Figure 6.10 - Image showing *Lot 1*, Left - 5mg ml^{-1} polymer, centre - 5 mg mL^{-1} polymer with 9x10^{9} bacteria, Right - 9x10^{9} bacteria. *Lot 2*, Left – 10 mg mL^{-1} polymer, centre - 10mg ml^{-1} polymer with 9x10^{9} bacteria, Right - 9x10^{9} bacteria. *Lot 3,* 10 mg mL^{-1} polymer, centre - 10 mg mL^{-1} polymer with 9x108 bacteria, Right - 9x10^{9} bacteria. The bacteria used were *Staphylococcus Aureus* S235 isolated from a wound infection. The experiment was carried out at room temperature.

With this in mind and taking into account the fact that no change in peak emission was observed in Figure 7.6, it is fair to assume that bacterial binding does not cause the colour change expected. This is demonstrated further by Figure 6.11.

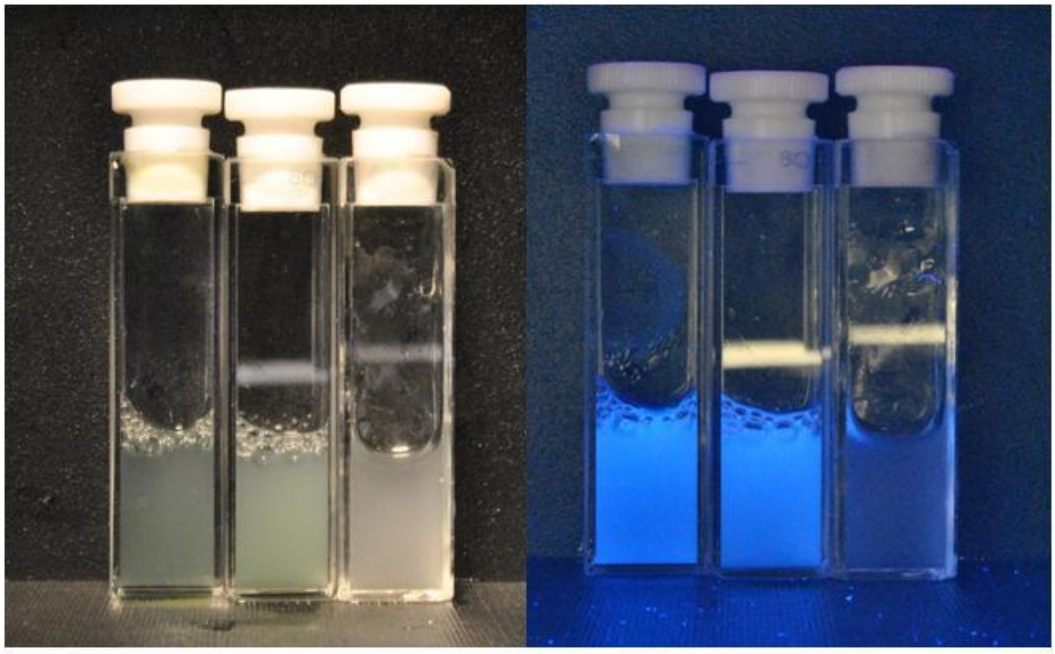

Figure 6.11 – (A) Left – 10 mg mL^{1} polymer, centre – 10 mg mL^{-1} polymer with $9x10^{9}$ bacteria, Right - $9x10^{9}$ bacteria with a black background under normal optical conditions. (B) Left – 10 mg mL^{-1} polymer, centre - 10 mg mL^{-1} polymer with $9x10^{9}$ bacteria, Right - $9x10^{9}$ bacteria with a black background exposed to 365nm UV light. The bacteria used were Staphylococcus aureus S235 isolated from a wound infection. The experiment was carried out at room temperature.

Any change in colour between the HB-P(NIPAM-co-AMMA)-NB/vanc containing samples (left and centre) can be accounted for by the cloudiness introduced by the addition of the bacteria. Any colour change is not sufficient for this to be used as a bacteria binding sensor.

As discussed previously, pendant groups can either be buried within the globule [126-127] or presented on the outside of the globule as a core shell type morphology.[85, 128-129] This could lead to a situation where the Nile Blue is presented on the outside of the particle in the globular conformation (Figure 6.12), which would not give rise to a change in environment. This explains the reason why no observable change was seen in the peak emission wavelength.

Figure 6.12 - Schematic of HB-PNIPAM-NB above and below LCST

6.4 Conclusions

By driving a relatively concentrated solution of HB-P(NIPAM-co-AMMA)-NB/vanc through its LCST there was an apparent change in the colour. However, after further investigation this should be attributed to diffraction of light by polymer particles and is not caused by a change in environment of the Nile Blue.

The introduction of Nile Blue as an end functionality does not give a colour change associated with coil collapse. There is no change in the peak emission and change caused by diffraction of light by the particles formed by coil collapse is too small to be sure of any change.

Compared to a polymer containing a dissolved Nile Blue the results were very different. There was an observable change in the peak emission which was not seen with an end bound Nile Blue label. This provides some evidence that the end bound Nile Blue does not experience a change in environment. However, the change in environment is possible by other means.

6.5 Further work

Work on this project has been continued by Dr. T. Swift, Dr. R. Hoskins, D. Pownall, and P. Teratanitorn sponsored by Smith & Nephew and The Welcome Trust. The simple attachment of Nile Blue to the polymer chain end has been antiquated by the *in situ* polymerisation of Nile Red acrylate in the NIPAM RAFT polymerisation. This introduces Nile Red into the polymer backbone where it will experience a larger change environment upon coil collapse, producing a larger solvatochromic effect.

7. Thesis Conclusions

HB-PNIPAM polymers were synthesised by RAFT polymerisation using the RAFT agent 4-VBPCD. The feed ratios of NIPAM, 4-VBPCD and ACVA were altered to produce polymers with a range of properties. Data from NMR studies of the HB-PNIPAM polymers showed that the feed ratios had a significant effect on the degree of branching. The LCST transition was studied by cloud point (turbidity) and VP-DSC. This data provided the first evidence that for some monomer feed ratios, the resultant polymer exhibited a core shell type morphology with a dehydrated inner core and a hydrated outer shell. Corroborative evidence of this 'core shell' structure was elucidated by dissolving the solvatochromic dye, Nile Red, within the polymer core and monitoring it by fluorescence emission across the LSCT. It was shown that the peak emission for Nile Red within globular HB-PNIPAM was consistently around 628 nm. Whereas, in the hydrated coil the Nile Red showed a variation in peak emission wavelength starting at around 660 nm for the lowest degree of branching and falling to around 630 nm for the highest degree of branching. The similarity of the peak emission of the 15:1 and 25:1 before and after the LCST suggests that there is no LCST transition taking place. However, turbidity and VP-DSC measurements show this not to be the case. From this it can be concluded that lack of change in the environment of the solvatochromic dye is likely to be caused by a globular moiety within the polymer core, which does not undergo a change in hydration upon coil collapse. This suggests a core shell structure (below the LCST), with a dehydrated core and hydrated outer shell which is able to undergo an LCST transition.

An alternative method for the analysis of GPC data for RAFT HB-PNIPAM polymers has been created. The traditional method of analysis was inappropriate for these polymers as the statistical analysis relies on the data fitting a Gaussian distribution. In the case of highly branched RAFT polymers, this is not the case. These distributions are often bimodal and as such should not be analysed using the usual technique. In order to take into account the whole distribution the median molecular weight should be used and the interquartile ranges should be calculated to give an indication of dispersity.

HB-PNIPAM polymers were used to passage cells. HB-PNIPAM-GRGDS has previously been used to lift cells from TCP and redeposit them into new well plates.[80] HB-PNIPAM polymers have been functionalised with RGD based peptide sequences, of the general formula GXGRGDS (where X is an amino acid). The GXGRGDS functionalised polymers have been used to lift and redeposit HDFs from TCP.

From this project it was possible to conclude that the flanking residue can have a large effect on the ability of the cells to lift and redeposit cells cultured on TCP. It was found that of the systems investigated GVGRGDS, GGGRGDS and GSGRGDS deposited the greatest number of cells.

The HB-PNIPAM particles were also successfully investigated as functional additives to photocurable polymers. HB-PNIPAM was dissolved in NVP and PEG based monomer systems and the resultant solution was crosslinked by UV light creating a BS-IPN. FTIR analysis showed that the HB-PNIPAM could only be partially extracted from these systems. The Data showed that a higher proportion of the HB-PNIPAM component was retained within the PEG system. The HB-PNIPAM component within the PVP and PEG based BS-IPNs were shown not to display an LCST (DSC, equilibrium water content and FTIR). This was beneficial in cell culture techniques as an LCST transition would likely cause delamination of the cell sheet,[72, 153] which would make imaging of cells difficult.

Addition of HB-PNIPAM-GRGDS to BS-IPNS was shown to have a beneficial effect of proliferation of cell types. When the concentration of HB-PNIPAM-GRGDS within a VPV based BS-IPN was varied, it was found that between 2.5 and 10 wt% HB-PNIPAM-GRGDS there was an increase in the spreading and proliferation of the cells. This was in agreement with the data reported by Hubbell,[56] where an RGD spacing of 440 nm was enough to support cellular adhesion with little spreading but with a spacing of 140 nm cells were observed to display typical adherent morphologies with good spreading and proliferation. It is suggested, based on the observed properties of the cells, that the 2.5 wt% HB-PNIPAM-GRGDS sample corresponds to the 440 nm spacing and the 10 wt% HB-PNIPAM-GRGDS corresponds to the 140 nm spacing. The migratory behaviour of the cells was observed and the HB-PNIPAM- GRGDS was seen to have no statistically significant effect by ANOVA above concentrations of 2.5 wt%.

BS-IPNs were synthesised with X-PEG and X-NVP as the matrix. The PEG based system was observed to have a much higher retention of the HB-PNIPAM component than the PVP system. It was suggested that this result was caused by an increase in crosslink density and a higher compatibility of the HB-PNIPAM within the PEG-DA system compared with the PVP system.

The X-PEG BS-IPNs were shown to have similar *in vitro* cell data to the PVP system. Although the increase in the rate of migration was not seen in the 2.5 and 5 wt% HB-PNIPAM GRGDS systems. However, a significant difference was seen between migration of the 10% HB-PNIAM-GRGRD sample and all other samples.

Both the X-PVP and X-PEG BS-IPNS systems were structured by projection microstereolithogrphy. It was concluded that these systems could be used to create medical devices such as tube type structures for peripheral nerve repair.

In order to create medical devices for implantation into the human body it is often a requirement that they be biodegradable to prevent adverse inflammatory response.[31] For this reason PTMC polymers were synthesised and methacrylate functionalised at a range of molecular weights. The mechanical properties of the polymers were assessed and it was found that the molecular weight of the prepolymers has the highest molecular weight prepolymer was found to produce the most flexible membrane. Although this was advantageous for soft tissue engineering the lower methacrylate functionality of the prepolymer made it difficult to crosslink via photopolymerisation. BS-IPN membranes were therefore synthesised using the 1:4 PTMC-MA. RN22s and HDFs were cultured on X-PTMC, 5%HB-PNIPAM-GRGDS BS-IPN and TCP. As with the NVP and PEG matrices HB-PNIPAM GRGDS was shown to have a positive effect on cell proliferation and viability.

The final experimental chapter used HB-PNIPAM-NB/vanc to create a colour change sensor for bacteria. HB-PNIPAM-vanc has been shown to bind bacteria, which induces a coil to globule transition.[130, 206] The solvatochromic dye Nile Red has been used to indicate the occurrence of the LCST of HB-PNIPAM.[90] Nile Blue has an amine functionality and can be readily tethered to the end groups of the HB-PNIPAM by NHS coupling reaction. Unfortunately, this polymer was shown not to produce a colour change by upon the coil to globule transition. Although this mean that the colour change sensor could not be made it did allow us to conclude that end groups do not penetrate into the globule.

8. Appendix

8.1NMR Spectra

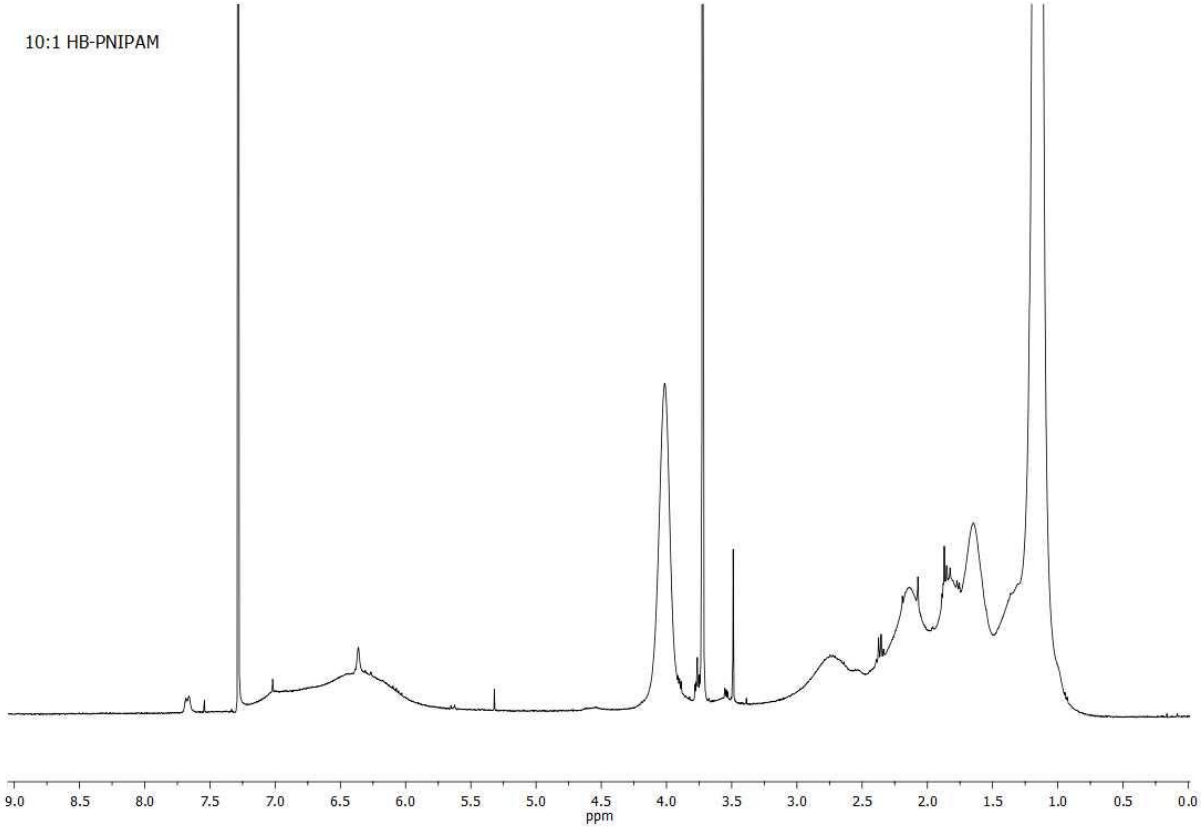

Figure A.1 – A ^{1}H NMR spectrum of 10:1 HB-PNIPAM

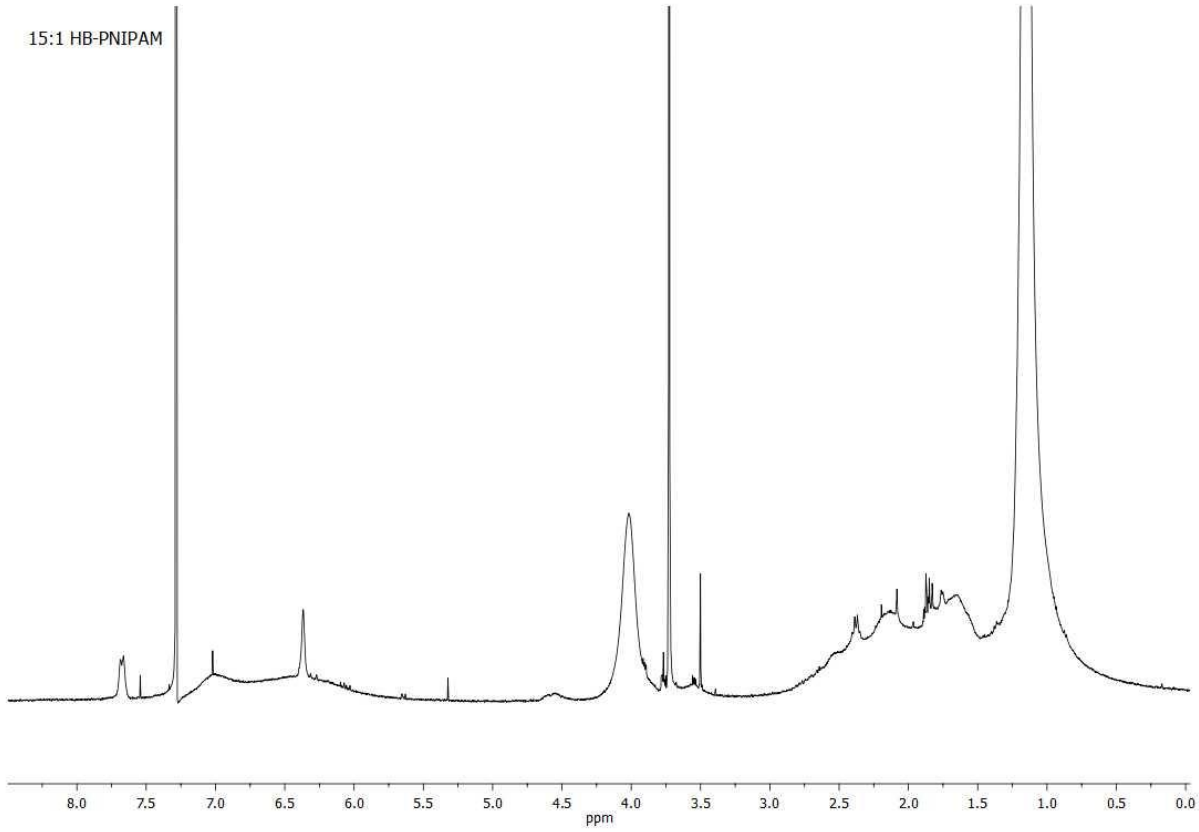

Figure A.2 - A ^{1}H NMR spectrum of 15:1 HB-PNIPAM

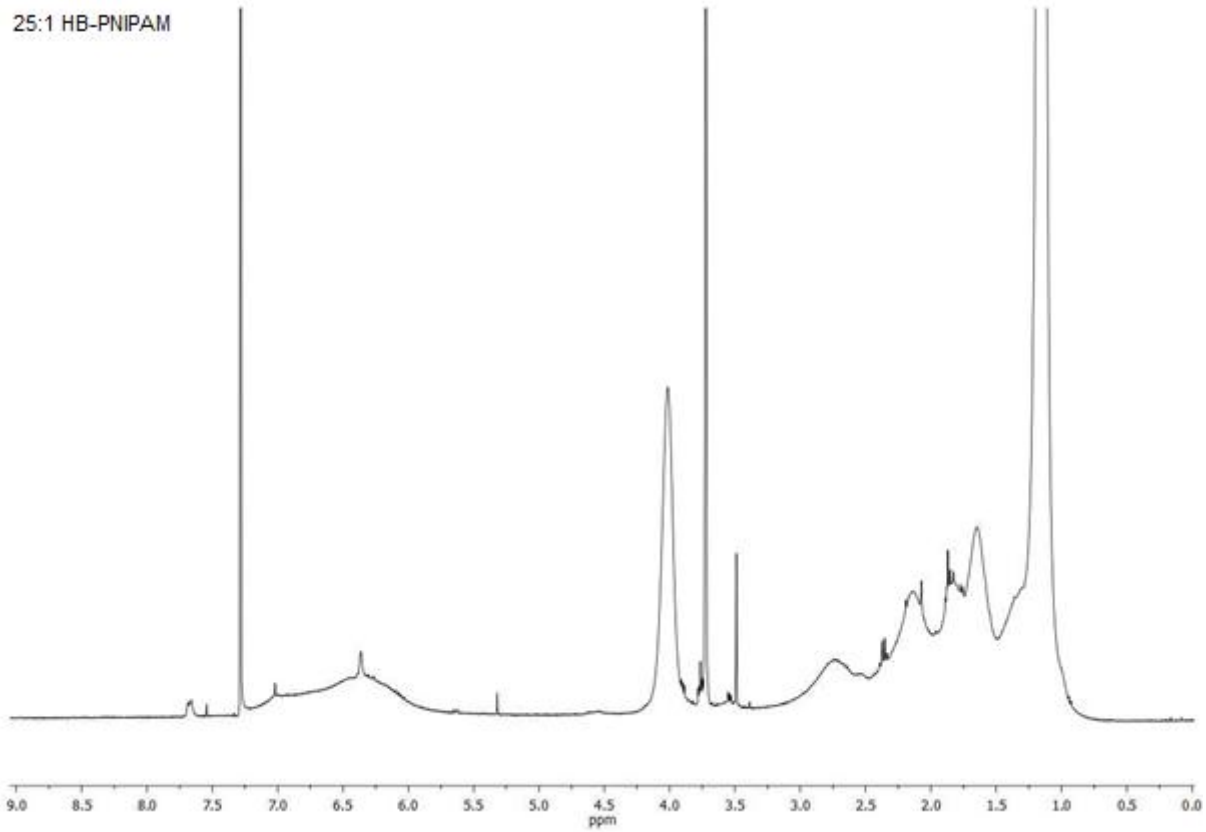

Figure A.3 - A ^{1}H NMR specturm of 25:1 HB-PNIPAM

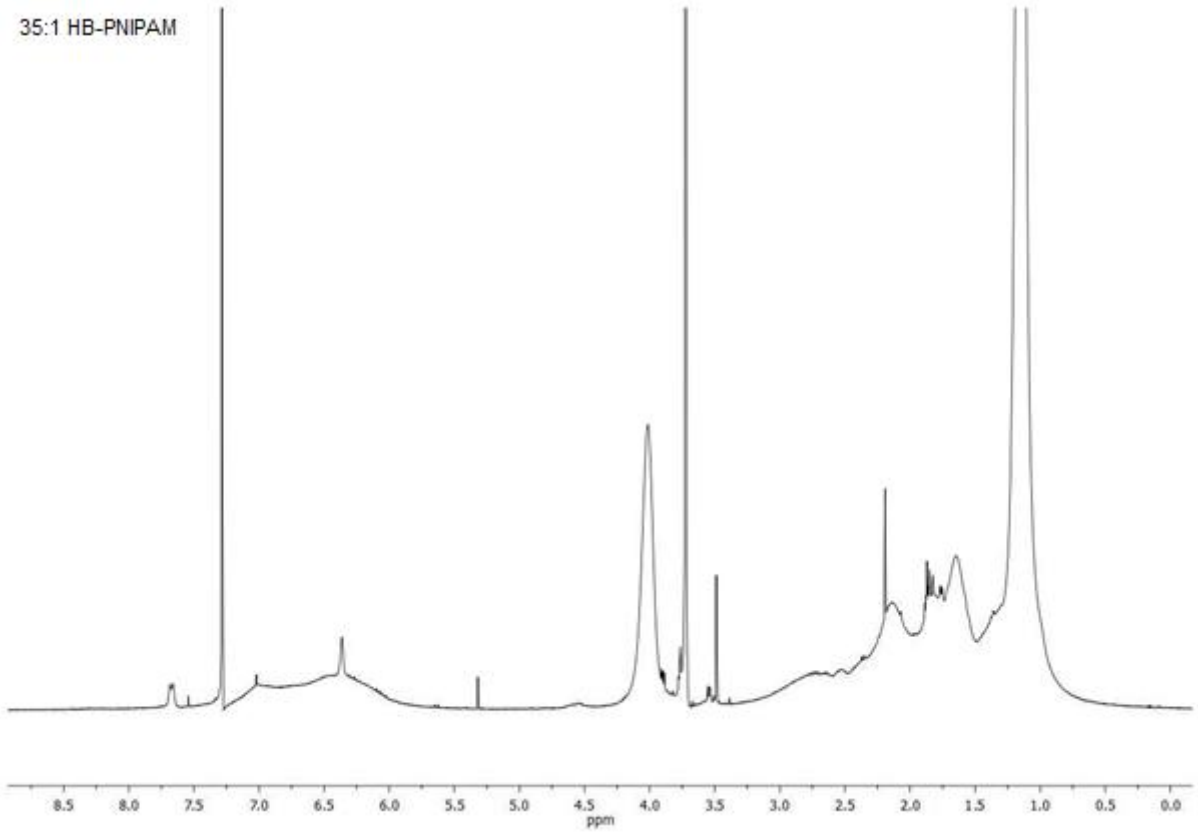

Figure A.4 - A ^{1}H NMR spectrum of 35:1 HB-PNIPAM

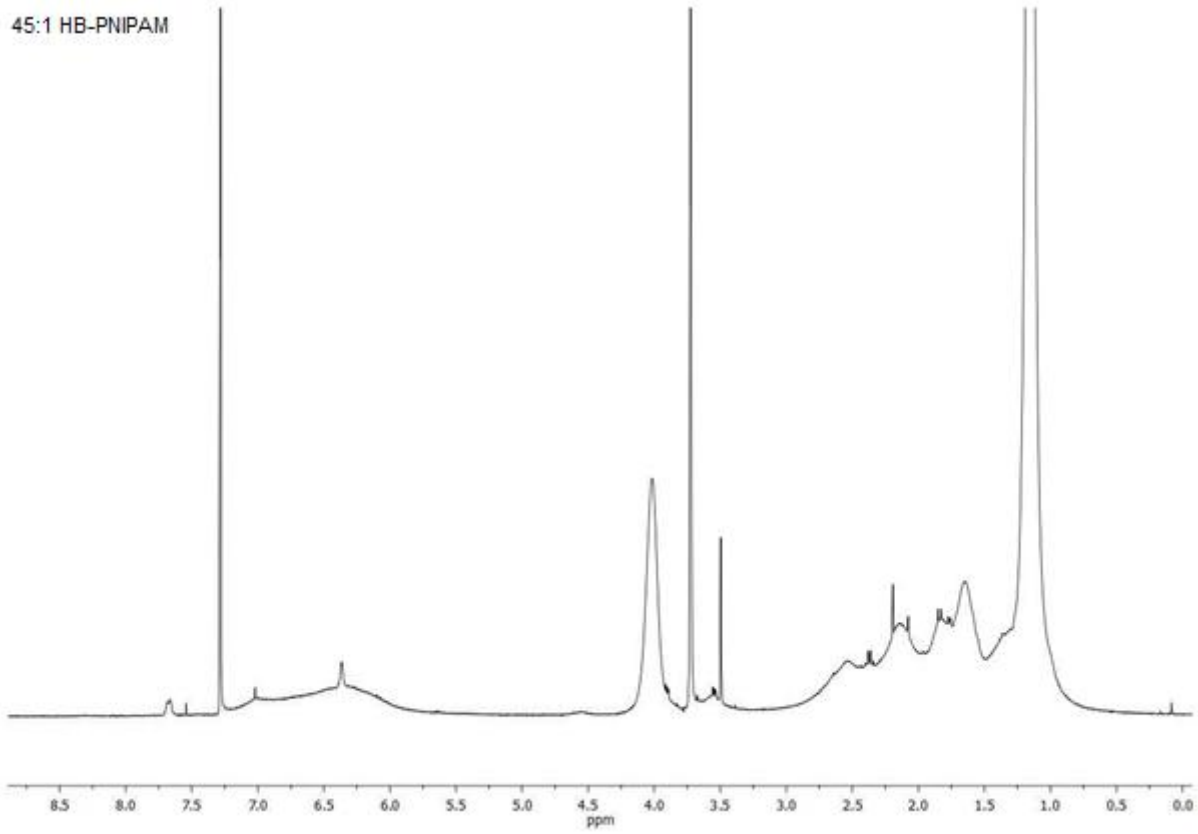

Figure A.5 – A ^{1}H NMR spectrum of 45:1 HB-PNIPAM

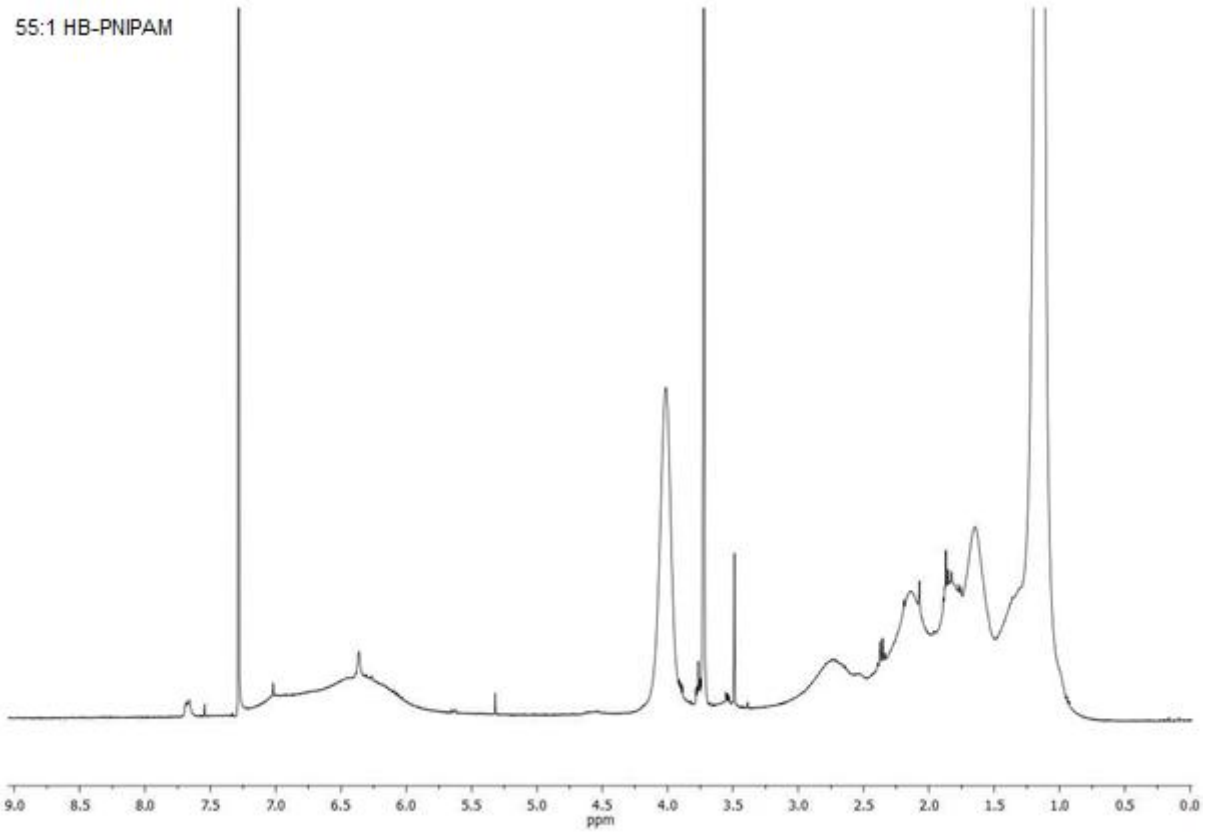

Figure A.6 - A ^{1}H NMR spectrum of 55:1 HB-PNIPAM

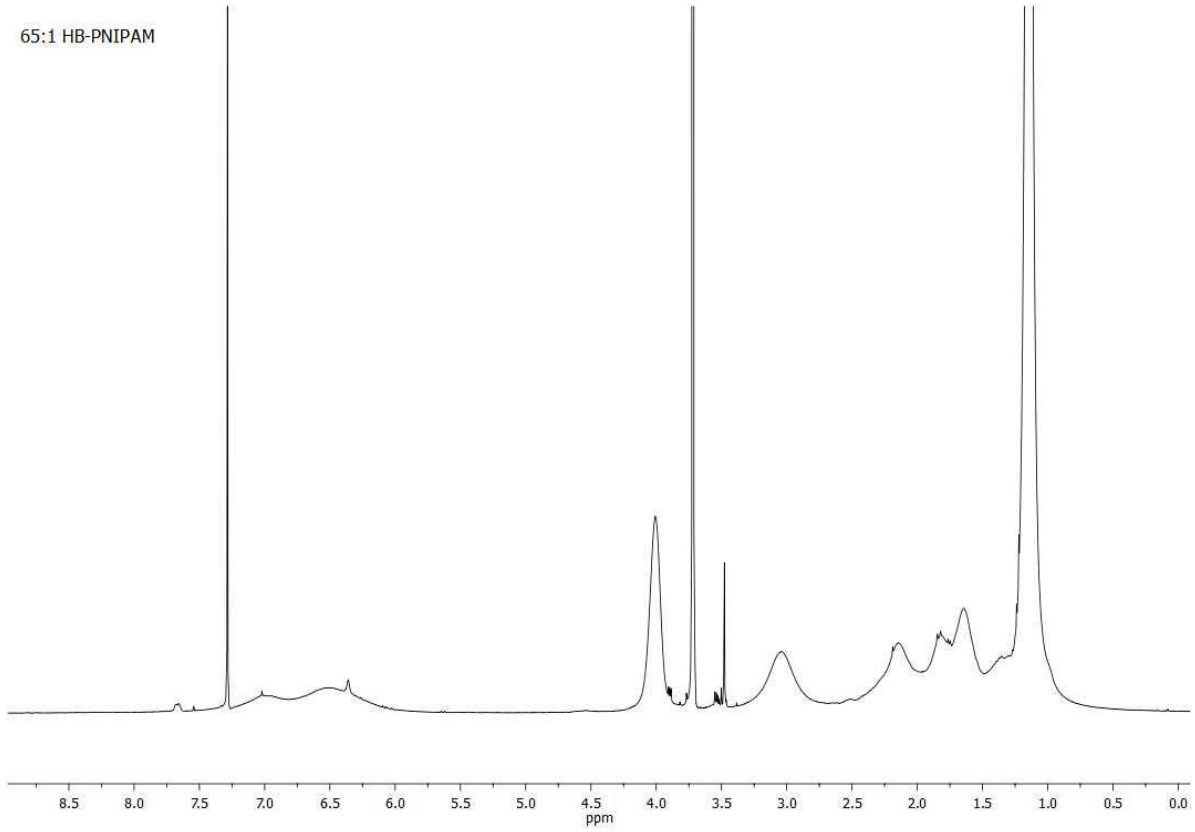

Figure A.7 - A ^{1}H NMR spectrum of 65:1 HB-PNIPAM

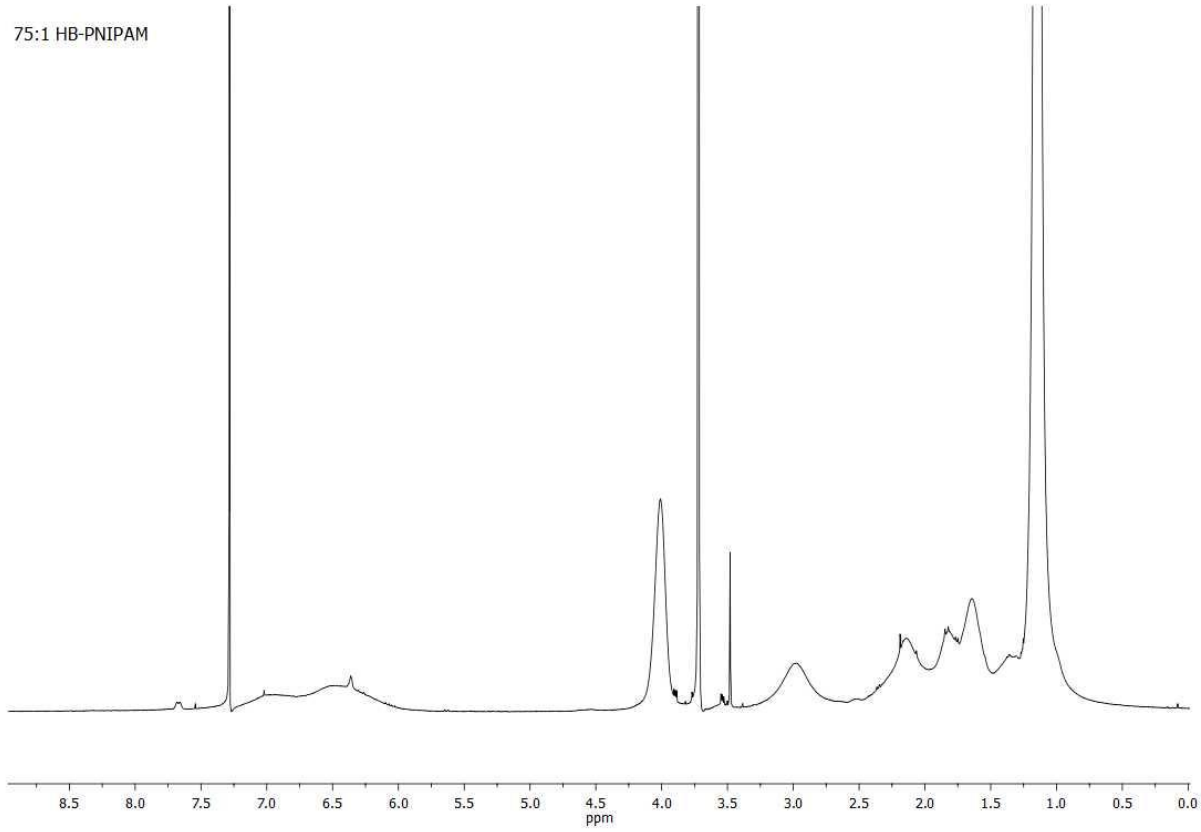

Figure A.8 - A ^{1}H NMR spectrum of 85:1 HB-PNIPAM

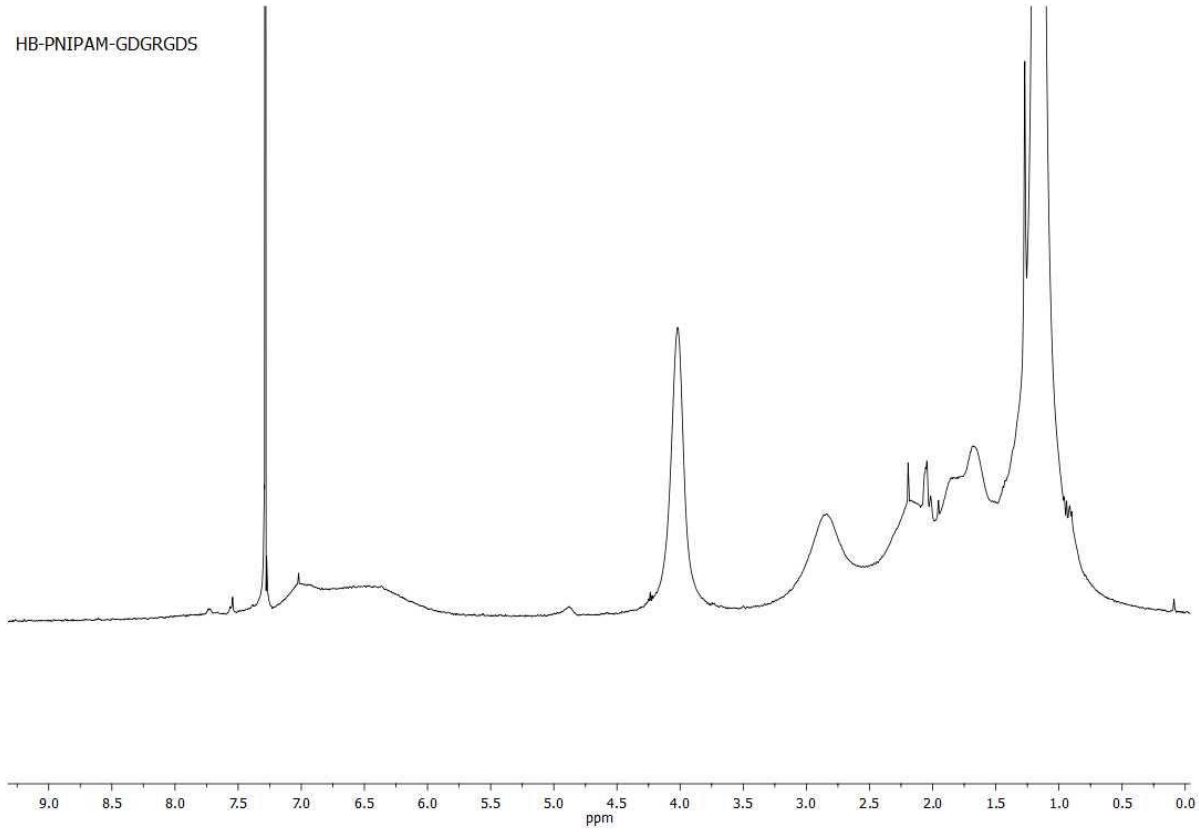

Figure A.9 - A ^{1}H NMR spectrum of HB-PNIPAM-GDGRGDS

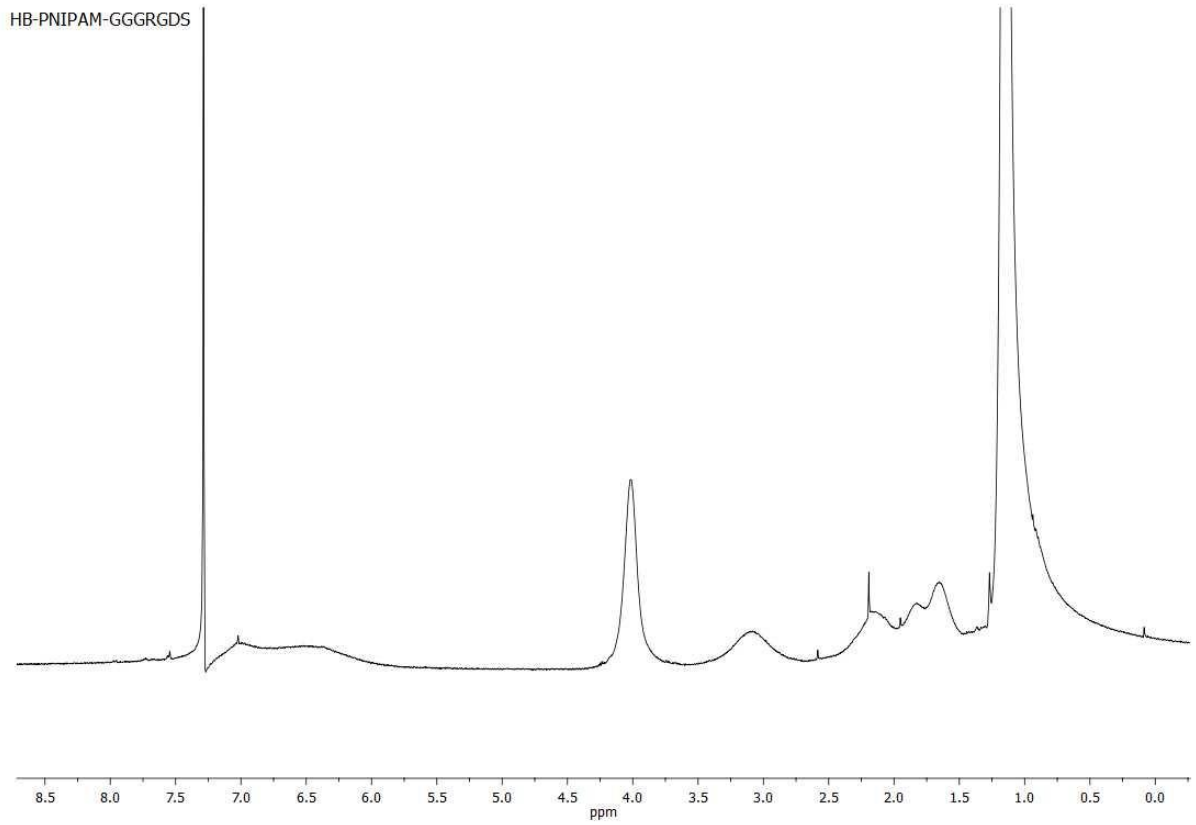

Figure A.10 - A ^{1}H NMR spectrum of HB-PNIPAM-GGGRGDS

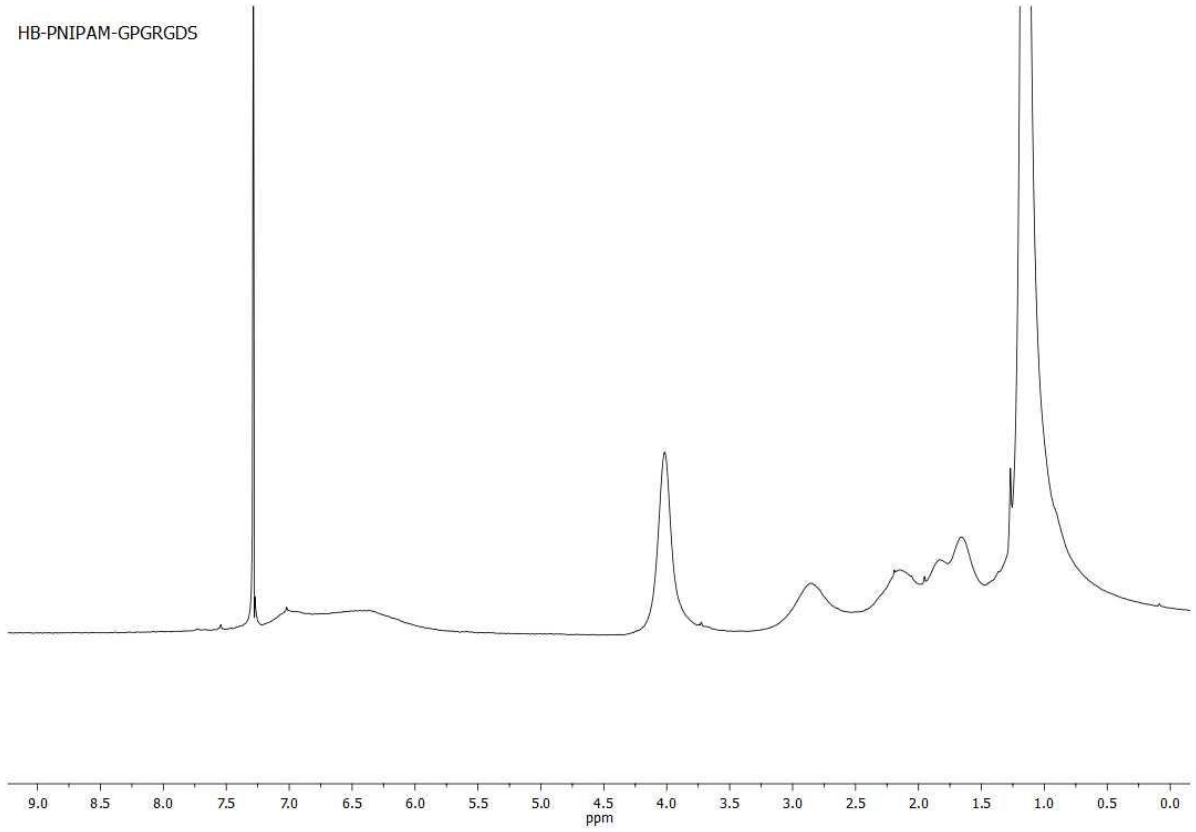

Figure A.11 - A ^{1}H NMR spectrum of HB-PNIPAM-GPGRGDS

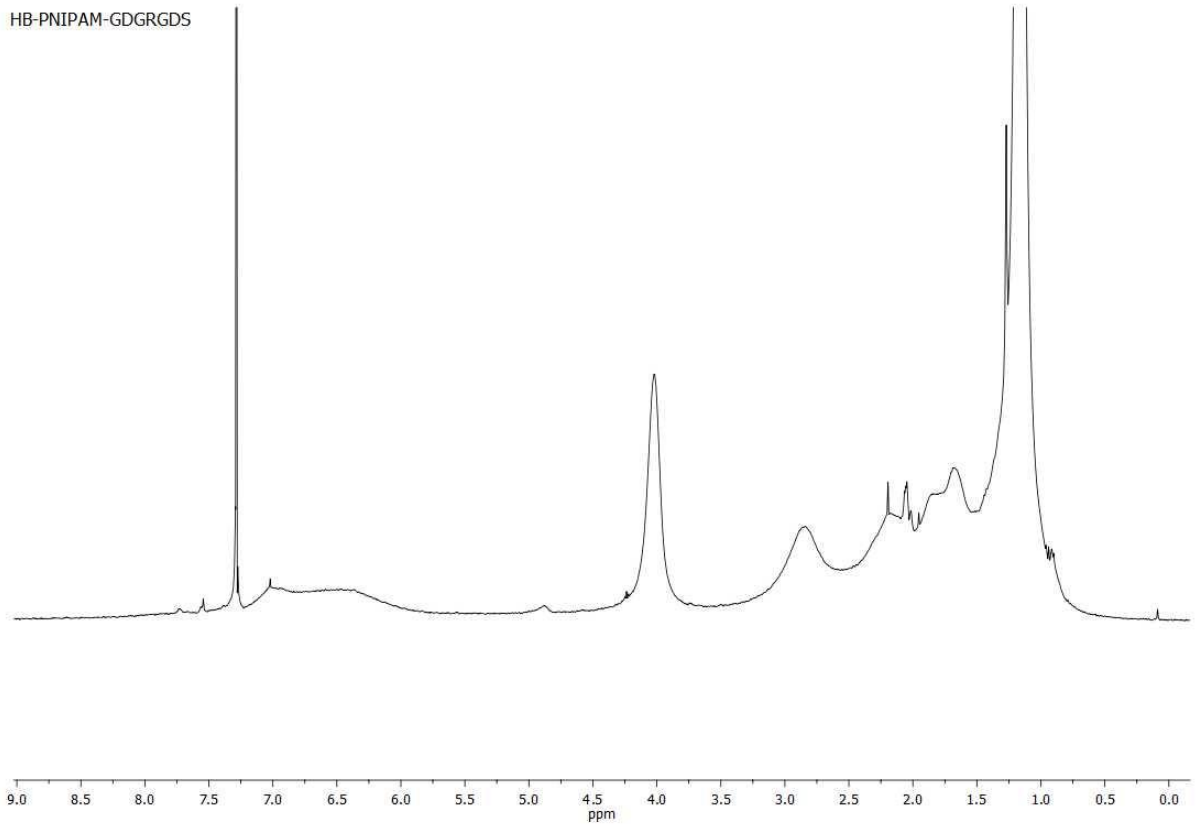

Figure A.12 - A ^{1}H NMR spectrum of HB-PNIPAM-GQGRGDS

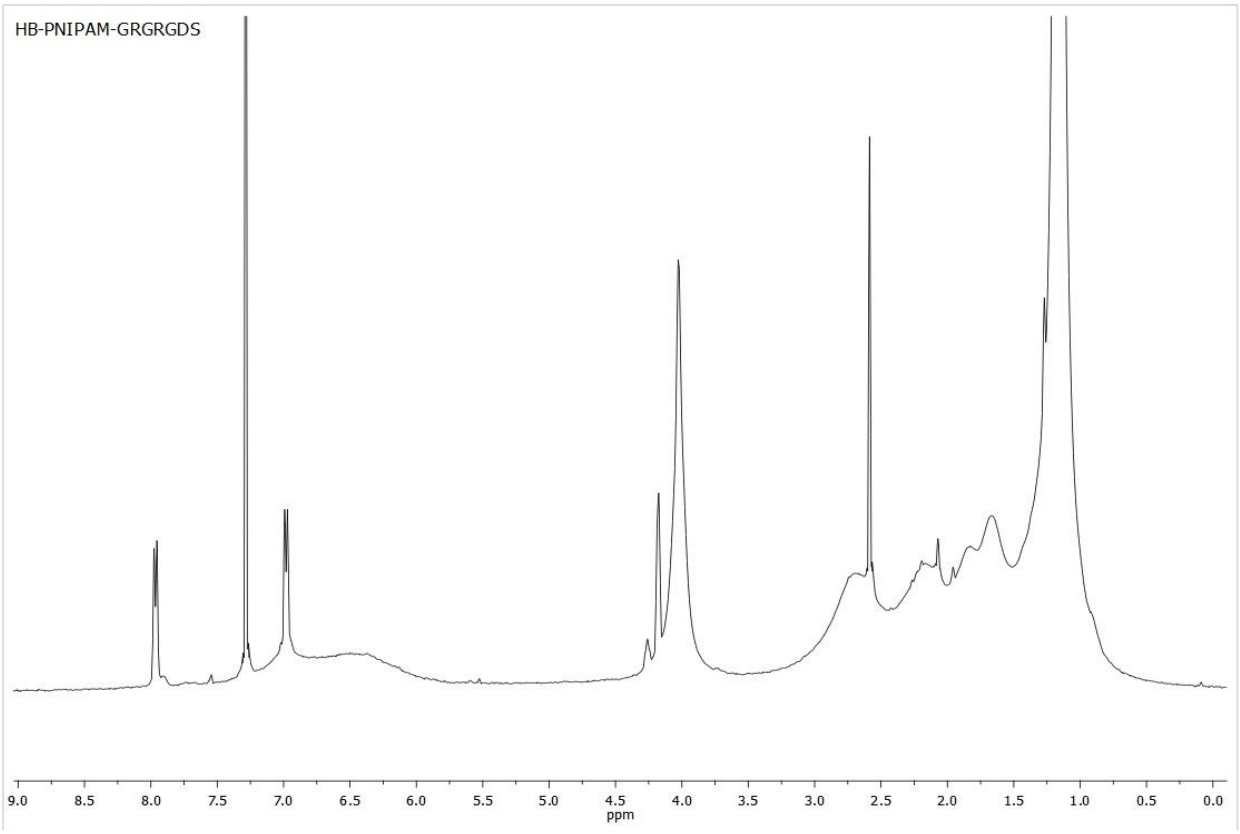

Figure A.13 - A ^{1}H NMR spectrum of HB-PNIPAM-GRGRGDS

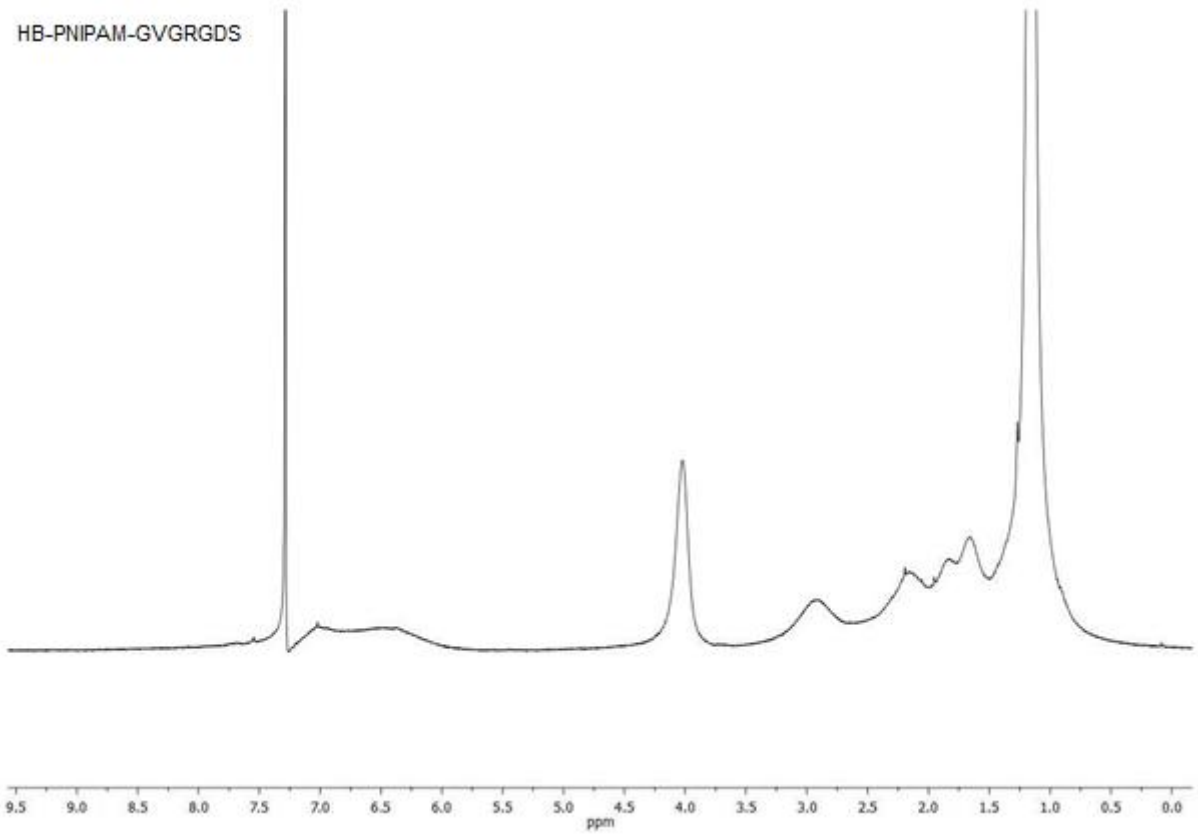

Figure A.14 - A ^{1}H NMR spectrum of HB-PNIPAM-GRGRGDS

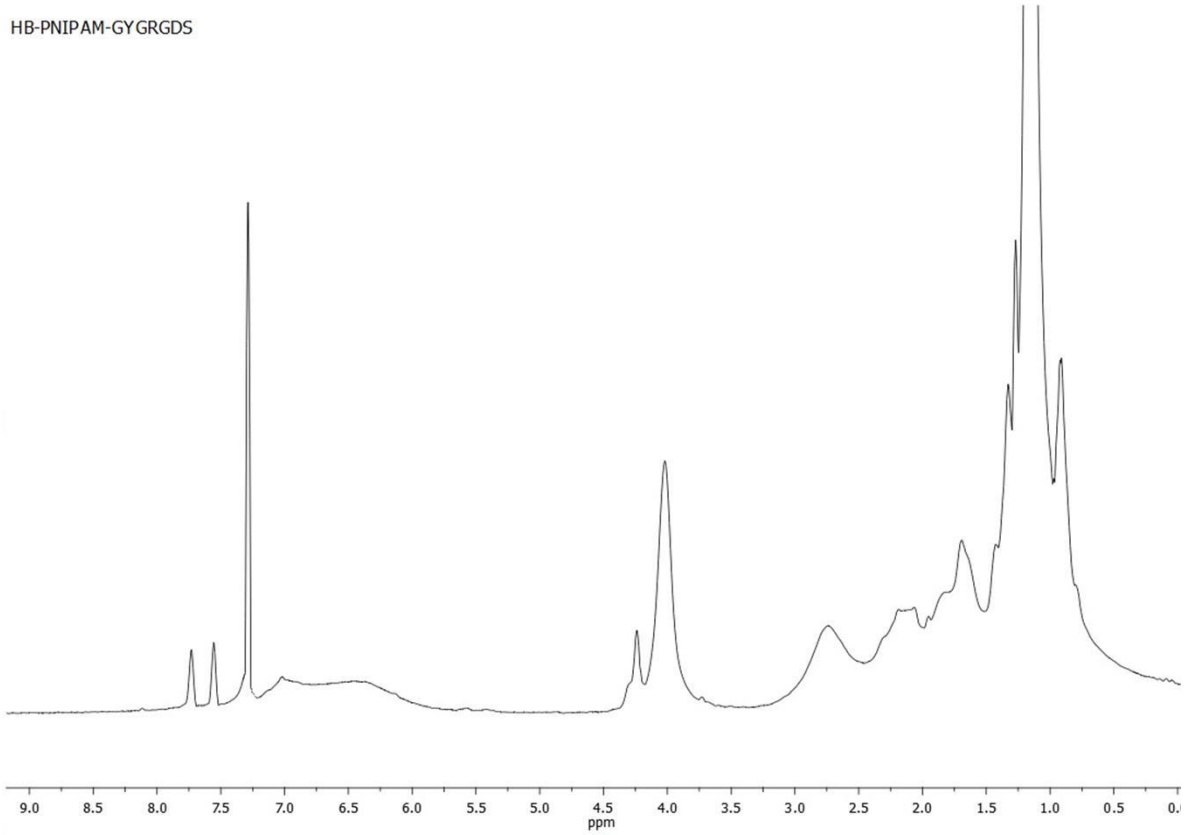

Figure A.15 - A ^{1}H NMR Spectrum of HB-PNIPAM-GYGRGDS

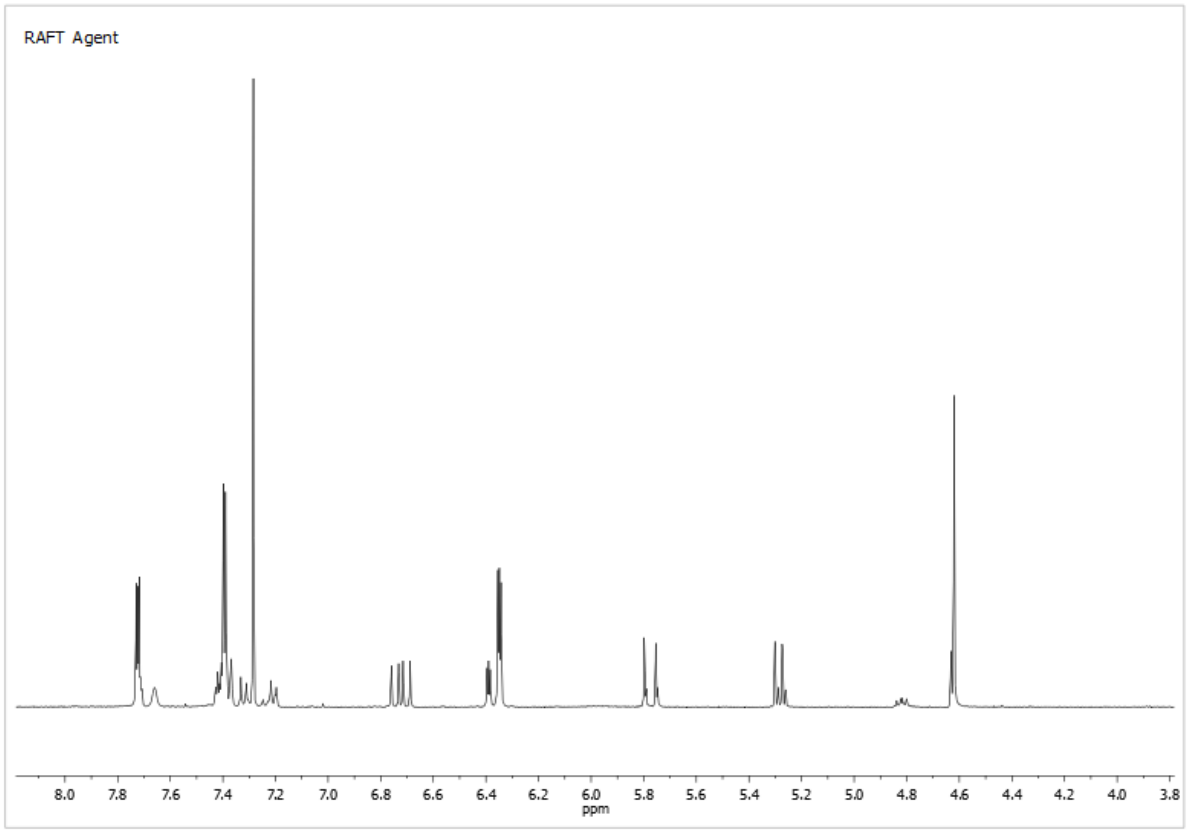

Figure A.16 - A ^{1}H NMR spectrum of RAFT agent (4-VPCD)

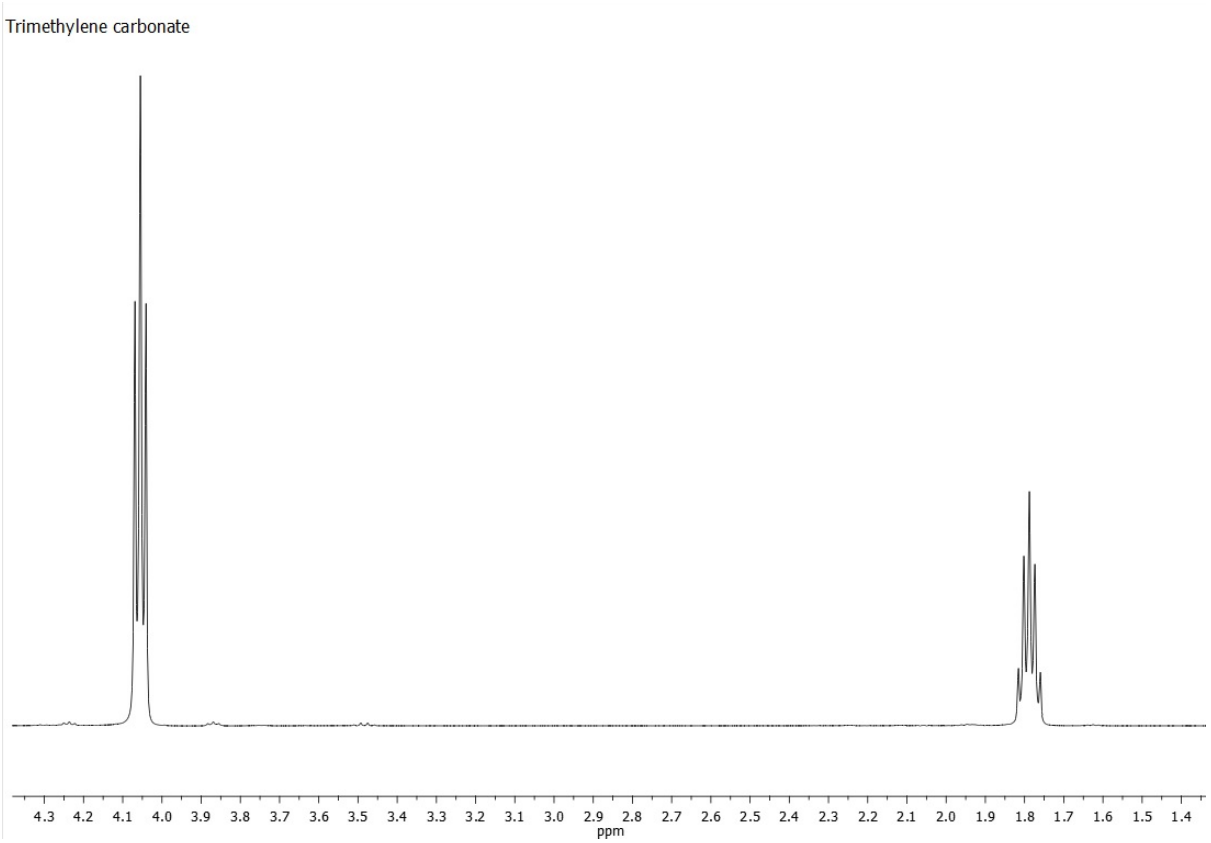

Figure A.17 - A ^{1}H NMR spectrum of trimethylene carbonate

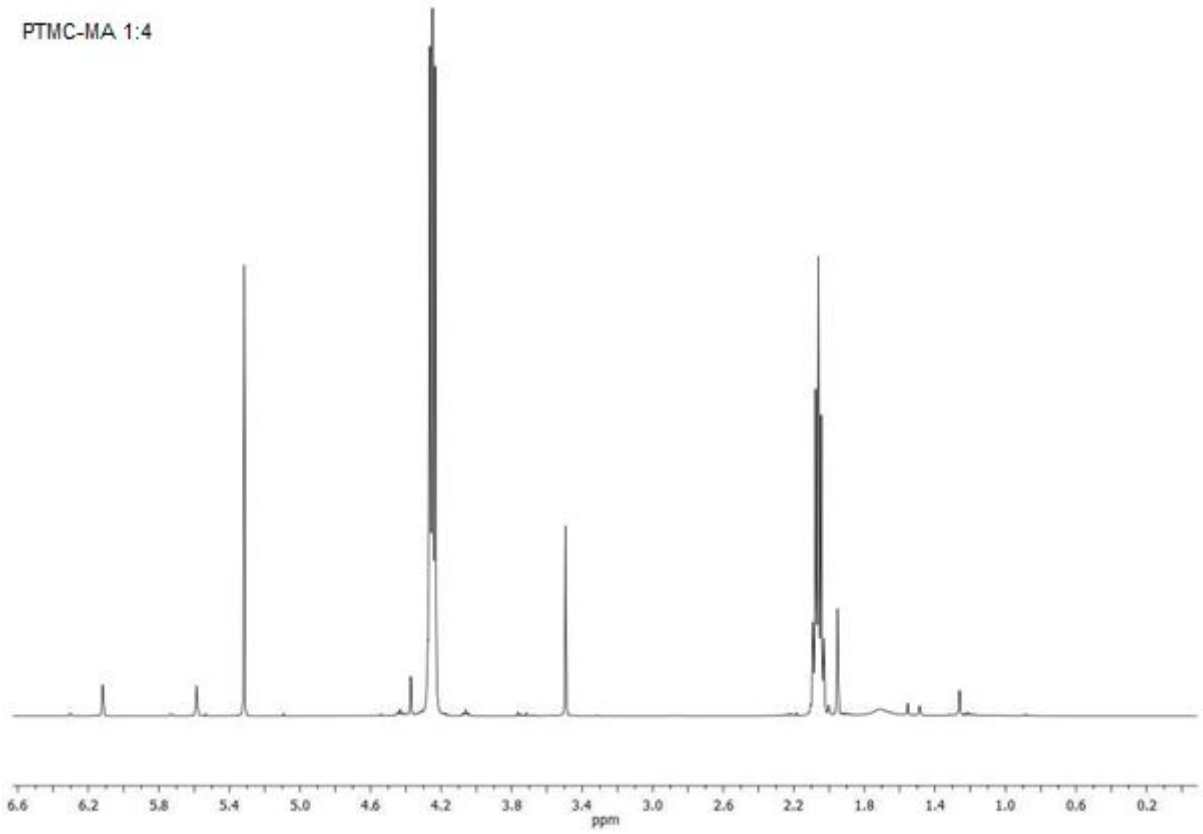

Figure A.18 - A ^{1}H NMR spectrum of PTCM-MA 1:4

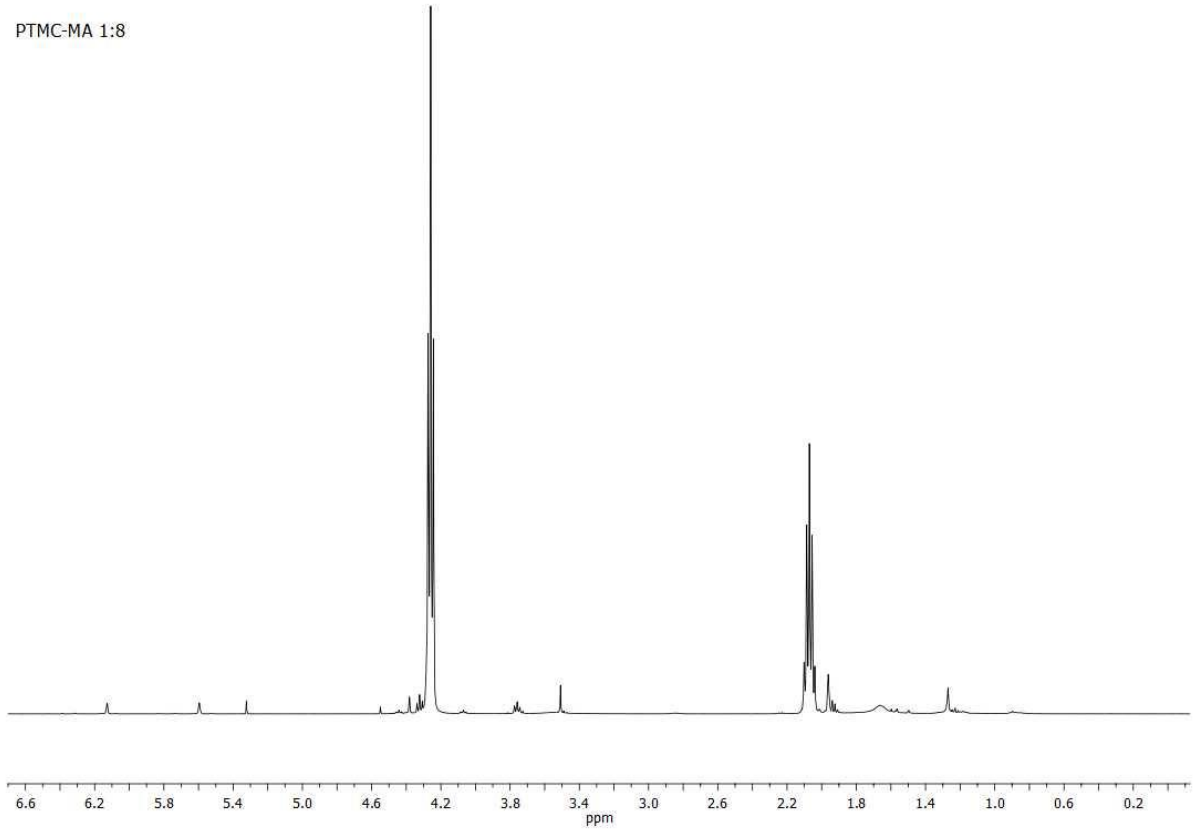

Figure A.19 - A ^{1}H NMR spectrum of PTCM-MA 1:8

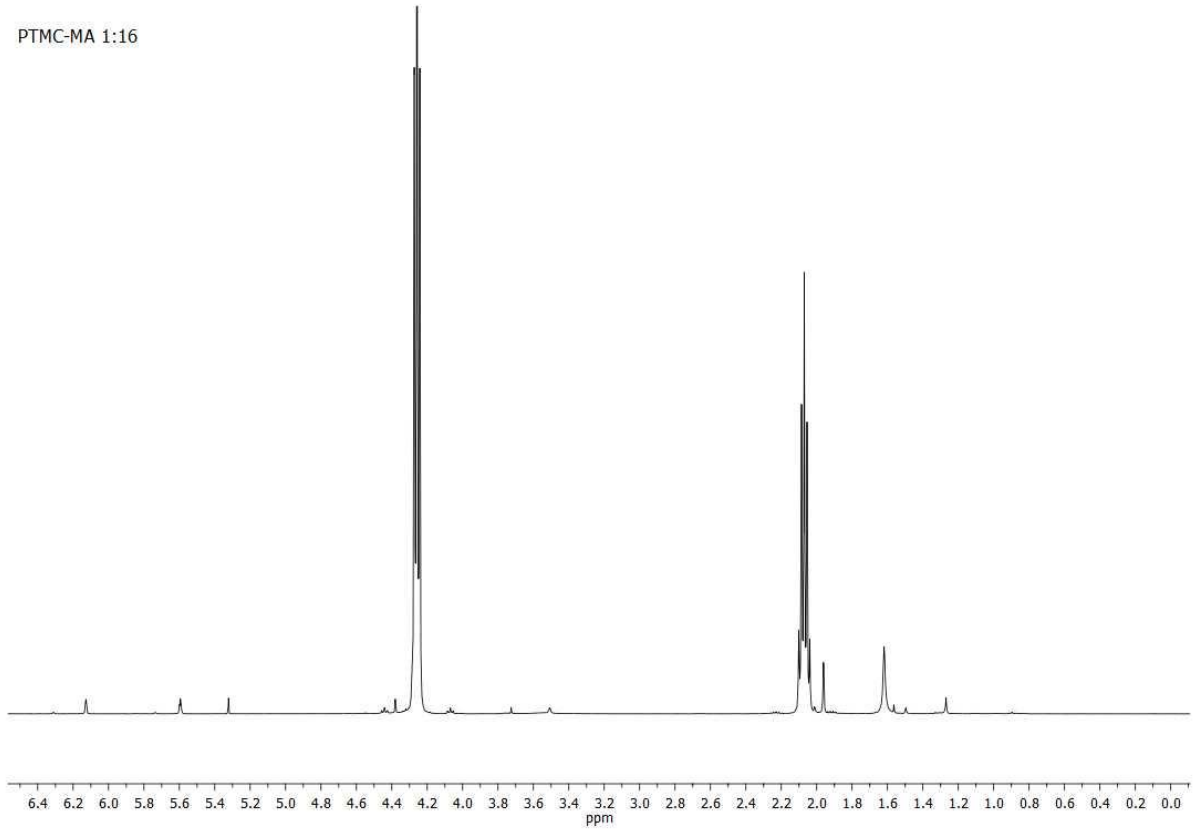

Figure A.20 - A ^{1}H NMR spectrum of PTCM-MA 1:16

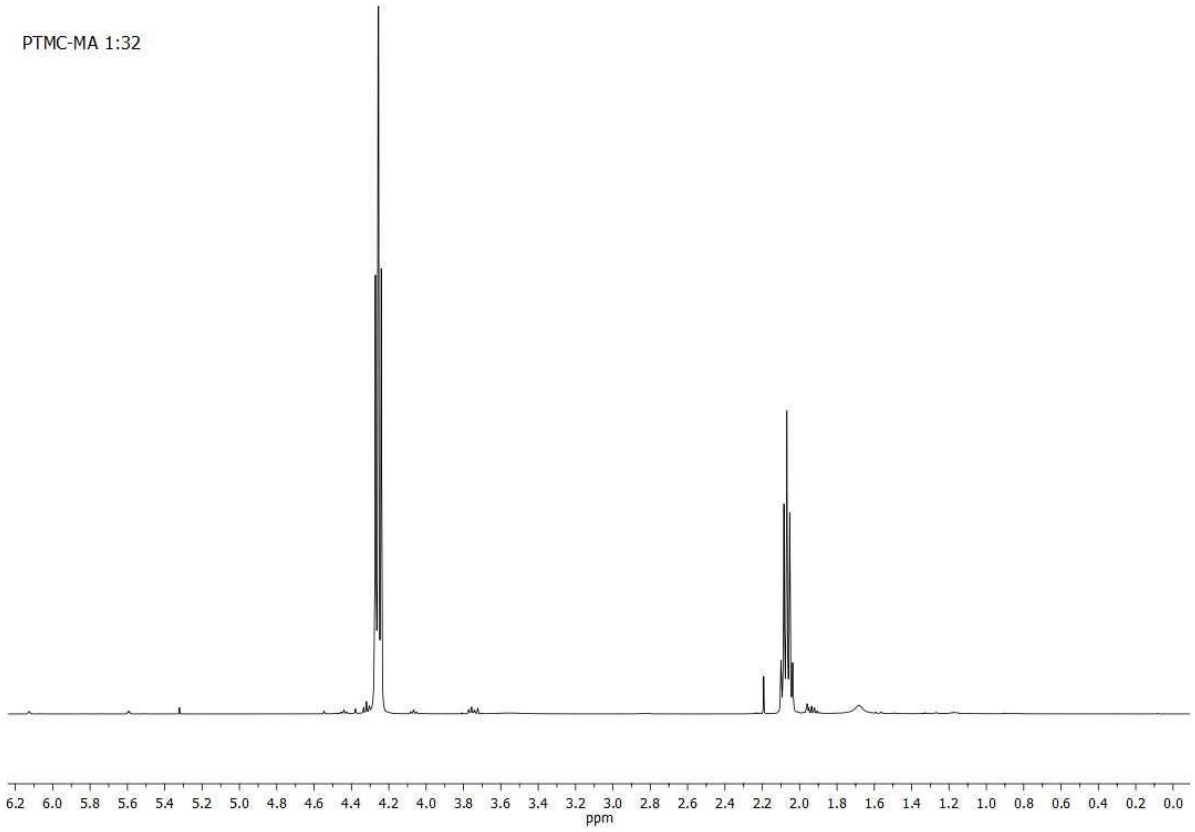

Figure A.21 - A ^{1}H NMR spectrum of PTCM-MA 1:32

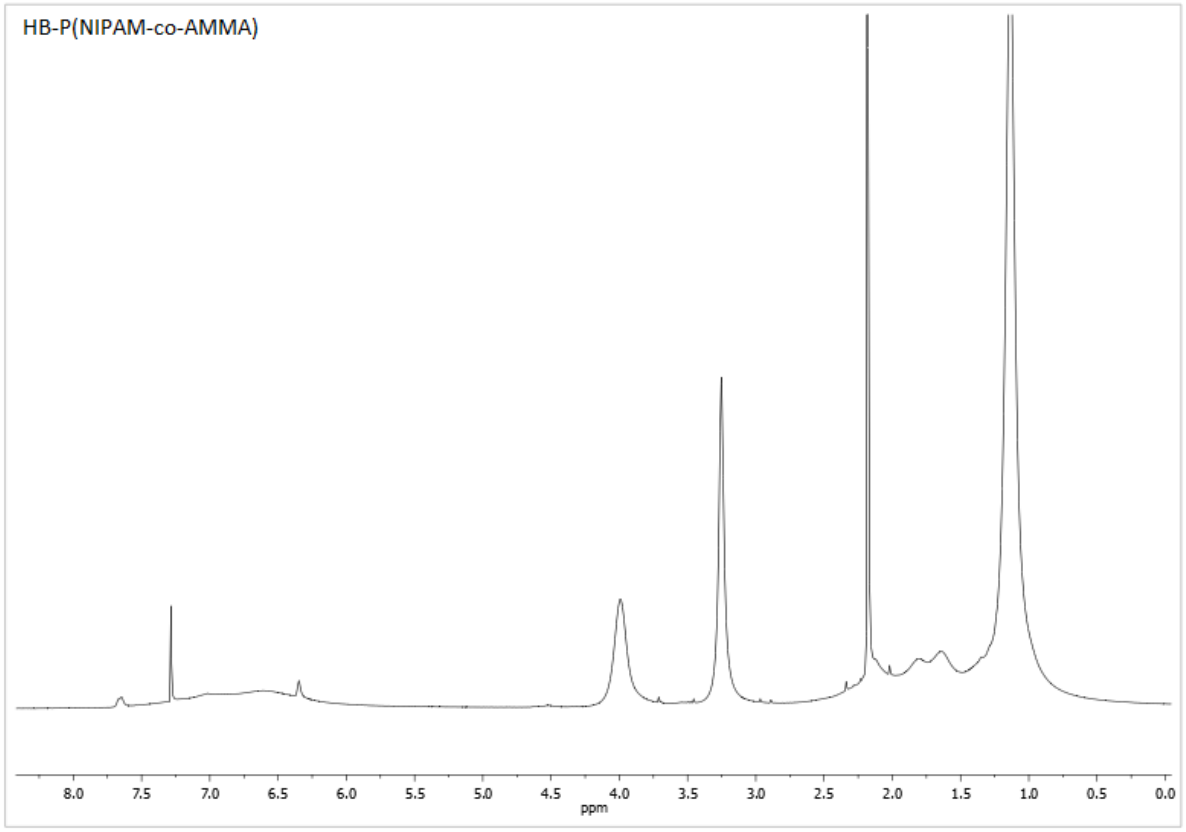

Figure A.22 – A ^{1}H NMR spectrum of HB-P(NIPAM-co-AMMA)

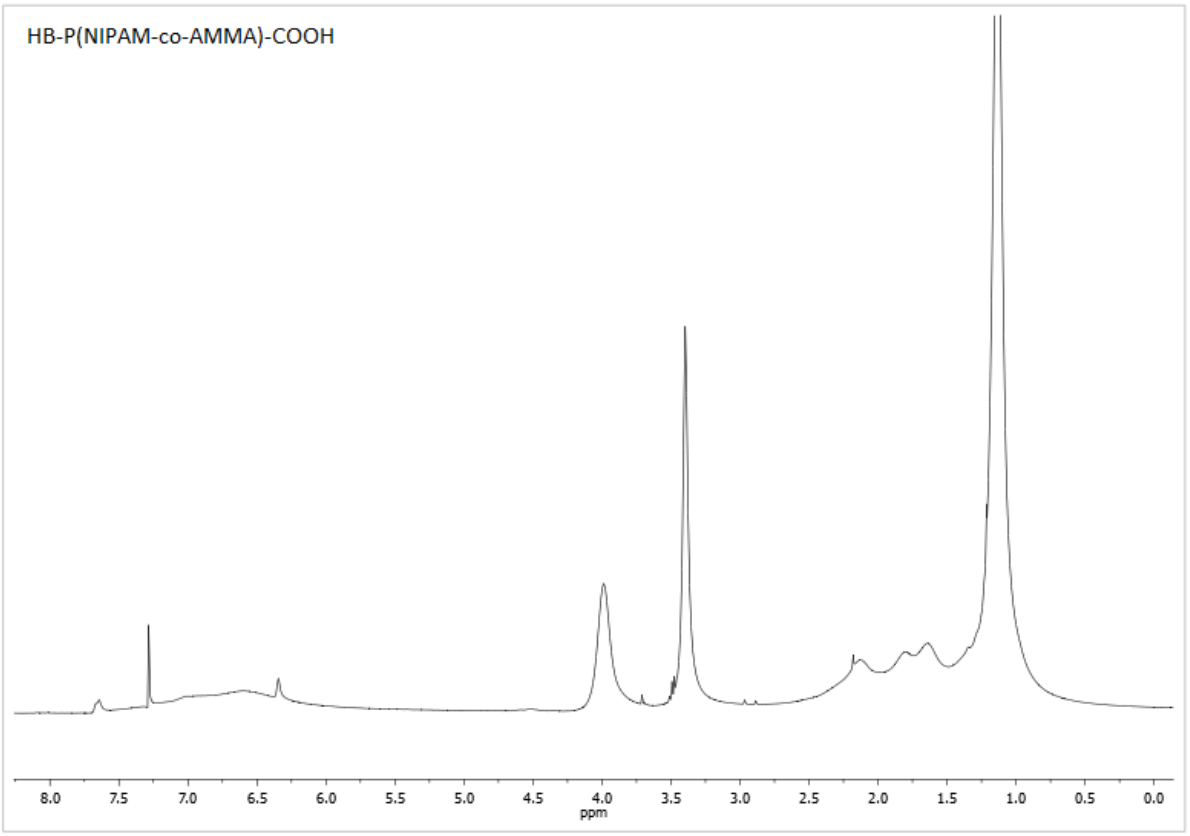

Figure A.23 - A ^{1}H NMR spectrum of HB-PNIPAM-co-AMMA)-COOH

8.2 FTIR Spectra

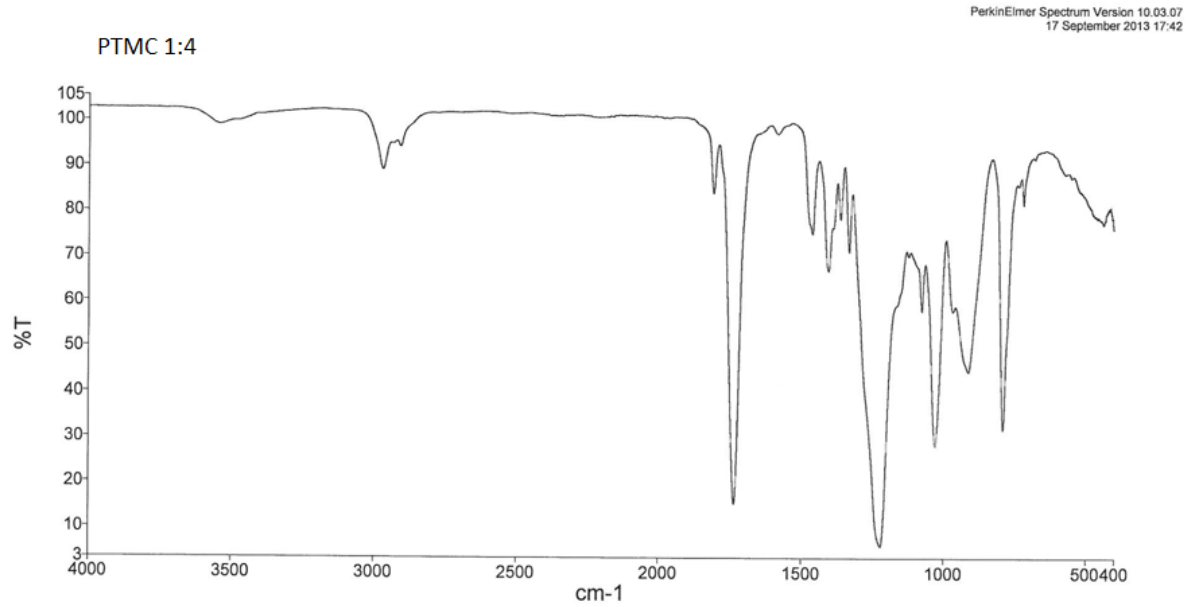

Figure A.24 - FTIR spectrum of PTMC 1:4

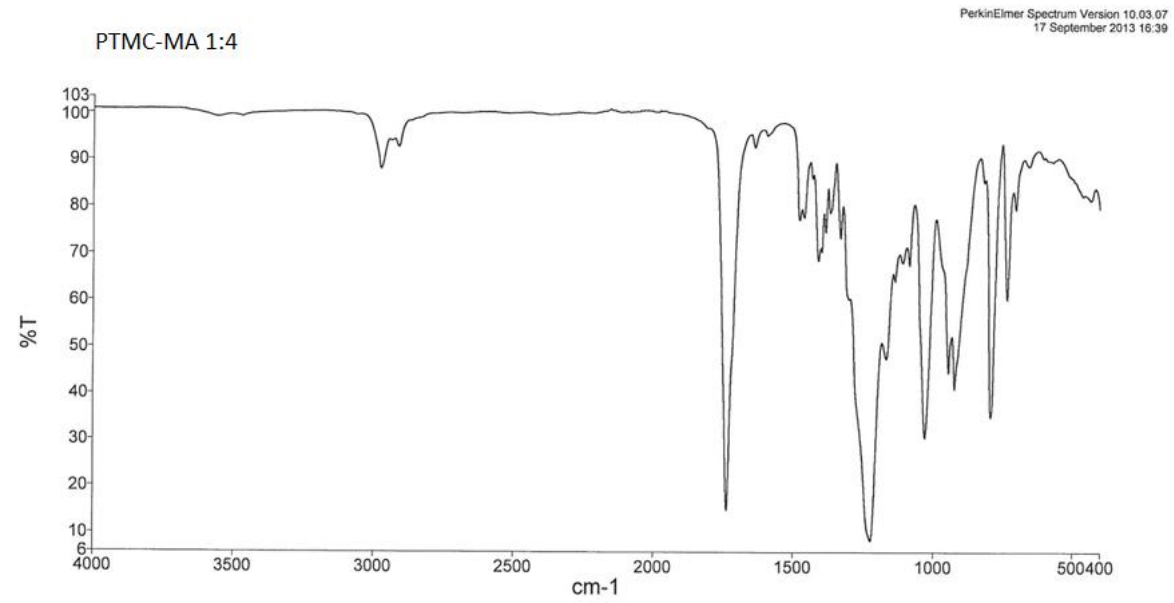

Figure A.25 - FTIR spectrum of PTMC-MA 1:4

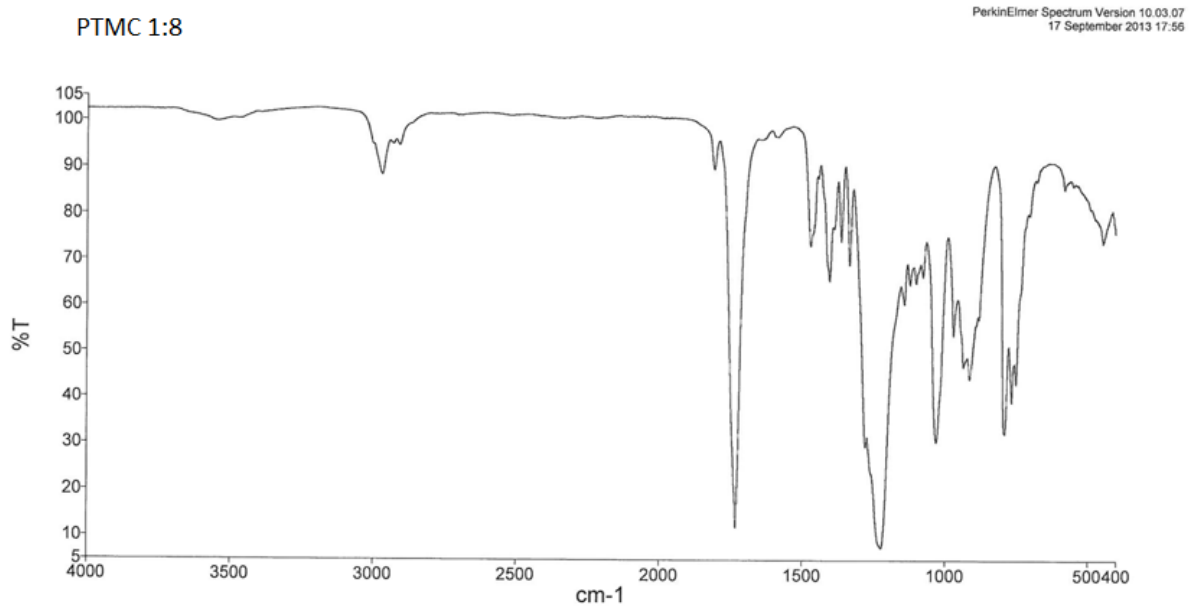

Figure A.26 - FTIR spectrum of PTMC 1:8

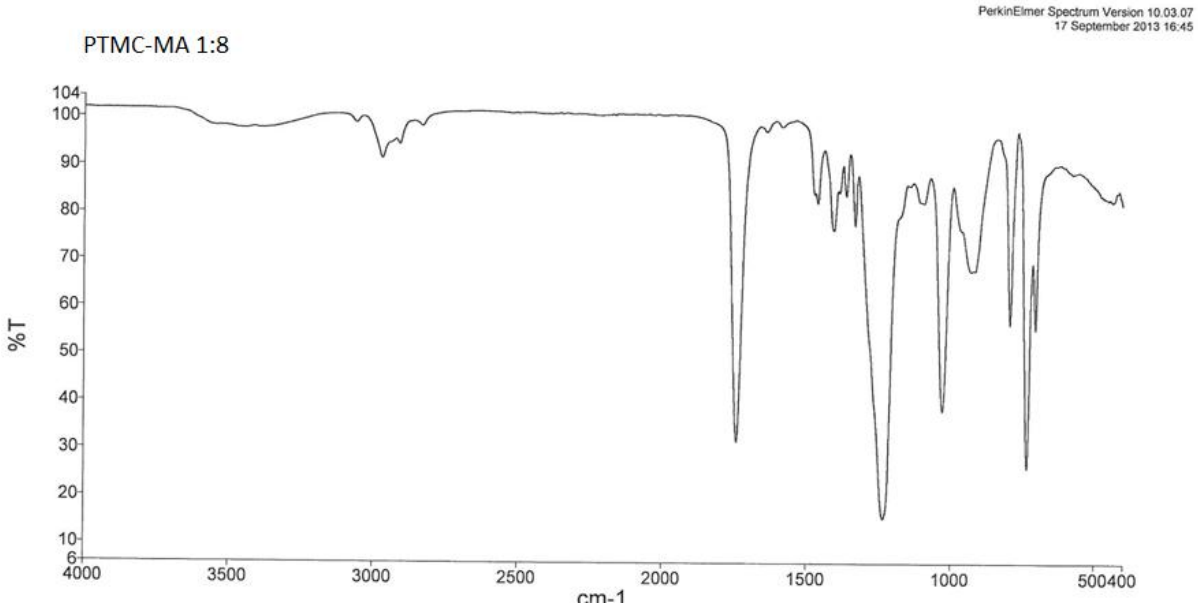

Figure A.27 - FTIR spectrum of PTMC-MA 1:8

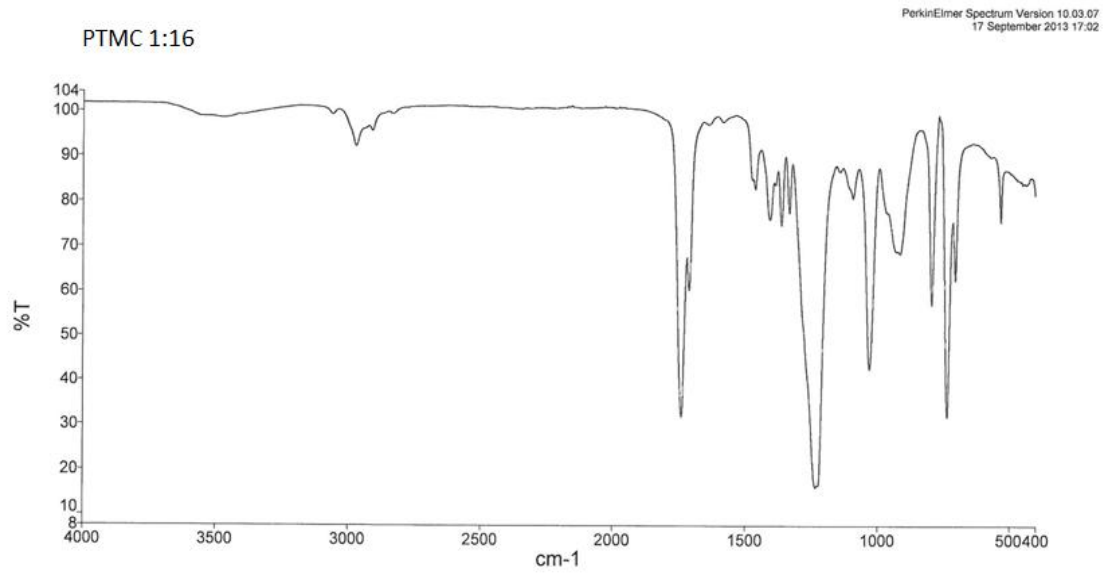

Figure A.28 - FTIR spectrum of PTMC 1:16

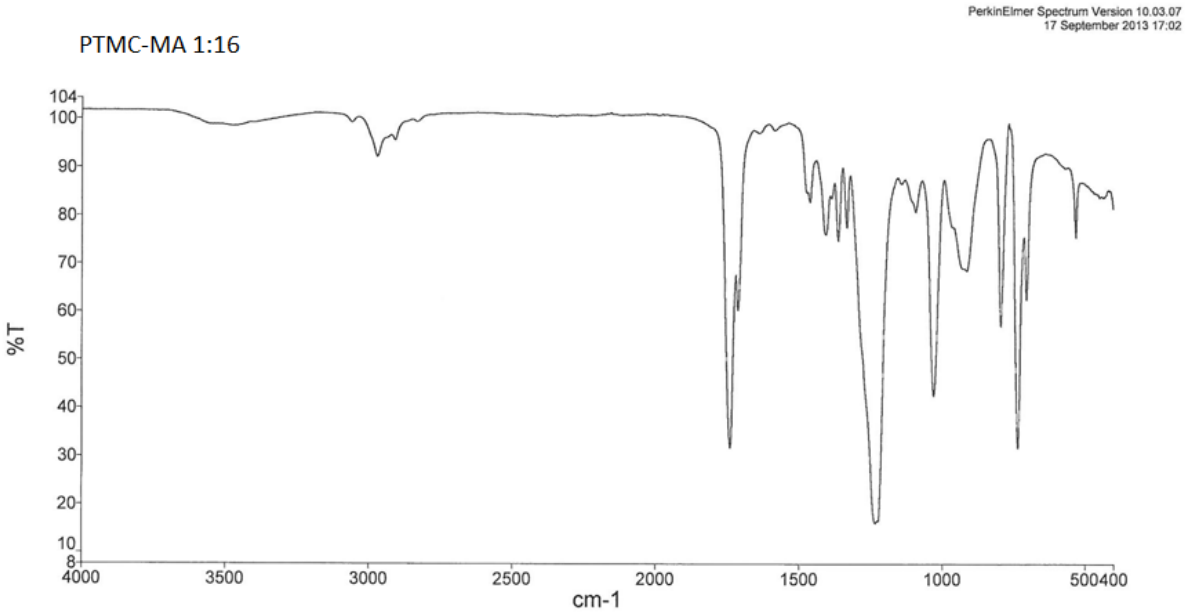

Figure A.29 - FTIR spectrum of PTMC-MA 1:16

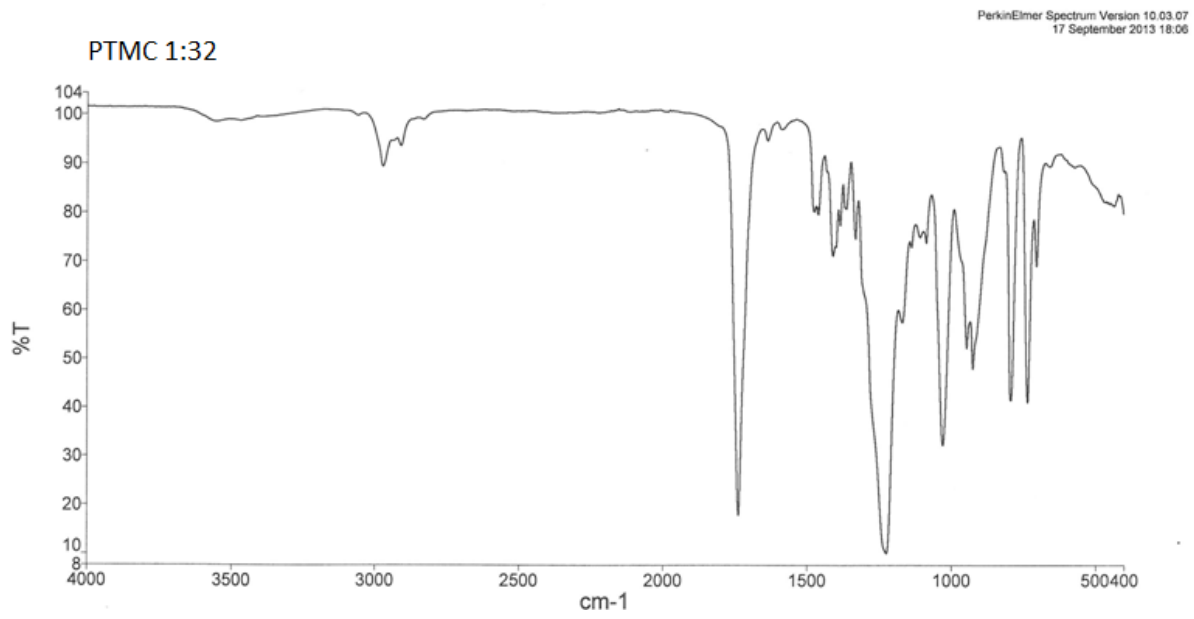

Figure A.30 - FTIR spectrum of PTMC 1:32

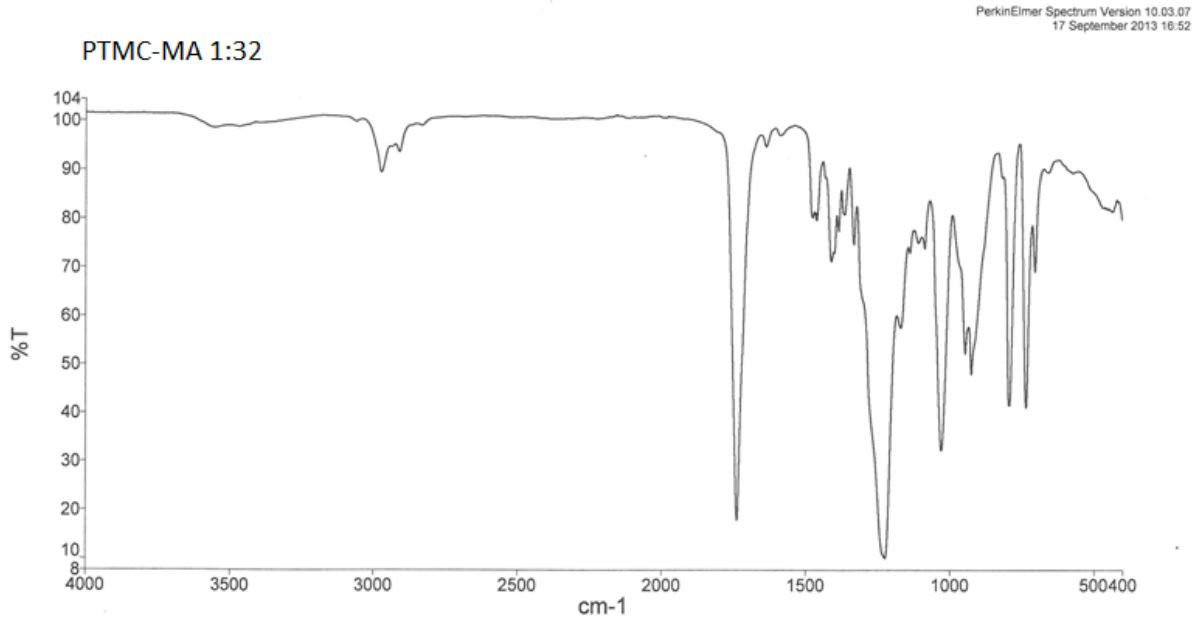

Figure A.31 - FTIR spectrum of PTMC-MA 1:32

8.3Non Gaussian Proof

Table A.1 - A table of D'Agostino & Pearsson omnibus normality test data proving non-Gausian nature of data

D'Agostino & Pearson omnibus normality test	10:1	15:1	25:1	35:1	45:1	55:1	65:1	75:1	85:1
P value	< 0.0001	< 0.0001	< 0.0001	< 0.0001	< 0.0001	< 0.0001	< 0.0001	< 0.0001	< 0.0001
Passed normality test (alpha=0.05)?	No	No	No	No	No	No	No	No	No
P value summary	****	****	****	****	****	****	****	****	****

Table A.2 - A table of Shapiro-Wilk normality test data proving non-Gausian nature of data

Shapiro-Wilk normality test	10:1	15:1	25:1	35:1	45:1	55:1	65:1	75:1	85:1
W	0.9072	0.9039	0.8939	0.8812	0.8823	0.8696	0.8714	0.8631	0.8744
P value	< 0.0001	< 0.0001	< 0.0001	< 0.0001	< 0.0001	< 0.0001	< 0.0001	< 0.0001	< 0.0001
Passed normality test (alpha=0.05)?	No	No	No	No	No	No	No	No	No
P value summary	****	****	****	****	****	****	****	****	****

Table A.3 – A table of KS normality test data proving non-Gausian nature of data

KS normality test	10:1	15:1	25:1	35:1	45:1	55:1	65:1	75:1	85:1
KS distance	0.09162	0.11	0.1227	0.1365	0.1457	0.1546	0.1484	0.1618	0.1475
P value	< 0.0001	< 0.0001	< 0.0001	< 0.0001	< 0.0001	< 0.0001	< 0.0001	< 0.0001	< 0.0001
Passed normality test (alpha=0.05)?	No	No	No	No	No	No	No	No	No
P value summary	****	****	****	****	****	****	****	****	****

8.4 HB-PNIPAM LCST

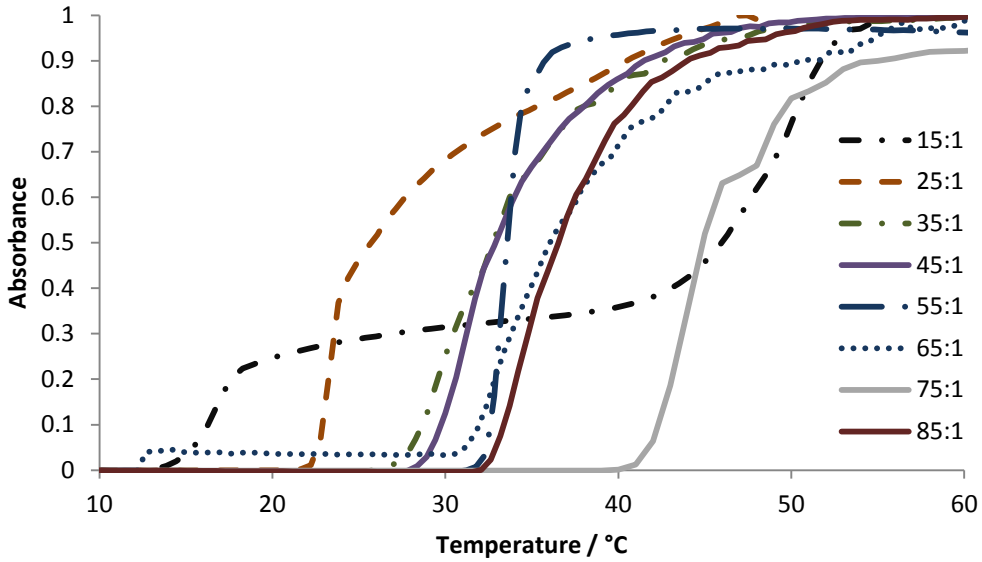

Figure A.32 - LCST of HB-PNIPAM polymers by cloud point

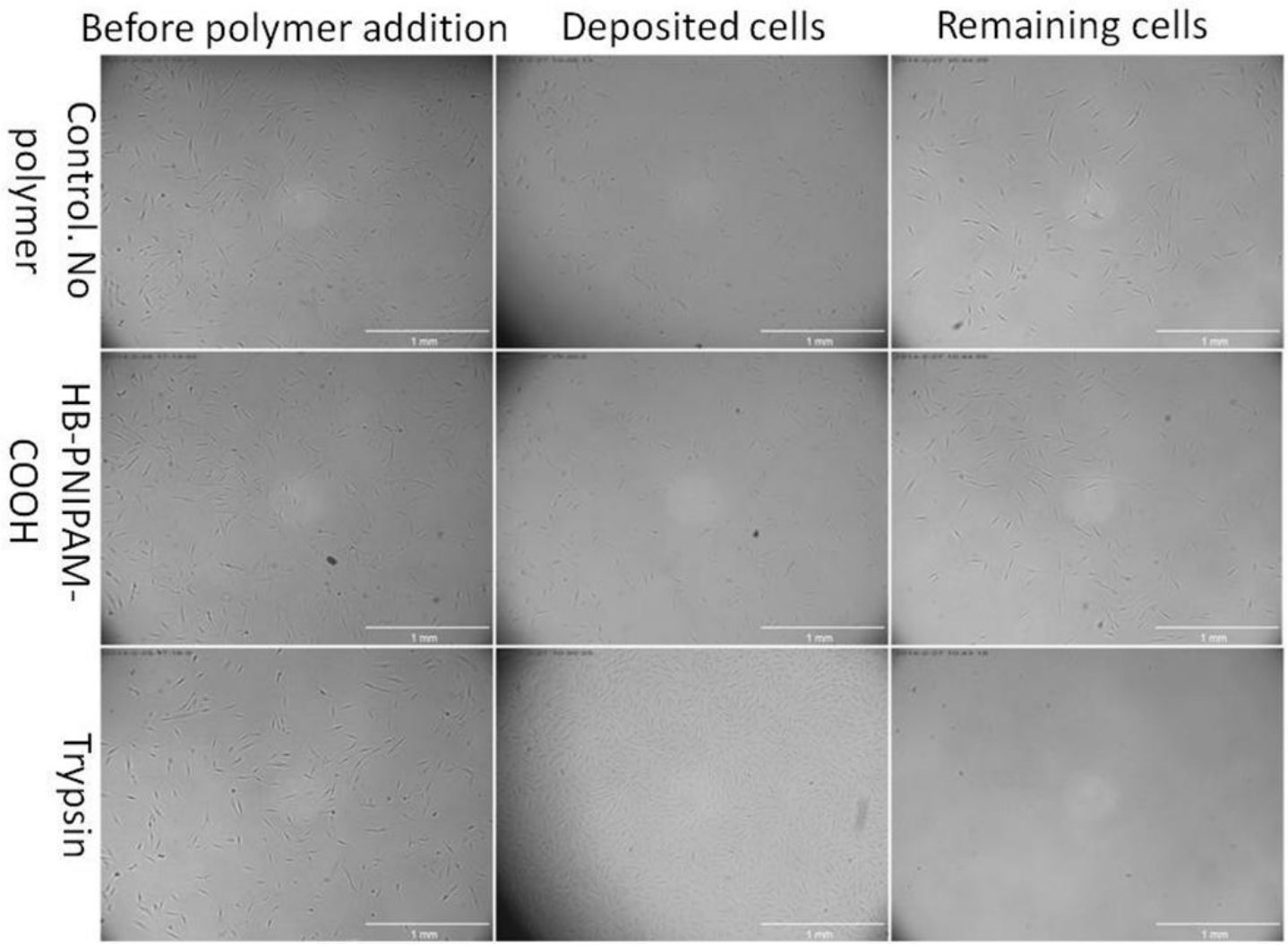

Figure A.33 - Phase contrast images of HDFs in culture before polymer addition and the deposited and remaining cells after the polymer has been used to lift and transfer the cells.

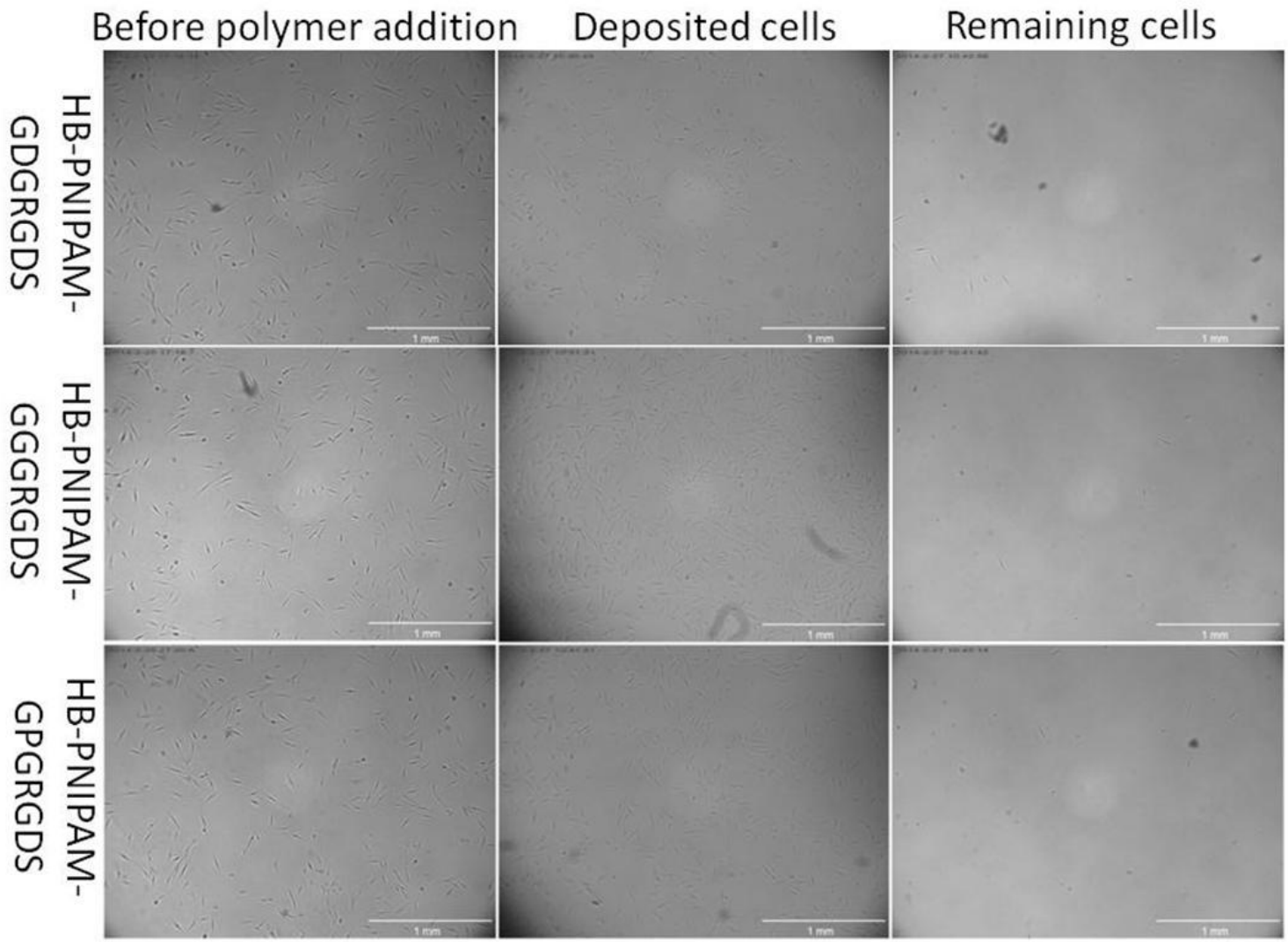

Figure A.34 - Phase contrast images of HDFs in culture before polymer addition and the deposited and remaining cells after the polymer has been used to lift and transfer the cells.

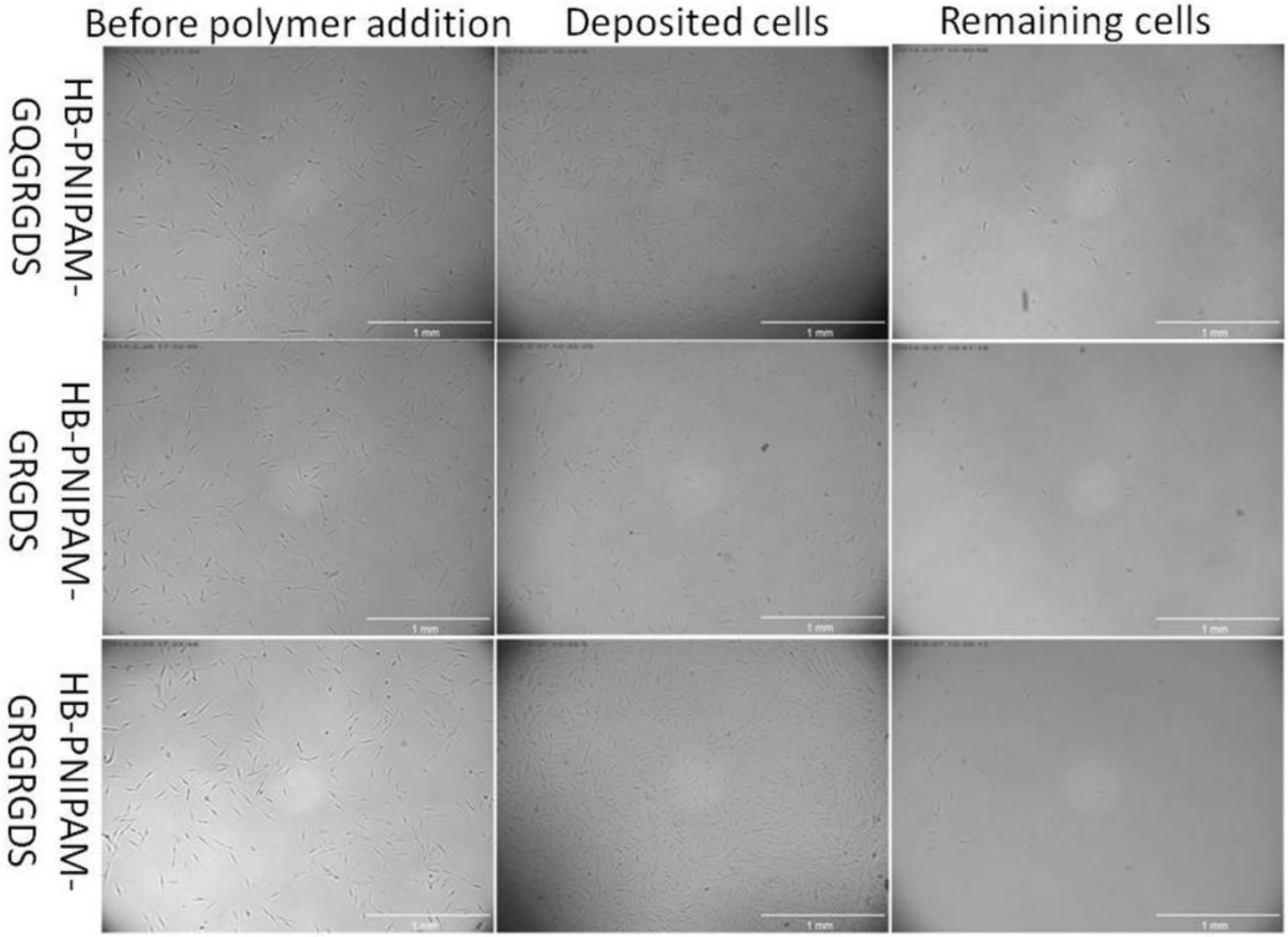

Figure A>35 - Phase contrast images of HDFs in culture before polymer addition and the deposited and remaining cells after the polymer has been used to lift and transfer the cells.

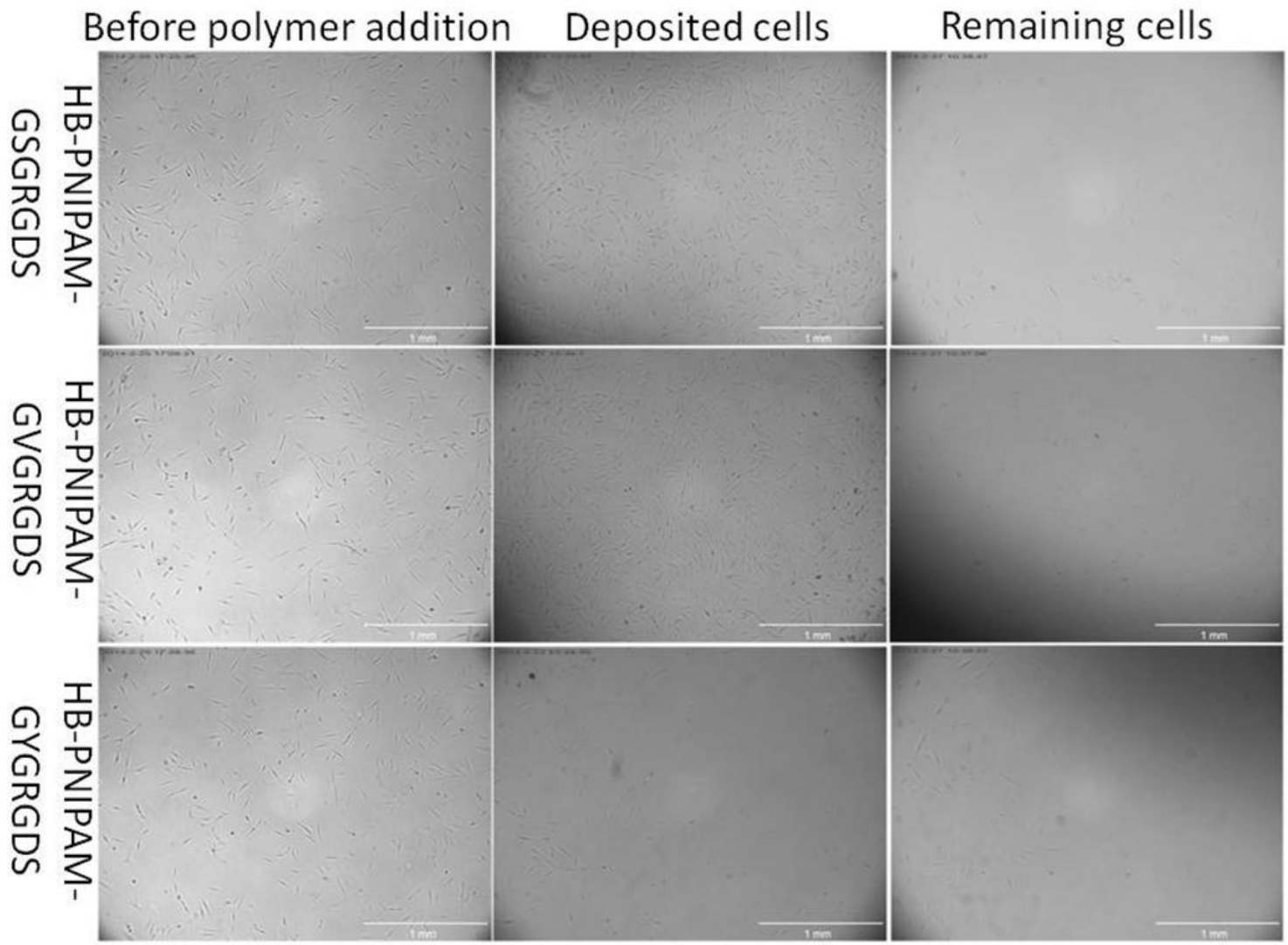

Figure A.36 - Phase contrast images of HDFs in culture before polymer addition and the deposited and remaining cells after the polymer has been used to lift and transfer the cells.

8.5 Determination of LCST by FTIR

The following data show the change in the wavenumber of the amide I carbonyl between 25 and 50°C, and the return to the original wavenumber upon cooling to 25°C. The return to the original wavenumber is important, as a loss of water from the sample can give a similar looking result. However, a dehydration of this kind will be non-reversible, so reducing the sample temperature to 25°C will not cause the reversible shift in peak position.

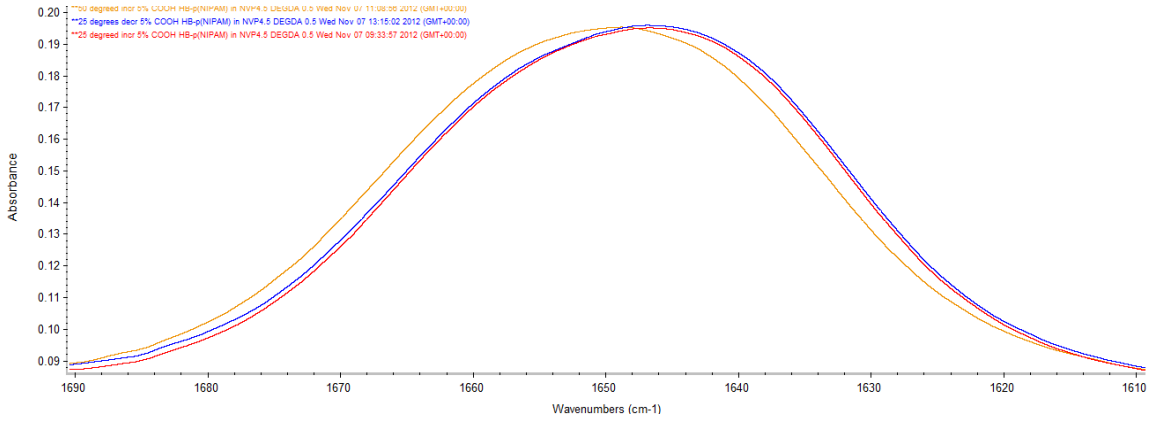

Figure A.37 - Amide I carbonyl shift of 5%HB-PNIPAM-GRGDS X-PVP BS-IPN. Red - initial 25°C, orange - 50°C and blue - final 25

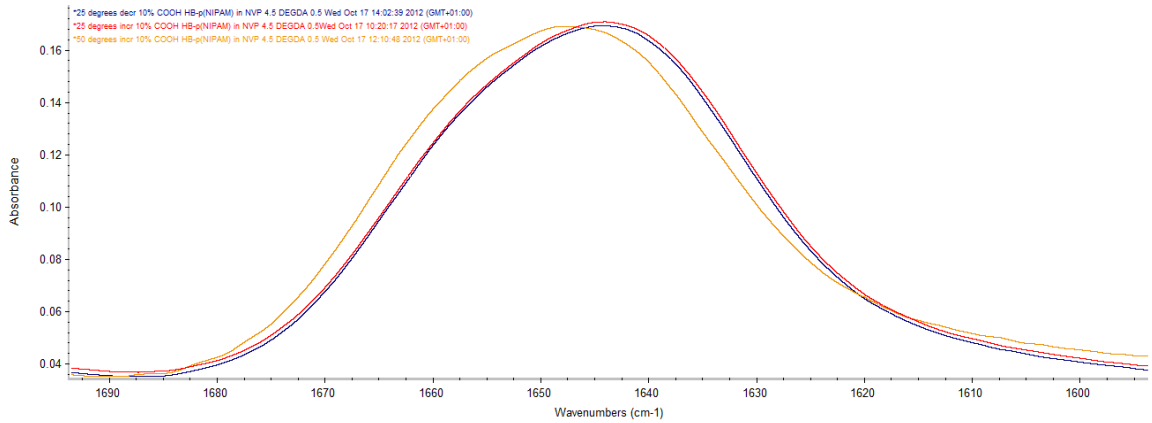

Figure A.38 - Amide I carbonyl shift of 10%HB-PNIPAM-GRGDS X-PVP BS-IPN. Red - initial 25°C, orange - 50°C and blue - final 25.°C

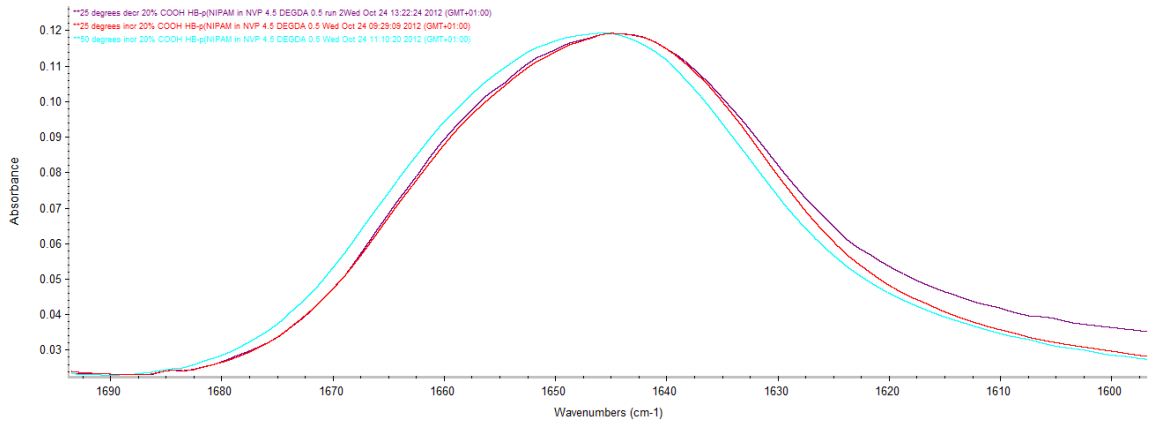

Figure A.39 - Amide I carbonyl shift of 20%HB-PNIPAM-GRGDS X-PVP BS-IPN. Red - initial 25°C, orange - 50°C and blue - final 25°C.

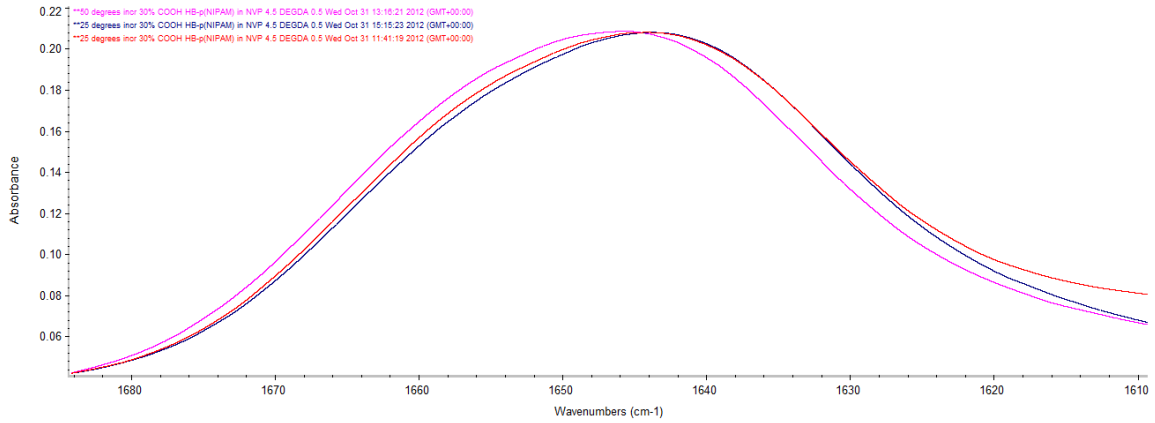

Figure A.40 - Amide I carbonyl shift of 30%HB-PNIPAM-GRGDS X-PVP BS-IPN. Red – initial 25°C, fuchsia 50°C and blue final

8.5.1 Concentrations of HB-PNIPAM by FTIR

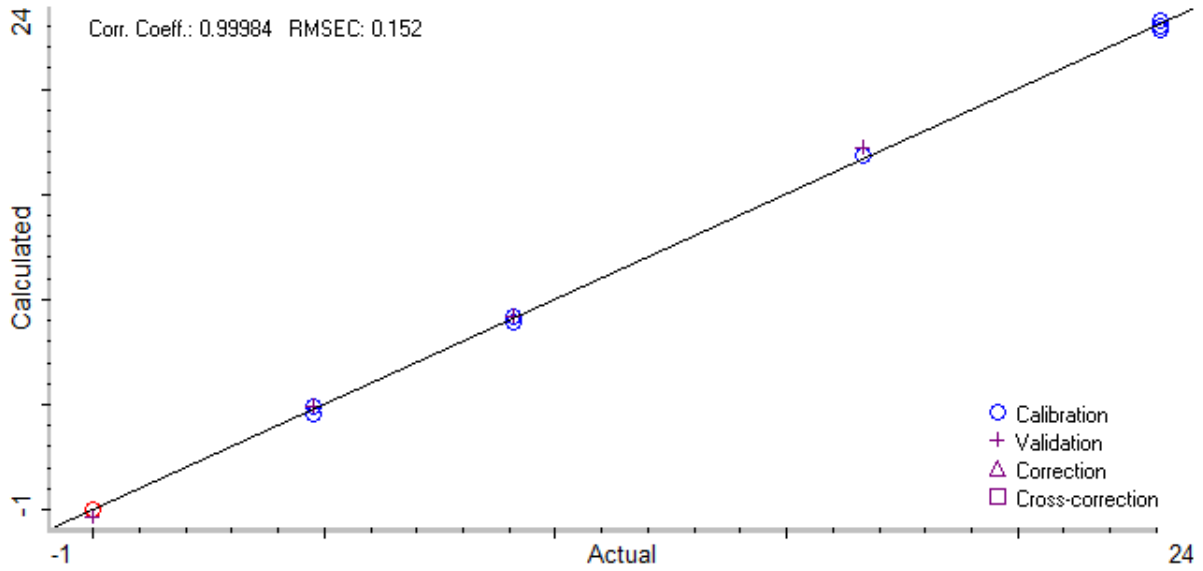

Figure A.41 - Actual percentage of HB-PNIPAM vs Calculated percentage of HB-PNIPAM for crosslinked PVP BS-IPN with HB-PNIPAM at 40% crosslinker.

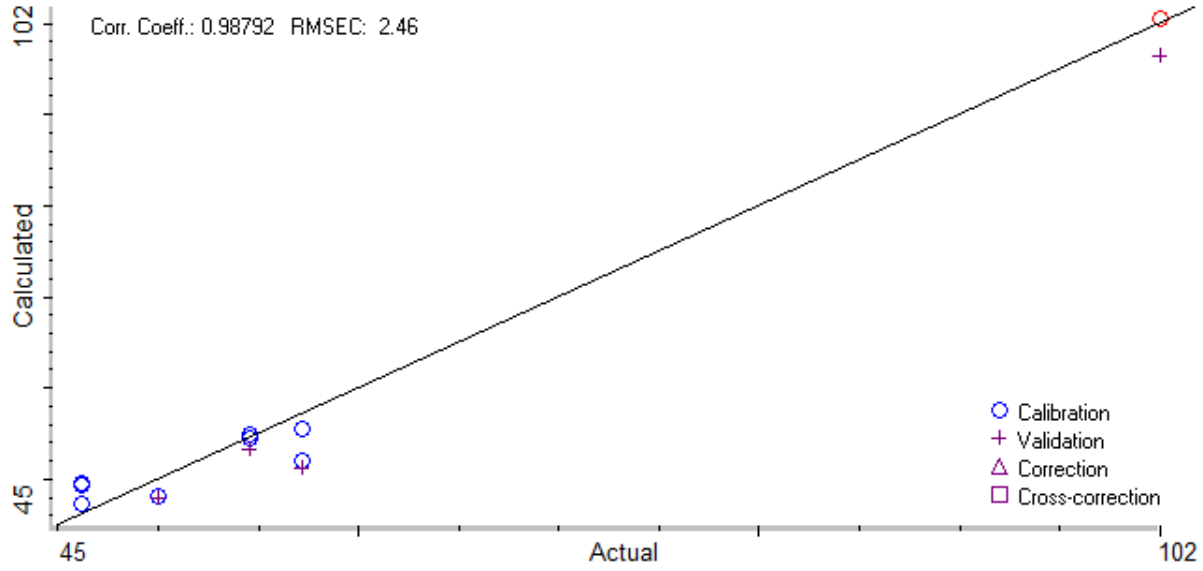

Figure A.42 - Actual percentage of PVP vs Calculated percentage of PVP for crosslinked PVP BS-IPN with HB-PNIPAM at 40% crosslinker.

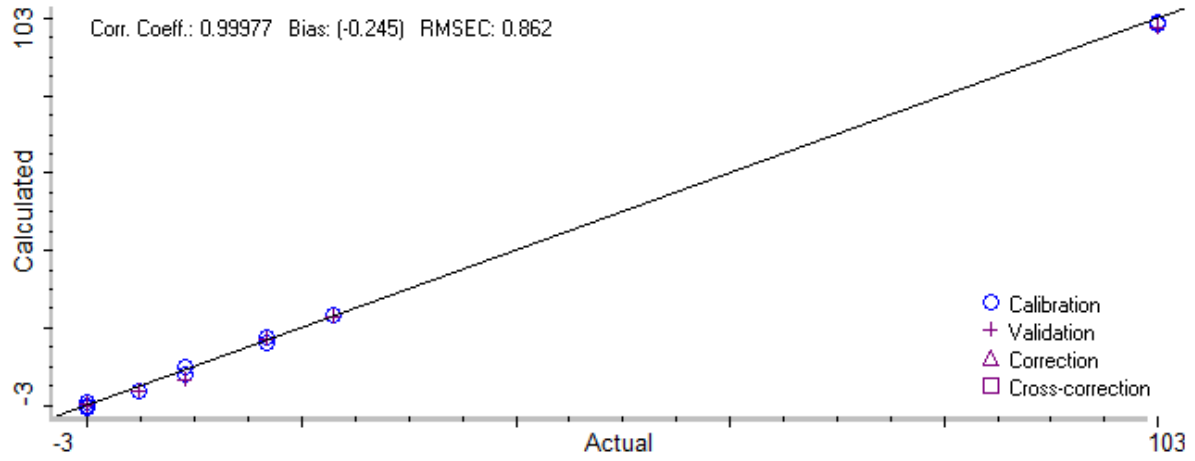

Figure A.43 - Actual percentage of HB-PNIPAM vs Calculated percentage of HB-PNIPAM for crosslinked PVP BS-IPN with HB-PNIPAM at 10% crosslinker.

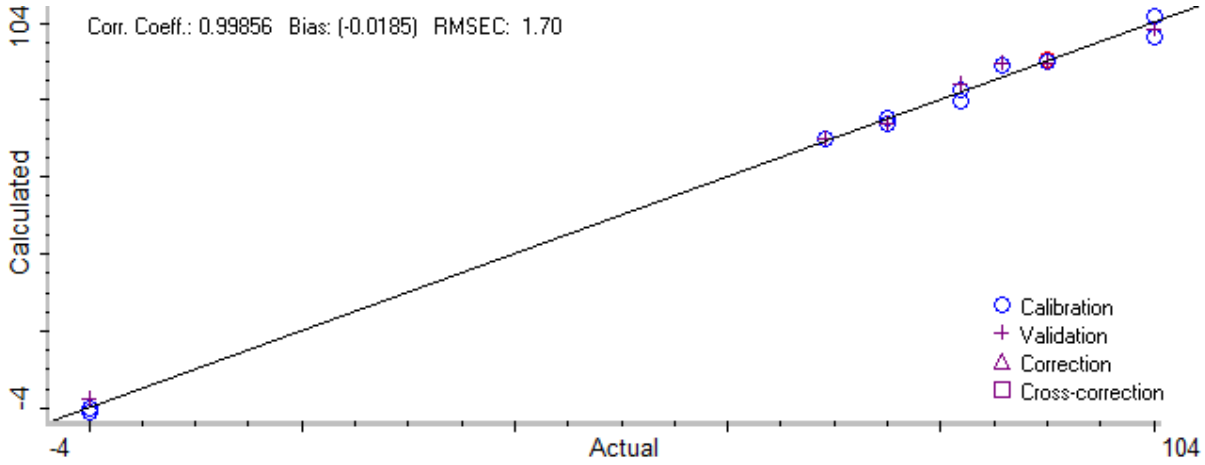

Figure A.44 - Actual percentage of PVP vs Calculated percentage of PVP for crosslinked PVP BS-IPN with HB-PNIPAM at 10% crosslinker.

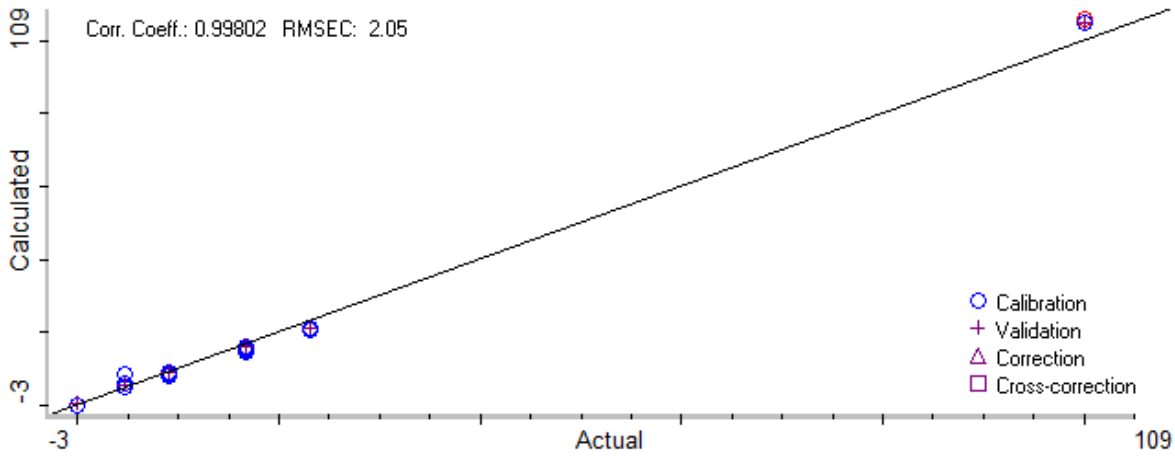

Figure A.45 - Actual percentage of HB-PNIPAM vs Calculated percentage of HB-PNIPAM for crosslinked PEG BS-IPN with HB-PNIPAM.

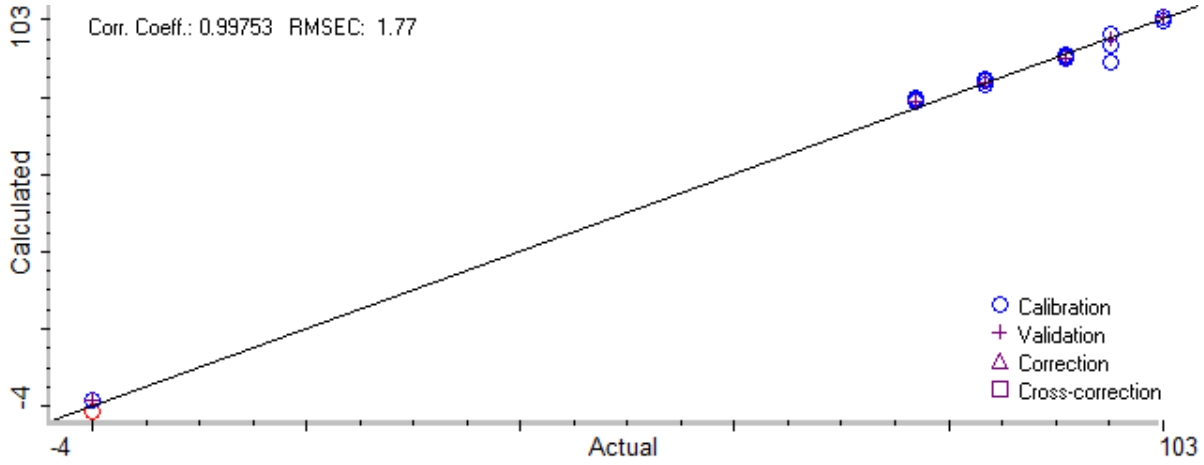

Figure A5.46 - Actual percentage of PEG vs Calculated percentage of PEG for crosslinked PEG BS-IPN with HB-PNIPAM.

8.6 Load vs Deflection Graphs for PTMC polymers

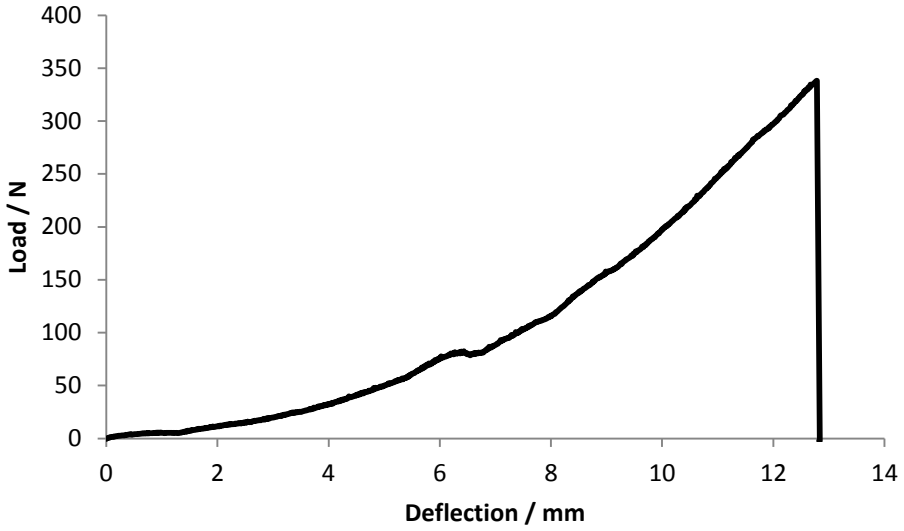

Figure A.47 - Load deflection curve for PTMC-MA 1:4 membrane sample 1, used to calculate stiffness

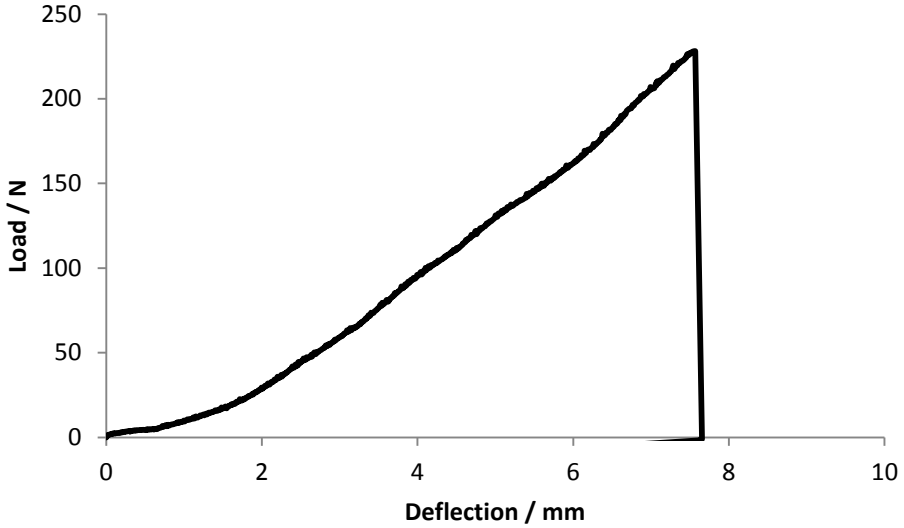

Figure A.48 - Load deflection curve for PTMC-MA 1:4 membrane sample 2, used to calculate stiffness

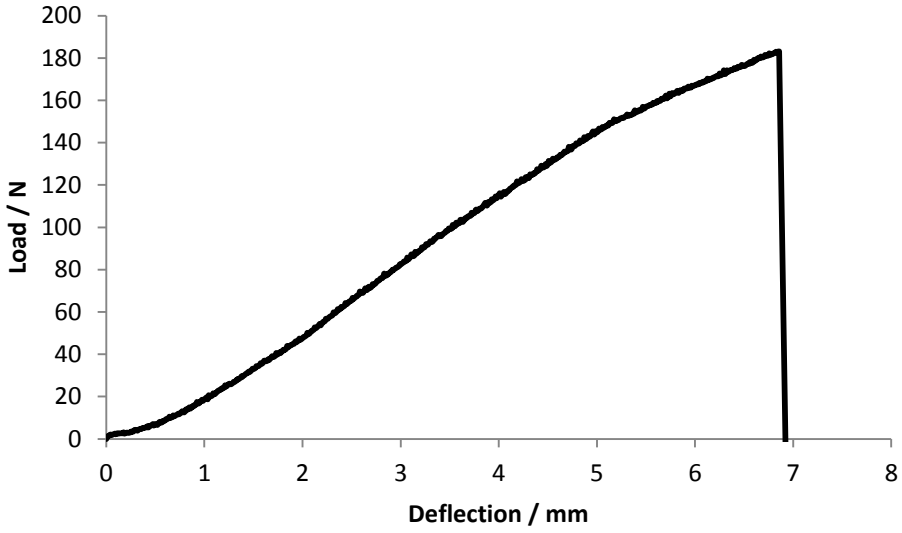

Figure A.49 - Load deflection curve for PTMC-MA 1:4 membrane sample 3, used to calculate stiffness

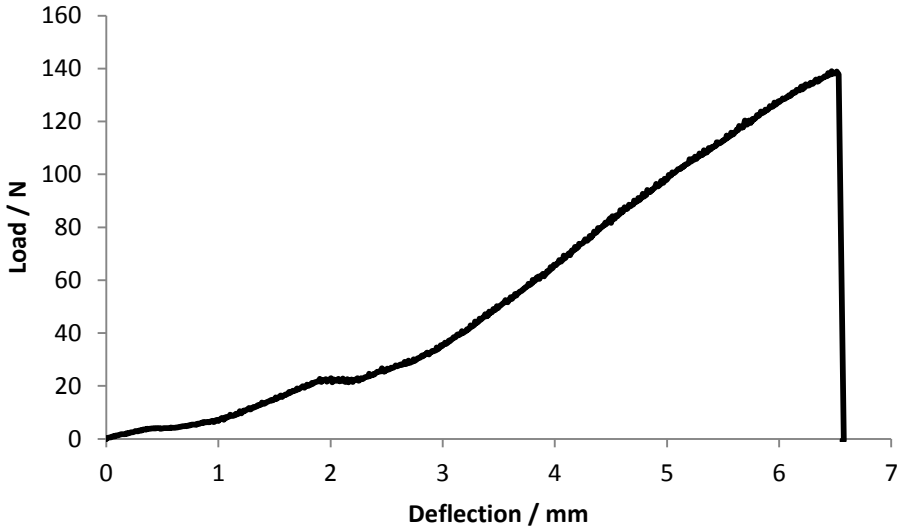

Figure A.50 - Load deflection curve for PTMC-MA 1:8 membrane sample 1, used to calculate stiffness

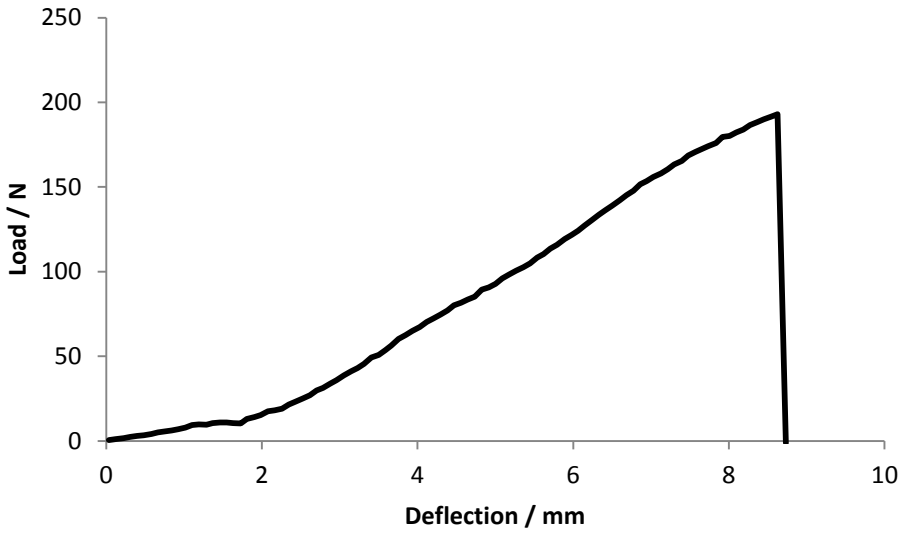

Figure A.51 - Load deflection curve for PTMC-MA 1:8 membrane sample 2, used to calculate stiffness

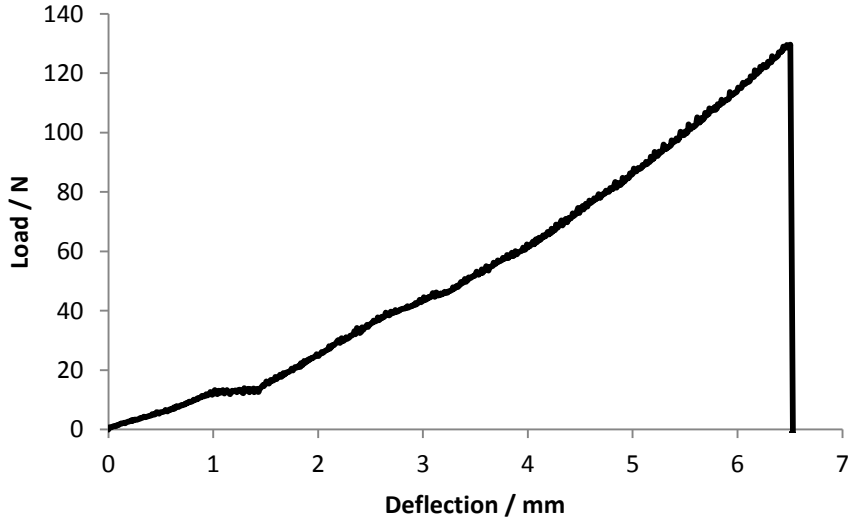

Figure A.52 - Load deflection curve for PTMC-MA 1:8 membrane sample 3, used to calculate stiffness

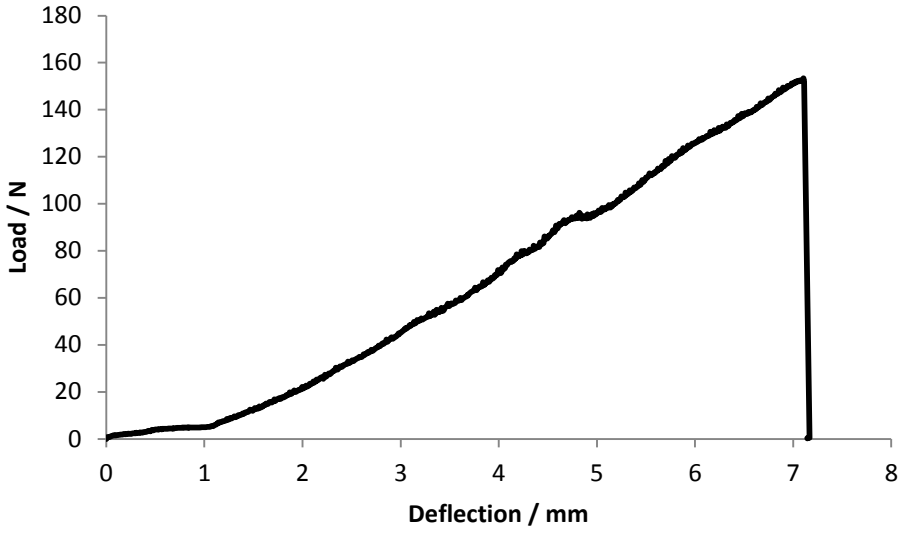

Figure A.53 - Load deflection curve for PTMC-MA 1:8 membrane sample 4, used to calculate stiffness

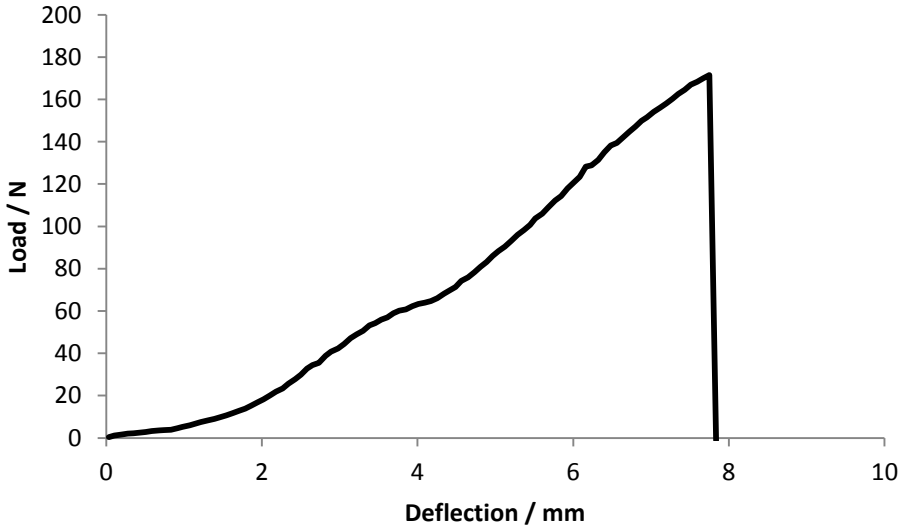

Figure A.54 - Load deflection curve for PTMC-MA 1:8 membrane sample 5, used to calculate stiffness

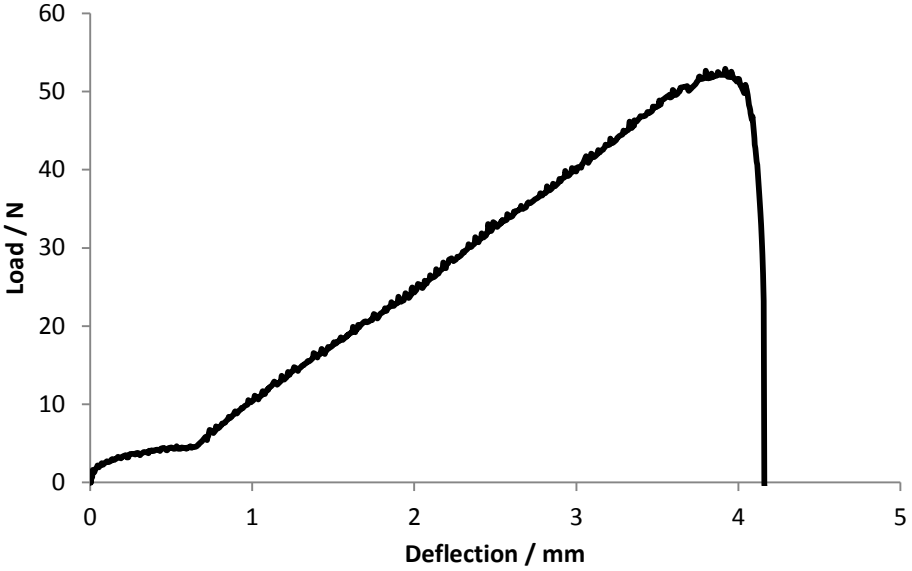

Figure A.55 - Load deflection curve for PTMC-MA 1:16 membrane sample 1, used to calculate stiffness

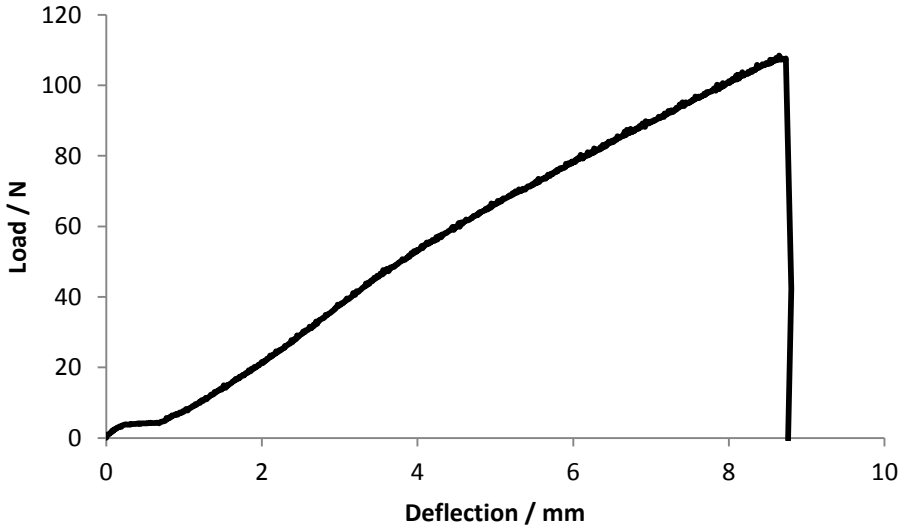

Figure A.56 - Load deflection curve for PTMC-MA 1:16 membrane sample 2, used to calculate stiffness

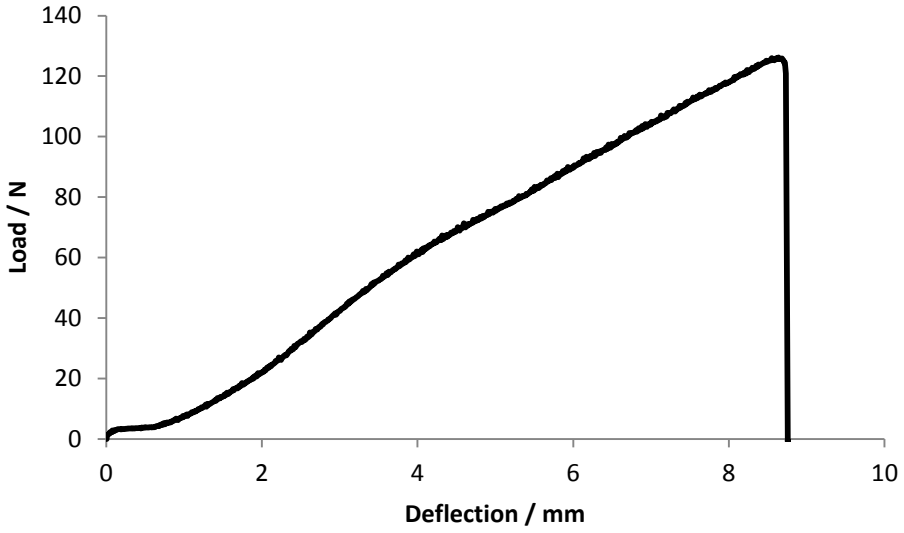

Figure A.57 - deflection curve for PTMC-MA 1:16 membrane sample 3, used to calculate stiffness

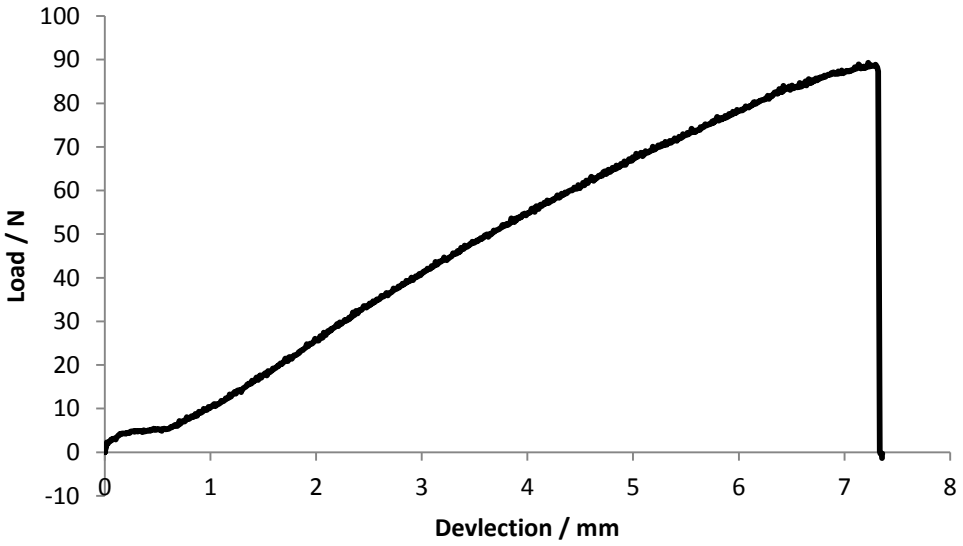

Figure A.58 - Deflection curve for PTMC-MA 1:16 membrane sample 4, used to calculate stiffness

9. References

1. Langer, R. and J. Vacanti, *Tissue engineering.* Science, 1993. **260**(5110): p. 920-926.
2. Griffith, L.G. and G. Naughton, *Tissue Engineering--Current Challenges and Expanding Opportunities.* Science, 2002. **295**(5557): p. 1009-1014.
3. Lee, C.H., A. Singla, and Y. Lee, *Biomedical applications of collagen.* International journal of pharmaceutics, 2001. **221**(1): p. 1-22.
4. Bailey, A. and R. Paul, *Collagen: a not so simple protein.* Journal of the Society of Leather Technologists and Chemists, 1998. **82**(3): p. 104-110.
5. Duranti, F., et al., *Injectable Hyaluronic Acid Gel for Soft Tissue Augmentation.* Dermatologic Surgery, 1998. **24**(12): p. 1317-1325.
6. Augst, A.D., H.J. Kong, and D.J. Mooney, *Alginate Hydrogels as Biomaterials.* Macromolecular Bioscience, 2006. **6**(8): p. 623-633.
7. Ravi Kumar, M.N.V., *A review of chitin and chitosan applications.* Reactive and Functional Polymers, 2000. **46**(1): p. 1-27.
8. Sionkowska, A., *Current research on the blends of natural and synthetic polymers as new biomaterials: Review.* Progress in Polymer Science, 2011. **36**(9): p. 1254-1276.
9. Seal, B.L., T.C. Otero, and A. Panitch, *Polymeric biomaterials for tissue and organ regeneration.* Materials Science and Engineering: R: Reports, 2001. **34**(4–5): p. 147-230.
10. Lewis, G., *Properties of acrylic bone cement: State of the art review.* Journal of Biomedical Materials Research, 1997. **38**(2): p. 155-182.
11. Park, S., et al., *Evaluation of Poly (lactic-co-glycolic Acid) Plate and Screw System for Bone Fixation.* Journal of Craniofacial Surgery, 2013. **24**(3): p. 1021-1025.
12. Veronese, F.M. and G. Pasut, *PEGylation, successful approach to drug delivery.* Drug Discovery Today, 2005. **10**(21): p. 1451-1458.
13. Inoue, T., et al., *An AB block copolymer of oligo (methyl methacrylate) and poly (acrylic acid) for micellar delivery of hydrophobic drugs.* Journal of Controlled Release, 1998. **51**(2): p. 221-229.
14. Schmaljohann, D., *Thermo- and pH-responsive polymers in drug delivery.* Advanced drug delivery reviews, 2006. **58**(15): p. 1655-1670.
15. Hyon, S.-H., et al., *Poly (vinyl alcohol) hydrogels as soft contact lens material.* Journal of Biomaterials Science, Polymer Edition, 1994. **5**(5): p. 397-406.
16. Opdahl, A., et al., *Surface mechanical properties of pHEMA contact lenses: Viscoelastic and adhesive property changes on exposure to controlled humidity.* Journal of Biomedical Materials Research Part A, 2003. **67A**(1): p. 350-356.
17. Xinming, L., et al., *Polymeric hydrogels for novel contact lens-based ophthalmic drug delivery systems: A review.* Contact Lens and Anterior Eye, 2008. **31**(2): p. 57-64.
18. Sun, J.-Y., et al., *Highly stretchable and tough hydrogels.* Nature, 2012. **489**(7414): p. 133-136.
19. Cadée, J.A., et al., *In vivo biocompatibility of dextran-based hydrogels.* Journal of Biomedical Materials Research, 2000. **50**(3): p. 397-404.
20. Karadağ, E., et al., *In vitro swelling studies and preliminary biocompatibility evaluation of acrylamide-based hydrogels.* Biomaterials, 1996. **17**(1): p. 67-70.
21. Molinaro, G., et al., *Biocompatibility of thermosensitive chitosan-based hydrogels: an in vivo experimental approach to injectable biomaterials.* Biomaterials, 2002. **23**(13): p. 2717-2722.
22. Gehrke, S.H., et al., *Factors Determining Hydrogel Permeability.* Annals of the New York Academy of Sciences, 1997. **831**(1): p. 179-184.
23. Drury, J.L. and D.J. Mooney, *Hydrogels for tissue engineering: scaffold design variables and applications.* Biomaterials, 2003. **24**(24): p. 4337-4351.

24. Hoare, T.R. and D.S. Kohane, *Hydrogels in drug delivery: Progress and challenges.* Polymer, 2008. **49**(8): p. 1993-2007.
25. Bourke, S.L., et al., *A photo-crosslinked poly (vinyl alcohol) hydrogel growth factor release vehicle for wound healing applications.* Aaps Pharmsci, 2003. **5**(4): p. 101-111.
26. Kissel, T., Y. Li, and F. Unger, *ABA-triblock copolymers from biodegradable polyester A-blocks and hydrophilic poly(ethylene oxide) B-blocks as a candidate for in situ forming hydrogel delivery systems for proteins.* Advanced drug delivery reviews, 2002. **54**(1): p. 99-134.
27. Gehrke, S.H., L.H. Uhden, and J.F. McBride, *Enhanced loading and activity retention of bioactive proteins in hydrogel delivery systems.* Journal of Controlled Release, 1998. **55**(1): p. 21-33.
28. Nguyen, K.T. and J.L. West, *Photopolymerizable hydrogels for tissue engineering applications.* Biomaterials, 2002. **23**(22): p. 4307-4314.
29. Sidwell, R.U., et al., *Localized granulomatous reaction to a semi-permanent hyaluronic acid and acrylic hydrogel cosmetic filler.* Clinical and Experimental Dermatology, 2004. **29**(6): p. 630-632.
30. Alijotas-Reig, J. and V. Garcia-Gimenez, *Delayed immune-mediated adverse effects related to hyaluronic acid and acrylic hydrogel dermal fillers: clinical findings, long-term follow-up and review of the literature.* Journal of the European Academy of Dermatology and Venereology, 2008. **22**(2): p. 150-161.
31. Christensen, L., et al., *Adverse reactions to injectable soft tissue permanent fillers.* Aesthetic plastic surgery, 2005. **29**(1): p. 34-48.
32. Park, K.M., et al., *Thermosensitive chitosan–Pluronic hydrogel as an injectable cell delivery carrier for cartilage regeneration.* Acta Biomaterialia, 2009. **5**(6): p. 1956-1965.
33. Ballios, B.G., et al., *A hydrogel-based stem cell delivery system to treat retinal degenerative diseases.* Biomaterials, 2010. **31**(9): p. 2555-2564.
34. Park, H., et al., *Injectable biodegradable hydrogel composites for rabbit marrow mesenchymal stem cell and growth factor delivery for cartilage tissue engineering.* Biomaterials, 2007. **28**(21): p. 3217-3227.
35. Peppas, N.A., et al., *Hydrogels in Biology and Medicine: From Molecular Principles to Bionanotechnology.* Advanced Materials, 2006. **18**(11): p. 1345-1360.
36. Atala, A. and D.J. Mooney, *Synthetic biodegradable polymer scaffolds*. 1997: Springer.
37. Hern, D.L. and J.A. Hubbell, *Incorporation of adhesion peptides into nonadhesive hydrogels useful for tissue resurfacing.* Journal of Biomedical Materials Research, 1998. **39**(2): p. 266-276.
38. Hassan, E., et al., *Amine functional hydrogels as selective substrates for corneal epithelialization.* Acta Biomaterialia, 2014. **10**(7): p. 3029-3037.
39. Sun, Y., et al., *Culture of dermal fibroblasts and protein adsorption on block conetworks of poly(butyl methacrylate-block-(2,3 propandiol-1-methacrylate-stat-ethandiol dimethacrylate)).* Biomaterials, 2007. **28**(4): p. 661-670.
40. Haddow, D.B., et al., *Plasma-polymerized surfaces for culture of human keratinocytes and transfer of cells to an in vitro wound-bed model.* Journal of Biomedical Materials Research - Part A, 2003. **64**(1): p. 80-87.
41. Nuttelman, C.R., et al., *Attachment of fibronectin to poly (vinyl alcohol) hydrogels promotes NIH3T3 cell adhesion, proliferation, and migration.* Journal of Biomedical Materials Research, 2001. **57**(2): p. 217-223.
42. Elbert, D.L. and J.A. Hubbell, *Conjugate addition reactions combined with free-radical cross-linking for the design of materials for tissue engineering.* Biomacromolecules, 2001. **2**(2): p. 430-441.
43. Ananthanarayanan, B., et al., *Neural stem cell adhesion and proliferation on phospholipid bilayers functionalized with RGD peptides.* Biomaterials, 2010. **31**(33): p. 8706-8715.

44. Ebara, M., et al., *Temperature-Responsive Cell Culture Surfaces Enable "On−Off" Affinity Control between Cell Integrins and RGDS Ligands.* Biomacromolecules, 2004. **5**(2): p. 505-510.
45. Hubbell, J.A., *Biomaterials in tissue engineering.* Nature Biotechnology, 1995. **13**(6): p. 565-576.
46. Hayman, E., M. Pierschbacher, and E. Ruoslahti, *Detachment of cells from culture substrate by soluble fibronectin peptides.* The Journal of cell biology, 1985. **100**(6): p. 1948-1954.
47. Cheng, S., et al., *Design and synthesis of novel cyclic RGD-containing peptides as highly potent and selective integrin .alpha.IIb.beta.3 antagonists.* Journal of Medicinal Chemistry, 1994. **37**(1): p. 1-8.
48. Ruoslahti, E. and M.D. Pierschbacher, *New perspectives in cell adhesion: RGD and integrins.* Science, 1987. **238**(4826): p. 491-497.
49. Verrier, S., et al., *Function of linear and cyclic RGD-containing peptides in osteoprogenitor cells adhesion process.* Biomaterials, 2002. **23**(2): p. 585-596.
50. Kostidis, S., et al., *The relative orientation of the Arg and Asp side chains defined by a pseudodihedral angle as a key criterion for evaluating the structure–activity relationship of RGD peptides.* Journal of Peptide Science, 2004. **10**(8): p. 494-509.
51. Porté-Durrieu, M.C., et al., *Cyclo-(DfKRG) peptide grafting onto Ti–6Al–4V: physical characterization and interest towards human osteoprogenitor cells adhesion.* Biomaterials, 2004. **25**(19): p. 4837-4846.
52. Kato, M. and M. Mrksich, *Using model substrates to study the dependence of focal adhesion formation on the affinity of integrin-ligand complexes.* Biochemistry, 2004. **43**(10): p. 2699-2707.
53. Aumailley, M., et al., *Arg-Gly-Asp constrained within cyclic pentapoptides Strong and selective inhibitors of cell adhesion to vitronectin and laminin fragment P1.* FEBS Letters, 1991. **291**(1): p. 50-54.
54. Kumagai, H., et al., *Effect of cyclic RGD peptide on cell adhesion and tumor metastasis.* Biochemical and Biophysical Research Communications, 1991. **177**(1): p. 74-82.
55. Pierschbacher, M.D. and E. Ruoslahti, *Influence of stereochemistry of the sequence Arg-Gly-Asp-Xaa on binding specificity in cell adhesion.* Journal of Biological Chemistry, 1987. **262**(36): p. 17294-17298.
56. Massia, S.P. and J.A. Hubbell, *An RGD spacing of 440 nm is sufficient for integrin alpha V beta 3-mediated fibroblast spreading and 140 nm for focal contact and stress fiber formation.* The Journal of cell biology, 1991. **114**(5): p. 1089-1100.
57. Ward, M.D. and D.A. Hammer, *A theoretical analysis for the effect of focal contact formation on cell-substrate attachment strength.* Biophysical journal, 1993. **64**(3): p. 936-959.
58. DiMilla, P.A., et al., *Maximal migration of human smooth muscle cells on fibronectin and type IV collagen occurs at an intermediate attachment strength.* The Journal of cell biology, 1993. **122**(3): p. 729-737.
59. Zygourakis, K., R. Bizios, and P. Markenscoff, *Proliferation of anchorage-dependent contact-inhibited cells: I. Development of theoretical models based on cellular automata.* Biotechnol Bioeng, 1991. **38**(5): p. 459-70.
60. Zygourakis, K., P. Markenscoff, and R. Bizios, *Proliferation of anchorage-dependent contact-inhibited cells. II: experimental results and validation of the theoretical models.* Biotechnol Bioeng, 1991. **38**(5): p. 471-9.
61. Merrifield, R.B., *Solid phase peptide synthesis. I. The synthesis of a tetrapeptide.* Journal of the American Chemical Society, 1963. **85**(14): p. 2149-2154.
62. Jones, J., *Amino acid and peptide synthesis*. Vol. 7. 1992: Oxford University Press.
63. Elloumi, I., et al., *Construction of epidermal growth factor fusion protein with cell adhesive activity.* Biomaterials, 2006. **27**(18): p. 3451-3458.

64. Underwood, P.A., J.G. Steele, and B.A. Dalton, *Effects of polystyrene surface chemistry on the biological activity of solid phase fibronectin and vitronectin, analysed with monoclonal antibodies.* Journal of cell science, 1993. **104**(3): p. 793-803.
65. Sawyer, A., et al., *The effect of the addition of a polyglutamate motif to RGD on peptide tethering to hydroxyapatite and the promotion of mesenchymal stem cell adhesion.* Biomaterials, 2005. **26**(34): p. 7046-7056.
66. Jacob, J.T., et al., *Corneal epithelial cell growth over tethered-protein/peptide surface-modified hydrogels.* Journal of Biomedical Materials Research Part B: Applied Biomaterials, 2005. **72B**(1): p. 198-205.
67. Reinhart-King, C.A., M. Dembo, and D.A. Hammer, *Endothelial Cell Traction Forces on RGD-Derivatized Polyacrylamide Substrata†.* Langmuir, 2002. **19**(5): p. 1573-1579.
68. Park, K.-H. and K. Yun, *Immobilization of Arg-Gly-Asp (RGD) sequence in a thermosensitive hydrogel for cell delivery using pheochromocytoma cells (PC12).* Journal of Bioscience and Bioengineering, 2004. **97**(6): p. 374-377.
69. Yamaoka, T., et al., *Synthesis and properties of malic acid-containing functional polymers.* International journal of biological macromolecules, 1999. **25**(1): p. 265-271.
70. Takezawa, T., Y. Mori, and K. Yoshizato, *Cell Culture on a Thermo-Responsive Polymer Surface.* Nat Biotech, 1990. **8**(9): p. 854-856.
71. Canavan, H.E., et al., *Cell sheet detachment affects the extracellular matrix: a surface science study comparing thermal liftoff, enzymatic, and mechanical methods.* Journal of Biomedical Materials Research Part A, 2005. **75**(1): p. 1-13.
72. Canavan, H.E., et al., *A Plasma-Deposited Surface for Cell Sheet Engineering: Advantages over Mechanical Dissociation of Cells.* Plasma Processes and Polymers, 2006. **3**(6-7): p. 516-523.
73. Canavan, H.E., et al., *Surface characterization of the extracellular matrix remaining after cell detachment from a thermoresponsive polymer.* Langmuir, 2005. **21**(5): p. 1949-1955.
74. Okano, T., et al., *Mechanism of cell detachment from temperature-modulated, hydrophilic-hydrophobic polymer surfaces.* Biomaterials, 1995. **16**(4): p. 297-303.
75. Reed, J.A., et al., *The effects of cell culture parameters on cell release kinetics from thermoresponsive surfaces.* Journal of applied biomaterials & biomechanics: JABB, 2008. **6**(2): p. 81.
76. Ebara, M., et al., *Copolymerization of 2-carboxyisopropylacrylamide with N-isopropylacrylamide accelerates cell detachment from grafted surfaces by reducing temperature.* Biomacromolecules, 2003. **4**(2): p. 344-349.
77. Kwon, O.H., et al., *Rapid cell sheet detachment from Poly (N‐isopropylacrylamide)‐grafted porous cell culture membranes.* Journal of Biomedical Materials Research, 2000. **50**(1): p. 82-89.
78. Xue, C., et al., *Protein Adsorption Modes Determine Reversible Cell Attachment on Poly(N-isopropyl acrylamide) Brushes.* Advanced Functional Materials, 2012. **22**(11): p. 2394-2401.
79. Hatakeyama, H., et al., *Bio-functionalized thermoresponsive interfaces facilitating cell adhesion and proliferation.* Biomaterials, 2006. **27**(29): p. 5069-5078.
80. Hopkins, S., et al., *Sub-micron poly(N-isopropylacrylamide) particles as temperature responsive vehicles for the detachment and delivery of human cells.* Soft Matter, 2009. **5**(24): p. 4928-4937.
81. Yamato, M., et al., *Temperature-responsive cell culture surfaces for regenerative medicine with cell sheet engineering.* Progress in Polymer Science, 2007. **32**(8–9): p. 1123-1133.
82. Patel, S., et al., *Regulation of endothelial cell function by GRGDSP peptide grafted on interpenetrating polymers.* Journal of Biomedical Materials Research Part A, 2007. **83**(2): p. 423-433.
83. Cooperstein, M.A. and H.E. Canavan, *Assessment of cytotoxicity of (N-isopropyl acrylamide) and Poly (N-isopropyl acrylamide)-coated surfaces.* Biointerphases, 2013. **8**(1): p. 19.

84. Cooperstein, M., *POLY (N-ISOPROPYL ACRYLAMIDE)-COATED SURFACES: INVESTIGATION OF CYTOTOXICITY WITH MAMMALIAN CELLS AND THE MECHANISM OF CELL DETACHMENT.* 2014.
85. Stephen Rimmer, S.C., Ramune Rutkaite, John W. Haycock, Linda Swanson, *Highly branched poly-(N-isopropylacrylamide)s with arginine-glycing-aspartic acid (RGD)- or COOH- chain ends that form sub micron stimulus-responsive particles above the critical solution temperature.* Communication, 2007. **3**: p. 971-973.
86. Chee, C.K., et al., *Fluorescence investigations of the thermally induced conformational transition of poly(N-isopropylacrylamide).* Polymer, 2001. **42**(12): p. 5079-5087.
87. Chee, C.K., et al., *Time-resolved fluorescence anisotropy studies of the temperature-induced intramolecular conformational transition of poly(N-isopropylacrylamide) in dilute aqueous solution.* Polymer, 1997. **38**(2): p. 483-486.
88. Vogt, A.P. and B.S. Sumerlin, *Tuning the Temperature Response of Branched Poly(N-isopropylacrylamide) Prepared by RAFT Polymerization.* Macromolecules, 2008. **41**(20): p. 7368-7373.
89. Carter, S., B. Hunt, and S. Rimmer, *Highly Branched Poly(N-isopropylacrylamide)s with Imidazole End Groups Prepared by Radical Polymerization in the Presence of a Styryl Monomer Containing a Dithioester Group.* Macromolecules, 2005. **38**(11): p. 4595-4603.
90. Plenderleith, R., T. Swift, and S. Rimmer, *Highly-branched poly (N-isopropyl acrylamide) s with core–shell morphology below the lower critical solution temperature.* RSC Advances, 2014. **4**(92): p. 50932-50937.
91. Robert, P., *Poly(N-isopropylacrylamide) (PNIPAM) is never hydrophobic.* Journal of Colloid and Interface Science, 2010. **348**(2): p. 673-674.
92. Cowie, J.M.G. and V. Arrighi, *Polymers: chemistry and physics of modern materials*. 2007: CRC press.
93. Green, W.A., *Industrial photoinitiators: a technical guide*. 2010: CRC Press.
94. A. D. JENKINS , P.K. and A.U.W.S. R. F. T. STEPTO *GLOSSARY OF BASIC TERMS IN POLYMER SCIENCE*
(IUPAC Recommendations 1996). INTERNATIONAL, UNION OF PURE
AND APPLIED CHEMISTRY, 1996. **68**(12): p. 2287-231 1,.
95. Beckwith, A.L.J., *Radicals in organic synthesis: Formation of carbon—carbon bonds. Von B. Giese, Pergamon Press, Oxford 1986. XIII, 294 S., Paperback $ 25.00. — ISBN 0-08-032494-0.* Angewandte Chemie, 1987. **99**(8): p. 824-825.
96. Cacioli, P., et al., *COPOLYMERIZATION OF omega -UNSATURATED OLIGO(METHYL METHACRYLATE): NEW MACROMONOMERS.* Journal of macromolecular science. Chemistry, 1986. **A23**(7): p. 839-852.
97. Chiefari, J., et al., *Living Free-Radical Polymerization by Reversible Addition−Fragmentation Chain Transfer: The RAFT Process.* Macromolecules, 1998. **31**(16): p. 5559-5562.
98. Krstina, J., et al., *Narrow polydispersity block copolymers by free-radical polymerization in the presence of macromonomers.* Macromolecules, 1995. **28**(15): p. 5381-5385.
99. Corpart, P., et al., *WO 9858974, 1998.* There is no corresponding record for this reference.
100. Delduc, P., C. Tailhan, and S.Z. Zard, *A convenient source of alkyl and acyl radicals.* J. Chem. Soc., Chem. Commun., 1988(4): p. 308-310.
101. Graeme Moad , E.R.a.S.H.T., *Living Radical Polymerisation by RAFT the Process - A First Update.* Australian Journal of Chemistry, 2006. **59**: p. 669-692.
102. Moad, G., E. Rizzardo, and S.H. Thang, *Radical addition-fragmentation chemistry in polymer synthesis.* Polymer, 2008. **49**(5): p. 1079-1131.
103. Graeme Moad , E.R.a.S.H.T., *Living Radical Polymerization by the RAFT Process.* Australian Journal of CHemistry, 2005. **5**(6): p. 379-410.
104. *Micro- and Nanoscale Processing of Biomaterials*. 2010.

105. Carter, S.R., et al., *Functional Graft Poly(N-isopropyl acrylamide)s Using Reversible Addition-Fragmentation Chain Transfer (RAFT) Polymerisation.* Macromolecular Bioscience, 2007. **7**(8): p. 975-986.
106. Moad, G., et al., *Advances in RAFT polymerization: the synthesis of polymers with defined end-groups.* Polymer, 2005. **46**(19): p. 8458-8468.
107. Perrier, S., P. Takolpuckdee, and C.A. Mars, *Reversible addition-fragmentation chain transfer polymerization: End group modification for functionalized polymers and chain transfer agent recovery.* Macromolecules, 2005. **38**(6): p. 2033-2036.
108. Schmid, C., *Efficient Switching of RAFT to Hydroxyl Capped Polymers as a Versatile Scaffold for Block Copolymer Synthesis*, in *Fakultät für Chemie und Biowissenschaften*. 2012, Karlsruher Institut für Technologie: Karlsruhe.
109. England, R.M. and S. Rimmer, *Synthesis of chain end functionalized linear and branched polymers by radical polymerisation in the presence of a silyl enol.* Chemical Communications, 2010. **46**(31): p. 5767-5769.
110. Scarpa, J.S., D.D. Mueller, and I.M. Klotz, *Slow hydrogen-deuterium exchange in a non-. alpha.-helical polyamide.* Journal of the American Chemical Society, 1967. **89**(24): p. 6024-6030.
111. Heskins, M. and J.E. Guillet, *Solution properties of poly (N-isopropylacrylamide).* Journal of Macromolecular Science—Chemistry, 1968. **2**(8): p. 1441-1455.
112. De Gennes, P., *Collapse of a flexible polymer chain II.* Journal de Physique Lettres, 1978. **39**(17): p. 299-301.
113. Schild, H.G., *Poly(N-isopropylacrylamide): experiment, theory and application.* Progress in Polymer Science, 1992. **17**(2): p. 163-249.
114. Wu, C. and X. Wang, *Globule-to-coil transition of a single homopolymer chain in solution.* Physical review letters, 1998. **80**(18): p. 4092.
115. Van der Goot, F., et al., *A'molten-globule'membrane-insertion intermediate of the pore-forming domain of colicin A.* 1991.
116. Galperin, A., T.J. Long, and B.D. Ratner, *Degradable, Thermo-Sensitive Poly(N-isopropyl acrylamide)-Based Scaffolds with Controlled Porosity for Tissue Engineering Applications.* Biomacromolecules, 2010. **11**(10): p. 2583-2592.
117. Stile, R.A., W.R. Burghardt, and K.E. Healy, *Synthesis and Characterization of Injectable Poly(N-isopropylacrylamide)-Based Hydrogels That Support Tissue Formation in Vitro.* Macromolecules, 1999. **32**(22): p. 7370-7379.
118. Tan, H., et al., *Thermosensitive injectable hyaluronic acid hydrogel for adipose tissue engineering.* Biomaterials, 2009. **30**(36): p. 6844-6853.
119. Kim, S. and K.E. Healy, *Synthesis and Characterization of Injectable Poly(N-isopropylacrylamide-co-acrylic acid) Hydrogels with Proteolytically Degradable Cross-Links.* Biomacromolecules, 2003. **4**(5): p. 1214-1223.
120. de las Heras Alarcón, C., S. Pennadam, and C. Alexander, *Stimuli responsive polymers for biomedical applications.* Chemical Society Reviews, 2005. **34**(3): p. 276-285.
121. Nelson, A., *Stimuli-responsive polymers: Engineering interactions.* Nat Mater, 2008. **7**(7): p. 523-525.
122. Klevens, R.M., et al., *Invasive methicillin-resistant Staphylococcus aureus infections in the United States.* Jama, 2007. **298**(15): p. 1763-1771.
123. Neu, H.C., *The crisis in antibiotic resistance.* Science, 1992. **257**(5073): p. 1064-1073.
124. Zhu, Y.-G., et al., *Diverse and abundant antibiotic resistance genes in Chinese swine farms.* Proceedings of the National Academy of Sciences, 2013. **110**(9): p. 3435-3440.
125. Burd, A., et al., *A comparative study of the cytotoxicity of silver-based dressings in monolayer cell, tissue explant, and animal models.* Wound Repair and Regeneration, 2007. **15**(1): p. 94-104.

126. Pasparakis, G. and C. Alexander, *Synthetic polymers for capture and detection of microorganisms.* Analyst, 2007. **132**(11): p. 1075-1082.
127. Pasparakis, G., A. Cockayne, and C. Alexander, *Control of bacterial aggregation by thermoresponsive glycopolymers.* Journal of the American Chemical Society, 2007. **129**(36): p. 11014-11015.
128. Liu, Y., et al., *Novel renewable immunosensors based on temperature-sensitive PNIPAAm bioconjugates.* Biosensors and bioelectronics, 2008. **24**(4): p. 710-715.
129. Ding, Z., et al., *Size-dependent control of the binding of biotinylated proteins to streptavidin using a polymer shield.* Nature, 2001. **411**(6833): p. 59-62.
130. Shepherd, J., et al., *Binding bacteria to highly branched poly(N-isopropyl acrylamide) modified with vancomycin induces the coil-to-globule transition.* Journal of the American Chemical Society, 2010. **132**(6): p. 1736-1737.
131. Hantzsch, A., *Über die Halochromie und »Solvatochromie« des Dibenzal-acetons und einfacherer Ketone, sowie ihrer Ketochloride.* Berichte der deutschen chemischen Gesellschaft (A and B Series), 1922. **55**(4): p. 953-979.
132. Reichardt, C., *Solvatochromic dyes as solvent polarity indicators.* Chemical Reviews, 1994. **94**(8): p. 2319-2358.
133. Kriz, G., G. Lampman, and D. Pavia, *Introduction to Spectroscopy.* Editora Thomson Learning, 1979. **3**.
134. Dutta, A.K., K. Kamada, and K. Ohta, *Spectroscopic studies of nile red in organic solvents and polymers.* Journal of Photochemistry and Photobiology A: Chemistry, 1996. **93**(1): p. 57-64.
135. Jose, J. and K. Burgess, *Benzophenoxazine-based fluorescent dyes for labeling biomolecules.* Tetrahedron, 2006. **62**(48): p. 11021-11037.
136. Greenspan, P. and S.D. Fowler, *Spectrofluorometric studies of the lipid probe, nile red.* Journal of lipid research, 1985. **26**(7): p. 781-789.
137. Fletcher, K.A., et al., *Behavior of the solvatochromic probes Reichardt's dye, pyrene, dansylamide, Nile Red and 1-pyrenecarbaldehyde within the room-temperature ionic liquid bmimPF6.* Green Chemistry, 2001. **3**(5): p. 210-215.
138. Ngeontae, W., et al., *Polymerized Nile Blue derivatives for plasticizer-free fluorescent ion optode microsphere sensors.* Analytica chimica acta, 2007. **599**(1): p. 124-133.
139. Inal, S., et al., *Structure-related differences in the temperature-regulated fluorescence response of LCST type polymers.* Journal of Materials Chemistry C, 2013. **1**(40): p. 6603-6612.
140. Sperling, L.H. and V. Mishra, *The current status of interpenetrating polymer networks.* Polymers for Advanced Technologies, 1996. **7**(4): p. 197-208.
141. Chikh, L., V. Delhorbe, and O. Fichet, *(Semi-)Interpenetrating polymer networks as fuel cell membranes.* Journal of Membrane Science, 2011. **368**(1-2): p. 1-17.
142. Ingavle, G.C., S.H. Gehrke, and M.S. Detamore, *The bioactivity of agarose–PEGDA interpenetrating network hydrogels with covalently immobilized RGD peptides and physically entrapped aggrecan.* Biomaterials, 2014. **35**(11): p. 3558-3570.
143. Lee, W.-F. and Y.-J. Chen, *Studies on preparation and swelling properties of the N-isopropylacrylamide/chitosan semi-IPN and IPN hydrogels.* Journal of Applied Polymer Science, 2001. **82**(10): p. 2487-2496.
144. Weng, L., et al., *Mechanically strong double network photocrosslinked hydrogels from N,N-dimethylacrylamide and glycidyl methacrylated hyaluronan.* Biomaterials, 2008. **29**(14): p. 2153-2163.
145. Stile, R.A., et al., *Poly(N-isopropylacrylamide)-based semi-interpenetrating polymer networks for tissue engineering applications. Effects of linear poly(acrylic acid) chains on rheology.* Journal of Biomaterials Science, Polymer Edition, 2004. **15**(7): p. 865-878.
146. Stile, R.A. and K.E. Healy, *Poly(N-isopropylacrylamide)-Based Semi-interpenetrating Polymer Networks for Tissue Engineering Applications. 1. Effects of Linear Poly(acrylic acid) Chains on Phase Behavior.* Biomacromolecules, 2002. **3**(3): p. 591-600.

147. Phillips, J.M. and W.J. Kao, *Macrophage Adhesion on Gelatin-Based Interpenetrating Networks Grafted with PEGylated RGD.* Tissue Engineering, 2005. **11**(5-6): p. 964-973.
148. Jaiswal, M., et al., *Cell adhesion and proliferation studies on semi-interpenetrating polymeric networks (semi-IPNs) of polyacrylamide and gelatin.* Journal of Biomedical Materials Research - Part B Applied Biomaterials, 2011. **98 B**(2): p. 342-350.
149. Liu, Y. and M.B. Chan-Park, *Hydrogel based on interpenetrating polymer networks of dextran and gelatin for vascular tissue engineering.* Biomaterials, 2009. **30**(2): p. 196-207.
150. Pescosolido, L., et al., *Hyaluronic acid and dextran-based semi-IPN hydrogels as biomaterials for bioprinting.* Biomacromolecules, 2011. **12**(5): p. 1831-1838.
151. Suri, S. and C.E. Schmidt, *Cell-laden hydrogel constructs of hyaluronic acid, collagen, and laminin for neural tissue engineering.* Tissue Engineering - Part A, 2010. **16**(5): p. 1703-1716.
152. Jaiswal, M., et al., *Polycaprolactone diacrylate crosslinked biodegradable semi-interpenetrating networks of polyacrylamide and gelatin for controlled drug delivery.* Biomedical Materials, 2010. **5**(6).
153. Wang, T., et al., *Rapid cell sheet detachment from alginate semi-interpenetrating nanocomposite hydrogels of PNIPAm and hectorite clay.* Reactive and Functional Polymers, 2011. **71**(4): p. 447-454.
154. Albertsson, A.C. and S. Karlsson, *Degradable polymers for the future.* Acta Polymerica, 1995. **46**(2): p. 114-123.
155. Amass, W., A. Amass, and B. Tighe, *A review of biodegradable polymers: uses, current developments in the synthesis and characterization of biodegradable polyesters, blends of biodegradable polymers and recent advances in biodegradation studies.* Polymer International, 1998. **47**(2): p. 89-144.
156. Holland, S., et al., *Advances in Pharmaceutical Sciences.* Advances in Pharmaceutical Sciences, 1992. **6**.
157. Jeong, B., et al., *Biodegradable block copolymers as injectable drug-delivery systems.* Nature, 1997. **388**(6645): p. 860-862.
158. Holland, S.J., B.J. Tighe, and P.L. Gould, *Polymers for biodegradable medical devices. 1. The potential of polyesters as controlled macromolecular release systems.* Journal of Controlled Release, 1986. **4**(3): p. 155-180.
159. de Ruiter, G.C., et al., *Designing ideal conduits for peripheral nerve repair.* Neurosurgical focus, 2009. **26**(2): p. E5.
160. Guo, B. and P. Ma, *Synthetic biodegradable functional polymers for tissue engineering: a brief review.* Science China Chemistry, 2014. **57**(4): p. 490-500.
161. Claeyssens, F., et al., *Three-Dimensional Biodegradable Structures Fabricated by Two-Photon Polymerization.* Langmuir, 2009. **25**(5): p. 3219-3223.
162. Martina, M. and D.W. Hutmacher, *Biodegradable polymers applied in tissue engineering research: a review.* Polymer International, 2007. **56**(2): p. 145-157.
163. Nimni, M.E., et al., *Chemically modified collagen: A natural biomaterial for tissue replacement.* Journal of Biomedical Materials Research, 1987. **21**(6): p. 741-771.
164. Holloway, J.L., A.M. Lowman, and G.R. Palmese, *Mechanical evaluation of poly(vinyl alcohol)-based fibrous composites as biomaterials for meniscal tissue replacement.* Acta Biomaterialia, 2010. **6**(12): p. 4716-4724.
165. Yankelson, L. and A.J. Domb, *Injectable biodegradable polymer compositions for soft tissue repair and augmentation*. 2014, Google Patents.
166. Steinberg, T., et al., *Biocompatible and biodegradable gradient layer system for regenerative medicine and for tissue support*. 2014, Google Patents.
167. Kumari, A., S.K. Yadav, and S.C. Yadav, *Biodegradable polymeric nanoparticles based drug delivery systems.* Colloids and Surfaces B: Biointerfaces, 2010. **75**(1): p. 1-18.
168. Oliveira, M.R., et al., *Tissue engineering: using collagen type I matrix for bone healing of bone defects.* Journal of Craniofacial Surgery, 2013. **24**(4): p. e394-e396.

169. Lai, E.S., C.M. Anderson, and G.G. Fuller, *Designing a tubular matrix of oriented collagen fibrils for tissue engineering.* Acta Biomaterialia, 2011. **7**(6): p. 2448-2456.
170. Koshy, S.T., et al., *Injectable, porous, and cell-responsive gelatin cryogels.* Biomaterials, 2014. **35**(8): p. 2477-2487.
171. Loth, T., et al., *Gelatin-based biomaterial engineering with anhydride-containing oligomeric cross-linkers.* Biomacromolecules, 2014.
172. Gil, E.S., et al., *Functionalized silk biomaterials for wound healing.* Advanced healthcare materials, 2013. **2**(1): p. 206-217.
173. Kundu, B., et al., *Silk fibroin biomaterials for tissue regenerations.* Advanced drug delivery reviews, 2013. **65**(4): p. 457-470.
174. Sun, J. and H. Tan, *Alginate-based biomaterials for regenerative medicine applications.* Materials, 2013. **6**(4): p. 1285-1309.
175. Qi, Y., et al., *Cartilage repair using mesenchymal stem cell (MSC) sheet and MSCs-loaded bilayer PLGA scaffold in a rabbit model.* Knee Surgery, Sports Traumatology, Arthroscopy, 2014. **22**(6): p. 1424-1433.
176. Zong, C., et al., *Biocompatibility and Bone-Repairing Effects: Comparison Between Porous Poly-Lactic-Co-Glycolic Acid and Nano-Hydroxyapatite/Poly (lactic acid) Scaffolds.* Journal of biomedical nanotechnology, 2014. **10**(6): p. 1091-1104.
177. Dechy-Cabaret, O., B. Martin-Vaca, and D. Bourissou, *Controlled ring-opening polymerization of lactide and glycolide.* Chemical Reviews, 2004. **104**(12): p. 6147-6176.
178. Miller, R.A., J.M. Brady, and D.E. Cutright, *Degradation rates of oral resorbable implants (polylactates and polyglycolates): rate modification with changes in PLA/PGA copolymer ratios.* Journal of Biomedical Materials Research, 1977. **11**(5): p. 711-719.
179. Buchholz, B., J. Hess, and K.R. Muller, *Process for the preparation of trimethylene carbonate*. 1993, Google Patents.
180. Pego, A., et al., *In vivo behavior of poly (1, 3 ‐ trimethylene carbonate) and copolymers of 1, 3 ‐ trimethylene carbonate with D, L ‐ lactide or ϵ ‐ caprolactone: Degradation and tissue response.* Journal of Biomedical Materials Research Part A, 2003. **67**(3): p. 1044-1054.
181. Pêgo, A.P., et al., *Biodegradable elastomeric scaffolds for soft tissue engineering.* Journal of Controlled Release, 2003. **87**(1–3): p. 69-79.
182. Zhang, Z., et al., *The in vivo and in vitro degradation behavior of poly (trimethylene carbonate).* Biomaterials, 2006. **27**(9): p. 1741-1748.
183. Pego, A., et al., *Preparation of degradable porous structures based on 1, 3-trimethylene carbonate and D, L-lactide (co) polymers for heart tissue engineering.* Tissue Engineering, 2003. **9**(5): p. 981-994.
184. P. Pêgo, A., et al., *Copolymers of trimethylene carbonate and ε-caprolactone for porous nerve guides: synthesis and properties.* Journal of Biomaterials Science, Polymer Edition, 2001. **12**(1): p. 35-53.
185. Pego, A.P., et al., *Adhesion and growth of human Schwann cells on trimethylene carbonate (co) polymers.* Journal of Biomedical Materials Research Part A, 2003. **67**(3): p. 876-885.
186. Habraken, W.J.E.M., et al., *Introduction of enzymatically degradable poly(trimethylene carbonate) microspheres into an injectable calcium phosphate cement.* Biomaterials, 2008. **29**(16): p. 2464-2476.
187. Xie, R., Y. Li, and L.-Y. Chu, *Preparation of thermo-responsive gating membranes with controllable response temperature.* Journal of Membrane Science, 2007. **289**(1–2): p. 76-85.
188. Hamid, R., et al., *Comparison of alamar blue and MTT assays for high through-put screening.* Toxicology in Vitro, 2004. **18**(5): p. 703-710.
189. Ralston, D.R., et al., *The requirement for basement membrane antigens in the production of human epidermal/dermal composites in vitro.* BRITISH JOURNAL OF DERMATOLOGY, 1999. **140**(4): p. 605-615.

190. Wang, M., et al., *Preparation and properties of chitosan-poly(N-isopropylacrylamide) semi-IPN hydrogels.* Journal of Polymer Science Part A: Polymer Chemistry, 2000. **38**(3): p. 474-481.
191. Zeng, M. and Z. Fang, *Preparation of sub-micrometer porous membrane from chitosan/polyethylene glycol semi-IPN.* Journal of Membrane Science, 2004. **245**(1–2): p. 95-102.
192. Plenderleith, R.A., et al., *Arginine–glycine–aspartic acid functional branched semi-interpenetrating hydrogels.* Soft Matter, 2015. **11**(38): p. 7567-7578.
193. Sammon, C., et al., *ATR–FTIR studies of a thermo-responsive ABA triblock copolymer gelator in aqueous solution.* Polymer, 2006. **47**(17): p. 6123-6130.
194. Maeda, Y., T. Nakamura, and I. Ikeda, *Changes in the Hydration States of Poly(N-alkylacrylamide)s during Their Phase Transitions in Water Observed by FTIR Spectroscopy†.* Macromolecules, 2001. **34**(5): p. 1391-1399.
195. Perlin, L., S. MacNeil, and S. Rimmer, *Production and performance of biomaterials containing RGD peptides.* Soft Matter, 2008. **4**(12): p. 2331-2349.
196. Smith, L.E., S. Rimmer, and S. MacNeil, *Examination of the effects of poly(N-vinylpyrrolidinone) hydrogels in direct and indirect contact with cells.* Biomaterials, 2006. **27**(14): p. 2806-2812.
197. Collett, J., et al., *Thermally responsive polymeric hydrogel brushes: synthesis, physical properties and use for the culture of chondrocytes.* Journal of The Royal Society Interface, 2007. **4**(12): p. 117-126.
198. Pateman, C.J., et al., *Nerve guides manufactured from photocurable polymers to aid peripheral nerve repair.* Biomaterials, 2015. **49**: p. 77-89.
199. Hollands, C., *The Animals (scientific procedures) Act 1986.* The Lancet, 1986. **328**(8497): p. 32-33.
200. Arcaute, K., et al. *Stereolithography of PEG hydrogel multi-lumen nerve regeneration conduits*. in *ASME 2005 International Mechanical Engineering Congress and Exposition*. 2005: American Society of Mechanical Engineers.
201. Ovsianikov, A., et al., *Three-dimensional laser micro- and nano-structuring of acrylated poly(ethylene glycol) materials and evaluation of their cytoxicity for tissue engineering applications.* Acta Biomaterialia, 2011. **7**(3): p. 967-974.
202. Zhu, K.J., et al., *Synthesis, properties, and biodegradation of poly(1,3-trimethylene carbonate).* Macromolecules, 1991. **24**(8): p. 1736-1740.
203. Ajiro, H., Y. Takahashi, and M. Akashi, *Thermosensitive Biodegradable Homopolymer of Trimethylene Carbonate Derivative at Body Temperature.* Macromolecules, 2012. **45**(6): p. 2668-2674.
204. Nederberg, F., et al., *Organocatalytic Ring Opening Polymerization of Trimethylene Carbonate.* Biomacromolecules, 2006. **8**(1): p. 153-160.
205. Shepherd, J., et al., *Hyperbranched poly(NIPAM) polymers modified with antibiotics for the reduction of bacterial burden in infected human tissue engineered skin.* Biomaterials, 2011. **32**(1): p. 258-267.
206. Sarker, P., et al., *Förster resonance energy transfer confirms the bacterial-induced conformational transition in highly-branched poly (N-isopropyl acrylamide with vancomycin end groups on binding to Staphylococcus aureus.* Soft Matter, 2014. **10**(31): p. 5824-5835.
207. Hargreaves, J.S. and S.E. Webber, *Photophysics of anthracene polymers: fluorescence, singlet energy migration, and photodegradation.* Macromolecules, 1984. **17**(2): p. 235-240.
208. Ruiz-Pérez, L., et al., *Conformation of poly (methacrylic acid) chains in dilute aqueous solution.* Macromolecules, 2008. **41**(6): p. 2203-2211.